

**A STUDY ON SOME ASPECTS OF HOT  
AND DENSE QCD MATTER**

*By*  
**RITESH GHOSH**  
**PHYS05201704023**

**Saha Institute of Nuclear Physics, Kolkata**

*A thesis submitted to the*

*Board of Studies in Physical Sciences*

*In partial fulfillment of requirements*

*For the Degree of*

**DOCTOR OF PHILOSOPHY**

*of*

**HOMI BHABHA NATIONAL INSTITUTE**



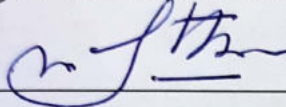
**October, 2022**



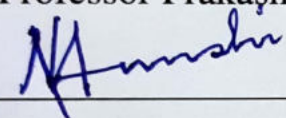
# Homi Bhabha National Institute

## Recommendations of the Viva Voce Committee

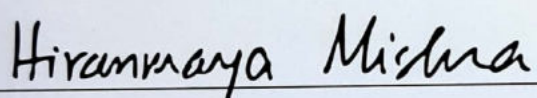
As members of the Viva Voce Committee, we certify that we have read the dissertation prepared by **Ritesh Ghosh** entitled "A study on some aspects of hot and dense QCD matter" and recommend that it maybe accepted as fulfilling the thesis requirement for the award of Degree of Doctor of Philosophy.

 25/10/22 Date:

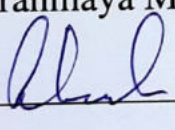
Chairman - Professor Prakash Mathews

 25/10/2022 Date:

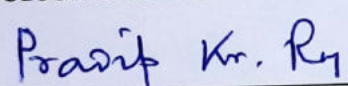
Guide / Convener - Professor Munshi Golam Mustafa

 25/10/2022 Date:

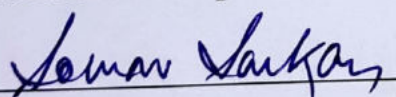
Examiner - Professor Hiranmaya Mishra

 25/10/2022 Date:

Member 1 - Professor Arnab Kundu

 25/10/2022 Date:

Member 2 - Professor Pradip Kumar Roy

 25/10/2022 Date:

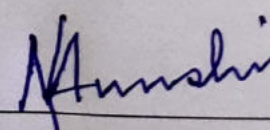
Member 3 - Professor Sourav Sarkar

Final approval and acceptance of this thesis is contingent upon the candidate's submission of the final copies of the thesis to HBNI.

I/We hereby certify that I/we have read this thesis prepared under my/our direction and recommend that it may be accepted as fulfilling the thesis requirement.

Date: 25/10/2022

Place: Kolkata

Guide: 



## STATEMENT BY AUTHOR

This dissertation has been submitted in partial fulfillment of requirements for an advanced degree at Homi Bhabha National Institute (HBNI) and is deposited in the Library to be made available to borrowers under rules of the HBNI.

Brief quotations from this dissertation are allowable without special permission, provided that accurate acknowledgment of source is made. Requests for permission for extended quotation from or reproduction of this manuscript in whole or in part may be granted by the Competent Authority of HBNI when in his or her judgment the proposed use of the material is in the interests of scholarship. In all other instances, however, permission must be obtained from the author.

Ritesh Ghosh  
25/10/22  
Ritesh Ghosh



## DECLARATION

I, hereby declare that the investigation presented in the thesis has been carried out by me. The work is original and has not been submitted earlier as a whole or in part for a degree / diploma at this or any other Institution / University.

Ritesh Ghosh  
25/10/22

Ritesh Ghosh





---

---

# LIST OF PUBLICATIONS

---

## Publications included in the thesis

### Journal:

- 1. Soft contribution to the damping rate of a hard photon in a weakly magnetized hot medium**  
*Ritesh Ghosh*, Bithika Karmakar, Munshi G. Mustafa, *Phys. Rev. D* **101** (2020) 5, 056007, [[arXiv:1911.00744](#) [hep-ph]].
- 2. Covariant formulation of gluon self-energy in presence of ellipsoidal anisotropy**  
*Ritesh Ghosh*, Bithika Karmakar, Arghya Mukherjee, *Phys. Rev. D* **102** (2020) 11, 114002, [[arXiv:2011.03374](#) [hep-ph]].
- 3. Chiral susceptibility in dense thermo-magnetic QCD medium within HTL approximation**  
*Ritesh Ghosh*, Bithika Karmakar, Munshi G. Mustafa, *Phys. Rev. D* **103** (2021) 7, 074019, [[arXiv:2103.08407](#) [hep-ph]].

4. **Shear Viscosity of hadronic matter at finite temperature and magnetic field**

*Ritesh Ghosh*, Najmul Haque, *Phys. Rev. D* **105** (2022) 11, 114029, [[arXiv:2204.01639 \[hep-ph\]](#)].

5. **Anisotropic tomography of heavy quark dissociation by using general propagator structure at finite magnetic field**

*Ritesh Ghosh*, Aritra Bandyopadhyay, Indrani Nilima, Sabyasachi Ghosh, *Phys. Rev. D* **106** (2022) 5, 054010, [[arXiv: 2204.02312](#)].

## **Other publications (not included in the thesis)**

1. **Heavy quark potential and LQCD based quark condensate at finite magnetic field**

Indrani Nilima, Aritra Bandyopadhyay, *Ritesh Ghosh*, Sabyasachi Ghosh, [[arXiv: 2204.02388](#)].

2. **Anisotropic pressure of deconfined QCD matter in presence of strong magnetic field within one-loop approximation**

Bithika Karmakar, *Ritesh Ghosh*, Aritra Bandyopadhyay, Najmul Haque, Munshi G. Mustafa, *Phys. Rev. D* **99** (2019) 9, 094002, [[arXiv:1902.02607 \[hep-ph\]](#)].

3. **Saha ionization equation in the early universe**

Aritra Das, *Ritesh Ghosh*, S. Mallik, *Astrophys.J.* **881** (2019), 40, [[arXiv:1812.10686 \[hep-ph\]](#)].

4. **Collective modes of gluons in an anisotropic thermo-magnetic medium**

Bithika Karmakar, *Ritesh Ghosh*, Arghya Mukherjee [[arXiv:2204.09646 \[hep-ph\]](#)].

5. **A study of shear viscosity coefficient of quark matter in Polyakov quark meson model for three flavors**

*Ritesh Ghosh*, [[arXiv:2112.11103](#) [hep-ph]].

**Conference papers:**

1. **Dynamics of QCD matter**

*Ritesh Ghosh*, *Int. J. Mod.Phys.E* **30** (2021) , 02, 2130001,

[[arXiv:2112.11103](#) [hep-ph]].

*Ritesh Ghosh*  
25/10/22  
Ritesh Ghosh



## **Dedication**

I dedicate the thesis to my parents for endless support and love in every moment. Thank you so much.



## ACKNOWLEDGMENTS

“ Gratitude opens the door to... the power, the wisdom,  
the creativity of the universe. You open the door  
through gratitude.”

——- *Deepak Chopra*

First and foremost I am extremely grateful to my supervisors, Prof. Munshi Golam Mustafa for his invaluable advice, motivation and continuous support. I have learned so many things from him about physics and life. Whenever I fell into problem in various academic and other issues, he always helped to get out of it. ‘Cha (tea)’ time in the afternoon will be always happily remembered.

After Munshi sir, I am thankful to Najmul da, "Mathematica Man". Whenever I faced any numerical problem, he solved it. I have learned many numerical things from him. I used to call him over phone frequently for discussions, but he was never irritated. I would like to thank Samir sir for his suggestions and discussions.

I feel very lucky to have senior like Arghya da. Whenever I talk to him, I learn something new. His physics understanding always helped me to think in new interesting way. He became friend from senior. I cherish the memory of Italy where we went to attend the academic school. I am also lucky to have Bithika di. From the beginning of my PhD, I asked silly and trivial questions and she always tried to explain without any annoyance. She helped me in many academic and non-academic issues. For her caring support, my PhD life became more easier. I would like to thank both Aritra da (AB and AD) and Aminul da for their discussions and suggestions. I am thankful to my collaborators Sabyasachi Ghosh, Indrani di and Manu for helpful discussions.

I acknowledge DST, INSPIRE for funding me for five years (from graduation to post-graduation). I also like to thank University Grants Commission (UGC) for funding me throughout my PhD tenure.

I am very thankful to all the members of Saha Institute of Nuclear Physics. I thank to Aranya da for suggesting Munshi sir as PhD guide. I also thank Augniv da, Supriyo da, Avik da (Choto and Boro), Udit da, Bithika di, Sukanya di for giving me a good environment in theory division (Room 3319). I would really miss the talented juniors Sabyasachi, Suman, Adil, Sandip, Pabitra. They always kept me happy. I thank Pritam Palit, Astik, Shuvam, Pooja, Saifuddin, Rezwana, Karimul, Suchanda, Pankaj who also became friends from the Post-Msc. I also thank Sukhendu, ashish, Aman, Vimal, Chiru da, Habib, Aditya. I am grateful to the theory office stuffs for helping in various matters.

I want to thank all the members of MSA-2 where I stayed for five years during the PhD tenure. I will definitely miss them. I want to thank Tanmoy, Upala, Dipali, Saikat, Promita and Lalit vaiya. Their presence always makes me happy. Hostel life was never boring for their craziness. Memory of the enjoyable trip to Darjeeling with Upala, Saikat, Tanmoy, Promita, Ayan and Arunima will be always remembered. Tanmoy became friend on the day when I missed the SINP scheduled bus. From that day, he gradually became one of my closest friends. Whenever I faced any problem, I consulted with him. Later Upala, Tanmoy, Dipali and me formed a close group where Saikat and Lalit often joined us as special guest. I also want to thank batch-mate Pritam, Anindita, juniors Pabitra, Lalit, Suman, Sandip, Adil, Soujanya, Sitaram, Gaurab, Suparna, Jaydip, Munmun, Shreyasi for making me laugh at hostel mess. I also thank senior Madhurima di, Rajkamal da, Sanjukta di and Pallavi. I am thankful to canteen, security and other working stuffs.

More importantly, I am very thankful to Upala, one of my closest friends and ‘mentor’, who inspired and supported me in many difficult situations. Her thinking and philosophy



have made me viewing everything in different ways. I am grateful to have such friendship with Upala who has been tolerating all my tantrums for five years.

Most immensely, I am grateful to my parents and my all family members for loving and unconditional support. I thank all my teachers from school days to PhD, all my childhood friends, school friends, college friends for supporting and helping me to reach this stage. I want to mention some friend's names like Suvo, Bhoda da, Arnab Bera, Arnab Sarkar, Arnab Barua, Arnab Seth, Souvik, Sourav, Partha Das, Partha Rana, Sudhakantha, Saswata, Swagata.

Ritesh Ghosh  
25/10/22  
Ritesh Ghosh



---

---

# CONTENTS

---

<b>Summary</b>	<b>v</b>
<b>Abbreviations</b>	<b>viii</b>
<b>List of Figures</b>	<b>ix</b>
<b>List of Tables</b>	<b>xiv</b>
<b>1 Introduction</b>	<b>1</b>
1.1 Quantum Chromodynamics . . . . .	2
1.2 Quark-gluon plasma . . . . .	5
1.3 Heavy ion collisions: Overview . . . . .	7
1.4 Theoretical approaches to study QCD . . . . .	10
1.5 Magnetic field in non-central heavy ion collisions . . . . .	12
1.6 Signatures of QGP . . . . .	15
1.6.1 Electromagnetic probe . . . . .	15
1.6.2 Strangeness Enhancement . . . . .	16
1.6.3 Quarkonia suppression . . . . .	17

1.6.4	Jet quenching . . . . .	17
1.6.5	Anisotropic flow . . . . .	18
1.7	Kinetic theory . . . . .	19
1.8	Hydrodynamics . . . . .	20
1.9	Plasma Instability . . . . .	23
1.10	Outline of this thesis . . . . .	24
<b>2</b>	<b>Basics of field theory at finite temperature</b>	<b>27</b>
2.1	Imaginary time formalism . . . . .	28
2.1.1	frequency sums . . . . .	31
2.1.2	Saclay Method . . . . .	35
2.2	Real time formalism . . . . .	39
<b>3</b>	<b>Covariant structure of Gauge-Boson propagator</b>	<b>43</b>
<b>4</b>	<b>Glueon self-energy in presence of ellipsoidal anisotropy</b>	<b>51</b>
4.1	Introduction . . . . .	51
4.2	Results . . . . .	55
4.3	Summary . . . . .	63
<b>5</b>	<b>Damping rate of a hard photon in a weakly magnetized hot medium</b>	<b>65</b>
5.1	Introduction . . . . .	65
5.2	SetUp . . . . .	68
5.3	Photon self-energy in hot magnetized medium . . . . .	71
5.3.1	Fermion propagator in weak field approximation . . . . .	72
5.3.2	Photon self-energy in weak magnetic field . . . . .	75
5.4	Imaginary parts of the components of the photon self-energy . . . . .	80

5.4.1	Imaginary parts of the magnetic field independent part, <i>i.e.</i> $\mathcal{O}[(eB)^0]$	82
5.4.2	Imaginary part of magnetic field dependent part of $\mathcal{O}[(eB)^2]$	86
5.5	Results	90
5.6	Summary	94
<b>6</b>	<b>Chiral susceptibility in thermo-magnetic QCD medium: within HTL approximation</b>	<b>97</b>
6.1	Introduction	98
6.2	Definition	100
6.3	General structure of Fermionic two point function	101
6.4	Chiral susceptibility for free fermion in the presence of weak magnetic field	104
6.5	HTL chiral Susceptibility in presence of weak magnetic field	105
6.6	Results	108
6.7	Summary	112
<b>7</b>	<b>Quarkonium in hot and magnetized QGP medium</b>	<b>113</b>
7.1	Introduction	114
7.2	Formalism	117
7.2.1	Heavy quark potential in presence of an external magnetic field	117
7.2.2	Imaginary part of the potential	118
7.2.3	Evaluation of the real and imaginary parts of $b(P)$	119
7.2.4	Final expression of Imaginary part of potential and Decay width	125
7.3	Results	126
7.4	Summary	137
<b>8</b>	<b>Hadronic viscosity coefficient at finite temperature and magnetic field</b>	<b>141</b>

8.1	Introduction . . . . .	142
8.2	Anisotropic Viscosity coefficients in non zero magnetic field . . . . .	143
8.3	Linear Sigma Model . . . . .	150
8.3.1	Thermodynamics . . . . .	152
8.3.2	Scattering amplitudes and interaction frequency . . . . .	153
8.4	Results . . . . .	160
8.5	Summary . . . . .	163
<b>9</b>	<b>Conclusions</b>	<b>165</b>
<b>A</b>	<b>Spectral representation of the propagators</b>	<b>173</b>
<b>B</b>	<b>Structure functions</b>	<b>191</b>
B.1	Sum-integrals . . . . .	198
B.1.1	One-loop sum integrals . . . . .	198
B.1.2	One-loop HTL sum integrals used in the magnetic case . . . . .	200
<b>C</b>	<b>Calculations related to heavy quark potential</b>	<b>203</b>
C.1	Gluon effective propagator in presence of magnetic field . . . . .	203
C.2	Frequency sum . . . . .	205
C.3	Definition of functions $X_{m,n}$ and $X_{m,n}^1$ . . . . .	206
C.4	Debye mass approximated $\text{Im } V$ . . . . .	206
<b>D</b>	<b>Charged scalar field</b>	<b>208</b>
D.1	wave function . . . . .	208
D.2	Quantization . . . . .	211
	<b>Bibliography</b>	<b>213</b>

---

---

# SUMMARY

---

Under extreme conditions such as high temperatures and densities, composite state of hadrons e.g. protons, neutrons, kaons, pions etc lose their identity and turn into a new state of their constituent elements quarks and gluons. This novel phase is called quark-gluon plasma (QGP). Such kind of state is presumed to be created after a few fraction of microseconds of the big bang having temperature higher than  $10^{12}$  K and small net baryon number. It can also exist in the core of the neutron stars where the mass densities ( $10^{15}$  gm/cm<sup>3</sup>) are much higher than the normal matter density. Relativistic Heavy Ion Collider (RHIC) at Brookhaven National Laboratory (BNL) and the Large Hadron Collider (LHC) at the European Organization for Nuclear Research (CERN) are designed to explore the properties of QGP state. The produced high temperature QGP phase at very low baryon densities mimics the early universe. Fixed target experiments are underway in FAIR (Facility for Antiproton and Ion Research) at GSI, Germany and NICA (Nuclotron-based Ion Collider Facility) at Joint Institute for Nuclear Research (JINR), Dubna to investigate the QCD phase diagram at high baryon density and low temperature. After the nuclear impact the system is in non-equilibrium and gradually expands and cools down. The local equilibrated QGP is formed and the dynamics of the system can be described by the hydro-

dynamics. The phase transition to the hadronic phase occurs and finally after the freeze-out the particles come out to the detector.

Main objective of this thesis is to study and explore the characteristics of various anisotropic systems created in several stages of heavy ion collisions. Broadly, we have studied two scenarios: One is the momentum space anisotropy created due to the rapid longitudinal expansion after the nuclear impact as the system expands along the collisional direction making the system much cooler in the longitudinal direction than the transverse direction. The other one is the anisotropy due to the background magnetic field. The former is studied by modeling of the non-equilibrium distribution function from the equilibrium case by suitable squeezing or stretching. The non-equilibrium plasma properties is described by studying the collective modes of the quasipartons in the framework of hard thermal loop perturbation theory. Due to the presence of non-equilibrium momentum distributions in QGP medium, existence of kinetic instabilities is expected. In this thesis covariant structure of gluon propagator has been formulated in presence of two anisotropy directions. The general structure is obtained in terms of six basis tensors. The collective modes can be calculated from the pole of the effective propagator. The collective modes and instability are discussed for ellipsoidal momentum anisotropy case.

The covariant structure of gluon propagator mentioned earlier can be used not only for the anisotropy arising from modeling of the non-equilibrium distribution function but also for the presence of the external magnetic field creating anisotropy in the medium. In recent time, more research interests are growing in non-central heavy ion collisions where the magnetic field is produced in the direction perpendicular to the reaction plane and the system becomes anisotropic. To study the magnetized QGP and hadronic matter is another direction of study which is explored in this thesis. Along with the temperature ( $T$ ), the presence of the magnetic field ( $B$ ) introduces extra scale in the system. Theoretically,



one can work in different regimes of magnetic field strength. Initially after the collision, very strong magnetic field is created. In the calculation one can use lowest Landau level (LLL) approximation as the magnetic field pushes the higher Landau levels to infinity compared to the LLL. The magnetic field decays rapidly with time depending upon the conductivity of the medium and one can work using weak field expansion. In weak field limit, we have calculated chiral susceptibility and photon damping rate in hot magnetized QCD/QED medium. Chiral susceptibility estimates the response of the chiral condensate with the variation of current quark mass and this quantity is important in study of chiral phase transition. The damping rate of the hard photon is associated with the mean free path of photon and hard photon production rate in QGP. So the study of those quantities is important in presence of magnetic field. In these studies Schwinger propagator and effective hard thermal loop (HTL) fermion propagator in weak field limit have been used. Here we worked in the scale hierarchy  $\sqrt{|q_f B|} < gT < T$ , where  $q_f$  is the charge of the quark with flavor  $f$ . In strong magnetic field, we have studied shear viscosity of hadronic matter using linear sigma model (LSM). The viscous coefficient is calculated in relaxation time approximation (RTA) where the point-like interaction rates of hadrons are evaluated through the S-matrix approach in the LLL approximation to obtain the temperature and magnetic field dependent relaxation time. In this case we use scale hierarchy  $\sqrt{|q_f B|} > T$ . We didn't confine ourselves only in the limiting cases i.e. strong and weak field limits, we have calculated heavy quark antiquark potential in the regime of arbitrary magnetic field strength i.e. considering all the Landau levels. Heavy quarkonia i.e. bound state of quark antiquark pair is an important signature of QGP and we have calculated the imaginary part of the Heavy Quark potential and the dissociation of heavy quarkonia in presence of arbitrary magnetic field. Here we have used the general structure of the gauge-boson propagator in a hot magnetized medium.

---

---

# ABBREVIATIONS

---

<b>BNL</b>	Brookhaven National Laboratory
<b>EoS</b>	Equation of State
<b>HIC</b>	Heavy ion collisions
<b>HQ</b>	Heavy Quark
<b>HTL</b>	Hard Thermal Loop
<b>LHC</b>	Large Hadron Collider
<b>LLL</b>	Lowest Landau Level
<b>NLO</b>	Next-to Leading Order
<b>QCD</b>	Quantum Chromodynamics
<b>QED</b>	Quantum Electrodynamics
<b>QGP</b>	Quark Gluon Plasma
<b>RHIC</b>	Relativistic Heavy ion collider

---



---

# LIST OF FIGURES

---

1.1	QCD running coupling as a function of energy scale. . . . .	3
1.2	Energy density and pressure scaled with $T^4$ as a function of temperature . . . . .	6
1.3	Schematic picture of space-time evolution of HIC. . . . .	8
1.4	Schematic sketch of QCD phase diagram. . . . .	10
1.5	Non-central heavy ion collision. . . . .	12
2.1	Wick rotation to imaginary time in complex time plane. . . . .	29
2.2	Contour for bosonic frequency sum. . . . .	32
2.3	The contour for the real time formalism. . . . .	41
4.1	The real and imaginary parts of the form factors are plotted in (a)–(f) as a function of $\omega/p$ for three different set of anisotropy tuple $\xi = (\xi_a, \xi_b) = (0, 0), (0, 10)$ and $(5, 10)$ . In each case, the imaginary parts are shown with comparatively thicker style. The spheroidal set is shown at fixed $\theta_p = \pi/4$ whereas for the ellipsoidal case, $(\theta_p, \phi_p) = (\pi/4, \pi/3)$ is considered. . . . .	56

4.2	Squared values of the mass scales corresponding to $\Omega_0$ and $\Omega_{\pm}$ are plotted in (a)–(c) as a function of $\theta_p$ for three different values of $\phi_p = \{\pi/2, \pi/4, \pi/6\}$ (shown in discrete style) considering $(\xi_a, \xi_b) = (5, 10)$ . The solid line represents the spheroidal case with $(\xi_a, \xi_b) = (0, 10)$ . . . . .	61
4.3	In the left panel, the squared value of the mass scale corresponding to $\Omega_-$ is plotted as a function of $\theta_p$ for three different values of $\phi_p = \{\pi/4, \pi/3, 5\pi/12\}$ (shown in discrete style) considering $(\xi_a, \xi_b) = (-0.5, -0.9)$ . The spheroidal case (shown in solid style) with $(\xi_a, \xi_b) = (0, -0.9)$ is also plotted for comparison. In the right panel, the growth rate for the $\Omega_-$ mode is plotted as a function of $p/m_D$ with $(\xi_a, \xi_b) = (-0.5, -0.9)$ and $(\theta_p, \phi_p) = (5\pi/12, 5\pi/12)$ . . . . .	62
5.1	Photon self-energy where the blob represents the effective electron propagator in magnetic field and double line represents bare electron propagator in magnetic field . . . . .	72
5.2	Choice of reference frame for computing the various components of photon self-energy. The magnetic field is along z-direction and $\theta_p$ is the angle between momentum of photon and the external magnetic field. . . . .	81
5.3	Plot of damping rate of photon with the propagation angle $\theta_p$ for $p = 3$ GeV, $T = 0.5$ GeV and $eB = m_{\pi}^2/4$ . . . . .	91
5.4	Plot of damping rate of photon with the energy for $T = 0.5$ GeV and $eB = m_{\pi}^2/4$ at propagation angles $\theta_p = \pi/10$ and $\pi/2$ . . . . .	91
5.5	Plot of damping rate of the hard photon with temperature at $p = 3$ GeV and $eB = m_{\pi}^2/4$ for two propagation angles $\pi/10$ and $\pi/2$ . . . . .	92
5.6	Plot of damping rate of the hard photon with the magnetic field strength at $T = 0.5$ GeV and $p = 3$ GeV for two propagation angles $\pi/10$ and $\pi/2$ . . . . .	93

5.7	Plot of damping rate of photon with $\Lambda$ for $\theta_p = \pi/4$ , $p = 3$ GeV, $T = 0.5$ GeV and $eB = m_\pi^2/4$ . . . . .	94
6.1	Variation of chiral susceptibility scaled with $T^2$ as a function of temperature for chemical potential 0, 100 and 200 MeV with zero magnetic field. . . . .	109
6.2	Variation of chiral susceptibility scaled with $T^2$ as a function of $T$ for magnetic field strength $ eB  = 0, m_\pi^2$ with $\mu = 0$ MeV (left) and $\mu = 100$ MeV (right). . . . .	110
6.3	Scaled chiral susceptibility is plotted as a function of magnetic field strength $ eB $ for temperature $T = 0.2$ GeV and $\mu = 0$ MeV and 100 MeV. . . . .	110
6.4	Variation of chiral susceptibility scaled with $T^2$ as a function of temperature for magnetic field strength $m_\pi^2$ for different values of renormalization scale. . . . .	111
7.1	One loop gluon self-energy. . . . .	120
7.2	Variation of $\text{Im } V$ with distance. We have shown two plots comparing with two recent results from Ref. [1] (left panel) and Ref. [2] (right panel) which requires certain fixed values of magnetic field ( $eB$ ) and temperature ( $T$ ), as depicted in the plot. We have considered both the cases, i.e. with vanishing $r_\perp$ and with vanishing $z$ . . . . .	127
7.3	Variation of $\text{Im } V$ with distance, i.e. with $z$ for vanishing $r_\perp$ (left panel) and with $r_\perp$ for vanishing $z$ (right panel), is shown considering different number of Landau levels where we show the difference between the LLL approximated result and the full result. . . . .	129
7.4	Variation of $\text{Im } V$ with distance comparing between full and Debye mass approximated expression. The variation is shown with $z$ for vanishing $r_\perp$ (dashed curve), with $r_\perp$ for vanishing $z$ (dotted curve), and with isotropic $r$ using Debye mass approximated expression (solid curve). . . . .	130

7.5	Variation of $\text{Im } V$ with $z$ for two different fixed values of $r_{\perp} - r_{\perp} = 0$ (upper-left panel) and $r_{\perp} = 0.5$ fm (upper-right panel) and with $r_{\perp}$ for two different fixed values of $z - z = 0$ (lower-left panel) and $z = 0.5$ fm (lower-right panel). For each of the plots we have chosen two different values of temperature and a fixed value of the external magnetic field. . . . .	131
7.6	Contour plot of $\text{Im } V$ showing the equal potential regions for different values of $r_{\perp}$ and $z$ . . . . .	132
7.7	Variation of $\text{Im } V$ with temperature shown for two different cases, i.e. for vanishing $r_{\perp}$ (left panel) and for vanishing $z$ (right panel). for each of the plots, we have chosen two different values of the external magnetic field which shows some interesting crossovers. . . . .	133
7.8	Variation of the decay width $\Gamma$ with respect to the external magnetic field for a fixed temperature shown for the case of Charm quark (left panel) and Bottom quark (right panel). Curves shown for the case of LLL approximated result, $m_D$ approximated result and full result. . . . .	135
7.9	Variation of the decay width $\Gamma$ with respect to the temperature for a fixed external magnetic field shown for the case of Charm quark (left panel) and Bottom quark (right panel). Curves shown for the case of LLL approximated result, $m_D$ approximated result and full result. . . . .	136
8.1	Energy density (left) and entropy density (right) as functions of temperature for three different vacuum sigma masses in presence(dashed line) and absence(solid line) of the magnetic field. . . . .	152

8.2	The ratio of shear viscosity to entropy density as a function of temperature for vacuum sigma masses $m_\sigma = 500$ MeV(left) and 700 MeV(right). In both the plots blue lines indicate the pure thermal case whereas the other lines represent the parallel components of shear viscosity coefficients to entropy ratio for $5m_\pi^2$ (red line), $10m_\pi^2$ (green line), $15m_\pi^2$ (black line). . . . .	160
8.3	Ratio of parallel $\eta_{\parallel}$ and perpendicular $\eta_{\perp}$ shear viscosity components to entropy as a function of temperature ( $T$ ) for vacuum sigma mass $m_\sigma = 500$ MeV (left) and $m_\sigma = 700$ MeV (right). Magnetic field strength is taken as $15m_\pi^2$ . . .	162
B.1	Self-energy diagram for a quark in presence of background magnetic field. The double line indicates the modified quark propagator in presence of weak magnetic field. . . . .	192

---

---

# LIST OF TABLES

---

1.1 Comparison of magnetic field strength of various sources. . . . . 14



---

## CHAPTER 1

---

# INTRODUCTION

---

“ An experiment is a question which science poses to nature, and a measurement is the recording of nature’s answer.”

— *Max Planck*

In nature Strong interaction is one of the four fundamental forces i.e. gravitational force, weak force, strong force and electromagnetic force. Strong force ‘glues’ the fundamental quarks into hadrons such as proton and neutron. In this chapter we would briefly discuss about quantum chromodynamics which describe the theory of strong interactions. Further, we review quark-gluon plasma and its experimental observations through heavy-ion collisions. After giving the outline of the thesis in the last section, we will gradually continue our journey throughout the rest of the thesis by investigating various properties of strongly interacting extreme matters.

## 1.1 Quantum Chromodynamics

The theory of strong interaction [3, 4] of quarks and gluons is governed by quantum chromodynamics (QCD). This is a theory of non-abelian gauge theory of SU(3) gauge group. QCD was established in analogy to the quantum electrodynamics (QED) which describes the action of electromagnetic force. In contrast to QED, where the theory is abelian of U(1) gauge group and there is only one type of electric charge, in QCD there are three kinds of charges of SU(3) gauge group called ‘colors’. Unlike QED, where the associated gauge boson ‘photon’ is not electrically charged, eight gauge bosons called ‘gluons’ in QCD carry color charges and interact with each other. Quarks also carry color charges in QCD. There are six flavors of quarks: up ( $u$ ), down ( $d$ ), strange ( $s$ ), top ( $t$ ), bottom ( $b$ ), charm ( $c$ ). Though, quarks are color charged, in nature color charge is not observed. They appear only through composite particles: (i) Baryons: They are built of three different color quarks producing color neutral particles and (ii) mesons: These are made of quarks and their anti-quarks. The anti-color of the anti-quark and the color of the quark produce color neutral mesons.

The behavior discussed above can be understood through the important properties namely asymptotic freedom [6, 7] and color confinement [3, 4] of the non-abelian gauge theory. The interaction strength between quarks and gluons decreases with the increasing energy due to the anti-screening of the color charges. This can be realized from the fact that the QCD coupling  $\alpha_s(Q)$  decreases with the energy or momentum transfer. In Fig. 1.1, the variation of QCD coupling with energy scale  $Q$  is shown graphically [5]. We can try to understand the behavior of QCD running coupling  $g = \sqrt{4\pi\alpha_s}$  which is given upto one

## 1.1. Quantum Chromodynamics

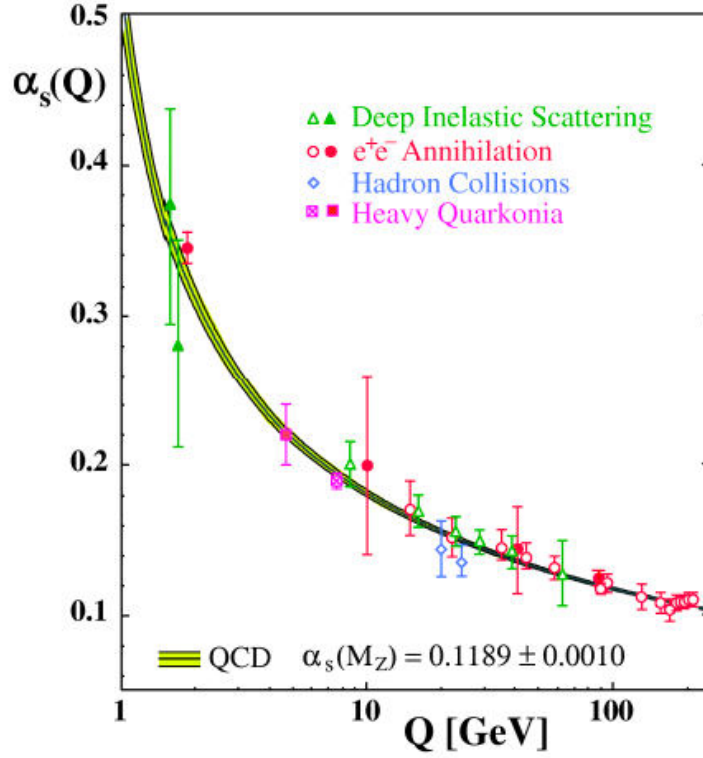


Figure 1.1: QCD running coupling as a function of energy scale. (Figure from Ref [5].)

loop order as [6, 7]

$$\alpha_s(Q^2) = \frac{g^2(Q^2)}{4\pi} = \frac{4\pi}{(11 - \frac{2}{3}N_f) \ln(\frac{Q^2}{\Lambda_{QCD}^2})}, \quad (1.1)$$

where  $N_f$  and  $Q^2$  represent the number of quark flavors and the four momentum transfer respectively.  $\Lambda_{QCD}$  is the typical QCD scale parameter. The running coupling decreases with increasing momentum transfer. In the high energy limit, the partons behave like free particles and this feature is called as asymptotic freedom. So, in the high energy domain, perturbative QCD can be a reliable theory. On the other hand, in the low energy, coupling becomes strong leading to the formation of colorless hadrons. This property is called

the color confinement. Non-perturbative physics is needed to understand the confinement nature. In QED, opposite nature to QCD i.e. screening of the electric charge can be found.

The QCD Lagrangian density describing the dynamics of quarks and gluons is given by

$$\mathcal{L} = \bar{\psi}_i \left( i\gamma^\mu (D_\mu)_{ij} - m\delta_{ij} \right) \psi_j - \frac{1}{4} F_{\mu\nu}^a F_a^{\mu\nu} + \mathcal{L}_{GF} + \mathcal{L}_{Ghost}, \quad (1.2)$$

where  $\psi_j(x)$  is the quark triplet field in the fundamental representation of SU(3) gauge group. So, here the indices  $i$  and  $j$  run from 1 to 3.  $\gamma^\mu$  are the Dirac matrices and  $m$  represents the quark mass.

The gauge covariant derivative is defined as

$$(D_\mu)_{ij} = \partial_\mu \delta_{ij} - ig(T_a)_{ij} A_\mu^a \quad (1.3)$$

with strong coupling strength  $g$ .  $A_\mu^a(x)$  are the gluon fields in the adjoint representation of SU(3) gauge group.  $T^a$  are the generators of the local SU(3) symmetry. The generators are given by  $T^a = \lambda^a/2$  where  $\lambda^a$  ( $a=1 \dots 8$ ) are Gell-Mann matrices. The gluon field strength tensor reads as

$$F_{\mu\nu}^a = \partial_\mu A_\nu^a - \partial_\nu A_\mu^a + gf^{abc} A_\mu^b A_\nu^c, \quad (1.4)$$

where indices  $a, b$  and  $c$  run from 1 to 8.  $f^{abc}$  denotes the structure constant of SU(3). In Eq. (1.2), the terms  $\mathcal{L}_{GF}$  and  $\mathcal{L}_{Ghost}$  take care of the gauge fixing and the Faddeev-Popov ghost terms respectively. The QCD Lagrangian possesses chiral symmetry in the limit of vanishing quark mass i.e.  $m = 0$ . But the ground state of QCD is not chirally symmetric and it is spontaneously broken by nonzero chiral condensate. At high temperature the chiral

## *1.2. Quark-gluon plasma*

symmetry is restored. At extremely high temperature quarks and gluons propagate freely in the deconfined phase called quark-gluon plasma (QGP) which will be introduced in the next section.

## **1.2 Quark-gluon plasma**

In the last section we learned about the asymptotic freedom where the coupling strength of the strong interaction decreases with decreasing length scale or increasing energy scale. If the energy of the system is increased, after some critical energy, the hadrons melt to the deconfined state of quarks and gluons forming quark gluon plasma (QGP) [8–11] state. The extreme state can be formed for high temperature and/or high density. If the nuclear matter density is increased gradually above certain critical baryon density, deconfined state of QCD matter is produced. Such kind of extreme state can be found in the core of the compact stars where the matter density is very high ( $\sim 10^{18} \text{ kg/m}^3$ ). Also, if the QCD vacuum is heated, after surpassing a certain critical temperature hadrons dissolve into deconfined state of quarks and gluons. This extreme state of matter is supposed to be present in the early universe after a few fraction of microseconds of the big bang and the temperature was of the order  $10^{12} \text{ K}$ . This strongly interacting matter is needed to study various properties of QCD matter e.g. the nature of QCD phase transitions. After big bang, the universe went through the several first or second order phase transition associated with the spontaneous symmetry breaking in non-abelian gauge theory. In the standard model of particle physics, there are two kind of symmetry breaking. At few hundred GeV temperature electroweak symmetry breaking take place and at temperature of a few MeV, hadrons to quark matter transition can occur. Except this confinement-deconfinement transition, chiral symmetry breaking related to the dynamical quark mass generation can occur at same

temperature scale. For massless quarks chiral symmetry is exact whereas, at high temperature, chiral symmetry restoration is approximate symmetry. To get more insights into the extreme matter, various heavy-ion experiments are operated to recreate the matter after few microseconds of the big bang in the early universe.

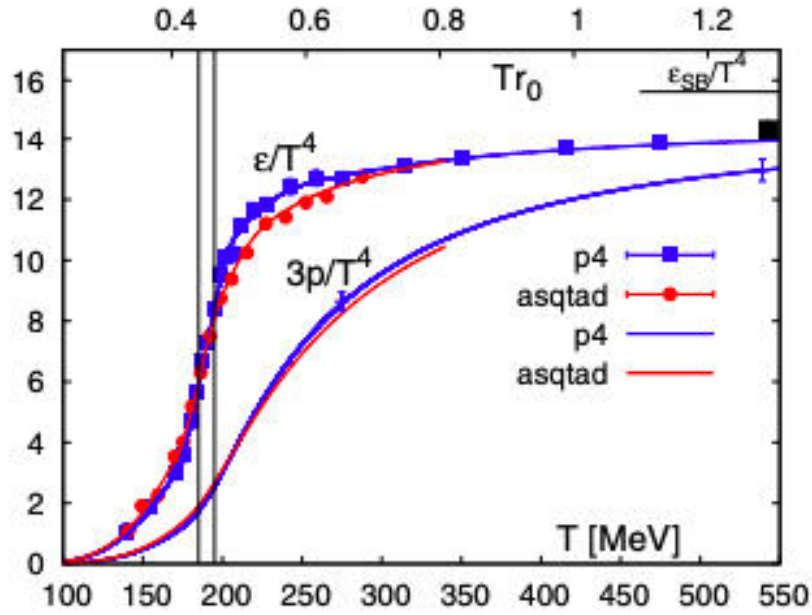


Figure 1.2: Energy density and pressure scaled with  $T^4$  as a function of temperature [12].

Lattice results for the energy density ( $\epsilon$ ) and pressure ( $P$ ) at vanishing chemical potential are shown [12] in Fig. 1.2. These are calculated using the staggered fermion actions *asqtad* and *p4*. The energy density scaled with  $T^4$  rises rapidly in the temperature range (170 – 200) MeV. This indicates the increase in entropy or number of the degrees of freedom.  $3P/T^4$  also rises rapidly in that temperature region but the rise is not as sharp as  $\epsilon/T^4$ . At the high temperature limit,  $\epsilon$  is significantly less than the Stefan-Boltzmann limit ( $\epsilon_{SB}$ ) revealing that it is far from the ideal gaseous state. The lattice results show that the transition at vanishing chemical potential is a crossover. More detailed discussions and

### 1.3. Heavy ion collisions: Overview

results can be found in Refs. [13–15]. In next section, we would discuss more about the extreme matter produced in the heavy-ion colliders.

## 1.3 Heavy ion collisions: Overview

To probe various features of the novel state of QGP, several experimental setups have been built e.g. Large Hadron Collider (LHC) at the European Organization for Nuclear Research (CERN) [16, 17], Relativistic Heavy Ion Collider (RHIC) at Brookhaven National Laboratory (BNL) [18–20]. In heavy ion collisions, two high energetic Lorentz contracted nuclei are collided. If the energy of the incoming ions are low i.e.  $\mathcal{O}(10 \text{ GeV})$  or below per nucleon, the nuclei effectively stop losing the kinetic energy and high baryon density is created at the center. This high baryon density matter is present at the core of the neutron star as mentioned earlier also. Future experiments are designed in Facility for Antiproton and Ion Research (FAIR) at Gesellschaft für Schwerionenforschung (GSI) [21, 22] and Nuclotron-based Ion Collider fAcility (NICA) at Joint Institute for Nuclear Research (JINR), Dubna [23, 24] to investigate the high density region of QCD phase diagram.

In the present days, highest reachable collisional energy in the ultra relativistic Heavy ion colliders are  $\sqrt{s} = 200 \text{ GeV}$  at RHIC and  $\sqrt{s} = 5.02 \text{ TeV}$  at LHC. In these cases Lorentz contracted nuclei pass through each other producing very high temperature at central area with almost zero baryon density. In Fig. 1.3, the space-time evolution of heavy ion collisions is presented through a schematic diagram. The descriptions of the stages of the collisions [25–27] are elaborated below.

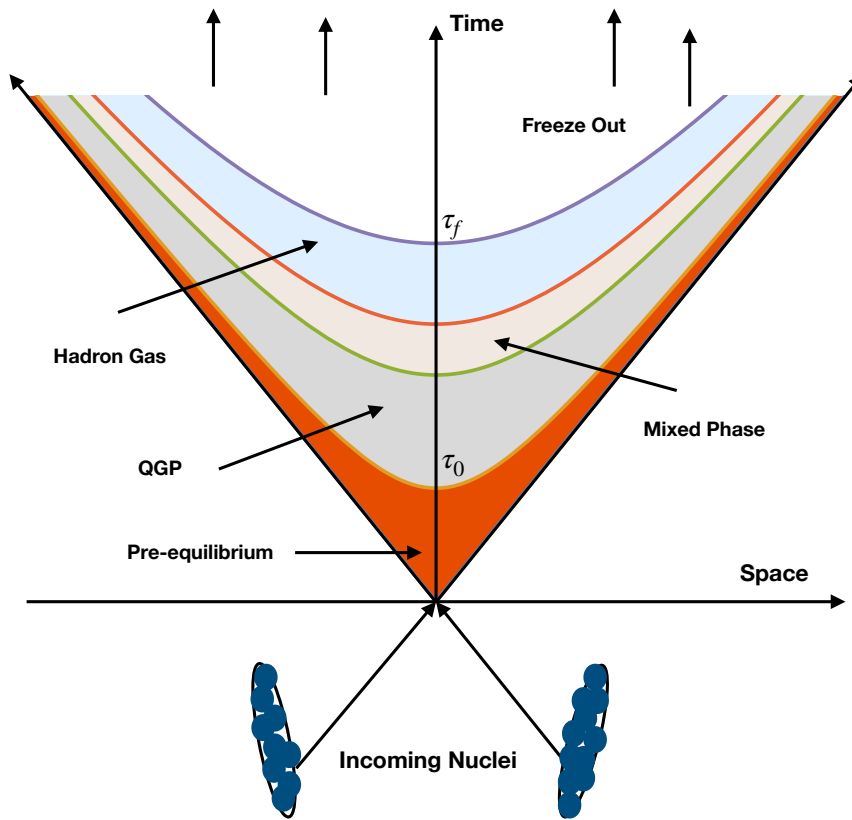


Figure 1.3: Schematic picture of space-time evolution of HIC.

- **Pre- uilibrium stage:**

Initially after the collisions, the created fireball is in non-equilibrium state. When the ultra relativistic heavy nuclei collide, huge entropy is produced. Theoretically, various models are introduced to study the highly non-equilibrium system. Color glass condensate (CGC) [28] is one example. After time  $\tau_0$ , the locally equilibrated QGP state is formed.

- **QGP stage:**

Due to the collisions of the incident partons, the system gradually cools down and equilibrates as it expands. The thermalization and equilibration processes are still arguable and



#### 1.4. Theoretical approaches to study QCD

unclear [29, 30]. The space-time evolution of quark-gluon plasma generated in relativistic heavy ion collisions are well explained by hydrodynamic simulations [31–33] which is applicable for the near-equilibrium systems. Recently anisotropic hydrodynamics (aHydro) [34, 35] has been developed which describe the highly momentum-space anisotropic i.e. far from equilibrium systems. In this framework momentum-space anisotropic one particle distribution function is considered. More discussions on momentum anisotropy would be presented in Chapter 4 of this thesis.

Various experimental results indicate the formation of such strongly interacting deconfined state of quarks and gluons. Subsequently, it goes through the phase transition to the hadronic phase.

##### • Freeze-out:

After transition to the hadronic phase, the system remains in equilibrium due to the inelastic collisions. Gradually freeze-out occurs after time  $\tau_f$  as the system expands and cools down. There are basically two type of freeze-out: One is chemical freeze-out, when the inelastic collisions are stopped and the number of hadron species do not change. When the mean free path of the particles becomes greater than the size of the system, the kinetic freeze-out occurs. From the kinetic freeze-out surface, the free streaming particles come to the detectors. The kinetic freeze-out temperature is generally lower than the chemical freeze-out temperature depending upon the hadronic species.

There are various theoretical methods to study QCD. In the next section, we discuss the theoretical tools used to study QCD and its phase structure, mainly QGP.

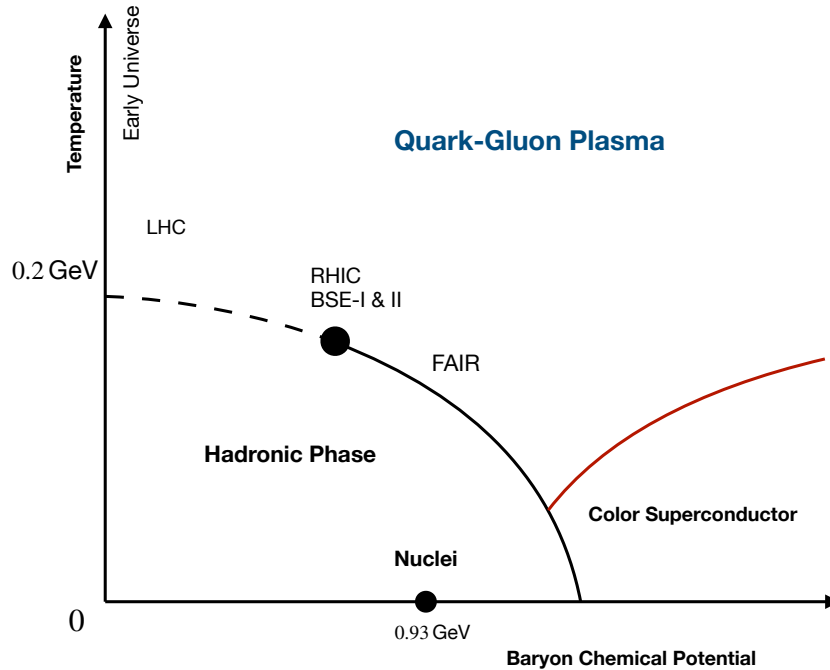


Figure 1.4: Schematic sketch of QCD phase diagram.

## 1.4 Theoretical approaches to study QCD

Several methods are developed to study the various aspects of QGP. Perturbative QCD are applicable for high energies when the QCD coupling is sufficiently small. So, the perturbative approaches are used for extremely high temperature. At finite temperature ordinary perturbation theory fails due to the infrared divergence. It was also shown that the gluon damping rate calculated using naive perturbation theory becomes gauge dependent [36–38]. The leading order contribution to the coupling can not be completed using ordinary perturbation theory as the higher order loops contribute to the leading order [39]. Resummation technique [40–43] was formulated to deal with the hot QCD. Later various thermodynamic quantities have been calculated using Hard thermal loop perturbation theory

#### 1.4. Theoretical approaches to study QCD

(HTLpt) [44–49].

At moderate or low temperature, perturbative calculation is not applicable. There is a successful numerical method called Lattice QCD (LQCD) [50–52] which is a first principle approach to study QCD in strong coupling regime. The theory is formulated on grids (lattices) of points in space and time. When the lattice size is taken infinitely large and lattice spacing is reduced to zero, the continuum QCD is reproduced. But the LQCD technique is not applicable for non zero baryonic chemical potential and this is the one of the limitations of this framework. This is well known sign problem [53].

Due to the shortcomings of LQCD and perturbative QCD, the effective theories have been modeled. Several effective QCD models are used to explore the non-perturbative regime. Effective models like Nambu-Jona-Lasinio (NJL) model [54–56], quark-meson model (QM) [57], Linear Sigma model (LSM) [58] and their Polyakov loop extended versions PNJL [59, 60] and Polyakov quark-meson (PQM) model [61], Hadron resonance gas (HRG) [62] model have acquired success to explain lattice data and the several parts of the QCD phase diagram shown in Fig. 1.4. LSM model is used in Chapter 8 to calculate shear viscosity coefficients of mesons.

In Fig. 1.4, the QCD phase diagram in  $T - \mu_B$  plane is represented.  $\mu_B$  is the baryon chemical potential. For low chemical potential, there is a crossover transition from hadronic phase to quark-gluon plasma phase at temperature around 150 MeV.  $\mu_B = 0$  case is well investigated by LQCD. For higher  $\mu_B$ , the transition is of first order and a critical point exists in between. The search for exact position of the critical point is an active field of research. At high chemical potential and low temperature, color superconducting phase is expected to exist.

In the next section, we are going to discuss about non-central heavy ion collisions and its consequences.

## 1.5 Magnetic field in non-central heavy ion collisions

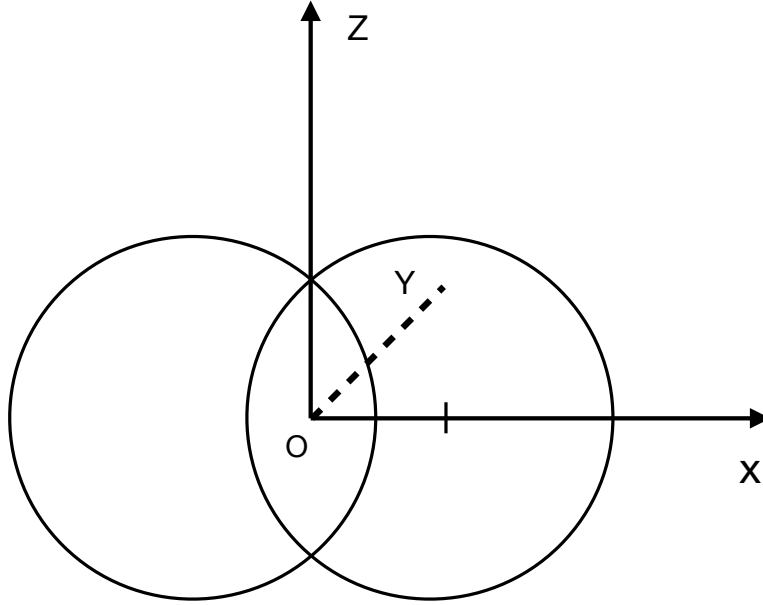


Figure 1.5: Non-central heavy ion collision.

The diagrammatic view of non-central HIC is shown in Fig. 1.5. In this figure,  $y$ -axis is the beam axis and  $z = 0$  plane is the reaction plane. The separation between the centers of two colliding nuclei is known as the impact parameter  $b$ . In recent times, more research interests are growing in non-central heavy ion collisions. Several studies indicate that non-central heavy ion collisions produce strong magnetic fields in the direction perpendicular to the reaction plane. The magnetic field strength simply can be estimated using the Biot-Savart law. If two nuclei of radius  $R$  with electric charge  $Ze$  collide with impact parameter  $b$ , then the magnetic field strength at center of mass frame reads as [63]

$$B \sim \gamma Ze \frac{b}{R^3}, \quad (1.5)$$

### 1.5. Magnetic field in non-central heavy ion collisions

where  $\gamma = \sqrt{s_{NN}}/2m_N$  is the Lorentz factor. At RHIC, using  $\sqrt{s_{NN}} = 200$  GeV,  $Z = 79$  for Au+Au collision and  $b \sim R_a \approx 7$  fm one gets  $B \sim 10^{18}$  Gauss. At LHC, using  $\sqrt{s_{NN}} = 5.02$  TeV,  $Z = 82$  for Pb+Pb one gets about 30 times larger value [64–66].

The magnitude of the produced magnetic field depends on several parameters such as impact parameter, collision energy, conductivity of the medium etc. The strong field produced in heavy ion collision (HIC) decays sharply with time. In Pb+Pb collision at  $\sqrt{s} = 2.76$  TeV, it is shown in Ref. [67] that for an insulating medium the magnetic field strength of  $\sim 100 m_\pi^2$  decays to a very low value within around 0.1 fm/c after nuclear impact [68]. However some studies [63, 69] have shown that the presence of finite electric conductivity of the medium can extend the life-time of the magnetic field. The presence of anisotropic field in the medium may affect the hot matter produced in the HIC. The various properties of QGP are needed to be investigated in the presence of magnetic fields. Different novel phenomena like chiral magnetic effect (CME) [70], thermodynamic properties [71–74], properties of quarkonia [1, 75], photon and dilepton production rate [76–80], transport coefficients [81, 82] and so on have been studied over the last few years. Using different effective models, the impacts of the external magnetic field have been investigated. It has been shown from various model studies [83–86] and earlier lattice QCD investigations [87] that the value of chiral condensate at finite temperature and magnetic field would be higher than the value of it at zero magnetic field. This property is called magnetic catalysis (MC). But later lattice studies [88–91] shows that the chiral condensate decreases with increasing magnetic field near the crossover temperature and this feature is called inverse magnetic catalysis (IMC). In recent times, several effective models [92–95] like NJL models explain this behavior by considering the magnetic field (eB) dependent coupling. The IMC effect can also be introduced by considering the non-local NJL model in presence of the magnetic field [96]. More comprehensive discussions can be found in

Refs. [97, 98].

Besides the non-central heavy ion collisions (HIC) magnetic fields also possess astrophysical consequences. The strong magnetic field can be found in the core of magnetars, neutron stars. As they are the sources of strongest magnetic fields in nature, the effect of the strong magnetic field in the dense phases of the strongly interacting matter is extremely important to study. Some sources and strengths of magnetic field from various sources are listed in table 1.1.

Magnetic field strength (Tesla)	Various sources
$10^{-12}$	Human brain
$10^{-5}$	Earth's magnetic field
$10^{-3}$	Refrigerator magnet
$10^0$	Loudspeaker magnet
$10^3$	magnetic field in lab
$10^6$	non-magnetar neutron star
$10^8 - 10^{11}$	magnetar
$10^{14}$	Heavy-ion collisions

Table 1.1: Comparison of magnetic field strength of various sources.

The presence of magnetic field in HIC introduces an extra scale in the system and the theoretical calculations become more challenging. In this situation one can work in different regimes of magnetic field strength. Initially, after the collisions, the magnetic field strength is very high and one works within the strong field limit. In presence of strong magnetic field, we may consider lowest Landau level (LLL) approximation [80, 99]. As mentioned earlier, the field strength decays rapidly with time and in this situation one can use weak field expansion [100]. Most of the current studies in the heavy-ion community

## 1.6. Signatures of QGP

focus on these two limiting cases. But in general one can compute any quantity in the regime of arbitrary magnetic field strength. In this thesis photon damping rate and chiral susceptibility in presence of weak magnetic field have been studied in Chapter 5 and 6 respectively. In Chapter 8 transport properties are discussed in presence of strong magnetic field. In Chapter 7 we obtain the imaginary part of heavy quark potential in arbitrary magnetic field strength.

## 1.6 Signatures of QGP

We learned from the previous sections that the produced QGP matter in HIC undergoes through the phase transition to hadronic matter. Due to the color confinement nature, only colorless hadrons and leptons can come out to the detectors. The hadrons are emanated predominately from the freeze-out surface whereas the leptons and photons are coming out from all the stages of the evolution (see Fig. 1.3). As the leptons and photons interact electromagnetically, they can be emitted without interacting much and can be used as direct probes. Now we are going to discuss some significant probes [101–103] involved in QGP identifications.

### 1.6.1 Electromagnetic probe

Real photons ( $\gamma$ ) and virtual photons ( $\gamma^*$ ) are considered as the electromagnetic probes of QGP. The virtual photons finally decay into lepton pairs (e.g.  $e^+e^-$ ,  $\mu^+\mu^-$ ). As they interact weakly with the medium, their mean free path become greater than size of the fireball  $\sim 10$  fm [104]. So they can carry the information from the early stages of the collisions. The hadrons interact strongly with the system and lose the the initial stage

information during the evolution of the system. These are used as the indirect probes. Extraction of the electromagnetic spectrum is complicated. Photons are produced from various mechanism such as hadronic decays, initial stage hard scattering before medium formation. These contribution to the spectrum should be removed to get the information from the thermal medium. More about the electromagnetic probes are discussed in Refs. [105–107].

## 1.6.2 Strangeness Enhancement

Strangeness enhancement is one of the most important signatures of QGP. The productions of strange particles are enhanced [108–110] in heavy ion collisions with respect to the  $pp$  collisions. Strange quark anti-quark pair can be produced from quark anti-quark or gluon fusion:

$$q\bar{q} \rightarrow s\bar{s}, \quad gg \rightarrow s\bar{s} \quad (q = u, d). \quad (1.6)$$

In this processes, the energy thresholds are  $2m_s = 190$  MeV where strange quark mass  $m_s$  is 95 MeV. In contrast, strange hadrons can be produced from nucleon nucleon reactions. But the energy threshold would be very high to produce strangeness because the mass of the strange hadrons are high enough. For example, energy threshold would be about 1 GeV to produce Kaon ( $m_{K^+} \approx 493$  MeV). Strangeness production is much easier if the plasma is formed. So this is a good signature suggesting the formation of QGP phase.

Strangeness enhancement can occur when baryon stopping is large [111, 112]. Due to the finite baryon density, light quark energy levels are occupied by many light quarks and the productions of those non-strange light quarks are suppressed resulting a high  $\bar{s}/\bar{q}$  ratio in QGP.



### 1.6.3 Quarkonia suppression

Bound state of quark and anti-quark pair ( $q\bar{q}$ ) is known as quarkonium.  $J/\psi$  is the bound state of charm quark and anti-quark ( $c\bar{c}$ ) whereas, the bound state of bottom quark and anti-quark ( $b\bar{b}$ ) is called as  $\Upsilon$ . Heavy quarkonia produced in very early stage of the nucleus nucleus collisions traverse the deconfined plasma phase. Due to the color screening nature of this medium, the binding of the  $q\bar{q}$  can be prohibited. If the screening radius becomes smaller than the binding radius, then the quarkonia can not be produced [113, 114]. If the QGP is produced in the nucleus nucleus collisions, quarkonia productions are suppressed in those collisions as compared to the proton proton or proton neutron collisions. Experimentally, quarkonium provides signal through the lepton pair decays [115]. Theoretically, quarkonium spectral functions are studied through various potential models [116, 117] and lattice QCD [118]. In this thesis, decay width of heavy quarkonium of magnetized QCD plasma is discussed in Section 7.

### 1.6.4 Jet quenching

In HIC experiments, high energetic scattered partons traverse the QGP medium losing their energy. Finally, they fragment into ‘jet’ particles and come to the detector. The partons lose their energy via radiative and collisional processes. Collisional energy loss occurs due to the scattering between medium partons and initial primary partons whereas, the radiative energy loss happen due to the gluon radiation. Due to the formation of medium, energy loss of jet is larger in nucleus nucleus collisions compared to the  $pp$  collisions. This phenomena is called “jet quenching” [119–123].

Experimentally, the jet energy loss is quantified through the measurement of the nuclear

modification factor  $R_{AA}$ , which characterizes the ratio of yield in nucleus-nucleus (A-A) to proton-proton (p-p) collisions scaled with  $\langle N_{coll} \rangle$ , the mean number of nucleon-nucleon collisions in a single A-A collisions. So it can be written as

$$R_{AA} = \frac{1}{\langle N_{coll} \rangle} \frac{dN_{AA}^2/dp_T d\eta}{dN_{pp}^2/dp_T d\eta}, \quad (1.7)$$

where  $dN_{XX}^2/dp_T d\eta$  is the differential yield of high- $P_T$  (transverse momentum) jets per event in X-X collisions. If A-A collision behaves like simple superposition of nucleon-nucleon, the nuclear modification factor  $R_{AA}$  would be unity. But, experimental results shows a suppression of jets indicating the formation of jets [124, 125].

## 1.6.5 Anisotropic flow

In non-central collisions (non zero impact factor), almond shape overlapped zone is formed by the Lorentz contracted nuclei. This initial spacial anisotropy of the deformed shape leads to the momentum anisotropy. Fourier decomposition of the invariant triple differential distributions is given by [126]

$$E \frac{d^3 N}{d^3 p} = \frac{d^2 N}{p_T dp_T dy} \frac{1}{2\pi} \left[ 1 + \sum_{n=1}^{\infty} 2v_n \cos n(\phi - \phi_R) \right], \quad (1.8)$$

where  $y$  is rapidity,  $p_T$  is the transverse momentum,  $\phi$  is the azimuthal angle,  $\phi_R$  is the reaction plane angle and  $E$  is the energy of the particle. The  $p_T$  and  $y$  dependent coefficients are given by

$$v_n(y, p_T) = \langle \cos[n(\phi - \phi_R)] \rangle, \quad (1.9)$$

### 1.7. Kinetic theory

where the angular brackets represent an average over the particles and sum over all events in the  $(p_T, y)$  bin under consideration. For central collision  $v_n = 0$  and only the radial flow exists. The coefficients  $v_1$  and  $v_2$  denote the direct flow and elliptic flow respectively. If the particles of the system interact, then the local thermal equilibrium would be attained and the system can be described by the thermodynamic quantities. The spatial anisotropy of the system creating the pressure gradient in transverse plane leads to anisotropic azimuthal distribution of particles. Then the nonzero  $v_n$  would exist. Flow coefficients indicate the level of thermalization of the QGP matter generated in the HIC. For more detailed analysis, see Refs. [127–129].

## 1.7 Kinetic theory

In this section we would briefly introduce the kinetic theory [130, 131] which can describe many particle system from Hamiltonian description of  $N \sim \mathcal{O}(10^{23})$  particles to the equations of fluid dynamics. The starting point is the Liouville's equation which describes the system by considering probability distribution over  $N$  particle phase space. But this is not easy to continue with the function of  $N$  variables. So one can focus on the one particle distribution function instead of the probability distribution function of  $N$  particles. In this way one can obtain a set of coupled equation explaining the dynamics of a system. This is known as Bogoliubov-Born-Green-Kirkwood-Yvon (BBGKY) hierarchy. Though it is not easy to deal with a set of coupled equations, depending upon the problems some approximations can be implemented by truncating the hierarchy to something manageable. One simple truncation leads to the Boltzmann equation which is based on the assumption that the time duration of collision is smaller than the time between two collisions. This kind of assumptions are applicable in dilute gas. The Boltzmann equation can be applicable in

some cases of relativistic thermal field theories such as dilute hadron gas.

An out of equilibrium isolated system evolves towards equilibrium state by increasing entropy. The system try to restore its equilibrium by transporting matter, momentum or energy. For example, viscosity is related to the momentum transfer whereas, thermal conductivity is related to the heat transfer. The microscopic mechanism of the momentum or energy transportation is involved with the interactions with the constituent particles of the system, so investigation of the transport phenomena can provide information about the nature of the interactions. So the transport properties can be good probe to understand the thermodynamic characteristic of a system. Transport coefficients are also used as the input of the hydrodynamic simulations [31, 132]. With these motivation we have studied the transport coefficients of hadronic matter in Chapter 8.

## 1.8 Hydrodynamics

The functional relationship between the state variables such as energy, pressure etc is called equations of state for the system. Following various conservation law, hydrodynamics provides those relations among the state variables or the macroscopic quantities. It gives the space time variation of the measurable macroscopic quantities. Although kinetic theory interprets the macroscopic quantities, it does not obtain their time variation within an evolving system. Whereas, hydrodynamics can provide time variation of those equations of macroscopic quantities for the system. The laws of ideal hydrodynamics were first constructed by Landau [133] for explaining the expansion of the strongly interacting matter formed in high energy hadronic collisions. Bjorken [134] found out a simple scaling solution providing a natural beginning point for more elaborate solutions in the ultra-relativistic regime. Because of the classical theory and local equilibrium assumption, the use of the

### 1.8. Hydrodynamics

Landau model was questionable for high energy physics for many years [135]. In those time, it was not truly believed that the highly excited system in nuclear collisions can be described in terms of a macroscopic theory [136]. and the Landau model was lying outside of ongoing physics [135]. Later, in Refs. [137, 138] the authors have shown that the utilization of hydrodynamics in explaining of data is a way to prove the existence of a new state of matter in laboratory.

To describe the ideal fluid dynamics, local thermal equilibrium condition is assumed. The system is characterized by energy density  $\epsilon$ , pressure  $P$ , charge density and fluid four velocity  $u^\mu$  at space-time point  $x^\mu$ . The four velocity is defined as

$$u^\mu = \frac{dx^\mu}{d\tau}, \quad (1.10)$$

where the proper time increment is given by

$$(d\tau)^2 = g_{\mu\nu} dx^\mu dx^\nu = (dt)^2 - (d\mathbf{x})^2 = (dt)^2(1 - \mathbf{v}^2), \quad (1.11)$$

with  $\mathbf{v} \equiv \frac{d\mathbf{x}}{dt}$ . So  $u^\mu$  can be written as

$$u^\mu(x) = \frac{dx^\mu}{dt} \frac{dt}{d\tau} = \gamma(1, \mathbf{v}(x)), \quad (1.12)$$

where  $\gamma = \frac{1}{\sqrt{1-\mathbf{v}^2(x)}}$  with normalization

$$u^\mu(x)u_\mu(x) = 1 \quad (1.13)$$

and  $\mathbf{v}(x)$  is the flow velocity. The fluid dynamics is governed by the conservation of

energy-momentum and the baryon number

$$\partial_\mu T^{\mu\nu} = 0, \quad (1.14)$$

$$\partial_\mu J_B^\mu = 0. \quad (1.15)$$

The energy-momentum tensor  $T^{\mu\nu}$  is given by

$$T^{\mu\nu} = (\epsilon + P)u^\mu u^\nu - g^{\mu\nu}P \quad (1.16)$$

and the baryon number current  $j_B^\mu$  can be written as  $j_B^\mu(x) = u^\mu(x)n_B(x)$ , where  $n_B$  is the baryon number density. From Eqs. (1.14) and (1.15), one can get five independent equations. One more equation can be obtained from the equation of state of the fluid relating the energy density  $\epsilon$  and pressure  $P$ . Space-time evolution of  $P(x)$ ,  $\epsilon(x)$ ,  $n_B(x)$  and the flow velocity components can be determined by solving the six equations mentioned above.

Contracting Eq. (1.14) with  $u_\nu$  and using  $u_\nu \partial_\mu u^\nu = 0$  from Eq. (1.13), one obtains

$$u^\mu \partial_\mu \epsilon + (\epsilon + P) \partial_\mu u^\mu = 0. \quad (1.17)$$

Using the thermodynamic relations  $\epsilon + P = Ts + \mu_B n$  and  $d\epsilon = Tds + \mu_B dn$  with the baryon number conservation, one can get the entropy conservation

$$\partial_\mu (su^\mu) = 0, \quad (1.18)$$

which is a natural consequence for considering ideal fluid. In case of ideal hydrodynamics limit, all the dissipative effects are neglected.

In ideal hydrodynamic limits, local thermodynamic equilibrium is considered where the

### 1.9. Plasma Instability

net flow of matter or energy is zero. The deviation from the equilibrium causes dissipation. In case of dissipative fluid, the energy-momentum tensor and baryon current get modified as

$$T^{\mu\nu} = (\epsilon + P)u^\mu u^\nu - P g^{\mu\nu} + \tau^{\mu\nu}, \quad (1.19)$$

$$j_B^\mu = n_B u^\mu + V_B^\mu, \quad (1.20)$$

where  $\tau^{\mu\nu}$  and  $V_B^\mu$  are dissipative quantities. The governing equations are obtained from the conservation laws of energy-momentum tensor and the baryon number.

## 1.9 Plasma Instability

As discussed in the last section, hydrodynamic model can explain the time evolution of the produced matter in the relativistic HIC experiments and it requires the locally equilibrated system. Collective flow and particle spectra studied within hydrodynamic models suggests that the equilibration time is less than 1 fm/c. For strongly coupled system this quick equilibration can be explained. But in case HIC, the produced matter behaves like weakly coupled plasma because of asymptotic freedom. So the question of fast equilibration arises for the weakly coupled plasma. The perturbation study suggests the time scale of 2–3 fm/c for thermalization. Recent studies show that the plasma instabilities can play important role to explain such fast equilibration [139–141].

After the nuclear impact, the system expands along the collisional direction [142]. Due to the rapid longitudinal expansion, the system becomes much cooler in the longitudinal direction than the transverse direction resulting the momentum space anisotropy,  $\langle p_L \rangle \ll \langle p_T \rangle$ . There are broadly two types of plasma instabilities [143] : (i) hydro-

dynamic instabilities and (ii) kinetic instabilities. Hydrodynamic instabilities are created by coordinate space inhomogeneities whereas the kinetic instabilities are associated with non-equilibrium momentum distribution of particles. In simple terms, it can be said that the collective modes possess positive imaginary part in their mode frequencies and it results in an exponential growth in the chromomagnetic and chromoelectric fields. The presence of such Chromo-Weibel instabilities can affect on the thermalization and isotropization of the medium. In Chapter 4 we have studied ellipsoidal momentum-space [144] anisotropic system and the occurrence of plasma instabilities.

We will end the introductory chapter by stating the scope of this thesis in the next section.

## 1.10 Outline of this thesis

In Chapter 2 we discuss some basics of finite temperature field theory which would be used in the rest of the thesis. Here we explain two methods i.e. imaginary time formalism and real time formalism in thermal field theory. We also show the Matsubara frequency sum rule used in imaginary time formalism.

In Chapter 3 the general structure of gauge-boson self-energy is formulated. The self-energy is constructed in presence of two anisotropy and thermal medium. Further the covariant structure of gauge-boson propagator has been obtained. In this thesis, this propagator is used to study ellipsoidal momentum anisotropy case and also the properties of the magnetized medium.

Gluon polarization in presence of ellipsoidal momentum-space anisotropy has been studied in Chapter 4. General structure of gluon propagator is used in this chapter. Gluon self-energy is calculated in real time formalism. Mass scales are introduced for each collec-



## 1.10. Outline of this thesis

tive modes. Also the unstable modes are studied in presence of the ellipsoidal momentum-space anisotropy.

In Chapter 5 weakly magnetized hot QED plasma comprising electrons and positrons is considered. We evaluate the damping rate of hard photon by calculating the imaginary part of the each transverse dispersive modes in a thermomagnetic QED medium. Considering the resummed fermion propagator in a weakly magnetized medium for the soft fermion and the Schwinger propagator for hard fermion, the soft contribution to the damping rate of hard photon is calculated. This formalism can easily be extended to QCD plasma.

In Chapter 6, we have computed the chiral susceptibility in QGP in the presence of a finite chemical potential and a weak magnetic field within hard thermal loop (HTL) approximation. We obtain a completely analytic expression for the chiral susceptibility in the weak magnetic field approximation. The effect of the thermomagnetic correction is discussed.

The Chapter 7 is devoted to study the imaginary part of the Heavy Quark (HQ) potential and subsequently the dissociation of heavy quarkonia, within the most general scenario of magnetized hot medium. We have investigated the rich anisotropic structure of the complex HQ potential which explicitly depends on the longitudinal and transverse distance. We have also compared our result with various approximated results available in the literature and explained the differences between them.

The shear viscous coefficient of hadronic matter in the presence of temperature and magnetic field using the linear sigma model has been calculated in Chapter 8. We estimate the shear viscosity over entropy density  $\eta/s$  in the relaxation time approximation. The point-like interaction rates of hadrons are evaluated through the S-matrix approach in the presence of a magnetic field to obtain relaxation time.

Finally we conclude in Chapter 9 with future directions of research.

## Notations and conventions:

In this thesis we follow the natural unit:  $\hbar = c = 1$ . In this convention  $[length] = [time] = [mass]^{-1} = [energy]^{-1}$ .

The metric tensor is given by  $g^{\mu\nu} = \text{diag}(1, -1, -1, -1)$ . Any four vector  $V^\mu$  is given as  $V^\mu = g^{\mu\nu}V_\nu = (v_0, \mathbf{v}) = (v_0, v_x, v_y, v_z)$ .  $\mathbf{v}$  is three vector with the magnitude  $|\mathbf{v}| = v = \sqrt{v_x^2 + v_y^2 + v_z^2}$ .

$V_\perp^\mu = (0, v_x, v_y, 0)$  and  $V_\parallel^\mu = (v_0, 0, 0, v_z)$  are the perpendicular and parallel components of the four vector  $V^\mu$  respectively.

The electromagnetic field tensor reads as

$$F_{\mu\nu} = \begin{pmatrix} 0 & E_x & E_y & E_z \\ -E_x & 0 & -B_z & B_y \\ -E_y & B_z & 0 & -B_x \\ -E_z & -B_y & B_x & 0 \end{pmatrix}.$$

The electric fields ( $E_i$ ) and magnetic fields ( $B_i$ ) are obtained as

$$\begin{aligned} E_i &= F_{0i} \\ B_i &= -\frac{1}{2}\epsilon_{ijk}F^{j,k}, \end{aligned}$$

where  $\epsilon_{ijk}$  is Levi-Civita tensor.

# BASICS OF FIELD THEORY AT FINITE TEMPERATURE

---

In this chapter we would discuss two formalisms i.e. imaginary time and real time formalism which are used in this thesis. We begin by reviewing the equilibrium statistical thermodynamics. A grand canonical ensemble in equilibrium at finite temperature  $T$  is described in terms of the partition function as

$$Z(\beta) = \text{Tr} \rho(\beta) = \text{Tr} e^{-\beta(H-\mu N)}, \quad (2.1)$$

where  $\beta$  is the inverse of temperature i.e.  $\beta = 1/T$  and  $\mu$  is the chemical potential of the particles in the system.  $H$  is the Hamiltonian of the system and  $N$  is the number operator.  $\rho(\beta)$  is the density matrix. In a canonical ensemble the system is allowed to exchange energy with the heat bath, whereas, in a grand canonical ensemble the system can exchange both energy and particles with the reservoir. The ensemble average of an observable  $\mathcal{O}$  is

defined as

$$\langle \mathcal{O} \rangle_\beta = \frac{1}{Z(\beta)} \text{Tr} \rho(\beta) \mathcal{O}. \quad (2.2)$$

Partition function is important function in thermodynamics and various thermodynamic quantities like pressure ( $P$ ), entropy density ( $S$ ), particle number density ( $n_i$ ) and energy density ( $\mathcal{E}$ ) can be calculated from the following relations:

$$P = \frac{\partial(T \ln Z)}{\partial V}, \quad (2.3)$$

$$S = \frac{1}{V} \frac{\partial(T \ln Z)}{\partial T}, \quad (2.4)$$

$$n_i = \frac{1}{V} \frac{\partial(T \ln Z)}{\partial \mu_i}, \quad (2.5)$$

$$\mathcal{E} = -P + TS + \mu_i N_i, \quad (2.6)$$

where  $V$  is the volume of the system. Usually the width of a system is larger than the inverse of the temperature, so that infinite volume limit is taken as a good approximation to describe the thermodynamics.

## 2.1 Imaginary time formalism

If a Schrodinger operator  $\mathcal{O}$  is given, we can define a operator in Heisenberg picture  $\mathcal{O}_H(t)$  as

$$\mathcal{O}_H(t) = e^{iHt} \mathcal{O} e^{-iHt}. \quad (2.7)$$

Thermal correlation function of two Heisenberg operators  $\mathcal{O}_H^1(t)$  and  $\mathcal{O}_H^2(t')$  can be

## 2.1. Imaginary time formalism

written as

$$\begin{aligned}
 \langle \mathcal{O}_H^1(t) \mathcal{O}_H^2(t') \rangle_\beta &= Z^{-1}(\beta) \text{Tr} [e^{-\beta H} \mathcal{O}_H^1(t) \mathcal{O}_H^2(t')] \\
 &= Z^{-1}(\beta) \text{Tr} [e^{-\beta H} \mathcal{O}_H^1(t) e^{\beta H} e^{-\beta H} \mathcal{O}_H^2(t')] \\
 &= Z^{-1}(\beta) \text{Tr} [\mathcal{O}_H^1(t + i\beta) e^{-\beta H} \mathcal{O}_H^2(t')] \\
 &= Z^{-1}(\beta) \text{Tr} [e^{-\beta H} \mathcal{O}_H^2(t') \mathcal{O}_H^1(t + i\beta)] \\
 &= \langle \mathcal{O}_H^2(t') \mathcal{O}_H^1(t + i\beta) \rangle_\beta.
 \end{aligned} \tag{2.8}$$

The cyclic properties of the trace operation is implemented here. The relation of equa-

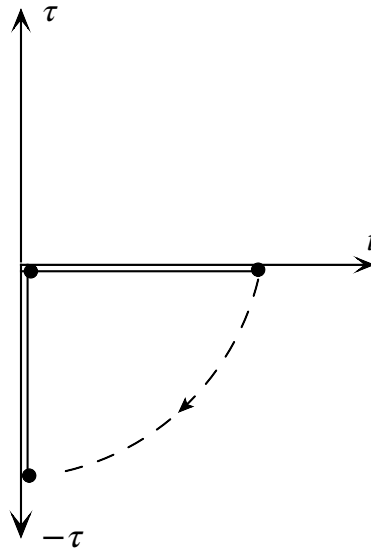


Figure 2.1: Wick rotation to imaginary time in complex time plane.

tion (2.8) is known as the Kubo-Martin-Schwinger (KMS) relation. This KMS relation leads to the periodicity for bosonic field and the anti-periodicity for fermionic fields in

various two point greens functions because of the commutation and anti-commutation relations, respectively. From Eq. (2.8) it can be said that the imaginary temperature is connected with the time as  $\beta = it = \tau$ . It can be realized by the Wick rotation in complex time plane from Fig. 2.1. It could be noticed that evolution operator ( $e^{-\beta H}$ ) has the form of time evolution operator ( $e^{-iHt}$ ) with  $\beta = it$ .

The Matsubara (imaginary) time formalism [145] presents a way of evaluating the partition function using a diagrammatic method. Now, for a field theory in  $(d+1)$  dimensional space-time at finite temperature, the partition function is written as,

$$Z(\beta) = \text{Tr} e^{-\beta H} = \int \mathcal{D}\phi \exp \left[ - \int_0^\beta d\tau \int d^d \mathbf{x} \mathcal{L}(\phi(\mathbf{x})) \right], \quad (2.9)$$

where  $\mathcal{L}$  is the Lagrangian density of the theory. For the bosonic case, the fields obey the periodic boundary condition

$$\phi(0, \mathbf{x}) = \phi(\beta, \mathbf{x}), \quad (2.10)$$

whereas the fermionic fields obey the anti-periodic boundary conditions

$$\phi(0, \mathbf{x}) = -\phi(\beta, \mathbf{x}). \quad (2.11)$$

The Feynman rules in finite temperature field theory are same as in zero temperature except that the imaginary time  $\tau$  becomes finite:  $0 \leq \tau \leq \beta$ . Due to the finite range of  $\tau$ , in the frequency space one has to perform a Fourier series decomposition involving the

## 2.1. Imaginary time formalism

discrete frequencies. So, the loop frequency integrals are replaced by loop frequency sums:

$$\int \frac{d^4 K}{(2\pi)^4} \rightarrow T \sum_{\omega_n} \int \frac{d^3 k}{(2\pi)^3} \quad (2.12)$$

with the sum over the Matsubara frequencies

$$k_0 = i\omega_n = 2ni\pi T \quad \text{for bosons,} \quad (2.13)$$

$$k_0 = i\omega_n = (2n + 1)i\pi T + \mu \quad \text{for fermions.} \quad (2.14)$$

### 2.1.1 frequency sums

**Bosonic case:**

Now we need to perform the the frequency sum. In general the bosonic frequency sum can be written as

$$\frac{1}{\beta} \sum_{n=-\infty}^{\infty} f(k_0 = i\omega_n = 2\pi inT). \quad (2.15)$$

Since hyperbolic cotangent has poles at  $n\pi i$  with residue unity, one can insert hyperbolic cotangent with suitable argument as

$$\frac{1}{\beta} \sum_{n=-\infty}^{\infty} f(k_0 = i\omega_n = 2\pi inT) \text{Res} \left[ \frac{\beta}{2} \coth \left( \frac{\beta k_0}{2} \right) \right]. \quad (2.16)$$

Here hyperbolic cotangent corresponds to poles at

$$k_0 = \frac{2\pi in}{\beta} = i\omega_n \quad (2.17)$$

with residues  $2/\beta$  and as a result  $\text{Res}\left[\frac{\beta}{2} \coth\left(\frac{\beta k_0}{2}\right)\right]$  leads to unity. From (2.16), one can write

$$\frac{1}{\beta} \sum_{n=-\infty}^{\infty} f(k_0) \text{Res}\left[\frac{\beta}{2} \coth\left(\frac{\beta k_0}{2}\right)\right] = \frac{1}{\beta} \sum_{n=-\infty}^{\infty} \frac{\beta}{2} \text{Res}\left[f(k_0) \coth\left(\frac{\beta k_0}{2}\right)\right]. \quad (2.18)$$

Using the residue theorem the sum over residues can be expressed as an integral over contour  $C$  in  $\mathbb{C}_{k_0}$  as

$$\frac{1}{\beta} \sum_{n=-\infty}^{\infty} \frac{\beta}{2} \text{Res}\left[f(k_0) \coth\left(\frac{\beta k_0}{2}\right)\right] = \frac{1}{2\pi i} \oint_C dk_0 \frac{1}{2} f(k_0) \coth\left(\frac{\beta k_0}{2}\right), \quad (2.19)$$

where the contour is shown in Fig. 2.2a. Some important points are noted below:

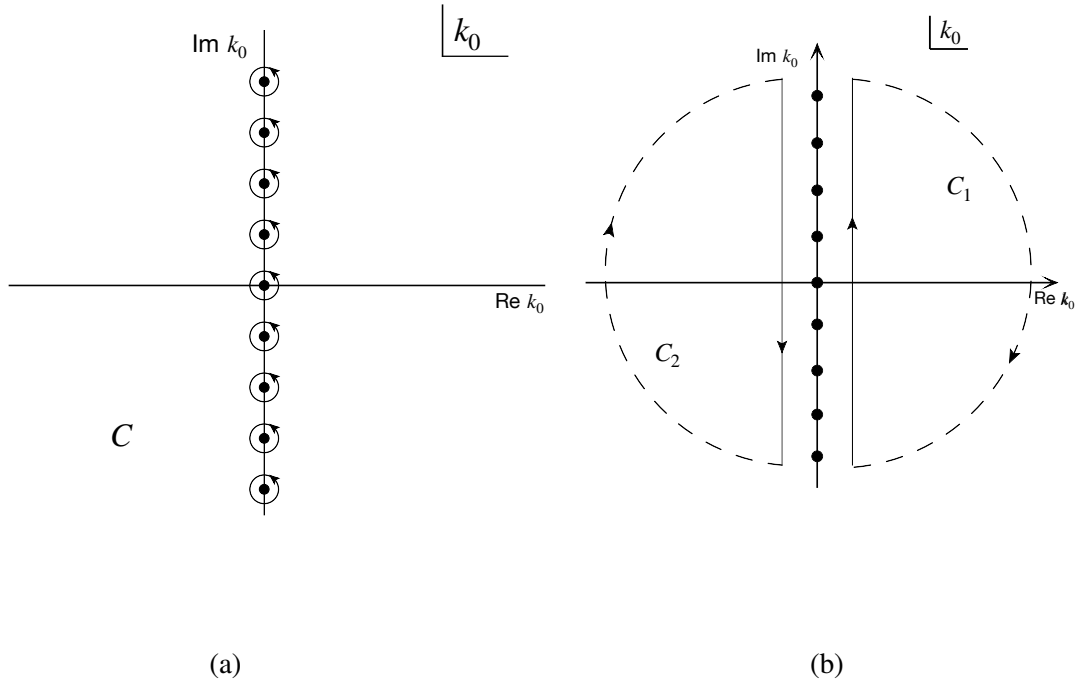


Figure 2.2: Contour for bosonic frequency sum.



## 2.1. Imaginary time formalism

- $\coth(\beta k_0/2)$  is bounded and analytic everywhere except the poles  $k_0 = i\omega_n = 2\pi iT$ .
- The function  $f(k_0 = i\omega_n)$  may have simple poles but no essential singularities or branch cuts.
- The function  $f(k_0)$  should not have singularities along the imaginary  $k_0$  axis.

Now the contour can be deformed as in Fig. 2.2b dividing the contour  $C$  in two half circles  $C_1$  and  $C_2$  in complex plane  $k_0$ .

So, the sum integral for the bosonic case can be written as

$$T \sum_{n=-\infty}^{\infty} f(k_0 = i\omega_n) = \frac{1}{2\pi i} \oint_{C_1 \cup C_2} dk_0 f(k_0 = i\omega_n) \left[ \frac{1}{2} + \frac{1}{\exp(\beta k_0) - 1} \right], \quad (2.20)$$

where we used the relation

$$\coth\left(\frac{\beta k_0}{2}\right) = 1 + \frac{2}{\exp(\beta k_0) - 1}. \quad (2.21)$$

It is noted from eq. (2.20), that the vacuum part ( $T = 0$ ) and medium part ( $T \neq 0$ ) are separated.

Finally, Eq. (2.20) can be decomposed as

$$\begin{aligned} T \sum_{n=-\infty}^{\infty} f(k_0 = i\omega_n) &= \frac{1}{2\pi i} \int_{-i\infty+\epsilon}^{i\infty+\epsilon} dk_0 f(k_0) \left[ \frac{1}{2} + \frac{1}{\exp(\beta k_0) - 1} \right] \\ &\quad - \frac{1}{2\pi i} \int_{i\infty-\epsilon}^{-i\infty-\epsilon} dk_0 f(k_0) \left[ \frac{1}{2} + \frac{1}{\exp(\beta k_0) - 1} \right]. \end{aligned} \quad (2.22)$$

Changing variable  $k_0 \rightarrow -k_0$  in the second integral and using the relation  $n_B(-k_0) =$

$-1 - n_B(k_0)$ , one can write

$$\begin{aligned}
 T \sum_{n=-\infty}^{\infty} f(k_0 = i\omega_n) &= \frac{1}{2\pi i} \int_{-i\infty}^{i\infty} dk_0 \frac{1}{2} [f(k_0) + f(-k_0)] \\
 &+ \frac{1}{2\pi i} \int_{-i\infty+\epsilon}^{i\infty+\epsilon} dk_0 [f(k_0) + f(-k_0)] n_B(k_0), \quad (2.23)
 \end{aligned}$$

where  $n_B(k_0) = \frac{1}{\exp(\beta k_0) - 1}$  is the Bose-Einstein distribution function including the medium effects. We can see that the sum is now converted into a convenient complex integral form.

### Fermionic case:

In the similar manner, one can obtain the fermionic frequency sum. The general form of the fermionic frequency sum reads as

$$\frac{1}{\beta} \sum_{n=-\infty}^{\infty} f(k_0 = i\omega_n = (2n + 1)\pi iT + \mu). \quad (2.24)$$

As the function  $\frac{\beta}{2} \tanh \frac{\beta(p_0 - \mu)}{2}$  has poles at  $p_0 = (2n + 1)\pi iT + \mu$  with residue unity, one can put hyperbolic tangent with suitable argument as

$$\frac{1}{\beta} \sum_{n=-\infty}^{\infty} f(k_0 = i\omega_n = (2n + 1)\pi iT + \mu) \text{Res} \left[ \frac{\beta}{2} \tanh \left( \frac{\beta(k_0 - \mu)}{2} \right) \right]. \quad (2.25)$$

As it is shown for the bosonic case, here we can write the frequency sum as

$$\frac{1}{\beta} \sum_{n=-\infty}^{\infty} f(k_0 = i\omega_n = (2n + 1)\pi iT + \mu)$$

## 2.1. Imaginary time formalism

$$\begin{aligned}
&= \frac{1}{2\pi i} \oint_C dk_0 \frac{1}{2} f(k_0) \tanh\left(\beta \frac{k_0 - \mu}{2}\right) \\
&= \frac{1}{2\pi i} \int_{-i\infty+\mu+\epsilon}^{i\infty+\mu+\epsilon} dk_0 f(k_0) \left[ \frac{1}{2} + \frac{1}{\exp(\beta(k_0 - \mu)) + 1} \right] \\
&- \frac{1}{2\pi i} \int_{-i\infty+\mu-\epsilon}^{i\infty+\mu-\epsilon} dk_0 f(k_0) \left[ \frac{1}{2} + \frac{1}{\exp(\beta(k_0 - \mu)) + 1} \right]. \tag{2.26}
\end{aligned}$$

After performing the fermionic/bosonic sums, one has to perform the loop momentum integration to calculate several thermodynamic quantities which will be discussed in some next chapters.

### 2.1.2 Saclay Method

Here, a convenient approach called Saclay-method is discussed to evaluate the frequency sums containing two or more propagators in Feynman loop diagrams. The bosonic propagator  $\Delta_B(K) = 1/(K^2 - m^2) = 1/(k_0^2 - \mathbf{k}^2 - m^2)$  in momentum space is written as

$$\Delta_B(K) = - \int_0^\beta d\tau e^{k_0\tau} \Delta_B(\tau, E_k), \tag{2.27}$$

where

$$\begin{aligned}
\Delta_B(\tau, E_k) &= -T \sum_{k_0=2n\pi iT} e^{-k_0\tau} \Delta_B(K) \\
&= \frac{1}{2E_k} \left[ \{1 + n_B(E_k)\} e^{-E_k\tau} + n_B(E_k) e^{E_k\tau} \right] \\
&= \sum_{s=\pm 1} \frac{s}{2E_k} \{1 + n_B(sE_k)\} e^{-sE_k\tau}. \tag{2.28}
\end{aligned}$$

The above equation can be derived from Eq. (2.23) using the contour integration.  $E_k = \sqrt{k^2 + m^2}$  is the particle energy and

$$n_B(E_k) = \frac{1}{e^{\beta E_k} - 1} \quad (2.29)$$

denotes the Bose-Einstein distribution.

The fermion propagator is represented as

$$S(K) = (\not{K} + m)\Delta_F(K). \quad (2.30)$$

The quantity  $\Delta_F(K)$  can be written in mixed representation as

$$\Delta_F(K) = - \int_0^\beta d\tau e^{k_0\tau} \Delta_F(\tau, E_k), \quad (2.31)$$

where

$$\begin{aligned} \Delta_F(\tau, E_k) &= -T \sum_{k_0=(2n+1)\pi iT} e^{-k_0\tau} \Delta_F(K) \\ &= \sum_{s=\pm 1} \frac{s}{2E_k} \{1 - n_F(sE_k)\} e^{-sE_k\tau}. \end{aligned} \quad (2.32)$$

$n_F(E_k) = \frac{1}{e^{\beta E_k} + 1}$  is the Fermi-Dirac distribution.

### Evolution of frequency sums:

We discuss the fermion-antifermion case. This kind of situation appears in gauge-boson self-energy calculation where the external line is a bosonic line.

## 2.1. Imaginary time formalism

### 1. Evolution of $T \sum_{k_0} \Delta_F(K) \Delta_F(Q)$ :

$$\begin{aligned}
& T \sum_{k_0=(2n+1)i\pi T} \Delta_F(K) \Delta_F(Q = P - K) \\
&= T \sum_{k_0} \int_0^\beta d\tau \int_0^\beta d\tau' e^{k_0\tau} \Delta_F(\tau, E_k) e^{q_0\tau'} \Delta_F(\tau', E_q) \\
&= \int d\tau \int d\tau' e^{p_0\tau'} T \sum_{k_0} e^{k_0(\tau-\tau')} \Delta_F(\tau, E_k) \Delta_F(\tau', E_q) \\
&= \int d\tau \int d\tau' e^{p_0\tau'} \delta(\tau - \tau') \Delta_F(\tau, E_k) \Delta_F(\tau', E_q) \\
&= \int d\tau e^{p_0\tau} \Delta_F(\tau, E_k) \Delta_F(\tau, E_q) \\
&= \sum_{s_1, s_2} \frac{s_1 s_2}{4E_k E_q} \int d\tau e^{p_0\tau} [1 - n_F(s_1 E_k)] [1 - n_F(s_2 E_q)] e^{-s_1 E_k - s_2 E_q \tau} \\
&= - \sum_{s_1, s_2} \frac{s_1 s_2}{4E_k E_q} \frac{1 - n_F(s_1 E_k) - n_F(s_2 E_q)}{p_0 - s_1 E_k - s_2 E_q}. \tag{2.33}
\end{aligned}$$

### 2. Evolution of $T \sum_{k_0} k_0 \Delta_F(K) \Delta_F(Q)$ :

$$\begin{aligned}
& T \sum_{k_0=(2n+1)i\pi T} k_0 \Delta_F(K) \Delta_F(Q = P - K) \\
&= T \sum_{k_0} \int_0^\beta d\tau \int_0^\beta d\tau' \frac{\partial}{\partial \tau} (e^{k_0\tau}) \Delta_F(\tau, E_k) e^{q_0\tau'} \Delta_F(\tau', E_q) \\
&= T \sum_{k_0} \int \frac{\partial}{\partial \tau} (e^{k_0\tau}) \Delta_F(\tau, E_k) d\tau \int d\tau' e^{q_0\tau'} \Delta_F(\tau', E_q). \tag{2.34}
\end{aligned}$$

We Use integration by parts to simplify the last line,

$$\begin{aligned}
 \int_0^\beta \frac{\partial}{\partial \tau} (e^{k_0 \tau}) \Delta_F(\tau, E_k) d\tau &= \Delta_F(\tau, E_k) e^{k_0 \tau} \Big|_0^\beta - \int_0^\beta e^{k_0 \tau} \frac{\partial}{\partial \tau} \Delta_F(\tau, E_k) d\tau \\
 &= -[\Delta_F(\beta, E_k) + \Delta_F(0, E_k)] - \int_0^\beta e^{k_0 \tau} \frac{\partial}{\partial \tau} \Delta_F(\tau, E_k) d\tau \\
 &= - \int_0^\beta e^{k_0 \tau} \frac{\partial}{\partial \tau} \Delta_F(\tau, E_k) d\tau. \tag{2.35}
 \end{aligned}$$

We have used  $e^{k_0 \beta} = -1$ . By using Eq. (2.32), It is also easy to show that the terms in the third bracket of the second line of Eq. (2.35) give zero. Putting Eq. (2.35) in Eq. (2.34) we get,

$$\begin{aligned}
 & T \sum_{k_0=(2n+1)i\pi T} k_0 \Delta_F(K) \Delta_F(Q) \\
 = & T \sum_{k_0} \int_0^\beta d\tau \int_0^\beta d\tau' e^{k_0 \tau} \frac{\partial}{\partial \tau} \Delta_F(\tau, E_k) e^{q_0 \tau'} \Delta_F(\tau', E_q) \\
 = & \int d\tau \int d\tau' e^{p_0 \tau'} T \sum_{k_0} e^{k_0(\tau-\tau')} \frac{\partial}{\partial \tau} \Delta_F(\tau, E_k) \Delta_F(\tau', E_q) \\
 = & \int d\tau \int d\tau' e^{p_0 \tau'} \delta(\tau - \tau') \frac{\partial}{\partial \tau} \Delta_F(\tau, E_k) \Delta_F(\tau', E_q) \\
 = & \int d\tau e^{p_0 \tau} \frac{\partial}{\partial \tau} \Delta_F(\tau, E_k) \Delta_F(\tau, E_q) \\
 = & - \sum_{s_1, s_2} \frac{s_2}{4E_q} \int d\tau e^{p_0 \tau} [1 - n_F(s_1 E_k)] [1 - n_F(s_2 E_q)] e^{-s_1 E_k - s_2 E_q} \tau \\
 = & \sum_{s_1, s_2} \frac{s_2}{4E_q} \frac{1 - n_F(s_1 E_k) - n_F(s_2 E_q)}{p_0 - s_1 E_k - s_2 E_q}. \tag{2.36}
 \end{aligned}$$

We have used here  $e^{p_0 \beta} = 1$  as the external line is a bosonic line i.e.  $p_0 = 2\pi i n T$ .

## 2.2 Real time formalism

Imaginary time formalism is applied to study the static and equilibrium properties of a system. The time dependence appears non-trivially through the analytical continuation. This formalism cannot describe the out of equilibrium systems. On the other hand, real time formalism is appropriate framework to handle the out of equilibrium systems and also to study the dynamical situations such as phase transition or evolution of the universe.

The real time formalism was originally proposed by Schwinger and Keldysh [146, 147]. Here we briefly discuss the real time method [148–150]. For better understanding we start with quantum mechanics. At finite temperature  $\beta^{-1} = T$ , the one important quantity is the partition function

$$\text{Tr} e^{-\beta H} = \int_{-\infty}^{\infty} dq \langle q, t | e^{-\beta H} | q, t \rangle. \quad (2.37)$$

This is the analogous to the transition amplitude for a system from  $q$  at time  $t$  to  $q'$  at time  $t'$  in vacuum theory

$$\langle q', t' | q, t \rangle = \langle q', t' | e^{-iH(t'-t)} | q, t \rangle, \quad (2.38)$$

where  $H$  is the Hamiltonian of the system. The operator  $e^{-iH(t'-t)}$  corresponds that the system evolves from time  $t$  to  $t'$ . Similarly, drawing the analogy with the vacuum case, one can think that the operator  $e^{-\beta H} = e^{-iH(\tau-i\beta-\tau)}$  evolves the system from time  $\tau$  to  $\tau - i\beta$  in the complex time path  $C$ .

## Chapter 2. Basics of field theory at finite temperature

Thermal scalar field propagator is defined as

$$\begin{aligned}
 D(x, x') &= i\langle T\phi(x)\phi(x') \rangle \\
 &= \theta(\tau - \tau')i\langle \phi(x)\phi(x') \rangle + \theta(\tau' - \tau)i\langle \phi(x')\phi(x) \rangle, \\
 &= \theta(\tau - \tau')D_+(x, x') + \theta(\tau' - \tau)D_-(x, x').
 \end{aligned} \tag{2.39}$$

$\tau$  and  $\tau'$  are the points on the contour.  $\theta(\tau - \tau')$  is the contour-ordered theta function.  $D_+(\mathbf{x}, \mathbf{x}'; \tau, \tau')$  is defined in domain  $-\beta \leq \text{Im}(\tau - \tau') \leq 0$  whereas,  $D_-(\mathbf{x}, \mathbf{x}'; \tau, \tau')$  is defined in domain  $\beta \geq \text{Im}(\tau - \tau') \geq 0$ . The thermal propagator satisfy the equation

$$(\square^2 + m^2)D(x, x') = \delta^4(x - x'), \tag{2.40}$$

with boundary condition

$$D_-(\mathbf{x}, \mathbf{x}'; \tau, \tau') = D_+(\mathbf{x}, \mathbf{x}'; \tau - i\beta, \tau') \tag{2.41}$$

known as KMS relation (shown in Eq. (2.8)). Going to the spacial Fourier transform space and solving the differential equation one can easily get

$$D(\mathbf{k}; \tau - \tau') = \frac{i}{2\omega} \left\{ [\theta(\tau - \tau') + n_B] e^{-i\omega(\tau - \tau')} + [\theta(\tau' - \tau) + n_B] e^{i\omega(\tau - \tau')} \right\}, \tag{2.42}$$

where  $n_B(\omega) = \frac{1}{e^{\beta\omega} - 1}$  is the single particle thermal distribution function with  $\omega^2 = \mathbf{k}^2 + m^2$ . Now we need to specify the contour and the suitable choice is shown in Fig. 2.3. The path traverses from  $-\bar{t}$  to  $+\bar{t}$  in real axis, then it continues in vertical path from  $\bar{t}$  to  $\bar{t} - i\beta/2$ . Then it runs from parallel to real axis upto  $-\bar{t} - i\beta/2$  and finally takes the vertical path upto  $-\bar{t} - i\beta$ .



## 2.2. Real time formalism

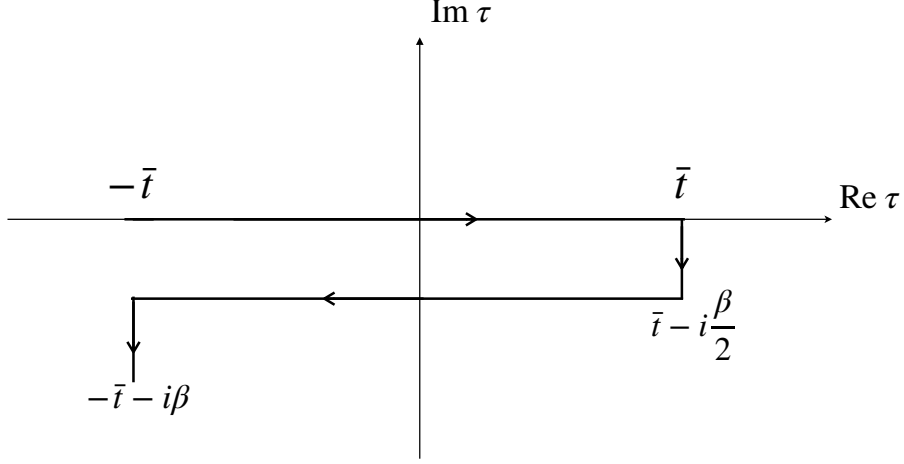


Figure 2.3: The contour for the real time formalism.

$D(\mathbf{k}, \tau_h, \tau_v) \rightarrow 0$  by Riemann-Lebesgue lemma where  $\tau_v$  and  $\tau_h$  are points on vertical and horizontal lines respectively. Both points on vertical lines are not considered as we are interested only in propagator having points on real axis. So, we are left with two lines parallel to real axes and the propagator can be written in form of  $2 \times 2$  matrix. The propagator is given in  $ij$ -th element as

$$D(\mathbf{k}; \tau_i - \tau'_j) = \frac{i}{2\omega} \left\{ [\theta(\tau_i - \tau'_j) + n_B] e^{-i\omega(\tau_i - \tau'_j)} + [\theta(\tau'_j - \tau_i) + n_B] e^{i\omega(\tau_i - \tau'_j)} \right\}. \quad (2.43)$$

Now we can write down the contour ordering in terms of the usual time ( $t$ ) ordering. When  $\tau$  and  $\tau'$  are on line 1 (real axis from  $-\bar{t}$  to  $\bar{t}$ ),  $\theta(\tau_1 - \tau'_1) = \theta(t - t')$ . If  $\tau$  and  $\tau'$  are on line 2 (real axis from  $\bar{t} - i\beta/2$  to  $-\bar{t} - i\beta/2$ ), it is written as  $\theta(\tau_2 - \tau'_2) = \theta(t' - t)$ . When the points are on different lines, we note that  $\theta(\tau_1 - \tau'_2) = 0$  and  $\theta(\tau_2 - \tau'_1) = 1$ .

Now the components of propagator in the momentum space are written by taking tem-

poral Fourier transform as

$$D_{ij}(\mathbf{k}, k_0) = \int_{-\infty}^{\infty} e^{ik_0(t-t')} D(\mathbf{k}; \tau_i, \tau'_j) dt. \quad (2.44)$$

Performing the integration, they can take the forms

$$D_{11} = \Delta_F(k) + 2i\pi n_B(\omega) \delta(k^2 - m^2), \quad (2.45)$$

$$D_{12} = 2i\pi \sqrt{n_B(\omega)(1 + n_B(\omega))} \delta(k^2 - m^2), \quad (2.46)$$

whereas the other components are written as

$$\begin{aligned} D_{21} &= D_{12}, \\ D_{22} &= -D_{11}^*. \end{aligned} \quad (2.47)$$

Finally, we can write the momentum space scalar propagator in terms of matrix as

$$D(k_0, \mathbf{k}) = \begin{bmatrix} \Delta_F(k) + 2i\pi n_B \delta(k^2 - m^2) & 2i\pi \sqrt{n_B(1 + n_B)} \delta(k^2 - m^2) \\ 2i\pi \sqrt{n_B(1 + n_B)} \delta(k^2 - m^2) & -\Delta_F(k)^* + 2i\pi n_B \delta(k^2 - m^2) \end{bmatrix}, \quad (2.48)$$

where  $\Delta_F(k)$  is the free scalar propagator. We use real time formalism to calculate gluon self-energy in chapter 4.

## COVARIANT STRUCTURE OF GAUGE-BOSON PROPAGATOR

---

In this chapter covariant structure of gluon self-energy and effective propagator is constructed for two independent anisotropy directions in presence of heat bath. In this case the general structure of gauge-boson self-energy are expressed as a linear combination of six linearly independent projection tensors. This chapter is based on the work presented in the following paper: *Covariant formulation of gluon self-energy in presence of ellipsoidal anisotropy*

*Ritesh Ghosh*, Bithika Karmakar, Arghya Mukherjee, *Phys. Rev. D* **102** (2020) 11, 114002, [[arXiv:2011.03374](https://arxiv.org/abs/2011.03374)].

In this thesis we are mainly interested in two anisotropy case: one is anisotropy due to the modeling of non-equilibrium distribution function by modifying the equilibrium distribution and the other anisotropy is due to the background magnetic field. Due to the presence of the anisotropy, the symmetry of the system is broken. In this chapter covariant

### Chapter 3. Covariant structure of Gauge-Boson propagator

structure of gauge-boson propagator is constructed for two independent anisotropy directions. We consider a thermal QCD medium with two anisotropic directions characterized by two independent four vectors  $a^\mu$  and  $b^\mu$  having unit norms. These two, together with the normalized heat bath velocity ( $u^\mu$ ) and the gluon momentum ( $P^\mu$ ), can be used to form a set of ten independent symmetric tensors so that the symmetric gluon polarization tensor can be expressed as a linear combination of them. A simple choice for this purpose may be the set of tensors  $P^\mu P^\nu$ ,  $u^\mu u^\nu$ ,  $b^\mu b^\nu$ ,  $a^\mu a^\nu$ ,  $P^\mu u^\nu + P^\nu u^\mu$ ,  $P^\mu b^\nu + P^\nu b^\mu$ ,  $P^\mu a^\nu + P^\nu a^\mu$ ,  $u^\mu b^\nu + b^\mu u^\nu$ ,  $u^\mu a^\nu + u^\nu a^\mu$  and  $b^\mu a^\nu + a^\mu b^\nu$ . Notice that, along with the four vectors, we have not considered the metric  $g^{\mu\nu}$  as usually done in isotropic or even in anisotropic case with one anisotropy direction. This is because, in case of two anisotropies, the metric itself no longer remains an independent tensor and can be expressed as a linear combination of the chosen set. Now, the constraints from the transversality condition  $P^\mu \Pi_{\mu\nu} = 0$  further reduce the number of independent basis tensors to six. In the rest frame of the heat bath with  $u^\mu = (1, 0, 0, 0)$ , one of the anisotropy directions can be taken along z, say  $b^\mu = (0, 0, 0, 1)$ , whereas the other anisotropy direction can be assumed to lie in the xz plane without any loss of generality. In the following we discuss a convenient method to obtain the basis tensors in a systematic way.

Let us first consider the general structure of the gauge boson self-energy in vacuum that can be written as

$$\Pi^{\mu\nu} = \left( g^{\mu\nu} - \frac{P^\mu P^\nu}{P^2} \right) \Pi(P^2) = V^{\mu\nu} \Pi(P^2). \quad (3.1)$$

Using the tensor  $V^{\mu\nu}$ , we obtain  $\tilde{u}^\mu = V^{\mu\nu} u_\nu$  which can be used to construct the first basis

tensor given by

$$A^{\mu\nu} = \frac{\tilde{u}^\mu \tilde{u}^\nu}{\tilde{u}^2}. \quad (3.2)$$

Now, it is useful to define the  $A^{\mu\nu}$  subtracted part of  $V^{\mu\nu}$  as  $U^{\mu\nu} = V^{\mu\nu} - A^{\mu\nu}$  which can be used to obtain  $\tilde{b}^\mu$  defined as  $\tilde{b}^\mu = U^{\mu\nu} b_\nu$  such that, it becomes orthogonal to  $\tilde{u}^\mu$  by construction. Similar to the earlier case, we obtain our second basis tensor using  $\tilde{b}^\mu$  as

$$B^{\mu\nu} = \frac{\tilde{b}^\mu \tilde{b}^\nu}{\tilde{b}^2}. \quad (3.3)$$

Another symmetric tensor that can be constructed intuitively using  $\tilde{b}^\mu$  and  $\tilde{u}^\mu$  together is given by

$$C^{\mu\nu} = \frac{\tilde{u}^\mu \tilde{b}^\nu + \tilde{b}^\mu \tilde{u}^\nu}{\sqrt{\tilde{u}^2} \sqrt{\tilde{b}^2}}. \quad (3.4)$$

To obtain the rest of the tensors, once again we go through the similar steps: at first we define  $R^{\mu\nu} = U^{\mu\nu} - B^{\mu\nu}$ , which, in this case, can be viewed as the  $A^{\mu\nu}$  and the  $B^{\mu\nu}$  subtracted part of our vacuum basis tensor  $V^{\mu\nu}$ . Then we obtain the  $\tilde{a}^\mu$  from  $a^\mu$  as  $\tilde{a}^\mu = R^{\mu\nu} a_\nu$ . This time, the newly constructed  $\tilde{a}^\mu$  becomes orthogonal to  $\tilde{b}^\mu$  as well as  $\tilde{u}^\mu$ . Note that, all the four vectors of the set  $\tilde{u}^\mu$ ,  $\tilde{b}^\mu$  and  $\tilde{a}^\mu$  are orthogonal to the gluon four momentum  $P^\mu$  and hence the basis tensors constructed using them trivially satisfy the transversality condition. Moreover, because of the orthogonality among the constructed four vectors, the extraction of the form factors gets simplified considerably. Now, with the constructed set, the rest of the independent symmetric tensors can also be obtained intuitively as

$$D^{\mu\nu} = \frac{\tilde{a}^\mu \tilde{a}^\nu}{\tilde{a}^2}, \quad (3.5)$$

### Chapter 3. Covariant structure of Gauge-Boson propagator

$$E^{\mu\nu} = \frac{\tilde{u}^\mu \tilde{a}^\nu + \tilde{a}^\mu \tilde{u}^\nu}{\sqrt{\tilde{u}^2} \sqrt{\tilde{a}^2}}, \quad (3.6)$$

$$F^{\mu\nu} = \frac{\tilde{a}^\mu \tilde{b}^\nu + \tilde{b}^\mu \tilde{a}^\nu}{\sqrt{\tilde{a}^2} \sqrt{\tilde{b}^2}}. \quad (3.7)$$

The general structure of the gauge boson self-energy in presence of two anisotropy directions medium can be expressed as a linear combination of the six basis tensors as

$$\Pi^{\mu\nu} = \alpha A^{\mu\nu} + \beta B^{\mu\nu} + \gamma C^{\mu\nu} + \delta D^{\mu\nu} + \sigma E^{\mu\nu} + \lambda F^{\mu\nu}. \quad (3.8)$$

It is worth mentioning here that though tensors like  $V^{\mu\nu}$  are used to obtain the set, once we declare our constructed set of tensors as independent, all the other symmetric and transverse tensors not belonging to the set become expressible as their linear combination. For example, it can be shown that

$$V^{\mu\nu} = A^{\mu\nu} + B^{\mu\nu} + D^{\mu\nu}. \quad (3.9)$$

Now, we can obtain the effective propagator from the Dyson-Schwinger equation

$$i\mathcal{D}^{\mu\nu} = i\mathcal{D}_0^{\mu\nu} + i\mathcal{D}_0^{\mu\rho} (i\Pi_{\rho\rho'}) i\mathcal{D}^{\rho'\nu}, \quad (3.10)$$

where the inverse bare propagator  $\mathcal{D}_0^{\mu\nu}$  without the explicit color indices is given by

$$(\mathcal{D}_0^{-1})^{\mu\nu} = -P^2 g^{\mu\nu} - \frac{1-\zeta}{\zeta} P^\mu P^\nu, \quad (3.11)$$

with  $\zeta$  representing the gauge fixing parameter. To obtain the effective propagator, let us

first consider the inner product identities among the basis tensors. To express the identities in a compact form, here we suppress the Lorentz indices of the basis tensors. Also the tensors  $C$ ,  $E$  and  $F$  are considered as a sum of two parts, for example  $C = \overline{C} + \underline{C}$  and in similar fashion for the other two where

$$\begin{aligned}\overline{C}_\nu^\mu &= \frac{\tilde{u}^\mu \tilde{b}_\nu}{\sqrt{\tilde{u}^2} \sqrt{\tilde{b}^2}}, & \underline{C}_\nu^\mu &= \frac{\tilde{b}^\mu \tilde{u}_\nu}{\sqrt{\tilde{u}^2} \sqrt{\tilde{b}^2}}, \\ \overline{E}_\nu^\mu &= \frac{\tilde{u}^\mu \tilde{a}_\nu}{\sqrt{\tilde{u}^2} \sqrt{\tilde{a}^2}}, & \underline{E}_\nu^\mu &= \frac{\tilde{a}^\mu \tilde{u}_\nu}{\sqrt{\tilde{u}^2} \sqrt{\tilde{a}^2}}, \\ \overline{F}_\nu^\mu &= \frac{\tilde{a}^\mu \tilde{b}_\nu}{\sqrt{\tilde{a}^2} \sqrt{\tilde{b}^2}}, & \underline{F}_\nu^\mu &= \frac{\tilde{b}^\mu \tilde{a}_\nu}{\sqrt{\tilde{a}^2} \sqrt{\tilde{b}^2}}.\end{aligned}$$

With this notation, the inner product between the basis tensors can be written in a compact form as

	$A$	$B$	$C$	$D$	$E$	$F$	
$A$	$A$	$0$	$\overline{C}$	$0$	$\overline{E}$	$0$	
$B$	$0$	$B$	$\underline{C}$	$0$	$0$	$\underline{F}$	
$C$	$\underline{C}$	$\overline{C}$	$A + B$	$0$	$\underline{F}$	$\overline{E}$	(3.12)
$D$	$0$	$0$	$0$	$D$	$\underline{E}$	$\overline{F}$	
$E$	$\underline{E}$	$0$	$\overline{F}$	$\overline{E}$	$A + D$	$\overline{C}$	
$F$	$0$	$\overline{F}$	$\underline{E}$	$\underline{F}$	$\underline{C}$	$B + D$	

where the composition rule for each entry of the multiplication table is defined as  $r_\rho^\mu c_\nu^\rho$  with  $r$  and  $c$  being members representing the row and the column respectively. Moreover, further contraction of the free indices as  $r_\rho^\mu c_\mu^\rho$  simplifies to

### Chapter 3. Covariant structure of Gauge-Boson propagator

	A	B	C	D	E	F
A	1	0	0	0	0	0
B	0	1	0	0	0	0
C	0	0	2	0	0	0
D	0	0	0	1	0	0
E	0	0	0	0	2	0
F	0	0	0	0	0	2

(3.13)

which will be useful to extract the coefficients of the basis tensors *i.e.*, the form factors from the polarization function. Using the properties of the basis tensors from Eq. (3.12) one can obtain the effective gluon propagator given by

$$\begin{aligned}
 \mathcal{D}^{\mu\nu} = & -\frac{\beta\delta - (\beta + \delta)P^2 - \lambda^2 + P^4}{\Delta} A^{\mu\nu} - \frac{\delta\alpha - (\delta + \alpha)P^2 - \sigma^2 + P^4}{\Delta} B^{\mu\nu} \\
 & - \frac{\gamma(P^2 - \delta) + \sigma\lambda}{\Delta} C^{\mu\nu} - \frac{\alpha\beta - (\alpha + \beta)P^2 - \gamma^2 + P^4}{\Delta} D^{\mu\nu} \\
 & - \frac{\sigma(P^2 - \beta) + \lambda\gamma}{\Delta} E^{\mu\nu} - \frac{\lambda(P^2 - \alpha) + \gamma\sigma}{\Delta} F^{\mu\nu} - \zeta \frac{P^\mu P^\nu}{P^4}.
 \end{aligned}
 \tag{3.14}$$

where the common denominator of the basis tensors,  $\Delta$  is given by

$$\begin{aligned}
 \Delta = & P^6 - (\alpha + \beta + \delta)P^4 - (\gamma^2 + \sigma^2 + \lambda^2 - \alpha\beta - \beta\delta - \delta\alpha)P^2 \\
 & + \alpha\lambda^2 + \beta\sigma^2 + \delta\gamma^2 - \alpha\beta\delta - 2\gamma\sigma\lambda.
 \end{aligned}
 \tag{3.15}$$

Notice that, in presence of two anisotropies, the denominator of the effective propagator



becomes a cubic equation of  $P^2$  and can be written as a product of three factors as

$$\Delta = (P^2 - \Omega_0)(P^2 - \Omega_+)(P^2 - \Omega_-), \quad (3.16)$$

where  $\Omega_0$  and  $\Omega_{\pm}$  can be written in terms of the form factors as

$$\Omega_0 = \frac{1}{3}(\alpha + \beta + \delta) - \frac{1}{3} \frac{\varpi}{\left(\frac{\chi + \sqrt{4\varpi^3 + \chi^2}}{2}\right)^{\frac{1}{3}}} + \frac{1}{3} \left(\frac{\chi + \sqrt{4\varpi^3 + \chi^2}}{2}\right)^{\frac{1}{3}}, \quad (3.17)$$

$$(3.18)$$

$$\begin{aligned} \Omega_+ &= \frac{1}{3}(\alpha + \beta + \delta) + \frac{1 + i\sqrt{3}}{6} \frac{\varpi}{\left(\frac{\chi + \sqrt{4\varpi^3 + \chi^2}}{2}\right)^{\frac{1}{3}}} \\ &\quad - \frac{1 - i\sqrt{3}}{6} \left(\frac{\chi + \sqrt{4\varpi^3 + \chi^2}}{2}\right)^{\frac{1}{3}}, \end{aligned} \quad (3.19)$$

$$\begin{aligned} \Omega_- &= \frac{1}{3}(\alpha + \beta + \delta) + \frac{1 - i\sqrt{3}}{6} \frac{\varpi}{\left(\frac{\chi + \sqrt{4\varpi^3 + \chi^2}}{2}\right)^{\frac{1}{3}}} \\ &\quad - \frac{1 + i\sqrt{3}}{6} \left(\frac{\chi + \sqrt{4\varpi^3 + \chi^2}}{2}\right)^{\frac{1}{3}}, \end{aligned} \quad (3.20)$$

where  $\varpi$  and  $\chi$  are given by

$$\varpi = \alpha(\beta - \alpha) + \beta(\delta - \beta) + \delta(\alpha - \delta) - 3(\gamma^2 + \lambda^2 + \sigma^2), \quad (3.21)$$

$$\begin{aligned} \chi &= (2\alpha - \beta - \delta)(2\beta - \delta - \alpha)(2\delta - \alpha - \beta) + 54\gamma\lambda\sigma \\ &\quad - 9\alpha(2\lambda^2 - \sigma^2 - \gamma^2) - 9\beta(2\sigma^2 - \gamma^2 - \lambda^2) - 9\delta(2\gamma^2 - \lambda^2 - \sigma^2). \end{aligned} \quad (3.22)$$

Once the form factors are extracted from the polarization function, the desired collective modes of the gluon can be obtained from the pole of the effective propagator.



# GLUON SELF-ENERGY IN PRESENCE OF ELLIPSOIDAL ANISOTROPY

---

In this chapter gluon collective modes for ellipsoidal momentum-space anisotropy is obtained from the pole of the propagator constructed in Chapter 3. Introducing the mass scale for collective modes, the presence of instability is also discussed. This chapter is based on the work presented in the following paper: *Covariant formulation of gluon self-energy in presence of ellipsoidal anisotropy*

Ritesh Ghosh, Bithika Karmakar, Arghya Mukherjee, *Phys. Rev. D* **102** (2020) 11, 114002, [[arXiv:2011.03374](https://arxiv.org/abs/2011.03374)].

## 4.1 Introduction

As discussed in introduction chapter 1, the plethora of knowledge gained through the non-perturbative lattice QCD simulations [151–153], perturbative hard thermal loop calculations [40, 154–156], effective hydrodynamical modeling [31, 32, 157] as well as AdS/CFT

inspired studies [158–161] have paved the way of achieving a remarkable advancement in our understanding of the experimental data available from the Relativistic Heavy Ion Collider (RHIC) facility at Brookhaven National Lab and the Large Hadron Collider (LHC) facility at European Center for Nuclear Research (CERN)[25, 162]. The concerted efforts from different heavy ion research communities suggest that the deconfined quark-gluon plasma(QGP) matter produced in the ultrarelativistic heavy ion collision experiments is most likely to possess substantial deviation from perfect local isotropic equilibrium [163]. In fact, soon after the initial nuclear impact, very large pressure anisotropy is expected in the center of the fireball with even larger anisotropy prevailing in the cooler regions of the plasma [35]. A promising way for hydrodynamical modeling of such highly momentum space anisotropic system is to consider the framework of anisotropic hydrodynamics [34, 164]. On the other hand, incorporating certain classes of anisotropic momentum distributions in the framework of hard thermal loop perturbation theory, the nonequilibrium plasma properties can be extracted by studying the collective modes of the quasipartons [141, 165]. A suitable parametrization for such distributions can be achieved following Refs. [166–168] where the one particle isotropic momentum space distribution function is deformed by introducing a directional dependency. This particular Romatschke-Strickland (RS) form has been widely used in different phenomenological applications such as photon and dilepton production from anisotropic QGP [169–171], anisotropic heavy quark potential [172], bottomonia suppression [173], plasma wakes [174, 175], nuclear modification factor [176], quasiparticle descriptions of particle production [177] and so on.

An important aspect of considering the nonequilibrium momentum distributions in QGP medium is the occurrence of kinetic instabilities. These are, in simple terms, the collective modes that possess a positive imaginary part in their mode frequencies resulting an exponential growth in the chromomagnetic and chromoelectric fields. The existence of

#### 4.1. Introduction

such Chromo-Weibel instabilities [178] can influence the thermalization and isotropization of the medium [179]. A recent review with a pedagogical introduction to the required theoretical tools for such studies can be found in Ref. [143]. In general, how many unstable modes are possible depends on the choice of the parameters. For example, in case of spheroidal anisotropy with Romatschke-Strickland parametrized form, the number of the possible unstable modes differs for the prolate and the oblate case which are obtained considering the negative and positive values for the anisotropy parameter respectively [166]. Moreover, there will be a directional dependence as well. In other words, depending on the angle of propagation with respect to the anisotropy direction, a stable collective mode may become unstable and can give rise to additional instabilities.

As already mentioned, the large momentum space anisotropy in early stages can be efficiently incorporated in the aHydro framework. This is because, unlike usual viscous hydrodynamic set up, here, the dominant anisotropic contributions to the distribution functions are captured in the leading order of hydrodynamic expansion. The second order anisotropic hydrodynamics as developed in [180] can take into account arbitrary transverse expansion and is consistent with the traditional dissipative hydrodynamics approach in the limiting case of small anisotropy. However, as argued in Ref. [181], the azimuthally symmetric ansatz in such approaches involving a single anisotropy parameter can further be generalized in a systematic way. More specifically, in the original anisotropic hydrodynamic setup, the leading order local rest frame distribution is taken to be of RS form and thus the two components of the pressure in the transverse plane can be different only after including the second order corrections. A generalization to include three different pressure components in the leading order of hydrodynamic expansion has been developed in Refs. [181–183] and recently has further been generalized in Ref. [184]. In the hard loop approach too, the generalized ellipsoidal distribution has been considered in the parton self-

#### Chapter 4. Gluon self-energy in presence of ellipsoidal anisotropy

energy studies [185] and implemented in phenomenological applications of photon and dilepton production [186, 187]. Obviously, the consideration of an ellipsoidal anisotropy increases the number of parameters compared to the spheroidal case, as, apart from one additional anisotropy parameter dependence, the collective properties of the partons in this case also possess azimuthal angular dependency. Recently, the gluonic unstable mode with an ellipsoidal anisotropic momentum distribution has been reported for the first time in Ref. [144]. It is observed that the growth rate of the unstable modes can become several times larger than the spheroidal case for certain propagation directions. Also the number of possible unstable modes are direction dependent. A convenient method to describe such directional dependency is to consider the static limits of the collective modes. In that case, one introduces mass scales corresponding to each of the collective modes and studies their angular dependency. The occurrence of a negative value in the mass scale in fact signifies the presence of an instability in the corresponding mode which are well studied in the spheroidal case. However, for the ellipsoidal case, such mass scales could not be defined in the formalism adopted in [144] where the general structure of the gluon polarization has not been considered. An important application of gluon self energy lies in the determination of the perturbative part of the heavy quark potential [172, 188, 189] which requires a covariant formulation of the general structure.

The primary objective of this work is to study the occurrence of the unstable modes in a similar fashion as done in case of spheroidal momentum space anisotropy using the general structure for the gluon polarization in presence of ellipsoidal momentum space anisotropy presented in Chapter 3. A suitable approach for constructing the tensor basis for gluon self energy is to choose the maximum possible mutually orthogonal set. The choice becomes useful for the derivation of the effective propagator where contractions among the basis tensors are involved. Once the effective gluon propagator is derived, one can obtain

## 4.2. Results

the collective modes from its pole. It should be mentioned here that the gluon collective modes can also be obtained by solving the characteristic equation without requiring any consideration of the general structure. In fact, this is the procedure adopted in Ref.[144]. However, the advantage of considering the general structure is that, the collective modes are expressed in terms of coordinate independent form factors which is essential for introducing the mass scales. In fact, the nontrivial angular dependence in the hard-thermal loop resummed potential enters through these mass scales [172].

## 4.2 Results

In this work we consider the hard-loop gluon polarization tensor in a non-equilibrium QGP medium given by [141]

$$\Pi^{\mu\nu}(p^0 = \omega, \mathbf{p}) = g_s^2 \int \frac{d^3\mathbf{k}}{(2\pi)^3} \frac{K^\mu}{E_k} \frac{\partial f(\mathbf{k})}{\partial K^\rho} \left[ g^{\rho\nu} - \frac{K^\rho P^\nu}{P \cdot K + i0^+} \right], \quad (4.1)$$

where  $g_s$  is the strong coupling constant and  $k^0 = E_k$  represents the energy of the massless partonic degrees of freedom that modify the gluon dispersion in presence of anisotropic medium. The effective distribution function  $f(\mathbf{k})$  is given by

$$f(\mathbf{k}) = 2N_c n_g(\mathbf{k}) + N_f [n_q(\mathbf{k}) + n_{\bar{q}}(\mathbf{k})], \quad (4.2)$$

where  $n_g(\mathbf{k})$  represents the gluon number density whereas  $n_q(\mathbf{k})$  and  $n_{\bar{q}}(\mathbf{k})$  are the quark and anti-quark number densities respectively.  $N_c$  and  $N_f$  are respectively the number of colors and quark flavors. A general method of constructing anisotropic momentum distribution function is to transform the argument of an isotropic momentum space distribution

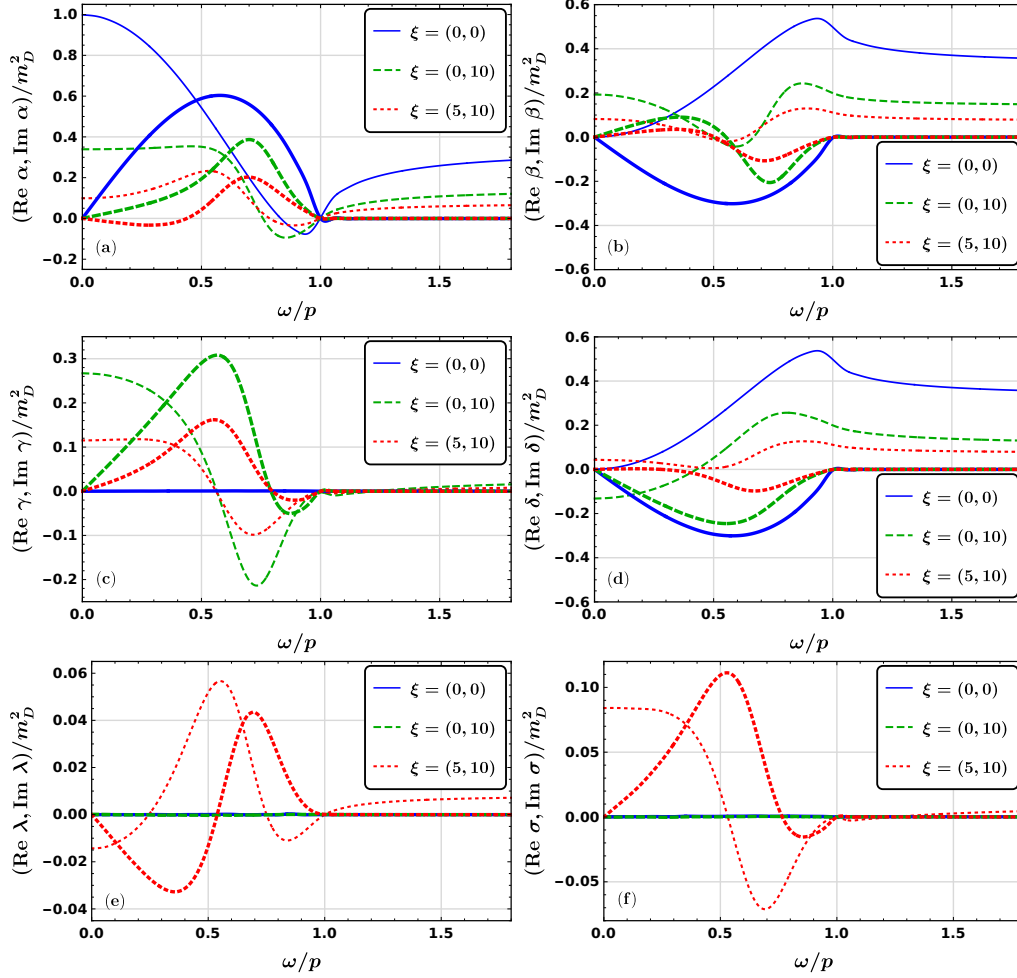


Figure 4.1: The real and imaginary parts of the form factors are plotted in (a)–(f) as a function of  $\omega/p$  for three different set of anisotropy tuple  $\xi = (\xi_a, \xi_b) = (0, 0), (0, 10)$  and  $(5, 10)$ . In each case, the imaginary parts are shown with comparatively thicker style. The spheroidal set is shown at fixed  $\theta_p = \pi/4$  whereas for the ellipsoidal case,  $(\theta_p, \phi_p) = (\pi/4, \pi/3)$  is considered.



## 4.2. Results

essentially by introducing deformations in a parametrized way. A discussion on the generalisation of the RS form to ellipsoidal anisotropies can be found in Refs.[144, 182]. In our case we use the ellipsoidal momentum distribution parametrized as [144, 185]

$$f_{\text{aniso}}(\mathbf{k}) \equiv f_{\text{iso}}\left(\frac{1}{\Lambda}\sqrt{\mathbf{k}^2 + \xi_a(\mathbf{k} \cdot \mathbf{a})^2 + \xi_b(\mathbf{k} \cdot \mathbf{b})^2}\right), \quad (4.3)$$

where  $\Lambda$  represents a temperature-like scale which, in the equilibrium limit, corresponds to the temperature. The gluon polarization tensor with such anisotropic parton distributions can be written as

$$\Pi^{\mu\nu}(\omega, \mathbf{p}, \xi) = m_D^2 \int \frac{d\Omega}{4\pi} v^\mu \frac{v^\nu + \xi_a(\mathbf{v} \cdot \mathbf{a})a^\nu + \xi_b(\mathbf{v} \cdot \mathbf{b})b^\nu}{(1 + \xi_a(\mathbf{v} \cdot \mathbf{a})^2 + \xi_b(\mathbf{v} \cdot \mathbf{b})^2)^2} \left[ g^{\nu\lambda} - \frac{v^\nu P^\lambda}{\omega - \mathbf{p} \cdot \mathbf{v} + i0^+} \right], \quad (4.4)$$

where  $\xi$  represents the anisotropy tuple  $(\xi_a, \xi_b)$  and  $m_D^2 = (N_c + N_f/2)\frac{g_s^2 \Lambda^2}{3}$  corresponds to the QCD Debye mass scale. In the above expression, the parton four velocity  $v^\mu = K^\mu/k$  and the components of  $\mathbf{a}$ ,  $\mathbf{b}$ ,  $\mathbf{v}$ , and  $\mathbf{p}$  in the rest frame of the medium are chosen as

$$\mathbf{a} = (1, 0, 0), \quad (4.5)$$

$$\mathbf{b} = (0, 0, 1), \quad (4.6)$$

$$\mathbf{v} = (\sin \theta_k \cos \phi_k, \sin \theta_k \sin \phi_k, \cos \theta_k), \quad (4.7)$$

$$\mathbf{p} = p(\sin \theta_p \cos \phi_p, \sin \theta_p \sin \phi_p, \cos \theta_p), \quad (4.8)$$

with  $d\Omega$  representing the differential solid angle corresponding to the internal angular coordinates  $(\theta_k, \phi_k)$ . It should be mentioned here that another common choice of reference frame is the parton specific co-ordinate as used in Ref. [144] where one reorients the axes so that the polar angle is measured with respect to the parton momentum. However, as we are interested in the evaluation of the form factors, the results do not depend on any specific

choice of the reference frame.

Now, as discussed in the previous section, the gluon self-energy can be decomposed in terms of six independent basis tensors. Utilizing the contraction relations among the basis tensors, the corresponding form factors can be obtained in terms of the self-energy components given in Eq. (4.4) as a two dimensional integral over the solid angle. However, because of the transversality condition and the symmetry under the exchange of the free indices, the number of independent components of the self-energy reduces to six. Thus, any chosen set of six independent components will be sufficient to determine the form factors. It should be mentioned here that, though in our work, the form factors are obtained numerically using the conventional quadrature routines, an alternative way involving the hypergeometric expansion method is expected to be much more efficient [144] for this purpose. The real and imaginary parts of the form factors are shown in Fig. 4.1, for three different situations, namely the isotropic case with  $\xi = (0, 0)$ , the spheroidal case with  $\xi = (0, 10)$  and the ellipsoidal case with  $\xi = (5, 10)$ . The spheroidal case is shown for  $\theta_p = \pi/4$  whereas for the ellipsoidal anisotropy,  $\theta_p$  and  $\phi_p$  are chosen as  $\pi/4$  and  $\pi/3$  respectively. The imaginary parts of the form factors in all the three cases exist only in the space-like region. It should be noted that when the isotropic medium is considered,  $\beta$  and  $\delta$  become degenerate whereas  $\gamma$ ,  $\lambda$  and  $\sigma$  become zero. This results in two distinct dispersive modes of the gluon among which one is degenerate *i.e.*,  $\Omega_0 = \alpha$  and  $\Omega_+ = \Omega_- = \beta = \delta$ . The analytic expression of the degenerate form factors is given by

$$\beta = \delta = \Pi_T = \frac{m_D^2 \omega^2}{2 p^2} \left[ 1 - \frac{\omega^2 - p^2}{2\omega p} \ln \frac{\omega + p}{\omega - p} \right], \quad (4.9)$$

whereas the dispersion for the other distinct mode can be obtained from

## 4.2. Results

$$\alpha = \Pi_L = \frac{m_D^2}{\tilde{u}^2} \left[ 1 - \frac{\omega}{2p} \ln \frac{\omega + p}{\omega - p} \right], \quad (4.10)$$

which are the familiar results of the gluon self-energy in isotropic thermal medium [150]. Here  $m_D^2 = (N_c + N_f/2) \frac{g_s^2 T^2}{3}$  and  $\tilde{u}^2 = -p^2/P^2$ . In the presence of spheroidal anisotropy,  $\sigma$  and  $\lambda$  remain zero. However,  $\beta$  and  $\delta$  are no longer degenerate. In that case the functions corresponding to the dispersive modes simplify to

$$\Omega_0 = \frac{1}{2} \left( \alpha + \beta + \sqrt{(\alpha - \beta)^2 + 4\gamma^2} \right), \quad (4.11)$$

$$\Omega_+ = \frac{1}{2} \left( \alpha + \beta - \sqrt{(\alpha - \beta)^2 + 4\gamma^2} \right), \quad (4.12)$$

$$\Omega_- = \delta. \quad (4.13)$$

which may be compared with the modes obtained in Ref. [166] (see for example Eq.(43) therein). Though we find a different combination of the form factors in the expressions due to the different choice of our basis tensors, it should be noticed that, in our case too, the arguments inside the square root appear as a sum of two complete squares, thereby allowing similar interpretation for the collective modes (see for example section VI of [166]). When ellipsoidal anisotropy is considered, it is observed that all the form factors are non-zero and they contribute in the gluon dispersion. However, It should be noticed that, for the fixed set of parameters chosen for the figure, the values of  $\lambda$  and  $\sigma$  are an order of magnitude smaller than the other form factors.

Now, following Ref. [166], a mass scale corresponding to a given form factor, say for example  $\alpha$ , can be defined in the static limit as

$$m_\alpha^2 = \lim_{\omega \rightarrow 0} \alpha. \quad (4.14)$$

It is evident from Fig. 4.1 that the imaginary part of each of the form factors vanishes at  $\omega \rightarrow 0$  limit. Thus, the mass scales as defined above are real quantities. Now, in a similar way, one can define the mass scales corresponding to the gluon dispersive modes as

$$m_{\Omega_{0,\pm}}^2 = \lim_{\omega \rightarrow 0} \Omega_{0,\pm}(\omega, p, \theta_p, \phi_p). \quad (4.15)$$

Their variation with the polar angle  $\theta_p$  is shown in Fig. 4.2 for three fixed values of  $\phi_p = \{\pi/2, \pi/4, \pi/6\}$ . For each modes, the corresponding spheroidal version is also shown for comparison. It is evident from the figures that the azimuthal symmetry of the spheroidal case is now broken with the introduction of additional anisotropy direction. Consequently, a non-trivial  $\phi_p$  dependence can be observed in the mass scales. As can be seen from the figure, the mass scale corresponding to  $\Omega_0$  remains positive throughout the range of  $\theta_p$  values as also found in the spheroidal case. Again, similar to the spheroidal anisotropy, negative values in the mass scale is observed for  $\Omega_\pm$  which correspond to instability [166]. However, it can be noticed that as the value of  $\phi_p$  approaches to  $\pi/2$ ,  $m_{\Omega_\pm}^2$  becomes positive at smaller values of  $\theta_p$ . In other words, with larger deviation from azimuthal anisotropy direction, the collective modes can be unstable only in shorter window of  $\theta_p$  values as compared to the spheroidal case. However, it should be noted that, the above observation is made with a particular set of anisotropy parameter where both  $\xi_a$  and  $\xi_b$  are positive. An interesting situation occurs for negative value of anisotropy parameter as shown in the left panel of Fig. 4.3. Here, the angular variation of  $m_{\Omega_-}^2$  is shown with  $(\xi_a, \xi_b) = (-0.5, -0.9)$ .

## 4.2. Results

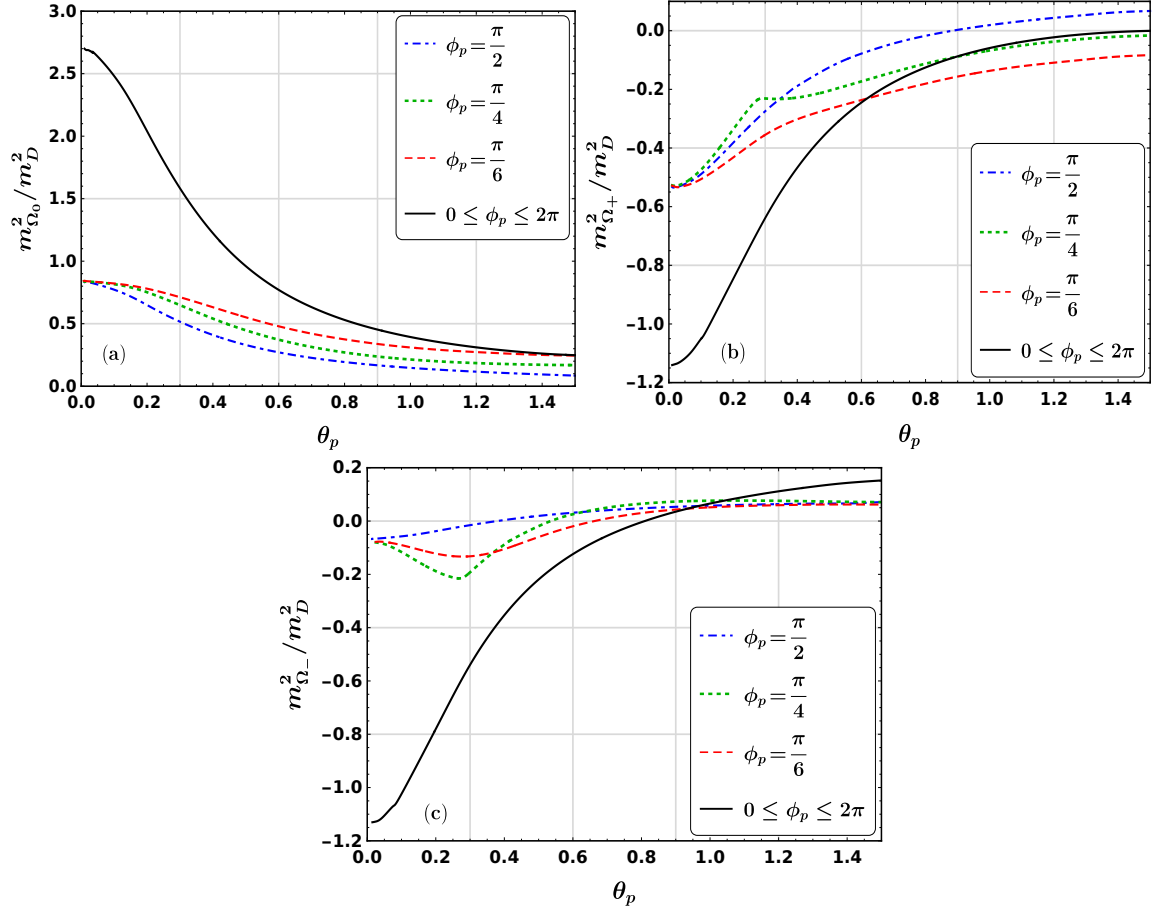


Figure 4.2: Squared values of the mass scales corresponding to  $\Omega_0$  and  $\Omega_{\pm}$  are plotted in (a)–(c) as a function of  $\theta_p$  for three different values of  $\phi_p = \{\pi/2, \pi/4, \pi/6\}$  (shown in discrete style) considering  $(\xi_a, \xi_b) = (5, 10)$ . The solid line represents the spheroidal case with  $(\xi_a, \xi_b) = (0, 10)$ .

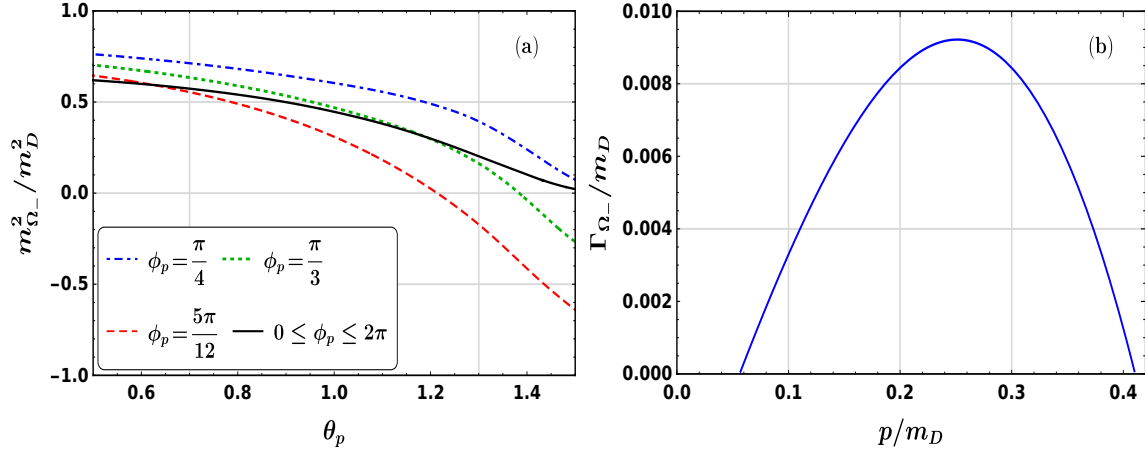


Figure 4.3: In the left panel, the squared value of the mass scale corresponding to  $\Omega_-$  is plotted as a function of  $\theta_p$  for three different values of  $\phi_p = \{\pi/4, \pi/3, 5\pi/12\}$  (shown in discrete style) considering  $(\xi_a, \xi_b) = (-0.5, -0.9)$ . The spheroidal case (shown in solid style) with  $(\xi_a, \xi_b) = (0, -0.9)$  is also plotted for comparison. In the right panel, the growth rate for the  $\Omega_-$  mode is plotted as a function of  $p/m_D$  with  $(\xi_a, \xi_b) = (-0.5, -0.9)$  and  $(\theta_p, \phi_p) = (5\pi/12, 5\pi/12)$ .

In this case, it is observed that, unlike the spheroidal case (which remains stable throughout the  $\theta_p$  range), the mass scale corresponding to  $\Omega_-$  can be negative indicating an unstable mode. The corresponding growth rate  $\Gamma_{\Omega_-}$  can be obtained by solving the dispersion with the replacement  $\omega \rightarrow i\Gamma_{\Omega_-}$  *i.e.*, by solving the equation

$$(\omega = i\Gamma_{\Omega_-})^2 - p^2 - \Omega_-(\omega = i\Gamma_{\Omega_-}, p, \theta_p, \phi_p) = 0. \quad (4.16)$$

The corresponding solution of the growth rate is shown in the right panel of Fig. 4.3 with  $\theta_p$  and  $\phi_p$  both fixed at  $5\pi/12$ . It should be mentioned here that in this case the growth rate of the unstable mode has amplitudes similar to the spheroidal case [166] whereas, with positive anisotropy parameters, a several times larger growth rate can be observed for certain angular values as reported in Ref. [144].

## 4.3 Summary

In this chapter, we have studied the gluon polarization in presence of ellipsoidal momentum-space anisotropy. The momentum distribution function in our case is parametrized with two anisotropy parameters  $\xi_a$  and  $\xi_b$ , represented together as an anisotropy tuple  $\xi = (\xi_a, \xi_b)$ . This is a simple generalisation of the spheroidal RS form that has been extensively used in the literature. The general structure of the gluon polarization tensor in presence of such ellipsoidal anisotropy has been used and subsequently, the gluon effective propagator is obtained. As shown earlier, from the pole of the effective propagator, the three collective modes can be obtained in terms of the form factors. The results obtained using our formulation are in agreement with the previous study incorporating ellipsoidal anisotropy [144]. It should be mentioned here that it is not mandatory to consider the general structure of the polarization function to obtain the collective modes, as, those can also be obtained solving the characteristic equation directly (see for example [144]). However, one of the important advantages of considering the general structure is that, the collective modes, as in our case, can be expressed in terms of the form factors which do not depend on the choice of the frame of reference. As a consequence, it is possible to define mass scales by taking the static limits of the functions characterizing the collective modes ( $\Omega_0$  and  $\Omega_{\pm}$ ) in a similar fashion as done in case of spheroidal anisotropy. The importance of such definition lies in the fact that, the existence of instability can be inferred systematically by studying the angular variations of the mass scales. More specifically, for the given external angles, the negative value of the squared mass indicates that the corresponding mode is unstable. In our analysis with  $\xi_a = -0.5$  and  $\xi_b = -0.9$ , we have observed that, unlike the spheroidal case, the mode corresponding to  $\Omega_-$  becomes unstable. The appearance of such additional unstable mode in presence of ellipsoidal anisotropy may have important influences on the

#### Chapter 4. Gluon self-energy in presence of ellipsoidal anisotropy

isotropization of the QGP medium produced in HIC experiments. As mentioned earlier, the formulation, as developed in this work, will be particularly useful in the studies concerning the heavy quark potential in presence of ellipsoidal anisotropy. The usual procedure to obtain the hard-thermal loop resummed perturbative part of the heavy quark potential is to consider the Fourier transform of the 00-component of the effective propagator (obtained in Eq. (3.14)) in the static limits. Consequently, the non-trivial angular dependence enters in the potential through the mass scales. It should be noted that, in this work, only the retarded part of the gluon self energy is considered. On the other hand, the imaginary part of the potential can be obtained from the Feynman effective propagator in the real time Keldysh formalism [172]. Due to the azimuthal angular dependence of mass scales, a non-trivial modification in the real as well as in the imaginary parts of the heavy quark potential is expected in presence of ellipsoidal anisotropy which will be an interesting future direction.



# DAMPING RATE OF A HARD PHOTON IN A WEAKLY MAGNETIZED HOT MEDIUM

---

In this chapter, we have calculated the damping rate of hard photon in weakly magnetized hot QED plasma. The damping rate is calculated from the imaginary part of the each transverse dispersive modes in a thermomagnetic QED medium. This formalism can easily be extended to QCD plasma. This chapter is based on the work presented in the following paper: *Soft contribution to the damping rate of a hard photon in a weakly magnetized hot medium*

Ritesh Ghosh, Bithika Karmakar, Munshi G. Mustafa, *Phys. Rev. D* **101** (2020) 05, 056007, [[arXiv:1911.00744](https://arxiv.org/abs/1911.00744)].

## 5.1 Introduction

Astrophysical plasma is almost always immersed in magnetic field. Extreme, magnetized plasma is found in interiors of neutron star, magnetospheres of magnetars and central en-

## Chapter 5. Damping rate of a hard photon in a weakly magnetized hot medium

gines of supernovae and gamma ray bursts [190]. The propagation of photon through the hot magnetized plasma, *viz.*, electron-positron plasma (EPP), is of great interest. Because the magnetar phenomena are found by analyzing the high-energy radiation detected at earth. Thus it is very important to have a good understanding of the propagation of photon through the EPP. Furthermore, the phenomenon of Faraday rotation *i.e.*, change of polarization of photon while propagating through a medium has been studied in Ref. [191] in a field theoretical viewpoint. This has also been detected in several astrophysical objects [192]. Also high-intensity laser beams are used to create ultrarelativistic EPP of temperature around 10 MeV [193]. This EPP may play an important role in various astrophysical situations. Some properties of such plasma, *viz.*, the equation of state, dispersion relation of collective plasma modes of photon and electron, damping rates, mean free paths, transport coefficients and particle production rates, are studied using QED at finite temperature [194, 195]. On the other hand, as mentioned earlier in Sec. 1.5, the magnetic field as high as  $(15 - 20)m_\pi^2$  can be generated [64] at LHC energies in noncentral heavy ion collisions. The photon is considered as a good probe of the QGP medium as photon only interacts electromagnetically. Thus, it comes out of the hot QCD system without interacting much. The damping rate of the hard photon is associated with the mean free path of photon [196] and hard photon production rate in QGP [104].

Damping rate of photon is related to the imaginary part of photon dispersion in the medium [197] which is again related to the scattering crosssection of the process that we find by cutting the photon self-energy diagram [198]. In lowest order coupling constant, photons are damped by Compton scattering and pair creation process. In case of low momentum transfer, the damping rate shows infrared singularity. Thus one should consider the effective resummed propagator instead of bare propagator for soft momentum of fermion. We will call this as the soft contribution to the damping rate of photon. The hard contri-

## 5.1. Introduction

bution refers to the case where all the fermions in loop have momentum order of or much greater than the system temperature  $T$ . Both soft and hard contributions to the damping rate of hard photon in thermal medium have been calculated in Ref. [197]. The dispersion relations of photon are modified for a hot magnetized medium [199]. So the damping rate of photon will also get modified in a thermomagnetic medium. In this article we intend to compute the soft contribution to the hard photon damping rate for a weakly magnetized hot medium in one loop approximation of photon self-energy. In a thermomagnetic medium this would be a good indicator as higher loop calculation contributing to higher order would be extremely involved.

We consider hard photon of momentum  $P^\mu = (p_0, \mathbf{p})$  where  $p = |\mathbf{p}| \gg T$  in a relativistic hot magnetized QED medium. To find the soft contribution of the damping rate we introduce a separation scale  $\Lambda$  where  $eT \ll \Lambda \ll T$  ( $gT \ll \Lambda \ll T$  in case of QCD). In the soft part of the damping rate, the contribution from soft loop momentum involving a fermion is taken into account up to the separation scale  $\Lambda$ . Here we assume that the magnetic field strength is weak *i.e.*,  $\sqrt{eB} < eT < T$  ( $\sqrt{q_f B} < gT < T$  for QCD). We use the recently obtained effective fermion propagator [200] in presence of weak magnetic field for the soft fermion and Schwinger propagator for the hard fermion in the loop. The Braaten-Pisarki-Yuan formalism [201] has been used here to calculate the imaginary part of photon self-energy. Extension to the case of damping rate of hard photon in weakly magnetized hot QCD medium is straightforward. We need to consider the loop fermions as quark and antiquark in that case.

In Sec. 5.2 we describe the set up to calculate the photon damping rate associated with imaginary part of photon self-energy. In Sec. 5.3 the self-energy is obtained in a weak field approximation. The imaginary parts of various components of photon self-energy is obtained in Sec. 5.4. Results are given in Sec. 5.5. We conclude in Sec. 5.6.

## 5.2 SetUp

We consider plasma of electrons and positrons at temperature  $T$ . The  $z$ -axis of the lab frame is oriented along the magnetic field. The form of effective gauge boson propagator can be used from Chapter 3 for single anisotropy direction. Here we use the notations of tensors and form factors evaluated in Ref. [199]. The general covariant structure of photon self-energy in a magnetized hot medium can be written as

$$\Pi^{\mu\nu} = \beta B^{\mu\nu} + \sigma R^{\mu\nu} + \delta Q^{\mu\nu} + \alpha N^{\mu\nu}, \quad (5.1)$$

where various form factors can be written as

$$\begin{aligned} \beta &= B^{\mu\nu} \Pi_{\mu\nu}, \\ \sigma &= R^{\mu\nu} \Pi_{\mu\nu}, \\ \delta &= Q^{\mu\nu} \Pi_{\mu\nu}, \\ \alpha &= \frac{1}{2} N^{\mu\nu} \Pi_{\mu\nu}. \end{aligned} \quad (5.2)$$

The general covariant structure of photon propagator can be obtained [199] as

$$\begin{aligned} D_{\mu\nu} &= \frac{\xi P_\mu P_\nu}{P^4} + \frac{(P^2 - \delta) B_{\mu\nu}}{(P^2 - \beta)(P^2 - \delta) - \alpha^2} + \frac{R_{\mu\nu}}{P^2 - \sigma} + \frac{(P^2 - \beta) Q_{\mu\nu}}{(P^2 - \beta)(P^2 - \delta) - \alpha^2} \\ &+ \frac{\alpha N_{\mu\nu}}{(P^2 - \beta)(P^2 - \delta) - \alpha^2}. \end{aligned} \quad (5.3)$$

We note that the thermal medium (absence of magnetic field) has two dispersive modes of photon *i.e.*, one degenerate transverse mode and one medium induced plasmon mode due to breaking of boost invariance. Now breaking of rotational invariance in the presence of

## 5.2. SetUp

a magnetic field leads to three dispersive modes of photon by lifting the degeneracy of the transverse modes. These three dispersive modes can be seen from the pole of Eq. (5.3). Now, the dispersion relations can be written as

$$P^2 - \sigma = 0, \quad (5.4)$$

$$(P^2 - \delta)(P^2 - \beta) - \alpha^2 = \left( P^2 - \frac{\beta + \delta + \sqrt{(\beta - \delta)^2 + 4\alpha^2}}{2} \right) \times \left( P^2 - \frac{\beta + \delta - \sqrt{(\beta - \delta)^2 + 4\alpha^2}}{2} \right) = 0. \quad (5.5)$$

In weak magnetic field approximation  $\alpha$  does not contribute upto  $\mathcal{O}[(eB)]^2$ , one gets simple form of the above dispersive modes [202]

$$\begin{aligned} P^2 - \sigma &= 0, \\ P^2 - \beta &= 0, \\ P^2 - \delta &= 0. \end{aligned} \quad (5.6)$$

Damping rate is defined as the imaginary part of photon dispersion relation. The medium induced longitudinal (plasmon) mode does not contribute to the damping rate <sup>1</sup> and the dispersion relations for two transverse modes of a photon are given, respectively, as

$$P^2 - \sigma = 0, \quad P^2 - \delta = 0, \quad (5.7)$$

Damping rates  $\gamma_\delta(p)$  and  $\gamma_\sigma(p)$  (for no overdamping *i.e.*  $\gamma_i \ll p_0$  where  $i = \delta, \sigma$ ) of hard

---

<sup>1</sup> The longitudinal dispersive mode merges with the light cone at high photon momentum.

photon are given by imaginary part of the form factors as [203]

$$\gamma_\sigma(p) = -\frac{1}{2p} \text{Im} \sigma(p_0 = p), \quad (5.8)$$

$$\gamma_\delta(p) = -\frac{1}{2p} \text{Im} \delta(p_0 = p). \quad (5.9)$$

The tensor structures of  $R^{\mu\nu}$  and  $Q^{\mu\nu}$  [199] are given as

$$R^{\mu\nu} = \begin{pmatrix} 0 & 0 & 0 & 0 \\ 0 & 0 & 0 & 0 \\ 0 & 0 & -1 & 0 \\ 0 & 0 & 0 & 0 \end{pmatrix}, \quad Q^{\mu\nu} = \begin{pmatrix} 0 & 0 & 0 & 0 \\ 0 & -\cos^2 \theta_p & 0 & \sin \theta_p \cos \theta_p \\ 0 & 0 & 0 & 0 \\ 0 & \sin \theta_p \cos \theta_p & 0 & -\sin^2 \theta_p \end{pmatrix}. \quad (5.10)$$

Using Eq.(5.10) in Eq.(5.2) we can write the form factors  $\sigma$  and  $\delta$  in weak field approximation as

$$\sigma = -\left(\Pi_0^{22} + \Pi_2^{22}\right), \quad (5.11)$$

$$\begin{aligned} \delta &= -\cos^2 \theta_p \left(\Pi_0^{11} + \Pi_2^{11}\right) - \sin^2 \theta_p \left(\Pi_0^{33} + \Pi_2^{33}\right) \\ &+ 2 \sin \theta_p \cos \theta_p \left(\Pi_0^{13} + \Pi_2^{13}\right). \end{aligned} \quad (5.12)$$

Combining Eq.(5.8) with Eq.(5.11) and Eq.(5.9) with Eq.(5.12), the damping rates become

$$\gamma_\sigma(p) = \frac{1}{2p} \left(\text{Im} \Pi_0^{22} + \text{Im} \Pi_2^{22}\right), \quad (5.13)$$

$$\begin{aligned} \gamma_\delta(p) &= \frac{1}{2p} \left[ \cos^2 \theta_p \left(\text{Im} \Pi_0^{11} + \text{Im} \Pi_2^{11}\right) + \sin^2 \theta_p \left(\text{Im} \Pi_0^{33} + \text{Im} \Pi_2^{33}\right) \right. \\ &\left. - 2 \sin \theta_p \cos \theta_p \left(\text{Im} \Pi_0^{13} + \text{Im} \Pi_2^{13}\right) \right] \end{aligned} \quad (5.14)$$

### 5.3. Photon self-energy in hot magnetized medium

The damping rates in Eqs.(5.13) and (5.14) can now be written as

$$\gamma_\sigma(p) = \gamma_{\text{th}}(p) + \gamma_\sigma^B(p), \quad (5.15)$$

$$\gamma_\delta(p) = \gamma_{\text{th}}(p) + \gamma_\delta^B(p). \quad (5.16)$$

where  $\gamma_{\text{th}}$  is the  $\mathcal{O}[(eB)^0]$  contribution or thermal contribution is given as

$$\begin{aligned} \gamma_{\text{th}}(p) &= \frac{1}{2p} \text{Im}\Pi_0^{22} = \frac{1}{2p} \left[ \cos^2 \theta_p \text{Im}\Pi_0^{11} + \sin^2 \theta_p \text{Im}\Pi_0^{33} \right. \\ &\quad \left. - 2 \sin \theta_p \cos \theta_p \text{Im}\Pi_0^{13} \right]. \end{aligned} \quad (5.17)$$

The thermomagnetic corrections of  $\mathcal{O}[(eB)^2]$  are given as

$$\gamma_\sigma^B(p) = \frac{1}{2p} \text{Im}\Pi_2^{22}, \quad (5.18)$$

$$\gamma_\delta^B(p) = \frac{1}{2p} \left[ \cos^2 \theta_p \text{Im}\Pi_2^{11} + \sin^2 \theta_p \text{Im}\Pi_2^{33} - 2 \sin \theta_p \cos \theta_p \text{Im}\Pi_2^{13} \right]. \quad (5.19)$$

We need to obtain the imaginary parts of 11, 22, 33 and 13 components of the photon self-energy  $\Pi^{\mu\nu}$  which are computed in the following sections.

## 5.3 Photon self-energy in hot magnetized medium

The photon self-energy as shown in Fig. 5.1 can be written as

$$\Pi_{\mu\nu}(P) = ie^2 \int \frac{d^4K}{(2\pi)^4} \left\{ \text{Tr}[\gamma_\mu S^*(K)\gamma_\nu S(Q)] + \text{Tr}[\gamma_\nu S^*(K)\gamma_\mu S(Q)] \right\}. \quad (5.20)$$

where  $S^*(K)$  is effective electron propagator and  $S(K)$  is Schwinger propagator for bare electron. As the external photon is hard, we consider one bare and one effective fermion

propagator in the loop. In the following we would obtain the propagators for fermion.

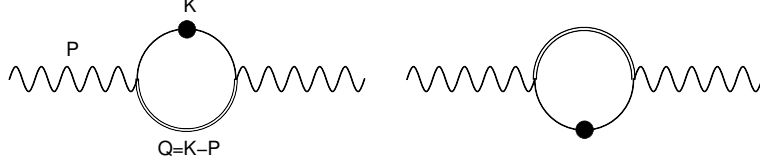


Figure 5.1: Photon self-energy where the blob represents the effective electron propagator in magnetic field and double line represents bare electron propagator in magnetic field

### 5.3.1 Fermion propagator in weak field approximation

In the weak magnetic field limit, *i.e.*,  $\sqrt{eB} < m_{\text{th}} \sim eT < T$  the Schwinger propagator for fermion can be written up to  $\mathcal{O}[(eB)^2]$  as [100]

$$\begin{aligned}
 S(K) &= \frac{\not{K} + m_f}{K^2 - m_f^2} + i\gamma^1\gamma^2 \frac{\not{K}_{\parallel} + m_f}{(K^2 - m_f^2)^2} (eB) \\
 &+ 2 \left[ \frac{\{(K \cdot u)\not{u} - (K \cdot n)\not{n}\} - \not{K}}{(K^2 - m_f^2)^3} - \frac{k_{\perp}^2 (\not{K} + m_f)}{(K^2 - m_f^2)^4} \right] (eB)^2 \\
 &+ \mathcal{O}[(eB)^3] \\
 &= S_0 + S_1 + S_2 + \mathcal{O}[(eB)^3].
 \end{aligned} \tag{5.21}$$

The general form of fermion self-energy in a weakly magnetized medium can be written as [200]

$$\Sigma(K) = -a\not{K} - b\not{u} - b'\gamma_5\not{u} - c'\gamma_5\not{n}. \tag{5.22}$$

In one loop order, the form factors are given as

$$a(k_0, k) = -\frac{m_{\text{th}}^2}{k^2} Q_1 \left( \frac{k_0}{k} \right), \tag{5.23}$$



### 5.3. Photon self-energy in hot magnetized medium

$$b(k_0, k) = \frac{m_{\text{th}}^2}{k} \left[ \frac{k_0}{k} Q_1\left(\frac{k_0}{k}\right) - Q_0\left(\frac{k_0}{k}\right) \right], \quad (5.24)$$

$$b'(k_0, k) = 4e^2 M^2(T, m_f, eB) \frac{k_3}{k^2} Q_1\left(\frac{k_0}{k}\right), \quad (5.25)$$

$$c'(k_0, k) = 4e^2 M^2(T, m_f, eB) \frac{1}{k} Q_0\left(\frac{k_0}{k}\right), \quad (5.26)$$

where Legendre function of second kind are given as

$$Q_0(x) = \frac{1}{2} \ln \left( \frac{x+1}{x-1} \right), \quad (5.27)$$

$$Q_1(x) = xQ_0(x) - 1, \quad (5.28)$$

and the thermomagnetic mass is given as

$$M^2(T, m_f, eB) = \frac{eB}{16\pi^2} \left[ \ln 2 - \frac{\pi T}{2m_f} \right], \quad (5.29)$$

whereas thermal mass is given as

$$m_{\text{th}}^2 = \frac{1}{8} e^2 T^2. \quad (5.30)$$

The effective fermion propagator can be written [200] as

$$\begin{aligned} S^*(K) &= P_- \frac{\not{L}(K)}{L^2} P_+ + P_+ \frac{\not{R}(K)}{R^2} P_- \\ &= S_L^*(K) + S_R^*(K), \end{aligned} \quad (5.31)$$

where chirality projection operators are given by

$$P_{\pm} = \frac{1}{2} (1 \pm \gamma_5), \quad (5.32)$$

## Chapter 5. Damping rate of a hard photon in a weakly magnetized hot medium

and  $L^\mu$  and  $R^\mu$  are given as

$$L^\mu = (1+a)K^\mu + (b+b')u^\mu + c'n^\mu, \quad (5.33)$$

$$R^\mu = (1+a)K^\mu + (b-b')u^\mu - c'n^\mu. \quad (5.34)$$

For simplicity of calculation we expand the effective fermion propagator in Eq. (5.31) in powers of  $eB$  and keep terms up to  $\mathcal{O}[(eB)^2]$  as

$$S^*(K) = S_0^*(K) + S_1^*(K) + S_2^*(K) + \mathcal{O}[(eB)^3], \quad (5.35)$$

where  $S_0^*(K)$  is  $\mathcal{O}[(eB)^0]$  and given as

$$S_0^*(K) = \frac{(1+a)\not{K} + b\not{t}}{D^2} = \frac{(1+a)\not{K} + b\not{t}}{D_+D_-}, \quad (5.36)$$

where  $D_\pm = (1+a)(k_0 \mp k) + b$ .

Equation (5.36) is the effective HTL fermion propagator [150, 204] in thermal medium.

The  $\mathcal{O}[(eB)]$  is obtained as

$$\begin{aligned} S_1^*(K) = & \frac{1}{D^4} \left[ 2(1+a)\not{K}\gamma_5 \left\{ -(1+a)k_3 c' - (1+a)k_0 b' - bb' \right\} \right. \\ & + \not{t}\gamma_5 \left\{ \left( (1+a)^2 K^2 - b^2 \right) b' - 2(a+1)bc'k_3 \right\} \\ & \left. + c\not{t}'\gamma_5 \left\{ \left( 2(1+a)k_0 + b \right) b + (a+1)^2 K^2 \right\} \right], \end{aligned} \quad (5.37)$$

whereas  $\mathcal{O}[(eB)^2]$  is obtained as

$$S_2^*(K) = \left[ \frac{\left( 2b' \left\{ (1+a)k_0 + b \right\} + 2c'k_3(1+a) \right)^2}{D^6} - \frac{b'^2 - c'^2}{D^4} \right] \left\{ (1+a)\not{K} + b\not{t} \right\}$$

### 5.3. Photon self-energy in hot magnetized medium

$$\begin{aligned}
& - \frac{\left(2b'\{(1+a)k_0+b\}+2c'k_3(1+a)\right)(b'\psi+c'\eta)}{D^4} \\
& = \left(\frac{h^2(k_0, k_\perp, k_3)}{D^6} - \frac{h'}{D^4}\right)\{(1+a)K+b\psi\} \\
& - \frac{h(k_0, k_\perp, k_3)}{D^4}(b'\psi+c'\eta), \tag{5.38}
\end{aligned}$$

where  $h = 2b'\{(1+a)k_0+b\} + 2c'k_3(1+a)$  and  $h' = b'^2 - c'^2$ .

### 5.3.2 Photon self-energy in weak magnetic field

Now the  $\mathcal{O}[(eB)^0]$  contribution of  $\Pi^{\mu\nu}$  given in Eq. (5.20) can be written as

$$\begin{aligned}
\Pi_0^{\mu\nu} & = ie^2 \int \frac{d^4K}{(2\pi)^4} \left\{ \text{Tr}[\gamma_\mu S_0^*(K)\gamma_\nu S_0(Q)] + \text{Tr}[\gamma_\nu S_0^*(K)\gamma_\mu S_0(Q)] \right\} \\
& = ie^2 \int \frac{d^4K}{(2\pi)^4} \left\{ \text{Tr} \left[ \gamma^\mu \left( \frac{\gamma_0 - \tilde{\gamma} \cdot \hat{\mathbf{k}}}{2D_+} + \frac{\gamma_0 + \tilde{\gamma} \cdot \hat{\mathbf{k}}}{2D_-} \right) \gamma^\nu \left( f_0^{(1)} \gamma^0 - f_0^{(0)} \tilde{\gamma} \cdot \mathbf{q} \right) \right] \right. \\
& + \left. \text{Tr} \left[ \gamma^\nu \left( \frac{\gamma_0 - \tilde{\gamma} \cdot \hat{\mathbf{k}}}{2D_+} + \frac{\gamma_0 + \tilde{\gamma} \cdot \hat{\mathbf{k}}}{2D_-} \right) \gamma^\mu \left( f_0^{(1)} \gamma^0 - f_0^{(0)} \tilde{\gamma} \cdot \mathbf{q} \right) \right] \right\} \\
& = 8ie^2 \int \frac{d^4K}{(2\pi)^4} \frac{1}{D_+ D_- Q^2} (1+a) \\
& \times \left\{ (K^\mu Q^\nu + K^\nu Q^\mu) - g^{\mu\nu} K \cdot Q \right\} + b \left\{ (Q^\mu u^\nu + Q^\nu u^\mu) - g^{\mu\nu} Q \cdot u \right\}, \tag{5.39}
\end{aligned}$$

where

$$\begin{aligned}
f_0^{(1)} & = \frac{q_0}{Q^2}, \quad f_0^{(0)} = \frac{1}{Q^2}, \\
f_1^{(1)} & = \frac{q_0}{Q^4}, \quad f_1^{(0)} = \frac{1}{Q^4}. \tag{5.40}
\end{aligned}$$

## Chapter 5. Damping rate of a hard photon in a weakly magnetized hot medium

The  $\mathcal{O}[(eB)]$  contribution of  $\Pi^{\mu\nu}$  is given as

$$\begin{aligned} \Pi_1^{\mu\nu} &= ie^2 \int \frac{d^4 K}{(2\pi)^4} \left\{ \text{Tr}[\gamma_\mu S_0^*(K) \gamma_\nu S_1(Q)] + \text{Tr}[\gamma_\nu S_0^*(K) \gamma_\mu S_1(Q)] \right. \\ &\quad \left. + \text{Tr}[\gamma_\mu S_1^*(K) \gamma_\nu S_0(Q)] + \text{Tr}[\gamma_\nu S_1^*(K) \gamma_\mu S_0(Q)] \right\}, \end{aligned} \quad (5.41)$$

which becomes zero.

The  $\mathcal{O}[(eB)^2]$  contribution of  $\Pi^{\mu\nu}$  is given as

$$\begin{aligned} \Pi_2^{\mu\nu} &= ie^2 \int \frac{d^4 K}{(2\pi)^4} \left\{ \text{Tr}[\gamma_\mu S_1^*(K) \gamma_\nu S_1(Q)] + \text{Tr}[\gamma_\nu S_1^*(K) \gamma_\mu S_1(Q)] \right. \\ &\quad + \text{Tr}[\gamma_\mu S_0^*(K) \gamma_\nu S_2(Q)] + \text{Tr}[\gamma_\nu S_0^*(K) \gamma_\mu S_2(Q)] \\ &\quad \left. + \text{Tr}[\gamma_\mu S_2^*(K) \gamma_\nu S_0(Q)] + \text{Tr}[\gamma_\nu S_2^*(K) \gamma_\mu S_0(Q)] \right\}. \end{aligned} \quad (5.42)$$

We calculate the above mentioned trace as follows. The trace of the first and second terms of Eq. (5.42) can be calculated as

$$\begin{aligned} &\text{Tr}[\gamma_\mu S_1^*(K) \gamma_\nu S_1(Q)] + \text{Tr}[\gamma_\nu S_1^*(K) \gamma_\mu S_1(Q)] \\ &= \frac{8(eB)}{D^2(Q^2 - m_f^2)^2} \left[ b' \left\{ (u^\mu n^\nu + u^\nu n^\mu)(Q \cdot u) - 2u^\mu u^\nu (Q \cdot n) + g^{\mu\nu} (Q \cdot n) \right\} \right. \\ &\quad \left. + c' \left\{ 2n^\mu n^\nu (Q \cdot u) - (n^\mu u^\nu + n^\nu u^\mu)(Q \cdot n) + g^{\mu\nu} (Q \cdot u) \right\} \right] - \frac{8(eB)}{D^4(Q^2 - m_f^2)^2} \\ &\quad \times \left[ h \left\{ (1+a) \left( g^{\mu\nu} \left( (K \cdot u)(Q \cdot n) - (K \cdot n)(Q \cdot u) \right) \right. \right. \right. \\ &\quad \left. \left. - (K^\mu u^\nu + K^\nu u^\mu) Q \cdot n + (K^\mu n^\nu + K^\nu n^\mu) Q \cdot u \right) \right. \\ &\quad \left. \left. + b \left( g^{\mu\nu} Q \cdot n + (u^\mu n^\nu + u^\nu n^\mu) Q \cdot u - 2u^\mu u^\nu Q \cdot n \right) \right\} \right]. \end{aligned} \quad (5.43)$$

### 5.3. Photon self-energy in hot magnetized medium

The trace of third and fourth terms in Eq. (5.42) can be obtained as

$$\begin{aligned}
& \text{Tr}[\gamma_\mu S_0^*(K)\gamma_\nu S_2(Q)] + \text{Tr}[\gamma_\nu S_0^*(K)\gamma_\mu S_2(Q)] \\
&= \frac{8(eB)^2}{D_+(Q^2 - m_f^2)^3} \left[ q_0 \left( \hat{K}^\mu g^{0\nu} + \hat{K}^\nu g^{0\mu} - g^{\mu\nu} \right) - q_3 \left( \hat{K}^\mu g^{3\nu} + \hat{K}^\nu g^{3\mu} - g^{\mu\nu} \hat{k}_3 \right) \right. \\
&\quad \left. - \left( \hat{K}^\mu Q^\nu + \hat{K}^\nu Q^\mu - g^{\mu\nu} \hat{K} \cdot Q \right) \right] - \frac{8(eB)^2 q_\perp^2}{D_+(Q^2 - m_f^2)^4} \left[ \hat{K}^\mu Q^\nu + \hat{K}^\nu Q^\mu - g^{\mu\nu} \hat{K} \cdot Q \right] \\
&\quad + \frac{8(eB)^2}{D_-(Q^2 - m_f^2)^3} \left[ q_0 \left( \hat{K}'^\mu g^{0\nu} + \hat{K}'^\nu g^{0\mu} - g^{\mu\nu} \right) - q_3 \left( \hat{K}'^\mu g^{3\nu} + \hat{K}'^\nu g^{3\mu} + g^{\mu\nu} \hat{k}_3 \right) \right. \\
&\quad \left. - \left( \hat{K}'^\mu Q^\nu + \hat{K}'^\nu Q^\mu - g^{\mu\nu} \hat{K}' \cdot Q \right) \right] \\
&\quad - \frac{8(eB)^2 q_\perp^2}{D_-(Q^2 - m_f^2)^4} \left[ \hat{K}'^\mu Q^\nu + \hat{K}'^\nu Q^\mu - g^{\mu\nu} \hat{K}' \cdot Q \right], \tag{5.44}
\end{aligned}$$

where  $\hat{K}'^\mu = (1, -\hat{\mathbf{k}})$ .

The trace of fifth and sixth terms in Eq. (5.42) are obtained as

$$\begin{aligned}
& \text{Tr}[\gamma_\mu S_2^*(K)\gamma_\nu S_0(Q)] + \text{Tr}[\gamma_\nu S_2^*(K)\gamma_\mu S_0(Q)] \\
&= \frac{8}{(Q^2 - m_f^2)} \left[ \left( \frac{h^2}{D^6} - \frac{h'}{D^4} \right) (1 + a) \left( K^\mu Q^\nu + K^\nu Q^\mu - g^{\mu\nu} K \cdot Q \right) \right. \\
&\quad + \left( b \left( \frac{h^2}{D^6} - \frac{h'}{D^4} \right) - b' \frac{h}{D^4} \right) \times \left( g^{\mu 0} Q^\nu + g^{\nu 0} Q^\mu - g^{\mu\nu} q_0 \right) \\
&\quad \left. - c' \frac{h}{D^4} \left( g^{\mu 3} Q^\nu + g^{\nu 3} Q^\mu - g^{\mu\nu} q_3 \right) \right]. \tag{5.45}
\end{aligned}$$

The photon self-energy in weak field approximation now can be decomposed using Eqs.(5.39),(5.41),(5.42) as

$$\Pi^{\mu\nu}(P) = \Pi_0^{\mu\nu}(P) + \Pi_2^{\mu\nu}(P), \tag{5.46}$$

where the first term is a pure thermal( $\mathcal{O}[(eB)^0]$ ) contribution and second term is thermo-

magnetic correction of  $\mathcal{O}[(eB)^2]$ .

Now the  $\mathcal{O}[(eB)^0]$  expression of  $\Pi^{11}$ ,  $\Pi^{22}$ ,  $\Pi^{33}$ , and  $\Pi^{13}$  can be written from Eq. (5.39)

as

$$\begin{aligned}
 \Pi_0^{11}(p_0, p) &= 8ie^2 \int \frac{d^4K}{(2\pi)^4} \frac{(1+a)(k_0q_0 + 2k_1q_1 - \mathbf{k} \cdot \mathbf{q}) + bq_0}{\left\{((1+a)k_0 + b)^2 - (1+a)^2k^2\right\} Q^2} \\
 &= -4e^2 \not\int \left[ \left( \frac{f_0^{(1)}}{D_+} + \frac{f_0^{(1)}}{D_-} \right) + (2\hat{k}_1q_1 - \hat{k} \cdot q) \left\{ \frac{f_0^{(0)}}{D_+} - \frac{f_0^{(0)}}{D_-} \right\} \right], \\
 \Pi_0^{22}(p_0, p) &= 8ie^2 \int \frac{d^4K}{(2\pi)^4} \frac{(1+a)(k_0q_0 + 2k_2q_2 - \mathbf{k} \cdot \mathbf{q}) + bq_0}{\left\{((1+a)k_0 + b)^2 - (1+a)^2k^2\right\} Q^2} \\
 &= -4e^2 \not\int \left[ \left( \frac{f_0^{(1)}}{D_+} + \frac{f_0^{(1)}}{D_-} \right) + (2\hat{k}_2q_2 - \hat{k} \cdot q) \left\{ \frac{f_0^{(0)}}{D_+} - \frac{f_0^{(0)}}{D_-} \right\} \right], \\
 \Pi_0^{33}(p_0, p) &= 8ie^2 \int \frac{d^4K}{(2\pi)^4} \frac{(1+a)(k_0q_0 + 2k_3q_3 - \mathbf{k} \cdot \mathbf{q}) + bq_0}{\left\{((1+a)k_0 + b)^2 - (1+a)^2k^2\right\} Q^2} \\
 &= -4e^2 \not\int \left[ \left( \frac{f_0^{(1)}}{D_+} + \frac{f_0^{(1)}}{D_-} \right) - (\hat{k} \cdot q - 2\hat{k}_3q_3) \left\{ \frac{f_0^{(0)}}{D_+} - \frac{f_0^{(0)}}{D_-} \right\} \right], \\
 \Pi_0^{13}(p_0, p) &= 8ie^2 \int \frac{d^4K}{(2\pi)^4} \frac{(1+a)(k_1q_3 + q_1k_3)}{\left\{((1+a)k_0 + b)^2 - (1+a)^2k^2\right\} Q^2} \\
 &= -4e^2 \not\int \left[ (\hat{k}_1q_3 + q_1\hat{k}_3) \left\{ \frac{f_0^{(0)}}{D_+} - \frac{f_0^{(0)}}{D_-} \right\} \right]. \tag{5.47}
 \end{aligned}$$

Using Eqs.(5.42),(5.43),(5.44) and (5.45), one can write the  $\mathcal{O}[(eB)^2]$  expression of  $\Pi^{11}$ ,  $\Pi^{22}$ ,  $\Pi^{33}$ , and  $\Pi^{13}$  as

$$\begin{aligned}
 \Pi_2^{11} &= -e^2 \not\int \left[ -\frac{8eB}{D^2(Q^2 - m_f^2)^2} \left\{ b'q_3 + c'q_0 \right\} \right. \\
 &\quad \left. + \frac{8eB}{D^4(Q^2 - m_f^2)^2} h \left\{ (1+a)(k_0q_3 - k_3q_0) + bq_3 \right\} \right]
 \end{aligned}$$

### 5.3. Photon self-energy in hot magnetized medium

$$\begin{aligned}
& + \frac{8(eB)^2}{D_+(Q^2 - m_f^2)^3} (\hat{k}_2 q_2 - \hat{k}_1 q_1) - \frac{8(eB)^2 q_\perp^2}{D_+(Q^2 - m_f^2)^4} (q_0 - \hat{k} \cdot q + 2\hat{k}_1 q_1) \\
& - \frac{8(eB)^2}{D_-(Q^2 - m_f^2)^3} (\hat{k}_2 q_2 - \hat{k}_1 q_1) - \frac{8(eB)^2 q_\perp^2}{D_-(Q^2 - m_f^2)^4} (q_0 + \hat{k} \cdot q - 2\hat{k}_1 q_1) \\
& + \frac{8}{(Q^2 - m_f^2)} \left\{ \left( \frac{h^2}{D^6} - \frac{h'}{D^4} \right) (1+a)(2k_1 q_1 + K \cdot Q) \right. \\
& \left. + \left( b \left( \frac{h^2}{D^6} - \frac{h'}{D^4} \right) - \frac{b'h}{D^4} \right) q_0 - \frac{c'h}{D^4} q_3 \right\}, \tag{5.48}
\end{aligned}$$

$$\begin{aligned}
\Pi_2^{22} & = -e^2 \not{\Sigma} \left[ -\frac{8eB}{D^2(Q^2 - m_f^2)^2} \left\{ b'q_3 + c'q_0 \right\} \right. \\
& + \frac{8eB}{D^4(Q^2 - m_f^2)^2} h \left\{ (1+a)(k_0 q_3 - k_3 q_0) + bq_3 \right\} \\
& + \frac{8(eB)^2}{D_+(Q^2 - m_f^2)^3} (\hat{k}_1 q_1 - \hat{k}_2 q_2) - \frac{8(eB)^2 q_\perp^2}{D_+(Q^2 - m_f^2)^4} (q_0 - \hat{k} \cdot q + 2\hat{k}_2 q_2) \\
& - \frac{8(eB)^2}{D_-(Q^2 - m_f^2)^3} (\hat{k}_1 q_1 - \hat{k}_2 q_2) - \frac{8(eB)^2 q_\perp^2}{D_-(Q^2 - m_f^2)^4} (q_0 + \hat{k} \cdot q - 2\hat{k}_2 q_2) \\
& + \frac{8}{(Q^2 - m_f^2)} \left\{ \left( \frac{h^2}{D^6} - \frac{h'}{D^4} \right) (1+a)(2k_2 q_2 + K \cdot Q) \right. \\
& \left. + \left( b \left( \frac{h^2}{D^6} - \frac{h'}{D^4} \right) - \frac{b'h}{D^4} \right) q_0 - \frac{c'h}{D^4} q_3 \right\}, \tag{5.49}
\end{aligned}$$

$$\begin{aligned}
\Pi_2^{33} & = -e^2 \not{\Sigma} \left[ \frac{8eB}{D^2(Q^2 - m_f^2)^2} \left\{ -b'q_3 + c'q_0 \right\} \right. \\
& + \frac{8eB}{D^4(Q^2 - m_f^2)^2} h \left\{ (1+a)(k_0 q_3 + k_3 q_0) + bq_3 \right\} \\
& + \frac{8(eB)^2}{D_+(Q^2 - m_f^2)^3} (-q_3 \hat{k}_3 + \hat{k} \cdot q) - \frac{8(eB)^2 q_\perp^2}{D_+(Q^2 - m_f^2)^4} (q_0 - \hat{k} \cdot q + 2q_3 \hat{k}_3)
\end{aligned}$$

$$\begin{aligned}
 & + \frac{8(eB)^2}{D_-(Q^2 - m_f^2)^3} (q_3 \hat{k}_3 - \hat{k} \cdot q) - \frac{8(eB)^2 q_\perp^2}{D_-(Q^2 - m_f^2)^4} (q_0 + \hat{k} \cdot q - 2q_3 \hat{k}_3) \\
 & + \frac{8}{(Q^2 - m_f^2)} \left\{ \left( \frac{h^2}{D^6} - \frac{h'}{D^4} \right) (1+a)(2k_3 q_3 + K \cdot Q) \right. \\
 & \left. + \left( b \left( \frac{h^2}{D^6} - \frac{h'}{D^4} \right) - \frac{b'h}{D^4} \right) q_0 + \frac{c'h}{D^4} q_3 \right\}, \tag{5.50}
 \end{aligned}$$

$$\begin{aligned}
 \Pi_2^{13} & = -e^2 \not{\int} \left[ \frac{8eB}{D^4(Q^2 - m_f^2)^2} h(1+a)(k_1 q_0) \right. \\
 & - \frac{8(eB)^2}{D_+(Q^2 - m_f^2)^3} \hat{k}_3 q_1 - \frac{8(eB)^2 q_\perp^2}{D_+(Q^2 - m_f^2)^4} \\
 & \times \left( \hat{k}_1 q_3 + \hat{k}_3 q_1 \right) + \frac{8(eB)^2}{D_-(Q^2 - m_f^2)^3} \hat{k}_3 q_1 + \frac{8(eB)^2 q_\perp^2}{D_-(Q^2 - m_f^2)^4} \left( \hat{k}_1 q_3 + \hat{k}_3 q_1 \right) \\
 & \left. + \frac{8}{(Q^2 - m_f^2)} \times \left\{ \left( \frac{h^2}{D^6} - \frac{h'}{D^4} \right) (1+a) (k_1 q_3 + k_3 q_1) + \frac{c'h}{D^4} q_1 \right\} \right]. \tag{5.51}
 \end{aligned}$$

## 5.4 Imaginary parts of the components of the photon self-energy

Before obtaining the imaginary parts, we discuss below the various approximations used in this calculation.

1. We have considered the momentum of photon as hard ( $p \gg T$ ). The momentum of soft fermion  $k \ll T$ . Thus we can take the following approximations:

$$n_F(\omega) \sim 1, \quad n_F(p - \omega) \sim e^{-p/T}, \quad e^{-p/T} \sim 0. \tag{5.52}$$

2. An upper cutoff  $\Lambda (< T)$  of the soft fermion momentum  $k$  has been introduced in the



#### 5.4. Imaginary parts of the components of the photon self-energy

integrations.

3. We consider  $m_f = m_{\text{th}}$  for electron.

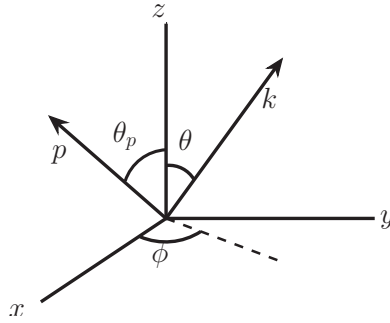


Figure 5.2: Choice of reference frame for computing the various components of photon self-energy. The magnetic field is along z-direction and  $\theta_p$  is the angle between momentum of photon and the external magnetic field.

4. To perform the various integrations we choose a frame of reference as shown in Fig. 5.2 in which the external momentum of the photon is in  $xz$  plane with  $0 < \theta_p < \pi/2$ . So one can write

$$\mathbf{p} \equiv (p \sin \theta_p, 0, p \cos \theta_p), \quad (5.53)$$

and then the loop momentum as

$$\mathbf{k} \equiv (k \sin \theta \cos \phi, k \sin \theta \sin \phi, k \cos \theta). \quad (5.54)$$

In the following subsection we will obtain imaginary parts of various self-energy components.

### 5.4.1 Imaginary parts of the magnetic field independent part, *i.e.* $\mathcal{O}[(eB)^0]$

We evaluate the imaginary parts of  $\Pi_0^{11}$ ,  $\Pi_0^{22}$ ,  $\Pi_0^{33}$ , and  $\Pi_0^{13}$  using the Braaten-Pisarski-Yuan method [197, 201].

$$\begin{aligned} \text{Im } \Pi_0^{11} &= -4e^2\pi(1 - e^{p/T}) \int \frac{d^3k}{(2\pi)^3} \int_{-\infty}^{\infty} \int_{-\infty}^{\infty} d\omega d\omega' n_F(\omega) n_F(\omega') \left\{ \rho_0^{(1)}(\omega') \left( \rho_{D_+}(\omega) \right. \right. \\ &\quad \left. \left. + \rho_{D_-}(\omega) \right) - (\hat{k} \cdot q - 2\hat{k}_1 q_1) \left( \rho_{D_+}(\omega) - \rho_{D_-}(\omega) \right) \rho_0^{(0)}(\omega') \right\} \delta(\omega + \omega' - p), \end{aligned} \quad (5.55)$$

$$\begin{aligned} \text{Im } \Pi_0^{22} &= -4e^2\pi(1 - e^{p/T}) \int \frac{d^3k}{(2\pi)^3} \int_{-\infty}^{\infty} \int_{-\infty}^{\infty} d\omega d\omega' n_F(\omega) n_F(\omega') \left\{ \rho_0^{(1)}(\omega') \left( \rho_{D_+}(\omega) \right. \right. \\ &\quad \left. \left. + \rho_{D_-}(\omega) \right) - (\hat{k} \cdot q - 2\hat{k}_2 q_2) \left( \rho_{D_+}(\omega) - \rho_{D_-}(\omega) \right) \rho_0^{(0)}(\omega') \right\} \delta(\omega + \omega' - p), \end{aligned} \quad (5.56)$$

$$\begin{aligned} \text{Im } \Pi_0^{33} &= -4e^2\pi(1 - e^{p/T}) \int \frac{d^3k}{(2\pi)^3} \int_{-\infty}^{\infty} \int_{-\infty}^{\infty} d\omega d\omega' n_F(\omega) n_F(\omega') \left\{ \rho_0^{(1)}(\omega') \left( \rho_{D_+}(\omega) \right. \right. \\ &\quad \left. \left. + \rho_{D_-}(\omega) \right) - (\hat{k} \cdot q - 2\hat{k}_3 q_3) \left( \rho_{D_+}(\omega) - \rho_{D_-}(\omega) \right) \rho_0^{(0)}(\omega') \right\} \delta(\omega + \omega' - p), \end{aligned} \quad (5.57)$$

$$\begin{aligned} \text{Im } \Pi_0^{13} &= -4e^2\pi(1 - e^{p/T}) \int \frac{d^3k}{(2\pi)^3} \int_{-\infty}^{\infty} \int_{-\infty}^{\infty} d\omega d\omega' n_F(\omega) n_F(\omega') \left\{ (\hat{k}_1 q_3 + q_1 \hat{k}_3) \right. \\ &\quad \left. \times \left( \rho_{D_+}(\omega) - \rho_{D_-}(\omega) \right) \rho_0^{(0)}(\omega') \right\} \delta(\omega + \omega' - p), \end{aligned} \quad (5.58)$$

#### 5.4. Imaginary parts of the components of the photon self-energy

where  $\rho_0^{(0)}, \rho_0^{(1)}, \rho_1^{(0)}, \rho_1^{(1)}, \rho_{D_+}$  and  $\rho_{D_-}$  are spectral representation of  $f_0^{(0)}, f_0^{(1)}, f_1^{(0)}, f_1^{(1)}$ ,  $1/D_+$  and  $1/D_-$  respectively. These spectral functions are obtained in Appendix A. We know that both  $\rho_{D_+}$  and  $\rho_{D_-}$  have pole containing the mass shell  $\delta$ -function + Landau cut part in space like region whereas  $\rho_0^{(0)}, \rho_0^{(1)}, \rho_1^{(0)}, \rho_1^{(1)}$  have only pole containing the mass shell  $\delta$  function. Since imaginary parts of various components of the self-energy contain the product of two spectral functions, it would then have the *pole-pole* and the *pole-cut* contributions.

The pole-pole parts of  $\text{Im}\Pi_{11}$ ,  $\text{Im}\Pi_{22}$ ,  $\text{Im}\Pi_{33}$  and  $\text{Im}\Pi_{13}$  contain  $\delta(p - \omega_{\pm} - q)$  where  $\omega_{\pm}$  is the energy of the fermion quasiparticle,  $\mathbf{k}$  and  $\mathbf{q} = \mathbf{k} - \mathbf{p}$  are the momenta of soft and hard fermion, respectively. Hence  $\omega_{\pm} > k$ . The  $\delta$ -function yields

$$p - \omega_{\pm} - q = 0$$

$$\cos \phi \approx \frac{\omega_{\pm}/k - \cos \theta \cos \theta_p}{\sin \theta \sin \theta_p}.$$

The value of  $\frac{\omega_{\pm}/k - \cos \theta \cos \theta_p}{\sin \theta \sin \theta_p}$  excludes the range  $[-1, 1]$  for all values of the parameters  $\theta$  and  $\theta_p$ . This restriction is valid for both thermal and the magnetic case. Thus pole-pole parts do not contribute in this calculation [104, 197]. In  $\mathcal{O}[(eB)^0]$  the contribution comes only from the *pole-cut* part.

#### **Pole-cut part of $\mathcal{O}[(eB)^0]$**

Now we would find the *pole-cut* part of the above self-energy components in Eqs.(5.55), (5.56), (5.57) and (5.58) as

Chapter 5. Damping rate of a hard photon in a weakly magnetized hot medium

$$\begin{aligned}
& \text{Im } \Pi_0^{11} \Big|_{\text{pole-cut}} \\
&= 2e^2 \pi (1 - e^{p/T}) \int \frac{d^3 k}{(2\pi)^3} \int_{-\infty}^{\infty} \int_{-\infty}^{\infty} d\omega d\omega' n_F(\omega) n_F(\omega') \left\{ \delta(\omega' - q) \Theta(k^2 - \omega^2) \right. \\
&\times \left. \left( \beta_+(\omega) + \beta_-(\omega) \right) - \frac{1}{q} (\hat{k} \cdot q - 2\hat{k}_1 q_1) \delta(\omega' - q) \Theta(k^2 - \omega^2) \left( \beta_+(\omega) - \beta_-(\omega) \right) \right\} \\
&\times \delta(p - \omega - \omega'), \\
&= -e^2 \pi \int_0^\Lambda \frac{k^2 dk}{2\pi^2} \int_0^\pi \frac{1}{2} \sin \theta d\theta \int_0^{2\pi} \frac{d\phi}{2\pi} \int_{-k}^k d\omega \left\{ \left( \beta_+(\omega) + \beta_-(\omega) \right) \right. \\
&- \left. \frac{1}{q} (\hat{k} \cdot q - 2\hat{k}_1 q_1) \times \left( \beta_+(\omega) - \beta_-(\omega) \right) \right\} \delta(p - \omega - q), \tag{5.59}
\end{aligned}$$

$$\begin{aligned}
& \text{Im } \Pi_0^{22} \Big|_{\text{pole-cut}} \\
&= 2e^2 \pi (1 - e^{p/T}) \int \frac{d^3 k}{(2\pi)^3} \int_{-\infty}^{\infty} \int_{-\infty}^{\infty} d\omega d\omega' n_F(\omega) n_F(\omega') \left\{ \delta(\omega' - q) \Theta(k^2 - \omega^2) \right. \\
&\times \left. \left( \beta_+(\omega) + \beta_-(\omega) \right) - \frac{1}{q} (\hat{k} \cdot q - 2\hat{k}_2 q_2) \delta(\omega' - q) \Theta(k^2 - \omega^2) \left( \beta_+(\omega) - \beta_-(\omega) \right) \right\} \\
&\times \delta(p - \omega - \omega') \\
&= -e^2 \pi \int_0^\Lambda \frac{k^2 dk}{2\pi^2} \int_0^\pi \frac{1}{2} \sin \theta d\theta \int_0^{2\pi} \frac{d\phi}{2\pi} \int_{-k}^k d\omega \left\{ \left( \beta_+(\omega) + \beta_-(\omega) \right) \right. \\
&- \left. \frac{1}{q} (\hat{k} \cdot q - 2\hat{k}_2 q_2) \times \left( \beta_+(\omega) - \beta_-(\omega) \right) \right\} \delta(p - \omega - q), \tag{5.60}
\end{aligned}$$

#### 5.4. Imaginary parts of the components of the photon self-energy

$$\begin{aligned}
& \text{Im } \Pi_0^{33} \Big|_{\text{pole-cut}} \\
&= 2e^2\pi(1 - e^{p/T}) \int \frac{d^3k}{(2\pi)^3} \int_{-\infty}^{\infty} \int_{-\infty}^{\infty} d\omega d\omega' n_F(\omega) n_F(\omega') \left\{ \delta(\omega' - q) \Theta(k^2 - \omega^2) \right. \\
&\times \left. \left( \beta_+(\omega) + \beta_-(\omega) \right) - \frac{1}{q} (\hat{k}_\perp q_\perp - \hat{k}_3 q_3) \delta(\omega' - q) \Theta(k^2 - \omega^2) \left( \beta_+(\omega) - \beta_-(\omega) \right) \right\} \\
&\times \delta(p - \omega - \omega') \\
&= -e^2\pi \int_0^\Lambda \frac{k^2 dk}{2\pi^2} \int_0^\pi \frac{1}{2} \sin \theta d\theta \int_0^{2\pi} \frac{d\phi}{2\pi} \int_{-k}^k d\omega \left\{ \left( \beta_+(\omega) + \beta_-(\omega) \right) \right. \\
&- \left. \frac{1}{q} (\hat{k}_\perp q_\perp - \hat{k}_3 q_3) \times \left( \beta_+(\omega) - \beta_-(\omega) \right) \right\} \delta(p - \omega - q), \tag{5.61}
\end{aligned}$$

$$\begin{aligned}
& \text{Im } \Pi_0^{13} \Big|_{\text{pole-cut}} \\
&= 2e^2\pi(1 - e^{p/T}) \int \frac{d^3k}{(2\pi)^3} \int_{-\infty}^{\infty} \int_{-\infty}^{\infty} d\omega d\omega' n_F(\omega) n_F(\omega') \left\{ \frac{\hat{k}_1 q_3 + q_1 \hat{k}_3}{q} \delta(\omega' - q) \right. \\
&\times \left. \left( \beta_+(\omega) - \beta_-(\omega) \right) \Theta(k^2 - \omega^2) \right\} \delta(p - \omega - \omega') \\
&= -e^2\pi \int_0^\Lambda \frac{k^2 dk}{2\pi^2} \int_0^\pi \frac{1}{2} \sin \theta d\theta \int_0^{2\pi} \frac{d\phi}{2\pi} \int_{-k}^k d\omega \frac{1}{q} (\hat{k}_1 q_3 + q_1 \hat{k}_3) \left( \beta_+(\omega) - \beta_-(\omega) \right) \\
&\times \delta(p - \omega - q). \tag{5.62}
\end{aligned}$$

Here we note that the terms with  $\delta(\omega' + q) \delta(p - \omega - \omega') \Theta(k^2 - \omega^2)$  will not contribute because  $k^2 - (p + q)^2$  can not be greater than zero. So we have excluded those terms.

## 5.4.2 Imaginary part of magnetic field dependent part of $\mathcal{O}[(eB)^2]$

Similar to  $\mathcal{O}[(eB)^0]$  case, the imaginary part of  $\Pi_2^{11}$ ,  $\Pi_2^{22}$ ,  $\Pi_2^{33}$  and  $\Pi_2^{13}$  can be written as

$$\begin{aligned}
 \text{Im } \Pi_2^{11} &= -8e^2\pi(1 - e^{p/T}) \int \frac{d^3k}{(2\pi)^3} \int_{-\infty}^{\infty} \int_{-\infty}^{\infty} d\omega d\omega' n_F(\omega) n_F(\omega') \\
 &\times \left[ eB \left\{ q_3 \rho_1^{(0)} \left( \rho_9^{(1)} + \rho_{10} - \rho_7 \right) - \rho_1^{(1)} \left( \rho_8 + k_3 \rho_9^{(0)} \right) \right\} \right. \\
 &+ (eB)^2 \left( \hat{k}_1 q_1 - \hat{k}_2 q_2 \right) \rho_2^{(0)} \left( \rho_{D-} - \rho_{D+} \right) - (eB)^2 q_{\perp}^2 \left\{ \rho_3^{(1)} \left( \rho_{D+} + \rho_{D-} \right) \right. \\
 &+ \left. \left. \left( 2\hat{k}_1 q_1 - \hat{k} \cdot \mathbf{q} \right) \rho_3^{(0)} \left( \rho_{D+} - \rho_{D-} \right) \right\} + \rho_0^{(1)} \left( \rho_{15}^{(1)} - \rho_{14}^{(1)} + \rho_{16} - \rho_{13} - \rho_{11} \right) \right. \\
 &+ \left. \left. \left( 2k_1 q_1 - \mathbf{k} \cdot \mathbf{q} \right) \rho_0^{(0)} \left( \rho_{15}^{(0)} - \rho_{14}^{(0)} \right) - q_3 \rho_0^{(0)} \rho_{12} \right] \\
 &\times \delta(p - \omega - \omega'),
 \end{aligned} \tag{5.63}$$

$$\begin{aligned}
 \text{Im } \Pi_2^{22} &= -8e^2\pi(1 - e^{p/T}) \int \frac{d^3k}{(2\pi)^3} \int_{-\infty}^{\infty} \int_{-\infty}^{\infty} d\omega d\omega' n_F(\omega) n_F(\omega') \\
 &\times \left[ eB \left\{ q_3 \rho_1^{(0)} \left( \rho_9^{(1)} + \rho_{10} - \rho_7 \right) - \rho_1^{(1)} \left( \rho_8 + k_3 \rho_9^{(0)} \right) \right\} \right. \\
 &+ (eB)^2 \left( \hat{k}_2 q_2 - \hat{k}_1 q_1 \right) \rho_2^{(0)} \left( \rho_{D-} - \rho_{D+} \right) - (eB)^2 q_{\perp}^2 \left\{ \rho_3^{(1)} \left( \rho_{D+} + \rho_{D-} \right) \right. \\
 &+ \left. \left. \left( 2\hat{k}_2 q_2 - \hat{k} \cdot \mathbf{q} \right) \rho_3^{(0)} \left( \rho_{D+} - \rho_{D-} \right) \right\} + \rho_0^{(1)} \left( \rho_{15}^{(1)} - \rho_{14}^{(1)} + \rho_{16} - \rho_{13} - \rho_{11} \right) \right. \\
 &+ \left. \left. \left( 2k_2 q_2 - \mathbf{k} \cdot \mathbf{q} \right) \rho_0^{(0)} \left( \rho_{15}^{(0)} - \rho_{14}^{(0)} \right) - q_3 \rho_0^{(0)} \rho_{12} \right] \\
 &\times \delta(p - \omega - \omega'),
 \end{aligned} \tag{5.64}$$

#### 5.4. Imaginary parts of the components of the photon self-energy

$$\begin{aligned}
\text{Im } \Pi_2^{33} &= -8e^2\pi(1 - e^{p/T}) \int \frac{d^3k}{(2\pi)^3} \int_{-\infty}^{\infty} \int_{-\infty}^{\infty} d\omega d\omega' n_F(\omega) n_F(\omega') \\
&\times \left[ eB \left\{ q_3 \rho_1^{(0)} \left( \rho_9^{(1)} + \rho_{10} - \rho_7 \right) + \rho_1^{(1)} \left( \rho_8 + k_3 \rho_9^{(0)} \right) \right\} \right. \\
&+ (eB)^2 \left( q_3 \hat{k}_3 - \hat{k} \cdot q \right) \rho_2^{(0)} \left( \rho_{D-} - \rho_{D+} \right) - (eB)^2 q_{\perp}^2 \left\{ \rho_3^{(1)} \left( \rho_{D+} + \rho_{D-} \right) \right. \\
&+ \left. \left. \left( 2q_3 \hat{k}_3 - \hat{k} \cdot q \right) \rho_3^{(0)} \left( \rho_{D+} - \rho_{D-} \right) \right\} + \rho_0^{(1)} \left( \rho_{15}^{(1)} - \rho_{14}^{(1)} + \rho_{16} - \rho_{13} - \rho_{11} \right) \right. \\
&+ \left. \left. \left( 2k_3 q_3 - \mathbf{k} \cdot \mathbf{q} \right) \rho_0^{(0)} \left( \rho_{15}^{(0)} - \rho_{14}^{(0)} \right) + q_3 \rho_0^{(0)} \rho_{12} \right] \\
&\times \delta(p - \omega - \omega'),
\end{aligned} \tag{5.65}$$

$$\begin{aligned}
\text{Im } \Pi_2^{13} &= -8e^2\pi(1 - e^{p/T}) \int \frac{d^3k}{(2\pi)^3} \int_{-\infty}^{\infty} \int_{-\infty}^{\infty} d\omega d\omega' n_F(\omega) n_F(\omega') \\
&\times \left[ eB \left\{ \rho_1^{(1)} k_3 \rho_9^{(0)} \right\} + (eB)^2 \hat{k}_3 q_1 \rho_2^{(0)} \left\{ \rho_{D-} - \rho_{D+} \right\} \right. \\
&- (eB)^2 q_{\perp}^2 \left\{ \left( \hat{k}_1 q_3 + \hat{k}_3 q_1 \right) \rho_3^{(0)} \left( \rho_{D+} - \rho_{D-} \right) \right\} \\
&+ \left. \left. \left( k_1 q_3 + k_3 q_1 \right) \rho_0^{(0)} \left( \rho_{15}^{(0)} - \rho_{14}^{(0)} \right) + q_1 \rho_0^{(0)} \rho_{12} \right] \delta(p - \omega - \omega'). \tag{5.66}
\end{aligned}$$

Various spectral functions are obtained in Appendix A. As discussed before we also note that the imaginary part of various components of the self-energy contain the *pole-pole* and the *pole-cut* contributions. As explained earlier the phase space does not allow the *pole-pole* part to contribute in this order. In  $\mathcal{O}[(eB)^2]$  the contribution comes only from the *pole-cut* part.

#### **Pole-cut part of $\mathcal{O}[(eB)^2]$**

Now the expressions of pole-cut parts of Eqs. (5.63), (5.64), (5.65) and (5.66) after using the approximations, are given below:

$$\begin{aligned}
 & \text{Im } \Pi_2^{11} \Big|_{\text{pole-cut}} \\
 = & 4e^2 \pi \int_0^\Lambda \frac{k^2 dk}{2\pi^2} \int \frac{1}{2} \sin \theta d\theta \int \frac{d\phi}{2\pi} \int_{-k}^k d\omega \int_{-\infty}^\infty d\omega' \left[ \delta'''(\omega' - \omega_q) \left\{ -\frac{(eB)^2 q_\perp^2}{96\omega_q^3} \right. \right. \\
 \times & \left. \left. \left( \beta_+ + \beta_- \right) - \frac{(eB)^2 q_\perp^2 (2\hat{k}_1 q_1 - \hat{k} \cdot q)}{96\omega_q^4} \left( \beta_+ - \beta_- \right) \right\} - \delta''(\omega' - \omega_q) \left\{ \frac{3(eB)^2}{64\omega_q^3} \right. \right. \\
 \times & \left. \left. \left( \frac{q_\perp^2 (\hat{k}_1 q_1 - \hat{k} \cdot q)}{\omega_q^2} - (\hat{k}_1 q_1 - \hat{k}_2 q_2) \right) \times \left( \beta_+ - \beta_- \right) + \frac{3(eB)^2 q_\perp^2}{128\omega_q^4} \left( \beta_+ + \beta_- \right) \right\} \right. \\
 + & \delta'(\omega' - \omega_q) \left\{ \frac{eB q_3}{4\omega_q^2} \left( \beta_9^{(1)} + \beta_{10} - \beta_7 \right) - \frac{eB}{4\omega_q} \left( \beta_8 + k_3 \beta_9^{(0)} \right) - \frac{(eB)^2}{16\omega_q^4} \left( \hat{k}_2 q_2 - \hat{k}_1 q_1 \right. \right. \\
 + & \left. \left. \frac{5q_\perp^2 (\hat{k}_1 q_1 - \hat{k} \cdot q)}{2\omega_q^2} \right) \left( \beta_+ - \beta_- \right) - \frac{(eB)^2 q_\perp^2}{32\omega_q^5} \left( \beta_+ + \beta_- \right) \right\} + \delta(\omega' - \omega_q) \left\{ \frac{eB q_3}{4\omega_q^3} \right. \\
 \times & \left. \left( \beta_9^{(1)} + \beta_{10} - \beta_7 \right) - \frac{(eB)^2}{16\omega_q^5} \left( 3\hat{k}_2 q_2 - 3\hat{k}_1 q_1 + \frac{5q_\perp^2 (\hat{k}_1 q_1 - \hat{k} \cdot q)}{2\omega_q^2} \right) \left( \beta_+ - \beta_- \right) \right. \\
 - & \left. \frac{1}{2} \left( \beta_{15}^{(1)} + \beta_{16} - \left( \beta_{14}^{(1)} + \beta_{11} + \beta_{13} \right) \right) - \frac{(2k_1 q_1 - \mathbf{k} \cdot \mathbf{q})}{2\omega_q} \left( \beta_{15}^{(0)} - \beta_{14}^{(0)} \right) \right. \\
 + & \left. \left. \frac{q_3}{2\omega_q} \beta_{12} \right\} \right] \times \delta(p - \omega - \omega'), \tag{5.67}
 \end{aligned}$$

$$\begin{aligned}
 & \text{Im } \Pi_2^{22} \Big|_{\text{pole-cut}} \\
 = & 4e^2 \pi \int_0^\Lambda \frac{k^2 dk}{2\pi^2} \int \frac{1}{2} \sin \theta d\theta \int \frac{d\phi}{2\pi} \int_{-k}^k d\omega \int_{-\infty}^\infty d\omega' \left[ \delta'''(\omega' - \omega_q) \left\{ -\frac{(eB)^2 q_\perp^2}{96\omega_q^3} \right. \right. \\
 \times & \left. \left. \left( \beta_+ + \beta_- \right) - \frac{(eB)^2 q_\perp^2 (2\hat{k}_2 q_2 - \hat{k} \cdot q)}{96\omega_q^4} \left( \beta_+ - \beta_- \right) \right\} - \delta''(\omega' - \omega_q) \left\{ \frac{3(eB)^2}{64\omega_q^3} \right. \right. \\
 \times & \left. \left. \left( \frac{q_\perp^2 (\hat{k}_2 q_2 - \hat{k} \cdot q)}{\omega_q^2} - (\hat{k}_2 q_2 - \hat{k}_1 q_1) \right) \times \left( \beta_+ - \beta_- \right) + \frac{3(eB)^2 q_\perp^2}{128\omega_q^4} \left( \beta_+ + \beta_- \right) \right\} \right. \\
 & \left. \left. \left. \right. \right. \right.
 \end{aligned}$$



#### 5.4. Imaginary parts of the components of the photon self-energy

$$\begin{aligned}
& + \delta'(\omega' - \omega_q) \left\{ \frac{eB q_3}{4\omega_q^2} (\beta_9^{(1)} + \beta_{10} - \beta_7) - \frac{eB}{4\omega_q} (\beta_8 + k_3 \beta_9^{(0)}) - \frac{(eB)^2}{16\omega_q^4} (\hat{k}_1 q_1 - \hat{k}_2 q_2 \right. \\
& + \left. \frac{5q_\perp^2 (\hat{k}_2 q_2 - \hat{k} \cdot \mathbf{q})}{2\omega_q^2} (\beta_+ - \beta_-) - \frac{(eB)^2 q_\perp^2}{32\omega_q^5} (\beta_+ + \beta_-) \right\} + \delta(\omega' - \omega_q) \left\{ \frac{eB q_3}{4\omega_q^3} \right. \\
& \times \left( \beta_9^{(1)} + \beta_{10} - \beta_7 \right) - \frac{(eB)^2}{16\omega_q^5} \left( 3\hat{k}_1 q_1 - 3\hat{k}_2 q_2 + \frac{5q_\perp^2 (\hat{k}_2 q_2 - \hat{k} \cdot \mathbf{q})}{2\omega_q^2} \right) (\beta_+ - \beta_-) \\
& - \left. \frac{1}{2} \left( \beta_{15}^{(1)} + \beta_{16} - (\beta_{14}^{(1)} + \beta_{11} + \beta_{13}) \right) - \frac{(2k_2 q_2 - \mathbf{k} \cdot \mathbf{q})}{2\omega_q} (\beta_{15}^{(0)} - \beta_{14}^{(0)}) + \frac{q_3}{2\omega_q} \beta_{12} \right\} \\
& \times \delta(p - \omega - \omega'), \tag{5.68}
\end{aligned}$$

$$\begin{aligned}
& \text{Im } \Pi_2^{33} \Big|_{\text{pole-cut}} \\
& = 4e^2 \pi \int_0^\Lambda \frac{k^2 dk}{2\pi^2} \int \frac{1}{2} \sin \theta d\theta \int \frac{d\phi}{2\pi} \int_{-k}^k d\omega \int_{-\infty}^\infty d\omega' \left[ \delta'''(\omega' - \omega_q) \left\{ -\frac{(eB)^2 q_\perp^2}{96\omega_q^3} \right. \right. \\
& \times \left( \beta_+ + \beta_- \right) - \frac{(eB)^2 q_\perp^2 (\hat{k}_3 q_3 - \hat{k}_\perp q_\perp)}{96\omega_q^4} (\beta_+ - \beta_-) \left. \right\} - \delta''(\omega' - \omega_q) \left\{ \frac{3(eB)^2}{64\omega_q^3} \right. \\
& \times \left. \left( \frac{q_\perp^2 (\hat{k}_3 q_3 - \hat{k}_\perp q_\perp)}{\omega_q^2} + \hat{k}_\perp q_\perp \right) \times (\beta_+ - \beta_-) + \frac{3(eB)^2 q_\perp^2}{128\omega_q^4} (\beta_+ + \beta_-) \right\} \\
& + \delta'(\omega' - \omega_q) \left\{ \frac{eB q_3}{4\omega_q^2} (\beta_9^{(1)} + \beta_{10} - \beta_7) + \frac{eB}{4\omega_q} (\beta_8 + k_3 \rho_9^{(0)}) - \frac{(eB)^2}{16\omega_q^4} (\hat{k}_\perp q_\perp \right. \\
& + \left. \frac{5q_\perp^2 (\hat{k}_3 q_3 - \hat{k}_\perp q_\perp)}{2\omega_q^2} (\beta_+ - \beta_-) - \frac{(eB)^2 q_\perp^2}{32\omega_q^5} (\beta_+ + \beta_-) \right\} + \delta(\omega' - \omega_q) \\
& \times \left\{ \frac{eB q_3}{4\omega_q^3} (\beta_9^{(1)} + \beta_{10} - \beta_7) - \frac{(eB)^2}{16\omega_q^5} \left( 3\hat{k}_\perp q_\perp + \frac{5q_\perp^2 (\hat{k}_3 q_3 - \hat{k}_\perp q_\perp)}{2\omega_q^2} \right) \right. \\
& \times \left( \beta_+ - \beta_- \right) - \frac{1}{2} \left( \beta_{15}^{(1)} + \beta_{16} - (\beta_{14}^{(1)} + \beta_{13} + \beta_{11}) \right) - \frac{(2k_3 q_3 - \mathbf{k} \cdot \mathbf{q})}{2\omega_q} \\
& \times \left. \left( \beta_{15}^{(0)} - \beta_{14}^{(0)} \right) - \frac{q_3}{2\omega_q} \beta_{12} \right\} \Big] \delta(p - \omega - \omega'), \tag{5.69}
\end{aligned}$$

$$\begin{aligned}
 & \text{Im } \Pi_2^{13} \Big|_{pole-cut} \\
 = & 4e^2\pi \int_0^\Lambda \frac{k^2 dk}{2\pi^2} \int \frac{1}{2} \sin \theta d\theta \int \frac{d\phi}{2\pi} \int_{-k}^k d\omega \int_{-\infty}^\infty d\omega' \left[ \delta'''(\omega' - \omega_q) \right. \\
 \times & \left\{ -\frac{(eB)^2 q_\perp^2 (\hat{k}_1 q_3 + \hat{k}_3 q_1)}{96\omega_q^4} (\beta_+ - \beta_-) \right\} - \delta''(\omega' - \omega_q) \left\{ \frac{3(eB)^2}{64\omega_q^3} \left( \frac{q_\perp^2 (\hat{k}_1 q_3 + \hat{k}_3 q_1)}{\omega_q^2} \right. \right. \\
 - & \left. \left. \hat{k}_3 q_1 \right) (\beta_+ - \beta_-) \right\} + \delta'(\omega' - \omega_q) \left\{ \frac{eB}{4\omega_q} k_1 \beta_9^{(0)} - \frac{(eB)^2}{16\omega_q^4} \left( -\hat{k}_3 q_1 + \frac{5q_\perp^2 (\hat{k}_1 q_3 + \hat{k}_3 q_1)}{2\omega_q^2} \right) \right. \\
 \times & \left. (\beta_+ - \beta_-) \right\} + \delta(\omega' - \omega_q) \left\{ -\frac{(eB)^2}{16\omega_q^5} \left( -3\hat{k}_3 q_1 + \frac{5q_\perp^2 (\hat{k}_1 q_3 + \hat{k}_3 q_1)}{2\omega_q^2} \right) (\beta_+ - \beta_-) \right. \\
 - & \left. \frac{(k_1 q_3 + k_3 q_1)}{2\omega_q} \left( \beta_{15}^{(0)} - \beta_{14}^{(0)} \right) - \frac{q_1}{2\omega_q} \beta_{12} \right\} \Big] \delta(p - \omega - \omega'). \tag{5.70}
 \end{aligned}$$

## 5.5 Results

We perform the integrations in Eq. (5.59), (5.60), (5.61), (5.62), (5.67), (5.68), (5.69) and (5.70) numerically. In this calculation we have taken  $m_\pi = 0.14$  GeV. The results are shown for  $\Lambda = 0.25$  GeV which satisfies  $eT \ll \Lambda \ll T$ .

The damping rate of photon in presence of magnetic field depends on the angle,  $\theta_p$ , between the momentum of photon and the magnetic field. Figure 5.3 shows the variation of the damping rate of a hard photon with the propagation angle. It increases with the increasing propagation angle. One can see that the two transverse modes of a hard photon are damped in a similar fashion. Since the magnetic field strength is very weak, this difference appears to be very small. We note that the magnetic correction is  $\sim \mathcal{O}[(eB)^2]$  and switching the magnetic field from  $z$  to  $-z$  direction would not affect the result. These two orientations of the magnetic field correspond to the propagation angle of photon  $\theta_p$  and  $\pi - \theta_p$ . These two situations are identical which correspond to the same damping rates of photon at  $\theta_p$  and  $\pi - \theta_p$ .

## 5.5. Results

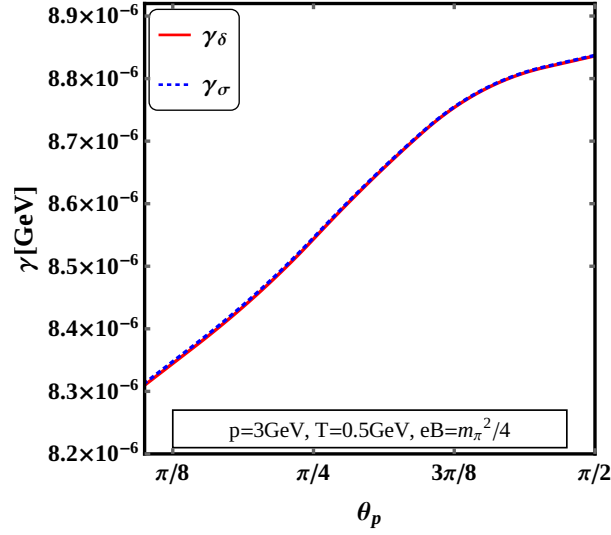


Figure 5.3: Plot of damping rate of photon with the propagation angle  $\theta_p$  for  $p = 3$  GeV,  $T = 0.5$  GeV and  $eB = m_\pi^2/4$ .

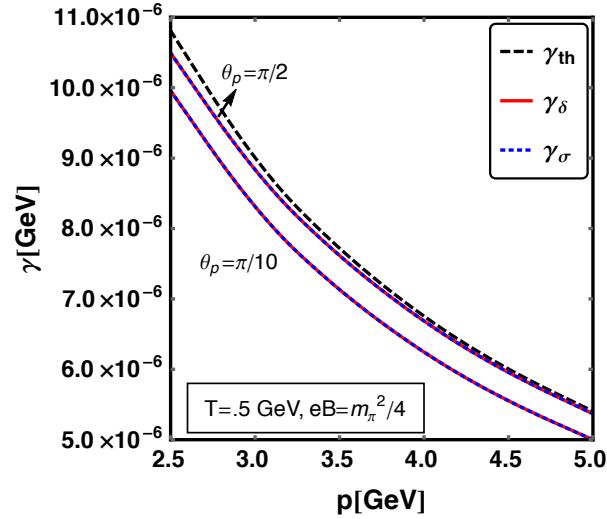


Figure 5.4: Plot of damping rate of photon with the energy for  $T = 0.5$  GeV and  $eB = m_\pi^2/4$  at propagation angles  $\theta_p = \pi/10$  and  $\pi/2$ .

## Chapter 5. Damping rate of a hard photon in a weakly magnetized hot medium

In Fig. 5.4 we display the damping rate as a function of photon momentum for two propagation angles  $\pi/10$  and  $\pi/2$ . The soft contribution of the damping rate in a thermal medium agrees well with that obtained in Ref. [197]. In presence of a thermomagnetic medium, the soft contribution to the damping rate is found to be reduced than that of the thermal one. For small propagation angle, the reduction of the damping rate is more compared to that of thermal medium. For higher momentum the damping rate approaches the thermal value as the temperature becomes the dominant scale as compared to the strength of the magnetic field considered.

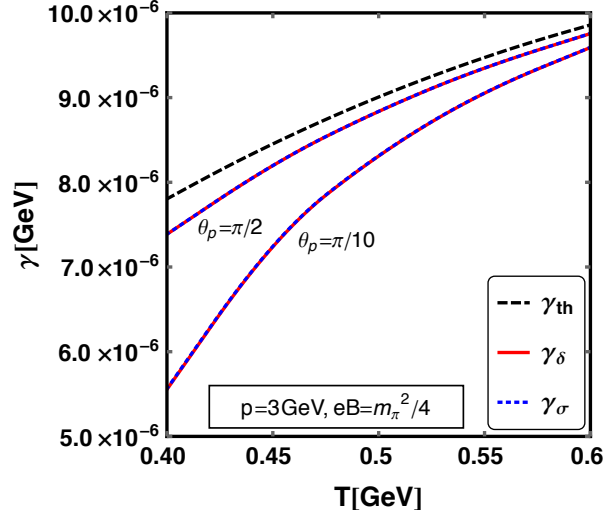


Figure 5.5: Plot of damping rate of the hard photon with temperature at  $p = 3$  GeV and  $eB = m_\pi^2/4$  for two propagation angles  $\pi/10$  and  $\pi/2$ .

Figure 5.5 displays the variation of damping rate with temperature for a specific value of momentum and magnetic field for two propagation angles  $\pi/10$  and  $\pi/2$ . It is found that the soft contribution to the damping rate increases with the increase in temperature both in thermal and thermomagnetic medium. For small propagation angle the damping rate is more reduced compared to that of large propagation angle. This observation is consistent with Fig. 5.4.

## 5.5. Results

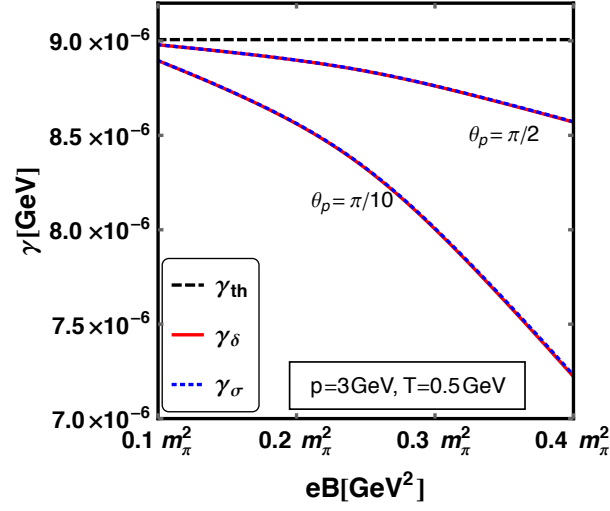


Figure 5.6: Plot of damping rate of the hard photon with the magnetic field strength at  $T = 0.5$  GeV and  $p = 3$  GeV for two propagation angles  $\pi/10$  and  $\pi/2$ .

Figure 5.6 shows the variation of the damping rate with the magnetic field strength for specific values of photon momentum and temperature for two propagation angles. The thermal damping rate ( $\mathcal{O}[(eB)^0]$ ) is represented by the black dashed horizontal line. The thermomagnetic damping rate decreases with the increasing magnetic field. At smaller propagation angles the photons are less damped than that of higher propagation angles which are consistent with Fig. 5.4.

Fig. 5.7 shows the variation of the photon damping rate with the separation scale  $\Lambda$  keeping the scale hierarchy  $eT \ll \Lambda \ll T$ . As the allowed phase space increases with the increase of  $\Lambda$ , the damping rate is also found to increase with it <sup>2</sup>. The magnetic correction to the thermal damping rate is negative. So, the difference between the thermal and thermomagnetic damping rate increases with  $\Lambda$ .

<sup>2</sup>Nevertheless, the damping rate is expected to be  $\Lambda$  independent when hard contribution is added.

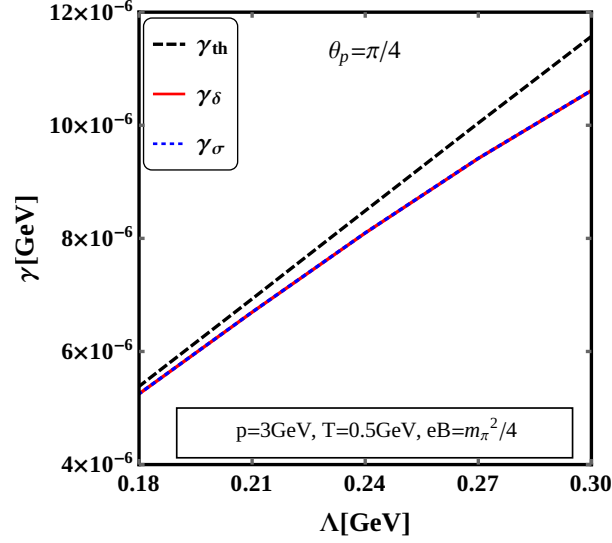


Figure 5.7: Plot of damping rate of photon with  $\Lambda$  for  $\theta_p = \pi/4$ ,  $p = 3$  GeV,  $T = 0.5$  GeV and  $eB = m_\pi^2/4$ .

## 5.6 Summary

We have calculated the soft contribution to the damping rate of a hard photon in a weakly magnetized QED medium where momentum of one of the fermion in the loop is considered as soft. The two degenerate transverse modes of photon in thermal medium are damped in a similar fashion in presence of weak magnetic field as shown in Fig. 5.3. The difference between two transverse modes is very marginal due to weak field approximation. The soft contribution to the damping rate in thermomagnetic medium is reduced compared to that of thermal medium. When the magnetic field is switched off thermomagnetic damping modes reduce to its thermal value. The effect of magnetic field is found to be dominant at low temperature and low photon momentum.

The soft contribution to the hard photon damping rate is  $\sim 10^{-6}$  GeV. Thus, a photon of a few GeV energy traversing in the QED medium of temperature  $\sim 0.5$  GeV and back-

### 5.6. Summary

ground magnetic field  $\sim 0.005 \text{ GeV}^2$  has a mean free path ( $\lambda = \gamma^{-1}/2$ ) of a few  $\text{\AA}$ . When the present calculation is extended to the case of relativistic heavy ion collisions, the mean free path of photon is found to be of a few hundred fm. This confirms that the mean free path of photon is larger than the size of the fireball and photon can be treated as a direct probe.

The damping rate is found to be dependent on the separation scale  $\Lambda$ . One needs to add the hard contribution with the soft contribution to cancel the  $\Lambda$  dependence of the result. The hard contribution to the photon damping rate comes from two-loop order with hard particles in the loop having momentum of the order of or higher than the temperature. This itself is a huge calculation which is in progress.





CHIRAL SUSCEPTIBILITY IN  
THERMO-MAGNETIC QCD MEDIUM:  
WITHIN HTL APPROXIMATION

---

In this chapter chiral susceptibility in QGP in the presence of a finite chemical potential and a weak magnetic field is computed. To calculate this we constructed the massive effective quark propagator in a thermomagnetic medium. A completely analytic expression for the chiral susceptibility in the weak magnetic field limit is obtained within HTL approximation. This chapter is based on the work presented in the following paper: *Chiral susceptibility in dense thermo-magnetic QCD medium within HTL approximation* Ritesh Ghosh, Bithika Karmakar, Munshi G. Mustafa, *Phys. Rev. D* **103** (2021) 07, 074019, [[arXiv:2103.08407](https://arxiv.org/abs/2103.08407)].

## 6.1 Introduction

It has been a long standing quest of heavy ion collision community to explore the phase diagram of QCD. Several large scale experiments *e.g.*, LHC at CERN, RHIC at BNL have been designed and performed for this purpose. Upcoming experiments at FAIR, NICA, JPARC are expected to examine the phase diagram of QCD at high baryon density. Two non-perturbative features of QCD vacuum are confinement and chiral symmetry breaking. With increasing temperature and/or baryon density the QCD vacuum undergoes a phase transition to deconfined and chiral symmetry restored phase. Besides the ongoing experiments, there are several theoretical tools *e.g.*, lattice calculations [205, 206], various effective models [207, 208], AdS/QCD correspondence [209], the functional renormalization-group method [210, 211] to study the phase diagram of QCD. Lattice results conclusively demonstrated that the phase transition at vanishing baryon chemical potential is a crossover. The order parameter of chiral symmetry breaking is quark-antiquark condensate which vanishes above the critical temperature in the chiral limit. Chiral susceptibility is the measure of fluctuation of the order parameter. It estimates the response of the chiral condensate with the variation of current quark mass. Measurement of fluctuations is an essential tool to investigate the properties of QCD matter at extreme conditions *e.g.*, electric charge fluctuation, quark number susceptibility can give insight to the degrees of freedom of the system. Chiral susceptibility has been studied in the framework of lattice QCD [212–216], hard thermal loop approximation [217], chiral perturbation theory [218], NJL model [219, 220], Dyson-Schwinger equation [221], etc.

Besides, production of magnetic field in non-central heavy ion collisions has added a new dimension to the understanding of QCD matter discussed in earlier chapters. The magnetic field can affect the dynamical chiral symmetry breaking. Some studies suggest

## 6.1. Introduction

that the chiral condensate increases in the presence of magnetic field. It is argued that in case of neutral spin-zero pair of fermion and antifermion, magnetic moments of both point along same direction. As a result, both magnetic moments can align along the magnetic field direction without creating any frustration in the fermion-antifermion pair [222]. This effect is linked to the increase in the phase transition temperature which is known as Magnetic Catalysis. However, several lattice studies [90] have found the opposite nature *i.e.*, the decrease in phase transition temperature at least for small magnetic fields. This effect has been named as Inverse Magnetic Catalysis. Also these studies revealed that the change in the chiral condensate strongly depends on the temperature and the quark mass. Recently, the chiral susceptibility was calculated using NJL model in Ref. [223] in the presence of chiral chemical potential and non-zero magnetic field. The magnetic field breaks the flavor symmetry. Hence two distinct peaks of chiral susceptibility for u and d quark have been observed at large magnetic field. The strong magnetic field produced in heavy ion collision sharply decays with time depending upon the conductivity of the medium. The QCD matter cools down after the collision and undergoes the chiral phase transition at around 160 MeV temperature. In this region the effect of weak magnetic field is particularly important. In this chapter, we consider the magnetic field to be small and use the scale hierarchy  $\sqrt{|q_f B|} < gT < T$ . In Ref. [217] the chiral susceptibility was computed with zero chemical potential within hard thermal loop (HTL) approximation. Here we, considering recently obtained effective quark propagator in the presence of weak magnetic field [200], determine the chiral susceptibility with finite chemical potential in the QCD medium using HTL approximation.

The chapter is organized as follows. In Sec. 6.2 we describe the static chiral susceptibility. We obtain the general structure of fermion self energy in presence of weak magnetic field and compute the effective propagator in Sec. 7.36. The free chiral susceptibility is cal-

Chapter 6. Chiral susceptibility in thermo-magnetic QCD medium: within HTL approximation

culated in Sec. 6.4. We compute the HTL chiral susceptibility within weak magnetic field approximation in Sec. 6.5. The results are described in Sec. 6.6. Finally, we summarize in Sec. 6.7.

## 6.2 Definition

The chiral condensate is defined as

$$\langle \bar{q}q \rangle = \frac{\text{Tr}[\bar{q}q e^{-\beta H}]}{\text{Tr}[e^{-\beta H}]} = \frac{\partial \Omega}{\partial m_f}, \quad (6.1)$$

where  $H$  is the Hamiltonian of the system.  $\Omega = -\frac{T}{V} \ln Z$  is the thermodynamic potential where  $Z$  is the partition function of a quark-antiquark gas. Quark condensate also can be written using quark propagator as

$$\langle \bar{q}q \rangle = -N_c N_f \sum_{\{P\}} \text{Tr} \left[ S(P) \right], \quad (6.2)$$

where  $N_c$  and  $N_f$  are the numbers of quark colors and flavors respectively. Susceptibility is the measure of the response of a system to small external force. Chiral susceptibility measures the response of chiral condensate to infinitesimal change of current quark mass  $m_f$  as

$$\chi_c = - \left. \frac{\partial \langle \bar{q}q \rangle}{\partial m_f} \right|_{m_f=0}. \quad (6.3)$$

## 6.3 General structure of Fermionic two point function

Recently covariant structure of fermion self-energy has been constructed in the presence of temperature and magnetic field in Ref. [200]. General covariant structure of fermion self energy in a weak thermomagnetic field can be written as

$$\Sigma(P) = -a\not{P} - b\not{u} - c'\gamma_5\not{u} - d'\gamma_5\not{u}, \quad (6.4)$$

where  $u_\mu$  is four velocity of fluid. The direction of magnetic field  $n_\mu$  can be written in terms of electromagnetic field tensor  $F^{\mu\nu}$  or its dual  $\tilde{F}^{\mu\nu}$  and fluid velocity  $u_\mu$  as

$$n_\mu \equiv \frac{1}{2B}\epsilon_{\mu\nu\rho\lambda}u^\nu F^{\rho\lambda} = \frac{1}{B}u^\nu\tilde{F}_{\mu\nu}. \quad (6.5)$$

For simplicity we have chosen the fluid rest frame and the magnetic field along  $z$ -direction as

$$u^\mu = (1, 0, 0, 0), \quad (6.6)$$

$$n_\mu = (0, 0, 0, 1). \quad (6.7)$$

The self-energy structure functions  $a$ ,  $b$ ,  $c'$  and  $d'$  in Eq. (6.4) can be calculated using Eqs. (B.1), (B.2), (B.3) and (B.4) in Appendix B. The structure functions in the presence of weak magnetic field are calculated upto  $\mathcal{O}(q_f B)$  for zero quark chemical potential in Ref. [200]. The calculations are generalized for finite quark chemical potential in Ref. [202]. Here, we compute the structure functions upto  $\mathcal{O}(q_f B)^2$  in presence of chemical potential in Appendix B.

Following the Dyson-Schwinger equation, the effective inverse propagator of massive

## Chapter 6. Chiral susceptibility in thermo-magnetic QCD medium: within HTL approximation

fermion can be written as

$$S_{\text{eff}}^{-1} = \not{P} - m_f \mathbb{I} - \Sigma. \quad (6.8)$$

Using Eq. (6.4) the structure of the inverse propagator of massive fermion in thermomagnetic medium can be written as

$$S_{\text{eff}}^{-1}(P) = (1 + a)\not{P} + b\not{\psi} + c'\gamma_5\not{\psi} + d'\gamma_5\not{\not{\psi}} - m_f \mathbb{I}. \quad (6.9)$$

To compute the chiral susceptibility in the presence of weak magnetic field one requires the effective fermion propagator as given in Eqs. (6.2) and (6.3). So we need to invert Eq. (6.9) to get the effective fermion propagator. For massless case, it is very easy to invert the effective inverse propagator to obtain the general structure of effective propagator in terms of  $\not{P}$ ,  $\not{\psi}$ ,  $\gamma_5\not{\psi}$  and  $\gamma_5\not{\not{\psi}}$ . To get the structure of the effective propagator in the massive case involving the Dirac matrices:  $\not{P}$ ,  $\not{\psi}$ ,  $\gamma_5\not{\psi}$ ,  $\gamma_5\not{\not{\psi}}$  and  $\mathbb{I}$ , we adopt the following trick used in Ref. [224].

Let us assume that we need to find the inverse of a matrix  $M$ . Now we need to choose a matrix  $R$  and multiply it with  $M$  to get a matrix  $U$  as

$$U = MR. \quad (6.10)$$

Now we can write inverse of the matrix  $M$  as

$$M^{-1} = RU^{-1}. \quad (6.11)$$

In our case we need to find the inverse of the matrix  $S_{\text{eff}}^{-1}$ . Now it is essential to choose  $R$

### 6.3. General structure of Fermionic two point function

in such a way that we get  $U$  in Eq. (6.10) in a very simple form. Then it would be easy to invert the matrix  $U$  and to find the inverse of our desired matrix  $S_{\text{eff}}^{-1}$ .

Thus we choose  $R$  as

$$R = (1 + a)\not{P} + b\not{t} - c'\gamma_5\not{t} - d'\gamma_5\not{t} - m_f\mathbb{I}. \quad (6.12)$$

From Eqs. (6.9) and (6.10), we have

$$U = S_{\text{eff}}^{-1}R = \alpha\not{P} + \beta\not{t} + \delta\gamma_5 + \lambda\mathbb{I}, \quad (6.13)$$

where

$$\begin{aligned} \alpha &= -2(1 + a)m_f, \\ \beta &= -2bm_f, \\ \delta &= 2((1 + a)c'p_0 + bc' + (1 + a)d'p_3), \\ \lambda &= (1 + a)^2P^2 + b^2 + c'^2 - d'^2 + m_f^2 + 2(1 + a)bp_0. \end{aligned} \quad (6.14)$$

We can now easily invert the matrix  $U$  to get

$$U^{-1} = \frac{1}{N^2}(\alpha\not{P} + \beta\not{t} + \delta\gamma_5 - \lambda\mathbb{I}), \quad (6.15)$$

where

$$N^2 = \alpha^2P^2 + 2\alpha\beta p_0 + \beta^2 + \delta^2 - \lambda^2. \quad (6.16)$$

Following Eq. (6.11), we get the effective fermion propagator  $S_{\text{eff}}$  as

$$\begin{aligned}
 S_{\text{eff}} &= RU^{-1} = \left( (1+a)\not{P} + b\not{\psi} - c'\gamma_5\not{\psi} - d'\gamma_5\not{\eta} - m_f\mathbb{I} \right) \\
 &\times \frac{\alpha\not{P} + \beta\not{\psi} + \delta\gamma_5 - \lambda\mathbb{I}}{\alpha^2 P^2 + 2\alpha\beta p_0 + \beta^2 + \delta^2 - \lambda^2}.
 \end{aligned} \tag{6.17}$$

The dispersion relation for massive fermion in weakly magnetized thermal medium can be obtained from the denominator of the effective propagator by setting it to zero.

## 6.4 Chiral susceptibility for free fermion in the presence of weak magnetic field

We consider weakly magnetized QCD medium. In the weak magnetic field limit, we work with the scale hierarchy,  $\sqrt{|q_f B|} < m_{\text{th}} \sim gT < T$ . Now treating  $q_f B$  as perturbation, the Schwinger propagator for a fermion in presence of weak magnetic field can be expanded and written up to  $\mathcal{O}[(q_f B)^2]$  as [100]

$$\begin{aligned}
 S(K) &= \frac{\not{K} + m_f}{K^2 - m_f^2} + i\gamma^1\gamma^2 \frac{\not{K}_{\parallel} + m_f}{(K^2 - m_f^2)^2} (q_f B) \\
 &+ 2 \left[ \frac{\{(K \cdot u)\not{\psi} - (K \cdot n)\not{\eta}\} - \not{K}}{(K^2 - m_f^2)^3} - \frac{k_{\perp}^2 (\not{K} + m_f)}{(K^2 - m_f^2)^4} \right] (q_f B)^2 \\
 &+ \mathcal{O}[(q_f B)^3] \\
 &= S_0 + S_1 + S_2 + \mathcal{O}[(q_f B)^3].
 \end{aligned} \tag{6.18}$$

We can write chiral condensate for free fermion in weak magnetic field upto  $\mathcal{O}[(q_f B)^2]$



### 6.5. HTL chiral Susceptibility in presence of weak magnetic field

from Eq. (6.18) as

$$\begin{aligned}\langle \bar{q}q \rangle_f &= -N_c N_f \sum_{\{P\}} \text{Tr} \left[ S_0(P) + S_1(P) + S_2(P) \right], \\ &= -4m_f N_c N_f \sum_{\{P\}} \left[ \frac{1}{P^2 - m_f^2} - 2(q_f B)^2 \frac{p_\perp^2}{(P^2 - m_f^2)^4} \right].\end{aligned}\quad (6.19)$$

Using the definition in Eq. (6.3) the chiral susceptibility for free fermion in weak magnetic field can be calculated as

$$\begin{aligned}\chi_c &= -\left. \frac{\partial \langle \bar{q}q \rangle}{\partial m_f} \right|_{m_f=0} = 4N_c N_f \sum_{\{P\}} \left[ \frac{1}{P^2} - 2(q_f B)^2 \frac{p_\perp^2}{(P^2)^4} \right] \\ &= \frac{N_c N_f}{6} T^2 \left[ 1 + 12\hat{\mu}^2 - (q_f B)^2 \frac{\mathfrak{J}(z)}{16\pi^4 T^4} \right],\end{aligned}\quad (6.20)$$

where  $\hat{\mu} = \mu/2\pi T$ .  $\mu$  is the quark chemical potential. The sum-integrals are calculated in Appendix B.1 and  $\mathfrak{J}(z)$  is given in Eq. (B.52).

## 6.5 HTL chiral Susceptibility in presence of weak magnetic field

Using the effective quark propagator in Eq. (6.17) chiral condensate  $\langle \bar{q}q \rangle$  takes the form,

$$\begin{aligned}\langle \bar{q}q \rangle &= -N_c N_f \sum_{\{P\}} \text{Tr}[S_{\text{eff}}(P)] \\ &= 4m_f N_c N_f \sum_{\{P\}} \frac{(1+a)^2 P^2 + 2(1+a) b p_0 + b^2 + d'^2 - c'^2 - m_f^2}{\alpha^2 P^2 + 2\alpha\beta p_0 + \beta^2 + \delta^2 - \lambda^2}.\end{aligned}\quad (6.21)$$

Chiral susceptibility in the massless limit can be calculated from Eq. (6.21) as

$$\begin{aligned}
 \chi_c &= -\frac{\partial \langle \bar{q}q \rangle}{\partial m_f} \Big|_{m_f=0} \\
 &= -4N_c N_f \sum_{\{P\}} \left[ (1+a)^2 P^2 + 2(1+a) b p_0 + b^2 + d'^2 - c'^2 \right] \\
 &\quad \times \frac{1}{4 \left[ (1+a)c' p_0 + bc' + (1+a)d' p_3 \right]^2 - \left[ (1+a)^2 P^2 + b^2 + c'^2 - d'^2 + 2(1+a) b p_0 \right]^2}, \tag{6.22}
 \end{aligned}$$

where the expressions of various structure functions are obtained in Appendix B. Now we expand the expression in Eq. (6.22) in the series of coupling constant  $g$  and keep upto  $\mathcal{O}(g)^4$  as

$$\begin{aligned}
 \chi_c &= 4N_c N_f \sum_{\{P\}} \left\{ \frac{1}{P^2} + 2m_{\text{th}}^2 \frac{1}{P^4} + m_{\text{th}}^4 \left( \frac{4}{P^6} + \frac{1}{p^2 P^4} - \frac{2}{p^2 P^4} \mathcal{T}_p + \frac{1}{p^2 p_0^2 P^2} \mathcal{T}_p^2 \right) \right. \\
 &\quad - m_{\text{eff}}'^2 \left( \frac{2}{3P^4} - \frac{2p_3^2}{p^2 P^4} - \frac{2}{P^4} \mathcal{T}_p + \frac{2p_3^2}{p^2 P^4} \mathcal{T}_p \right) \\
 &\quad \left. - m_{\text{eff}}^4 \left( \frac{4p_3^2}{p^2 P^6} + \frac{p_3^2}{p^4 P^4} - \frac{2p_3^2}{p^4 P^4} \mathcal{T}_p + \frac{3}{p_0^2 P^4} \mathcal{T}_p^2 + \frac{p_3^2}{p^4 P^4} \mathcal{T}_p^2 - \frac{4p_3^2}{p^2 p_0^2 P^4} \mathcal{T}_p^2 \right) \right\}, \tag{6.23}
 \end{aligned}$$

where

$$\begin{aligned}
 m_{\text{th}}^2 &= \frac{g^2 C_F T^2}{8} (1 + 4\hat{\mu}^2), \\
 m_{\text{eff}}'^2 &= \frac{g^2 C_F (q_f B)^2 T}{32 \pi m_f^3}, \\
 m_{\text{eff}}^2 &= 4g^2 C_F \frac{q_f B}{16\pi^2} \left[ -\frac{1}{4} \aleph(z) - \frac{\pi T}{2m_f} - \frac{\gamma_E}{2} \right], \tag{6.24}
 \end{aligned}$$

with  $\aleph(z)$  defined in Eq. (B.51) and  $C_F = (N_c^2 - 1)/2N_c$  is QCD Casimir factor. Using the

### 6.5. HTL chiral Susceptibility in presence of weak magnetic field

sum-integrals listed in Appendix B.1 we find the expression for the chiral susceptibility as

$$\begin{aligned}
\chi_c &= \frac{N_c N_f T^2}{6} \left[ 1 + 12\hat{\mu}^2 + \frac{3}{\pi^2} \left( \frac{\Lambda}{4\pi T} \right)^{2\epsilon} \left( \frac{1}{\epsilon} - \aleph(z) \right) \frac{m_{\text{th}}^2}{T^2} \right. \\
&+ \frac{1}{\pi^2} \left( \frac{\Lambda}{4\pi T} \right)^{2\epsilon} \left( \frac{1}{\epsilon} + \frac{4}{3} - \aleph(z) \right) \frac{m_{\text{eff}}'^2}{T^2} + \frac{\mathfrak{J}(z)}{32\pi^4} (\pi^2 - 6) \frac{m_{\text{th}}^4}{T^4} \\
&\left. - \frac{\mathfrak{J}(z)}{24\pi^4} (\pi^2 - 6) \frac{m_{\text{eff}}^4}{T^4} \right]. \tag{6.25}
\end{aligned}$$

We note that the logarithmic divergence comes from the thermal part. A new divergence appears in presence of the magnetic field. We renormalize the chiral susceptibility within  $\overline{MS}$  renormalization scheme using the following counter term

$$\Delta\chi_c^{\text{counter}} = -\frac{N_c N_f}{6\pi^2\epsilon} (3m_{\text{th}}^2 + m_{\text{eff}}'^2). \tag{6.26}$$

The renormalized chiral susceptibility is given as

$$\begin{aligned}
\chi_c &= \frac{N_c N_f T^2}{6} \left[ 1 + 12\hat{\mu}^2 + \frac{3}{\pi^2} \left( 2 \ln \hat{\Lambda} - 2 \ln 2 - \aleph(z) \right) \frac{m_{\text{th}}^2}{T^2} \right. \\
&+ \frac{1}{3\pi^2} \left( 4 - 3\aleph(z) + 6 \ln \hat{\Lambda} - 6 \ln 2 \right) \frac{m_{\text{eff}}'^2}{T^2} + \frac{\mathfrak{J}(z)}{32\pi^4} (\pi^2 - 6) \frac{m_{\text{th}}^4}{T^4} \\
&\left. - \frac{\mathfrak{J}(z)}{24\pi^4} (\pi^2 - 6) \frac{m_{\text{eff}}^4}{T^4} \right], \tag{6.27}
\end{aligned}$$

with  $\hat{\Lambda} = \Lambda/2\pi T$  and  $\hat{\mu} = \mu/2\pi T$ . The obtained result is completely analytic in presence of chemical potential and weak magnetic field. Here we note that the Eq. (6.27) consists of  $\mathcal{O}[(q_f B)^0]$  and  $\mathcal{O}[(q_f B)^2]$  terms. The  $\mathcal{O}[(q_f B)^0]$  reproduces the thermal chiral susceptibility without chemical potential obtained in Ref. [217]. The  $\mathcal{O}[(q_f B)^2]$  terms are the thermomagnetic correction to the thermal chiral susceptibility.

## 6.6 Results

We consider magnetic field dependent running coupling [225] as

$$\alpha_s(\Lambda^2, |eB|) = \frac{\alpha_s(\Lambda^2)}{1 + b_1 \alpha_s(\Lambda^2) \ln \left( \frac{\Lambda^2}{\Lambda^2 + |eB|} \right)}, \quad (6.28)$$

where the one loop running coupling at renormalization scale reads as

$$\alpha_s(\Lambda^2) = \frac{1}{b_1 \ln \left( \Lambda^2 / \Lambda_{\overline{\text{MS}}}^2 \right)}, \quad (6.29)$$

with  $b_1 = \frac{11N_c - 2N_f}{12\pi}$ ,  $\Lambda_{\overline{\text{MS}}} = 204$  MeV requiring  $\alpha_s = 0.326$  at 1.5 GeV [226]. We choose the renormalization scale as  $\Lambda = 2\pi \sqrt{T^2 + \mu^2/\pi^2}$ . The following results are shown considering two light quark flavors  $u$  and  $d$ .

In Fig. 7.1 the chiral susceptibility scaled with temperature squared is plotted with temperature in absence of magnetic field for zero and non zero quark chemical potential. The effect of quark chemical potential is prominent in the low temperature region as can be seen from the figure. Similar plot for thermal QCD medium and zero chemical potential was obtained in Ref. [217]. For low temperature the chiral susceptibility increases rapidly for both zero and non zero chemical potential. Here we note that the increase of the chiral susceptibility in the low temperature region does not indicate the chiral phase transition. It is due to the temperature dependence of the coupling constant and for the choice of the renormalization scale [217]. At very high temperature the chiral susceptibility reaches the free value asymptotically.

## 6.6. Results

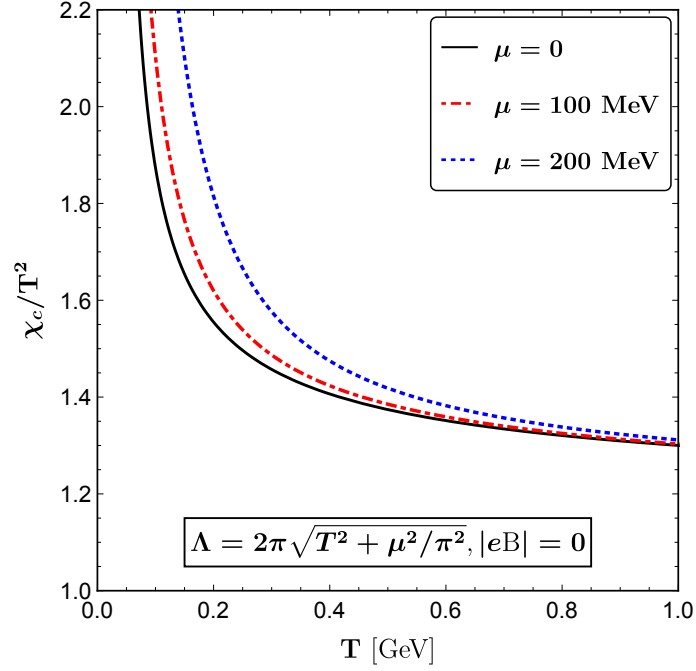


Figure 6.1: Variation of chiral susceptibility scaled with  $T^2$  as a function of temperature for chemical potential 0, 100 and 200 MeV with zero magnetic field.

The variation of chiral susceptibility scaled with temperature squared for zero and finite magnetic field is plotted with temperature in Fig. 6.2. In the left panel of Fig. 6.2 we have shown the effect of weak magnetic field on the chiral susceptibility for zero quark chemical potential, whereas, the same for finite quark chemical potential is shown in the right panel. In presence of magnetic field chiral susceptibility is slightly increased than that of thermal medium in the low temperature region. Since we are working in weak magnetic field limit, the increase in susceptibility due to magnetic field is small. As temperature increases the effect of magnetic field reduces as temperature becomes the dominant scale.

It should be noted that the scale hierarchy of weakly magnetized medium is  $\sqrt{|q_f B|} < gT < T$ . This particular condition is satisfied for around  $T > 0.14 \text{ GeV}$  as we have considered  $|eB| = m_\pi^2 = 0.14^2 \text{ GeV}^2$  in Fig.2. Thus the weak field and HTL approximations are valid at high temperature. This is consistent with our study because we calculate the

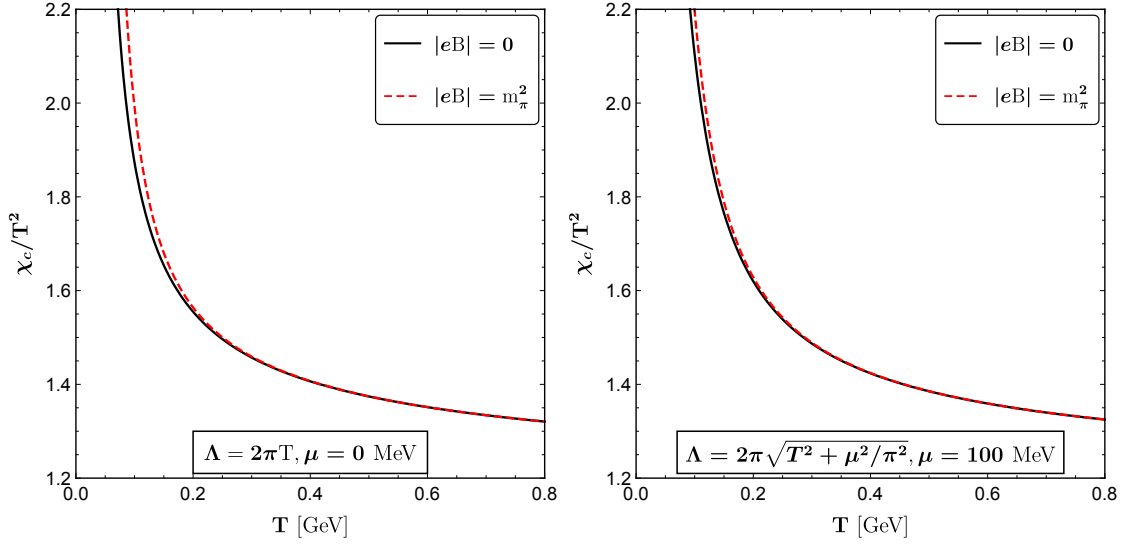


Figure 6.2: Variation of chiral susceptibility scaled with  $T^2$  as a function of  $T$  for magnetic field strength  $|eB| = 0, m_\pi^2$  with  $\mu = 0$  MeV (left) and  $\mu = 100$  MeV (right).

chiral susceptibility of the medium in perturbative region.

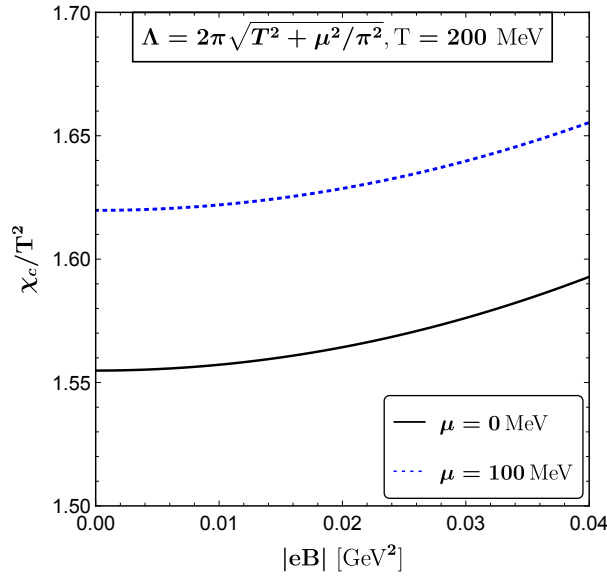


Figure 6.3: Scaled chiral susceptibility is plotted as a function of magnetic field strength  $|eB|$  for temperature  $T = 0.2$  GeV and  $\mu = 0$  MeV and 100 MeV.

## 6.6. Results

The effect of magnetic field can be seen clearly from Fig. 6.3 where the variation of the scaled chiral susceptibility is shown with magnetic field for fixed temperature  $T = 200$  MeV. Here we notice the slow increase in the chiral susceptibility with increasing magnetic field for both with and without chemical potential. Here we note that the weak field approximation is valid in this case because  $\sqrt{|q_f B|} < T$  is satisfied.

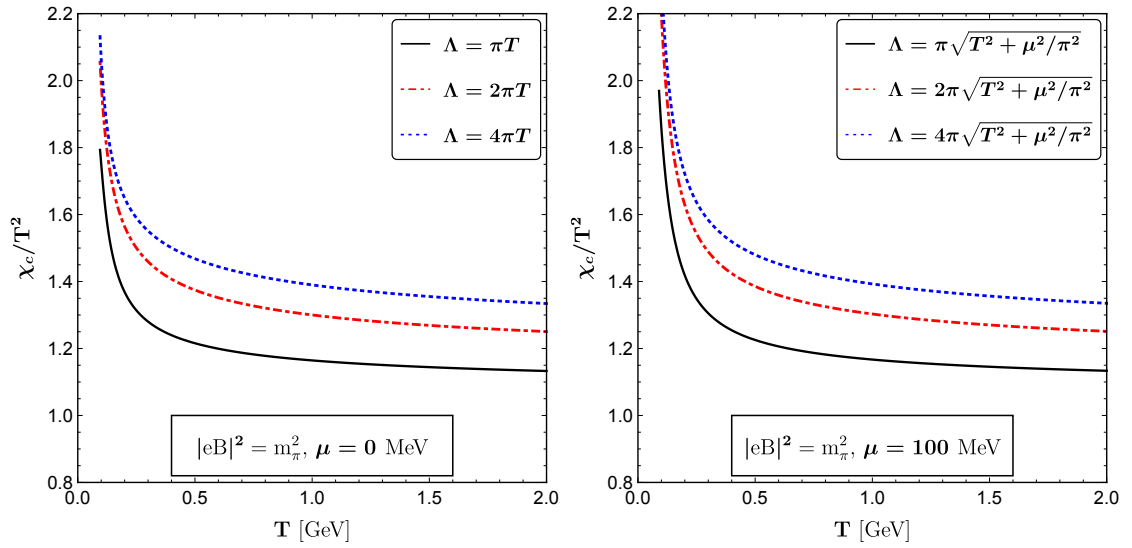


Figure 6.4: Variation of chiral susceptibility scaled with  $T^2$  as a function of temperature for magnetic field strength  $m_\pi^2$  for different values of renormalization scale.

In Fig. 6.4 the sensitivity of the chiral susceptibility with renormalization scale is shown in the presence of a constant weak magnetic field. Here chiral susceptibility scaled with  $T^2$  is plotted with temperature for zero (left panel) and finite (right panel) chemical potential by varying renormalization scale  $\Lambda$  by factor 2 around its central value  $2\pi\sqrt{T^2 + \mu^2/\pi^2}$ .

Here we note that HTL approximation is valid above the phase transition temperature where the scale hierarchy  $\sqrt{|q_f B|} < gT < T$  is maintained. We have shown the plots of chiral susceptibilities at low temperature just to show the steep increase in the plots.

## 6.7 Summary

We have investigated the effect of magnetic field on the chiral susceptibility of quark-gluon plasma within HTL approximation in presence of finite chemical potential. The general structure of effective massive fermion propagator is constructed for thermo-magnetic medium. Then the self-energy structure functions upto  $\mathcal{O}[(q_f B)^2]$  in presence of chemical potential have been calculated in the weak magnetic field regime using the scale hierarchy  $\sqrt{|q_f B|} < gT < T$ . Quark condensate is computed using effective quark propagator in presence of magnetic field. Finally we obtain completely analytic expression for chiral susceptibility in hot and dense weakly magnetized QCD medium. We have subtracted the UV divergence via  $\overline{MS}$  renormalization scheme. It is found that the chiral susceptibility is increased due to the presence of chemical potential as well as the background magnetic field. At high temperature the effect of magnetic field on chiral susceptibility becomes feeble.



# QUARKONIUM IN HOT AND MAGNETIZED QGP MEDIUM

---

In this chapter we have explored the imaginary part of the Heavy Quark (HQ) potential and subsequently the dissociation of heavy quarkonia at finite temperature and magnetic field. The present work contain three new ingredients. First one is considering all Landau level summation, for which present work can be applicable in entire magnetic field domain - from weak to strong. Second one is the general structure of the gauge boson propagator in a hot magnetized medium, which is used here in heavy quark potential problem first time. Third one is a rich anisotropic structure of the complex heavy quark potential, which explicitly depends on the longitudinal and transverse distance. This chapter is based on the work presented in the following paper: *Anisotropic tomography of heavy quark dissociation by using general propagator structure at finite magnetic field*

Ritesh Ghosh, Aritra Bandyopadhyay, Indrani Nilima, Sabyasachi Ghosh, [Communicated], [[arXiv:2204.02312](https://arxiv.org/abs/2204.02312)].

## 7.1 Introduction

As mentioned earlier in Chapter 1 several theoretical efforts [227, 228] have been made to study the modification of the strongly interacting matter in presence of an external magnetic field produced in noncentral HICs. In this chapter we have focused on one important signature of quark matter and its behavior in presence of an arbitrary external magnetic field, i.e. heavy quarkonia. Because of their large mass and resistant behaviour towards thermal medium heavy quarkonia is considered as one of the most dynamic probes to study the characteristics of the quark matter. There are mainly two lines of theoretical approaches to determine quarkonium spectral functions, viz. the potential models [113, 114, 116, 117, 229, 230] and the lattice QCD studies [118, 231]. In lattice QCD simulation approach, one studies the spectral functions derived from Euclidean meson correlation [232]. Because of the decreasing temporal range at large temperature, construction of spectral functions is problematic and hence the results suffer from discretization effects and statistical errors and, thus, are still inconclusive. This is why potential models have been used widely to study the heavy quarkonia at finite temperatures. Pioneering studies to explore the heavy quarkonia and its dissociation at finite temperature using potential models has been done by Satz et. al. [113, 114]. In Ref. [113], they predicted a suppression of the bound state of  $c\bar{c}$  pair, which is being caused by the shortening of the screening length for color interactions in the quark matter.

A very short lifetime ( $\sim$  few fm/c) of the quark matter in HIC experiments further emphasizes the need to explore the effects of magnetic field on the properties of heavy quarkonia. There are also several studies in the literature which have explored the effect of magnetic field on the evaluation of quarkonia [233–236]. Modification of the heavy quark potential is one of the most important aspect of the theoretical up gradation required to

### 7.1. Introduction

study the properties of heavy quarkonia in a magnetized medium, which is studied recently by Refs. [1, 237]. The effect of a constant uniform magnetic field on the static quarkonium potential at zero and finite temperature and on the screening masses have been studied in Refs. [238] and [239]. For heavy quark diffusion phenomenology at finite magnetic field, see Refs. [240, 241].

In this chapter we will investigate the properties of heavy quarkonia at finite magnetic field using the most general structure of the gluon propagator in a hot magnetized medium. Several recent studies have presented various general structures of the fermion and gauge boson self energies vis-a-vis propagators at finite temperature and in presence of an external magnetic field [199, 200, 242–249] using different independent tensor structures. For the present work we have chosen the effective gluon propagator in a hot and magnetized medium from Ref. [199]. The medium modified heavy quark potential is the sum of both Coulombic and string terms [250] and it is directly dependent on the temporal component of the gluon propagator through the inverse of dielectric permittivity. For obtaining the imaginary parts of medium modified heavy quark potential we will extract the imaginary part of the resummed gluon propagator in terms of real and imaginary parts of gluon self energy form factors. Moreover, the form factors can be divided into fermionic and gluonic contributions and the magnetic field dependent contribution arises only from the fermionic contribution. Subsequently, this will give the imaginary part of the dielectric permittivity, which in turn will give the imaginary parts of the in-medium heavy quark potential [231, 251–254].

When we notice recent Refs. [1, 237] for the research topic on heavy quark potential at finite temperature and magnetic field, then we can find limitation of their application zone of magnetic field. Ref. [1] can be applicable in the strong field limit, where lowest Landau level (LLL) approximation take dominant contribution, whereas Ref. [2] is done

## Chapter 7. Quarkonium in hot and magnetized QGP medium

in the weak field limit. In this regards, present work can be applicable to entire magnetic field domain from weak to strong as we are considering all Landau level summations. Unlike to Refs. [1, 2], where they had neglected the Debye mass ( $m_D$ ) independent terms in the calculation of the form factors, those terms will be automatically incorporated in our calculation. This contribution has been taken care by using general structure of gluon propagator at finite temperature and magnetic field. Apart from these two ingredients - (1) considering all Landau level summation and (2) considering general structure of gluon propagator at finite temperature and magnetic field, we also have shown the anisotropic structure of heavy quark potential, which can be naturally expected at finite magnetic field but ignored in earlier Refs. [1, 2].

This chapter is organized as follows. In section 7.2, we will discuss the formalism used to execute this work. In subsection 7.2.1 we discuss about the formalism of Heavy quark potential in presence of an external magnetic field. Subsections 7.2.2 and 7.2.3 deal with the formalism of imaginary part of the potential and evaluation of the real and imaginary parts of form factor  $b(P)$  respectively. Moreover in subsection 7.2.4, we will discuss about the final anisotropic expression of potential and decay width expression. Section 7.3 refers to the results and discussions after which we conclude in section 7.4.

## 7.2 Formalism

### 7.2.1 Heavy quark potential in presence of an external magnetic field

To understand the melting of the quarkonia near crossover temperature, one needs to incorporate the non-perturbative effect in the heavy-quark potential. The Cornell potential consisting of the Coulomb and string-like part can describe the vacuum behavior of quarkonium bound state very well. In-medium behavior of the potential is not well-known in literature. There are several proposals to parametrize the real and imaginary part of potential and we would use one of them, by the virtue of which we can write down the in medium heavy quark potential in real space as [255, 256]

$$V(r) = \int \frac{d^3p}{(2\pi)^{3/2}} \left( e^{i\mathbf{p}\cdot\mathbf{r}} - 1 \right) \frac{V_{\text{Cornell}}(p)}{\epsilon(p)}, \quad (7.1)$$

where  $\epsilon(p)$  is the dielectric permittivity which contains the medium information and  $V_{\text{Cornell}}$  is the Cornell potential in momentum space, which is given by

$$V_{\text{Cornell}}(p) = -\sqrt{2/\pi} \frac{\alpha}{p^2} - \frac{4\sigma}{\sqrt{2\pi}p^4}, \quad (7.2)$$

with  $\alpha = C_F\alpha_s$ ,  $C_F = (N_c^2 - 1)/2N_c$  and  $\sigma$  is the string tension.

Inverse of dielectric permittivity  $\epsilon(p)$  is related with the temporal component of the effective gluon propagator  $D^{\mu\nu}$  by the definition [1]

$$\epsilon^{-1}(p) = \lim_{p_0 \rightarrow 0} p^2 D^{00}(P). \quad (7.3)$$

In presence of an external magnetic field one needs to consider appropriate modifications in the gluon propagator. The general structure of a gauge boson propagator in a hot magnetized medium is given in appendix C.1 and from eq (C.10) one can easily extract the temporal component as

$$D^{00}(P) = \frac{P^2 - d}{(P^2 - b)(P^2 - d) - a^2} B^{00}(P), \quad (7.4)$$

where  $a(P)$ ,  $b(P)$  and  $d(P)$  are the corresponding form factors whose explicit expressions are given in appendix C.1. Now in the vanishing limit of  $p_0$ , form factor  $a(P)$  also vanishes [257]. So we are not considering the form factor  $a(P)$  in our case. Hence in our case the temporal component of the effective propagator can be further simplified as

$$D^{00}(P) = \frac{1}{(P^2 - b)} B^{00}(P). \quad (7.5)$$

## 7.2.2 Imaginary part of the potential

Instead of going to real part of potential, we will focus directly on its imaginary part as it will be connected with heavy quark dissociation probability, which is our matter of interest. From Eq. (7.1), one can straightway extract the imaginary part of the in medium heavy quark potential as

$$\begin{aligned} \text{Im}V(r) &= \int \frac{d^3p}{(2\pi)^{3/2}} \left( e^{i\mathbf{p}\cdot\mathbf{r}} - 1 \right) V_{\text{Cornell}}(p) \text{Im} \epsilon^{-1}, \\ &= \int \frac{d^3p}{(2\pi)^{3/2}} \left( e^{i\mathbf{p}\cdot\mathbf{r}} - 1 \right) V_{\text{Cornell}}(p) p^2 \left( \lim_{p_0 \rightarrow 0} \text{Im} D^{00}(P) \right). \end{aligned} \quad (7.6)$$

## 7.2. Formalism

In the spectral function representation one can evaluate the imaginary part of the effective gauge boson propagator ( $D^{\mu\nu} = C_i \mathcal{P}_i^{\mu\nu}$ , where  $C_i$  are the form factors and  $\mathcal{P}_i^{\mu\nu}$  are the projection operators) as [258]

$$\text{Im } D^{\mu\nu}(P \equiv \{p_0, \mathbf{p}\}) = -\pi (1 + e^{-p_0/T}) \rho^{\mu\nu}(p_0, \mathbf{p}), \quad (7.7)$$

where  $\rho^{\mu\nu}$  is the spectral function, represented as

$$\rho^{\mu\nu}(p_0, \mathbf{p}) = \frac{1}{\pi} \frac{e^{p_0/T}}{e^{p_0/T} - 1} \rho_i \mathcal{P}_i^{\mu\nu}, \quad (7.8)$$

with  $\rho_i$  being the imaginary parts of the respective form factors, i.e.  $\rho_i = \text{Im } C_i$ . Using this approach, from equation (7.5) the imaginary part of the temporal component of the gluon propagator can be written in terms of the self energy form factor  $b(P)$  as

$$\text{Im } D^{00}(p_0, \mathbf{p}) = -\pi(1 + e^{-p_0/T}) \times \frac{1}{\pi} \frac{e^{p_0/T}}{e^{p_0/T} - 1} \frac{\text{Im } b}{(P^2 - \text{Re } b)^2 + (\text{Im } b)^2} \frac{1}{\bar{u}^2}, \quad (7.9)$$

where we have used  $B^{00}(P) = \frac{1}{\bar{u}^2}$ , with  $\bar{u} = -\frac{\mathbf{p}^2}{p_0^2 - \mathbf{p}^2}$ . In the next subsection we will evaluate the real and imaginary part of the form factor  $b(P)$ .

### 7.2.3 Evaluation of the real and imaginary parts of $b(P)$

The form factor  $b(P)$  can be divided into quark and gluonic contributions as

$$b(P) = b_q(P) + b_g(P) = -\frac{p_0^2 - p^2}{p^2} \left[ \Pi_q^{00}(P) + \Pi_g^{00}(P) \right], \quad (7.10)$$

where  $\Pi_{q/g}^{00}$  are quark/gluonic parts of the temporal component of the one loop gluon self energy in a hot magnetized medium.

### Gluonic contribution

Since gluons are not affected by magnetic field, the gluonic contribution of the one loop self energy is similar to the  $B = 0$  case [1], i.e.

$$\Pi_g^{00} = m_{Dg}^2 \left[ 1 - \frac{p_0}{2p} \ln \left| \frac{p_0 + p}{p_0 - p} \right| + i\pi \frac{p_0}{2p} \Theta(p^2 - p_0^2) \right], \quad (7.11)$$

where  $m_{Dg}^2 = \frac{g^2 T^2 N_c}{3}$  and  $\Theta$  is the step-function. This implies in the  $p_0 \rightarrow 0$  limit we can write down the real and imaginary part of the form factor  $b_g(P)$  as

$$\lim_{p_0 \rightarrow 0} \text{Re } b_g(P) = m_{Dg}^2, \quad (7.12)$$

$$\lim_{p_0 \rightarrow 0} \text{Im } b_g(P) = \lim_{p_0 \rightarrow 0} m_{Dg}^2 \frac{\pi p_0}{2p} \Theta(p^2). \quad (7.13)$$

### Fermionic contribution

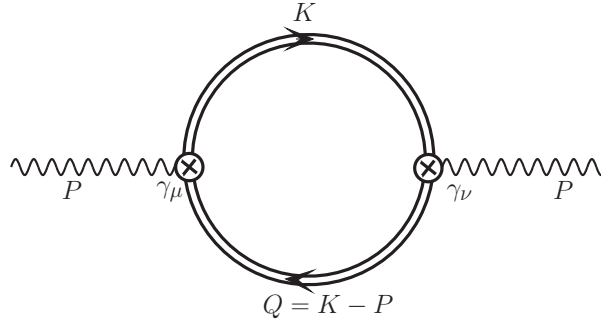


Figure 7.1: One loop gluon self-energy.

To evaluate the fermionic contribution we are going to review the one loop gluon self-energy calculation from quark-antiquark loop in presence of arbitrary magnetic field. Quark-antiquark are affected by magnetic field, so the propagator should be modified in presence



## 7.2. Formalism

of the magnetic field. Translation invariant part of the fermion propagator  $G(t, \mathbf{r})$  can be written in mixed coordinate-momentum space as [76, 228]

$$G(t, \mathbf{r}) = \int \frac{d\omega dk_z}{(2\pi)^2} e^{ik_z z - i\omega t} G(\omega, k_z, \mathbf{r}_\perp), \quad (7.14)$$

where

$$G(\omega, k_z, \mathbf{r}_\perp) = i \frac{e^{-\mathbf{r}_\perp^2 / (4d_f^2)}}{2\pi d_f^2} \sum_{l=0}^{\infty} \frac{D_l(\omega, k_z, \mathbf{r}_\perp)}{\omega^2 - k_z^2 - m_f^2 - 2l|eB|}. \quad (7.15)$$

In this case, the magnetic field  $\mathbf{B}$  is in the z-direction and the vector potential is given by Landau gauge i.e.  $\mathbf{A} \equiv (-By, 0, 0)$ . The numerator of eq. (7.15) is given by

$$\begin{aligned} D_l(\omega, k_z, \mathbf{r}_\perp) &= (\omega\gamma^0 - k_z\gamma^3 + m) \left[ P_+ L_l \left( \frac{\mathbf{r}_\perp^2}{2d_f^2} \right) + P_- L_{l-1} \left( \frac{\mathbf{r}_\perp^2}{2d_f^2} \right) \right] \\ &\quad - \frac{i}{d_f^2} (\mathbf{r}_\perp \cdot \boldsymbol{\gamma}_\perp) L_{l-1}^1 \left( \frac{\mathbf{r}_\perp^2}{2d_f^2} \right), \end{aligned} \quad (7.16)$$

where  $P_\pm = \frac{1}{2}[1 \pm i \text{sign}(q_f B) \gamma^1 \gamma^2]$  are spin projectors and  $d_f = \frac{1}{\sqrt{|q_f B|}}$ .  $L_n^\alpha(x)$  are the generalized Laguerre polynomials and  $L_{-1}^\alpha(x) = 0$  by definition. So the gauge-boson self-energy can be written as

$$\begin{aligned} \Pi_q^{\mu\nu}(i\omega_m, \mathbf{p}) &= g^2 T \frac{1}{2} \sum_{n=-\infty}^{\infty} \int \frac{dk_z}{2\pi} d^2 \mathbf{r}_\perp e^{-i\mathbf{r}_\perp \cdot \mathbf{p}_\perp} \\ &\quad \times \text{Tr} \left[ \gamma^\mu G(i\omega_n, \mathbf{k}_z, \mathbf{r}_\perp) \gamma^\nu G(i\omega_n - i\omega_m, \mathbf{k}_z - \mathbf{p}_z, -\mathbf{r}_\perp) \right]. \end{aligned} \quad (7.17)$$

Here fermionic and bosonic Matsubara frequencies are  $\omega_n = (2n+1)\pi T$  and  $\omega_m = 2m\pi T$  respectively. Eq. (7.17) can be further simplified as

$$\begin{aligned} \Pi_q^{\mu\nu}(i\omega_m, \mathbf{p}) &= -g^2 T \frac{1}{2} \sum_{n=-\infty}^{\infty} \int \frac{dk_z}{2\pi} d^2\mathbf{r}_\perp e^{-i\mathbf{r}_\perp \cdot \mathbf{p}_\perp} \frac{e^{-\mathbf{r}_\perp^2/(2d_f^2)}}{(2\pi d_f^2)^2} \\ &\times \sum_{l=0}^{\infty} \sum_{l'=0}^{\infty} \frac{1}{k_0^2 - E_{l,k_z}} \frac{S^{\mu\nu}}{q_0^2 - E_{l',q_z}}, \end{aligned} \quad (7.18)$$

where the fermionic energies are defined as  $E_{l,k_z,f} = \sqrt{m_f^2 + k_z^2 + 2l|q_f B|}$ . Here we define  $S^{\mu\nu}$  as the trace

$$S^{\mu\nu} = \text{Tr}[\gamma^\mu D_1(i\omega_n, \mathbf{k}_z, \mathbf{r}_\perp) \gamma^\nu D_1'(i\omega_n - i\omega_m, \mathbf{k}_z, \mathbf{r}_\perp)]. \quad (7.19)$$

Since we are only interested to find the temporal component of the one loop self energy, we can straightway put  $\mu = \nu = 0$  to get

$$\begin{aligned} \Pi_q^{00}(i\omega_m, \mathbf{p}) &= -g^2 T \frac{1}{2} \sum_{n=-\infty}^{\infty} \int \frac{dk_z}{2\pi} d^2\mathbf{r}_\perp e^{-i\mathbf{r}_\perp \cdot \mathbf{p}_\perp} \frac{e^{-\mathbf{r}_\perp^2/(2d_f^2)}}{(2\pi d_f^2)^2} \\ &\times \sum_{l=0}^{\infty} \sum_{l'=0}^{\infty} \frac{1}{k_0^2 - E_{l,k_z}} \frac{1}{q_0^2 - E_{l',q_z}} \\ &\times \left\{ 2(L_l L_{l'} + L_{l-1} L_{l'-1})(k_0 q_0 + k_3 q_3 + m_f^2) + \frac{4\mathbf{r}_\perp^2}{d_f^4} L_{l-1}^1 L_{l'-1}^1 \right\} \\ &= -g^2 T \frac{1}{2} \sum_{n=-\infty}^{\infty} \int \frac{dk_z}{2\pi} \sum_{l=0}^{\infty} \sum_{l'=0}^{\infty} \frac{1}{k_0^2 - E_{l,k_z}} \frac{1}{q_0^2 - E_{l',q_z}} \frac{1}{4\pi^2 d_f^4} \\ &\times \left\{ 4\pi d_f^2 (X_{l,l'} + X_{l-1,l'-1})(k_0 q_0 + k_3 q_3 + m_f^2) + 8\pi X_{l-1,l'-1}^1 \right\} \\ &= -\frac{g^2}{4\pi^2} \frac{1}{2} \sum_{f=u,d} \frac{1}{d_f^4} \int \frac{dk_z}{2\pi} \sum_{l,l'=0}^{\infty} \sum_{s_1, s_2=\pm 1} \frac{n_F(E_{l,k_z,f}) - n_F(s_1 E_{l',q_z,f})}{4s_1 E_{l,k_z,f} E_{l',q_z,f}} \\ &\times \frac{1}{is_2 \omega_m + E_{l,k_z,f} - s_1 E_{l',q_z,f}} (I_{1,f} + I_{2,f}), \end{aligned} \quad (7.20)$$

## 7.2. Formalism

where the functions  $I_{1,f}$  and  $I_{2,f}$  are defined as

$$\begin{aligned} I_{1,f} &= 4\pi d_f^2 \left( s_1 E_{k_z,l} E_{q_z,l'} + k_z q_z + m_f^2 \right) \left[ X_{l,l'} + X_{l-1,l'-1} \right], \\ I_{2,f} &= 8\pi X_{l-1,l'-1}^1. \end{aligned} \quad (7.21)$$

The associated function  $X_{m,n}$  and  $X_{m,n}^1$  are defined in Appendix C.3. Finally we can write down the real part of the temporal component of the self energy in the limit of  $p_0 \rightarrow 0$  as

$$\begin{aligned} \Pi_q^{00}(p_0, \mathbf{p}) \Big|_{p_0 \rightarrow 0} &= -\frac{g^2}{8\pi^2} \sum_{f=u,d} \frac{1}{d_f^4} \int \frac{dk_z}{2\pi} \sum_{l,l'=0}^{\infty} \sum_{s_1, s_2 = \pm 1} \\ &\quad \left( \frac{n_F(E_{l,k_z,f}) - n_F(s_1 E_{l',q_z,f})}{4s_1 E_{l,k_z,f} E_{l',q_z,f}} \frac{I_{1,f} + I_{2,f}}{E_{l,k_z,f} - s_1 E_{l',q_z,f}} \right) \Big|_{p_0 \rightarrow 0} \end{aligned} \quad (7.22)$$

Now to find out the imaginary part of the self-energy, we need to perform analytic continuation to the real value of gluon energy. By replacing  $i\omega_m \rightarrow p_0 + i\epsilon$ , the imaginary part of the temporal component of the gluon self-energy is given by,

$$\begin{aligned} \text{Im}\Pi_q^{00}(p_0, \mathbf{p}) &= \frac{g^2}{4\pi} \frac{1}{2} \sum_{f=u,d} \frac{1}{d_f^4} \int \frac{dk_z}{2\pi} \sum_{l,l'=0}^{\infty} \sum_{s_1, s_2 = \pm 1} \frac{n_F(E_{l,k_z,f}) - n_F(s_1 E_{l',q_z,f})}{4s_1 s_2 E_{l,k_z,f} E_{l',q_z,f}} \\ &\quad \times \delta(s_2 p^0 + E_{l,k_z,f} - s_1 E_{l',q_z,f}) (I_{1,f} + I_{2,f}). \end{aligned} \quad (7.23)$$

In the limit of our interest, i.e.  $p_0 \rightarrow 0$ , only two delta function will contribute i.e. for  $s_2 = \pm 1$  when  $s_1 = 1$ . We can write the above equation as

$$\begin{aligned} \text{Im}\Pi_q^{00}(p_0, \mathbf{p}) \Big|_{p_0 \rightarrow 0} &= \frac{1}{2} \frac{g^2}{4\pi} \sum_{f=u,d} \frac{1}{d_f^4} \int \frac{dk_z}{2\pi} \sum_{l,l'=0}^{\infty} \sum_{s_2 = \pm 1} \frac{1}{4s_2 E_{l,k_z,f} E_{l',q_z,f}} \frac{\partial n_F(E_k)}{\partial E_k} s_2 p_0 \\ &\quad \times \delta(E_{l,k_z,f} - E_{l',q_z,f}) (I_{1,f} + I_{2,f}) \end{aligned} \quad (7.24)$$

$$= \frac{1}{2} \frac{2g^2}{4\pi} p_0 \sum_{f=u,d} \frac{1}{d_f^4} \int \frac{dk_z}{2\pi} \sum_{l,l'=0} \frac{I_{1,f} + I_{2,f}}{4E_{l,k_z,f} E_{l',q_z,f}} \frac{\partial n_F(E_k)}{\partial E_k} \delta(E_{l,k_z,f} - E_{l',q_z,f}) \quad (7.25)$$

Now we use the following property of the Dirac delta function

$$\delta(f(x)) = \sum_n \frac{\delta(x - x_n)}{\left| \frac{\partial f(x)}{\partial x} \right|_{x=x_n}}, \quad (7.26)$$

with  $x_n$  as the zeros of the function  $f(x)$ , to obtain the solutions for  $k_z$  as

$$k_{z0} = \frac{2(l' - l)|q_f B| + p_z^2}{2p_z}. \quad (7.27)$$

Using the value of  $k_{z0}$  subsequently we obtain the explicit expressions of fermionic energies as

$$E_{k_z,l} \Big|_{k_z=k_{z0}} = \sqrt{m_f^2 + 2l|q_f B| + \left( \frac{p_z^2 + 2(l' - l)|q_f B|}{2p_z} \right)^2}, \quad (7.28)$$

$$E_{q_z,l'} \Big|_{k_z=k_{z0}} = \sqrt{m_f^2 + 2l'|q_f B| + \left( \frac{p_z^2 - 2(l' - l)|q_f B|}{2p_z} \right)^2}. \quad (7.29)$$

Hence, finally we can write

$$\text{Im}\Pi_q^{00}(p_0, \mathbf{p}) \Big|_{p_0 \rightarrow 0} = -\beta \frac{2g^2}{4\pi} \frac{1}{2} p_0 \sum_{f=u,d} \frac{1}{d_f^4} \frac{1}{2\pi} \sum_{l,l'=0} \frac{I_{1,f} + I_{2,f}}{4p_z E_{l,k_z,f}} n_F(E_k) (1 - n_F(E_k)) \Big|_{k_z=k_{z0}} \quad (7.30)$$

So, the real and imaginary parts of the form factor  $b_q$  in the limit of  $p_0 \rightarrow 0$  are respectively given in Eq. (7.22) and Eq. (7.30).

## 7.2.4 Final expression of Imaginary part of potential and Decay width

Using Eqs. (7.12), (7.13), (7.22) and (7.30) in Eq. (7.9) within the limit  $p_0 \rightarrow 0$ , we find

$$\begin{aligned} \text{Im } D^{00}(\mathbf{p}) &= -2 \frac{1}{(p^2 + \text{Re } b(p_0 = 0, \mathbf{p}))^2} \times \left( \frac{\pi T m_{Dg}^2}{2p} \right. \\ &\quad \left. - \frac{g^2}{4\pi} \sum_{f=u,d} \frac{1}{d_f^4} \frac{1}{2\pi} \sum_{l,l'=0} \frac{I_{1,f} + I_{2,f}}{4 p_z E_{l,k_z,f}} n_F(E_k) (1 - n_F(E_k)) \Big|_{k_z=k_{z0}} \right) \end{aligned} \quad (7.31)$$

where

$$\begin{aligned} \text{Re } b(p_0 = 0, \mathbf{p}) &= \text{Re } b_q(p_0 = 0, \mathbf{p}) + \text{Re } b_g(p_0 = 0, \mathbf{p}), \\ &= \text{Re } \Pi_q^{00}(p_0 = 0, \mathbf{p}) + m_{Dg}^2. \end{aligned} \quad (7.32)$$

As the expression for  $\text{Im } D^{00}$  is an explicit function of  $p_z$  and  $p_\perp$ , so we need to accordingly break up the phase space due to anisotropy of the external magnetic field along the ‘ $z$ ’ direction. By doing that, Eq. (7.6) will be transformed into

$$\begin{aligned} \text{Im } V(r_\perp, z) &= - \int \frac{p_\perp dp_\perp dp_z d\phi_p}{(2\pi)^{3/2}} \left( e^{ip_\perp(x \cos \phi_p + y \sin \phi_p) + izp_z} - 1 \right) \\ &\quad \times \left( \sqrt{2/\pi} \frac{\alpha}{p^2} + \frac{4\sigma}{\sqrt{2\pi} p^4} \right) p^2 \text{Im } D^{00}(p_z, p_\perp), \\ &= - \int \frac{p_\perp dp_\perp}{(2\pi)^{3/2}} \int_0^\infty dp_z 4\pi \left( J_0(p_\perp r_\perp) \cos z p_z - 1 \right) \\ &\quad \times \left( \sqrt{2/\pi} \frac{\alpha}{p^2} + \frac{4\sigma}{\sqrt{2\pi} p^4} \right) p^2 \text{Im } D^{00}(p_z, p_\perp). \end{aligned} \quad (7.33)$$

Eq. (7.33) is our final expression for the imaginary part of the heavy quark potential.

We will now use the imaginary part of the potential to calculate decay width ( $\Gamma$ ). So

using the first-order time-independent perturbation theory, decay width( $\Gamma$ ) can be estimated from the given equation [1, 252]

$$\Gamma(T, B) = - \int d^3\mathbf{r} |\Psi(r)|^2 \text{Im} V(\hat{r}; T, B), \quad (7.34)$$

Here  $\psi(r)$  is the Coulombic wave function for the ground state is given by

$$\psi(r) = \frac{1}{\sqrt{\pi a_0^3}} e^{-r/a_0}, \quad (7.35)$$

where  $a_0 = 2/(m_Q\alpha)$ . Substituting the imaginary part of equation given in (7.33) into (7.34) we estimate the decay width for given temperature and magnetic field. We would discuss the decay width of two quarkonia,  $J/\psi$  (the ground state of charmonium,  $c\bar{c}$ ) and  $\Upsilon$  (bottomonium,  $b\bar{b}$ ).

## 7.3 Results

In this section we will discuss our results about the imaginary part of the HQ potential and the decay rate. For our present study we have chosen  $N_c = 3$ ,  $N_f = 2$  and the strong running coupling constant  $g$  as

$$g^2(T) = \frac{24\pi^2}{(11N_c - 2N_f) \ln\left(\frac{2\pi T}{\Lambda_{\overline{\text{MS}}}}\right)}, \quad (7.36)$$

with  $\Lambda_{\overline{\text{MS}}} = 0.176$  GeV [155]. We also want to mention here, that there are recent studies which explore the thermo-magnetic behavior of the strong coupling  $g$  [92, 225, 259, 260], which will be interesting to incorporate in future works. We have taken the value of string tension as  $\sigma = 0.174$  GeV<sup>2</sup> [261]. Considering the anisotropy encountered in our studies,

### 7.3. Results

throughout the results section we will discuss two cases, i.e. with varying  $z$  for a fixed  $r_{\perp}$  and vice versa.

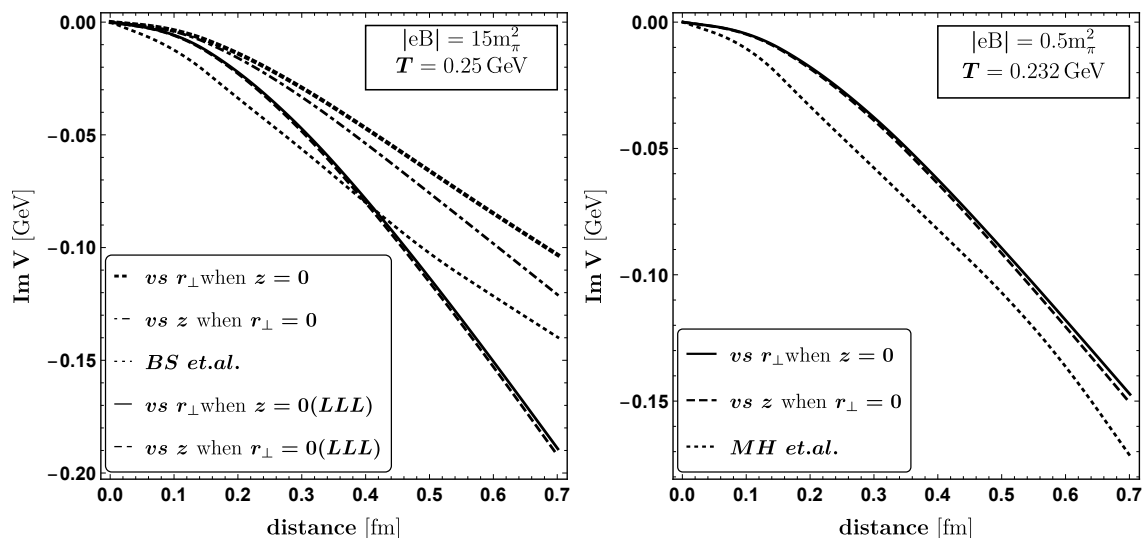


Figure 7.2: Variation of  $\text{Im } V$  with distance. We have shown two plots comparing with two recent results from Ref. [1] (left panel) and Ref. [2] (right panel) which requires certain fixed values of magnetic field ( $eB$ ) and temperature ( $T$ ), as depicted in the plot. We have considered both the cases, i.e. with vanishing  $r_{\perp}$  and with vanishing  $z$ .

As mentioned in the introduction, recently several studies have explored the heavy quark potential in a magnetized medium restricting themselves to limiting cases involving strong or weak magnetic field approximations. In this context, present work can be applicable in entire domain of magnetic field from weak to strong as we are considering all Landau level summation. Therefore, we have started our numerical presentation from Fig. 7.2, where we have compared our result with two such recent results, strong field or LLL approximated result from Singh et.al. [1] and weak field or perturbatively expanded result from Hasan et.al. [2]. Since our present calculation has captured the anisotropic outcomes of magnetic field, so potential become function of  $r_{\perp}$  and  $z$  but earlier Refs. [1, 2] provide isotropic potential in terms of  $r$  only. Hence, the comparison will not be very

straight forward. In the left panel, we have compared our anisotropic results for  $r_{\perp} = 0$  and for  $z = 0$  with the LLL approximated results from Ref. [1] which shows noticeable difference between them. One of the source of this difference is that our results carry all Landau level summation but Ref. [1] is LLL approximation. To find other sources of difference, we have generated our LLL approximated results which also differs from that of Ref [1]. Origin of this difference between the two LLL approximated results can be traced back to the structure of the coefficient function  $b$  where we have made no approximations unlike Ref [1], where they have neglected the Debye mass ( $m_D$ ) independent terms. Also anisotropic and isotropic structures are another level of differences. Similar difference can again be observed in the right panel of fig. 7.2 where we have compared our general results for both  $r_{\perp} = 0$  and  $z = 0$  with that of an weakly approximated one from Ref [2]. Hence, the left and right panels of Fig. 7.2 indicate that our results in weak and strong fields both limits can not merged with earlier estimations [1, 2] because of general structure of magnetized gluon propagator and anisotropic structure of potential, considered in the present work.

To further emphasise the deficiency of the LLL approximation, in fig. 7.3 we have plotted the variation of the imaginary part of the HQ potential with distance for various increasing values of the Landau levels and compared them with respect to the LLL approximated result. Again, we have shown two different cases in two panels of fig. 7.3, left panel showing  $r_{\perp} = 0$  case and right panel showing  $z = 0$  case. For both the cases one can identify that the LLL approximated result is hugely overestimating the values for the imaginary part of the HQ potential, whereas with increasing values of the number of Landau levels  $n$ , the gap with the full result is getting diminished. We have considered  $n = 50$  as full results since we notice that the values are not changing beyond  $n = 10$ .

In fig. 7.4, we have again compared our general result with the Debye mass approxi-



### 7.3. Results

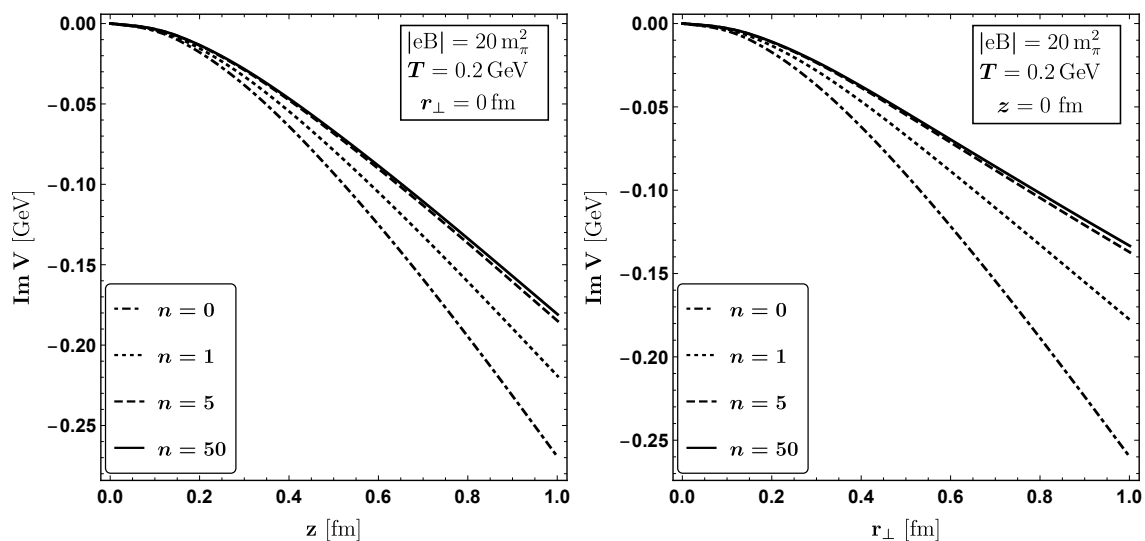


Figure 7.3: Variation of  $\text{Im } V$  with distance, i.e. with  $z$  for vanishing  $r_{\perp}$  (left panel) and with  $r_{\perp}$  for vanishing  $z$  (right panel), is shown considering different number of Landau levels where we show the difference between the LLL approximated result and the full result.

mated results, but this time for arbitrary values of external fields. As our observable, again we have chosen the imaginary part of the HQ potential. In appendix C.4, we have given the expression for the Debye mass approximated imaginary part of the HQ potential, which is isotropic in nature (i.e. no explicit dependence on  $r_{\perp}$  and  $z$ ), unlike our most general result. So, in fig. 7.4, we have shown this Debye mass approximated isotropic curve (solid curve) with our anisotropic curves (dashed and dotted curves). The anisotropic curves are plotted from our main result, i.e. eq. (7.33) using eq. (7.31). Among the two curves, the dashed curve shows the variation with  $z$  for vanishing  $r_{\perp}$  whereas the dotted curve shows the variation with  $r_{\perp}$  for vanishing  $z$ . On the other hand, the solid curve is drawn using eq. C.17 where one can see that the magnetic field effect is coming solely through the Debye mass, subsequently providing incomplete information. In this scenario, we are getting the isotropic space dependency of the potential. One can observe from fig. 7.4 that the

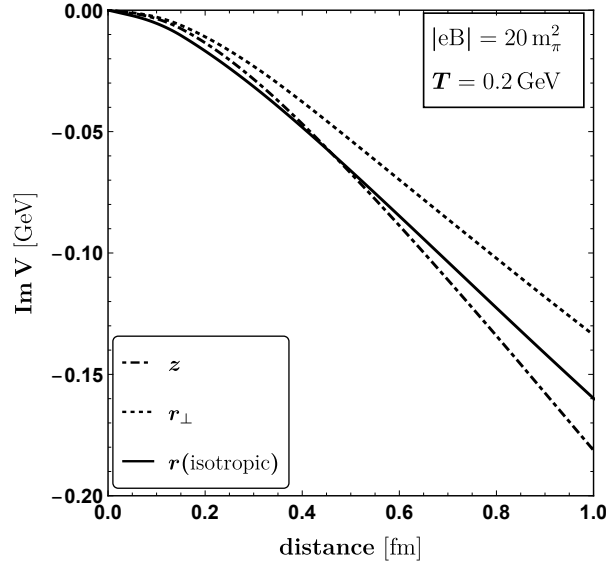


Figure 7.4: Variation of  $\text{Im } V$  with distance comparing between full and Debye mass approximated expression. The variation is shown with  $z$  for vanishing  $r_{\perp}$  (dashed curve), with  $r_{\perp}$  for vanishing  $z$  (dotted curve), and with isotropic  $r$  using Debye mass approximated expression (solid curve).

difference between the full result and the Debye mass approximated result increases significantly with increasing distance, thereby emphasizing the importance of considering the anisotropic nature of the full HQ potential in presence of arbitrary values of external magnetic fields. So, from Fig. (7.2) to (7.4) are devoted to show our ingredient details in the heavy quark potential at finite  $T$ ,  $B$  with respect to earlier calculations [1, 2]. Next, we will zoom-in more the anisotropic tomography of this heavy quark potential due to magnetic field, which is probably first time addressed in the literature.

Fig. 7.5 have explored the anisotropic nature of the heavy quark potential in presence of the external magnetic field, applied along the  $z$  direction. In upper panel of fig. 7.5 we have shown the variation of the imaginary part of the HQ potential with respect to the longitudinal distance  $z$  for two different fixed values of the transverse distance  $r_{\perp} = 0$  (upper-left panel) and  $r_{\perp} = 0.5$  fm (upper-right panel). For both the plots we have fixed

### 7.3. Results

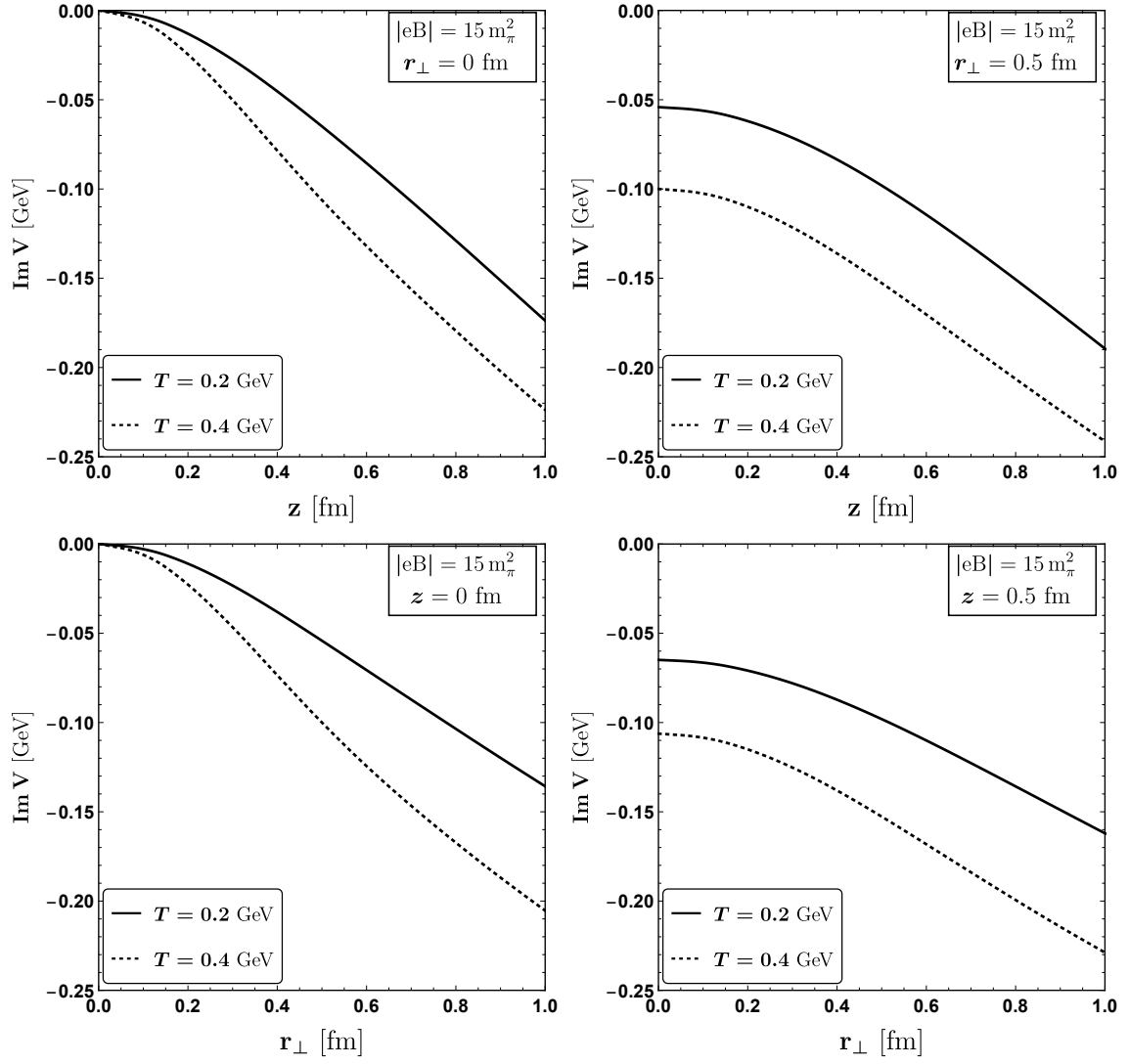


Figure 7.5: Variation of  $\text{Im } V$  with  $z$  for two different fixed values of  $r_{\perp}$  -  $r_{\perp} = 0$  (upper-left panel) and  $r_{\perp} = 0.5$  fm (upper-right panel) and with  $r_{\perp}$  for two different fixed values of  $z$  -  $z = 0$  (lower-left panel) and  $z = 0.5$  fm (lower-right panel). For each of the plots we have chosen two different values of temperature and a fixed value of the external magnetic field.

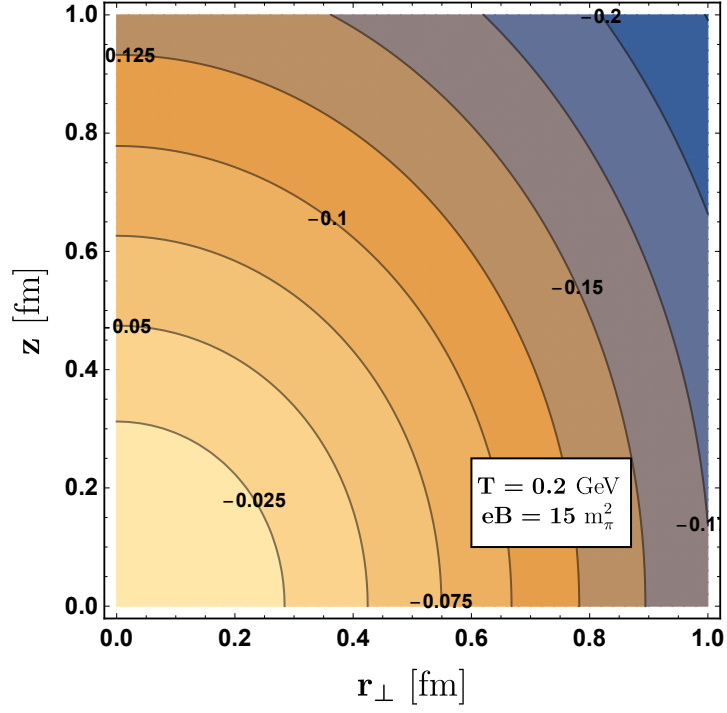


Figure 7.6: Contour plot of  $\text{Im } V$  showing the equal potential regions for different values of  $r_{\perp}$  and  $z$ .

the external magnetic field to  $eB = 15m_{\pi}^2$  and shown the variation for two different values of the temperature, i.e.  $T = 0.2$  and  $T = 0.4$  GeV. For the plot with  $r_{\perp} = 0$ , at lower values of  $z$ , both the curves start from vanishing  $\text{Im } V$ , as expected. Also for both the plots one can notice that with higher values of temperature, the magnitude of  $\text{Im } V$  also becomes higher. The curves show a gradually decreasing behaviour of the imaginary part of the HQ potential with increasing distance, as was also evident from figures. 7.2 and 7.3. Lower panel of Fig. 7.5 shows similar behaviours, where we have fixed  $z$  to two different values of  $z = 0$  (lower-left panel) and  $z = 0.5$  fm (lower-right panel) and varied  $\text{Im } V$  with respect to  $r_{\perp}$ .

In fig. 7.6 we have shown the overall spatial dependence of the imaginary part of the

### 7.3. Results

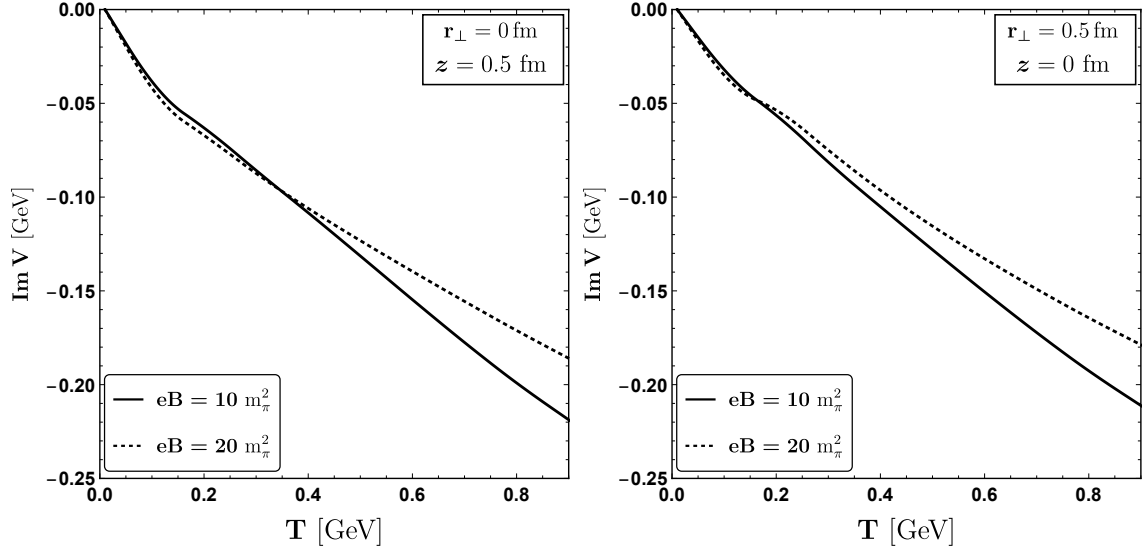


Figure 7.7: Variation of  $\text{Im } V$  with temperature shown for two different cases, i.e. for vanishing  $r_{\perp}$  (left panel) and for vanishing  $z$  (right panel). For each of the plots, we have chosen two different values of the external magnetic field which shows some interesting crossovers.

HQ potential in the form of a contour plot where we have varied both  $z$  and  $r_{\perp}$  within the range of 0 to 1 fm. For this plot, we have fixed the values of the temperature and the magnetic field as 0.2 GeV and  $15 m_{\pi}^2$  respectively. The equal potential (imaginary) regions are represented by different curves and the corresponding values for the imaginary parts of the HQ potential is depicted on top of each curve. Reader should notice that equi-potential curves are elliptic in nature instead of circle. Finite magnetic field make this transformation from circle to ellipse, meaning isotropic to anisotropic transformation. So this anisotropic tomography of heavy quark potential may be used as a signature of magnetic field, produced in heavy ion collision. Though this task is very non-trivial but we will try to search the possibility by presenting our results in different angle. The contour plot (fig. 7.6) will be modified with temperature and magnetic field, which is explored in next paragraph.

In fig. 7.7, we have presented the variation of the imaginary part of the HQ potential with respect to the temperature for two different values of the external magnetic field, i.e.  $eB = 10m_\pi^2$  and  $eB = 20m_\pi^2$ . We have considered the case of vanishing transverse distance in the left panel with a fixed value of  $z = 0.5$  fm. It can be observed that for vanishing temperatures, curves for different magnetic field merges into giving a vanishing  $\text{Im } V$  as in-medium dissociation phenomena of quarkonia can't be expected in vacuum or  $T = 0$ . When the temperature starts to increase gradually, at first the curve for the higher magnetic field gives higher values for imaginary part of the HQ potential. However, after a certain temperature, we observe a crossing between the curves. This feature can be understood in the following way: In the low temperature region, magnetic field is the most dominating scale. As the temperature starts to increase, a competition between the magnetic field and the temperature takes place. The nature of the curves get inverted with the enhancement of the temperature, as the temperature scale becomes more dominant for  $eB = 10 m_\pi^2$ , compare to  $eB = 20 m_\pi^2$ . Similar behaviors have also been observed in the right panel where we have vanishing  $z$  and a fixed  $r_\perp = 0.5$  fm. So, according to Fig. 7.7, dissociation probability is enhanced and suppressed by magnetic field in the low and high temperature respectively. If we concentrate within  $T = 0.1-0.4$  GeV,  $eB = 10-20m_\pi^2$  as covering domain of expanding QGP and heavy quark dissociation temperature range broadly as  $T_d = 0.15-0.35$  GeV, then along  $z$ -axis, dissociation probability can be enhanced due to magnetic field, while opposite impact of magnetic field can be occurred along  $r_\perp$ -axis. This comment is based on the left and right panels of Fig. 7.7, which are plotted at  $r_\perp = 0, z = 0.5$  fm and  $r_\perp = 0.5$  fm,  $z = 0$  respectively. However, for exact knowledge of enhancing and suppressing dissociation domain, one should notice the variation of all four parameters -  $r_\perp, z, T$  and  $eB$ .

From the earlier discussion, we can see a rich anisotropic tomography of heavy quark

### 7.3. Results

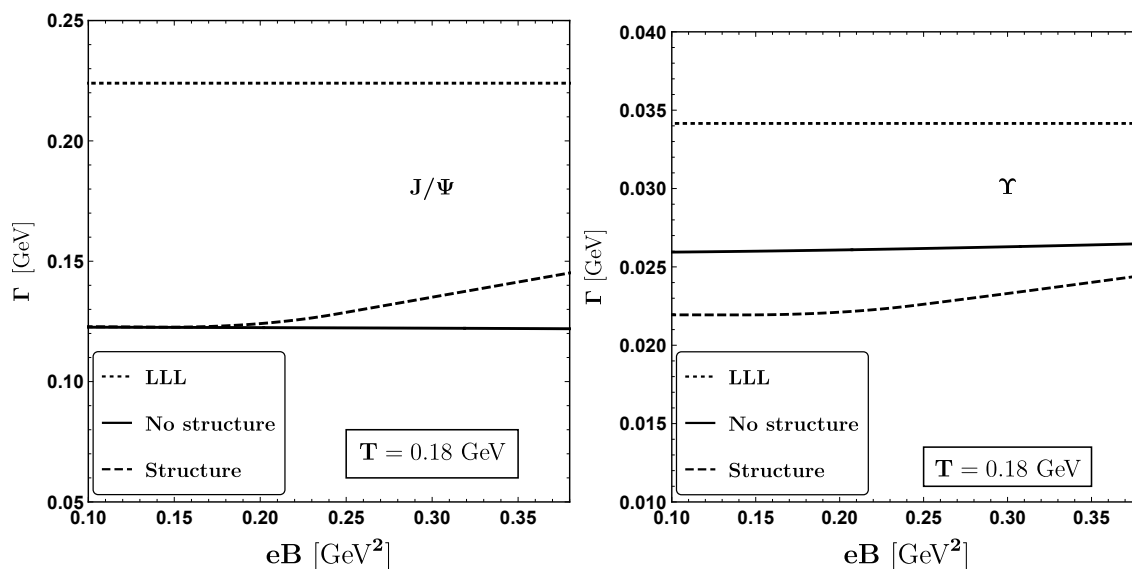


Figure 7.8: Variation of the decay width  $\Gamma$  with respect to the external magnetic field for a fixed temperature shown for the case of Charm quark (left panel) and Bottom quark (right panel). Curves shown for the case of LLL approximated result,  $m_D$  approximated result and full result.

dissociation by varying  $r_\perp$ ,  $z$ ,  $T$  and  $eB$  but when we go towards experimental quantity - heavy quark dissociation probability, this anisotropic tomography will be integrated and we will get only temperature and magnetic field dependent dissociation, which carry the anisotropic information through its integrated values, which will be different from corresponding integrated values isotropic potential. Using Eq. (7.34), this integrated values of heavy quark dissociation are obtained. In figs. 7.8 and 7.9, we have studied the variation of the decay width with respect to the external magnetic field and temperature respectively. In the calculation we take the bottomonium and charmonium masses as  $m_b = 4.66 \text{ GeV}$  and  $m_c = 1.275 \text{ GeV}$  respectively [1, 262]. For each of the cases, we have shown two plots, for charm (left panel) and bottom (right panel) quarks. In fig. 7.8 we have fixed the temperature at  $T = 180 \text{ MeV}$  and in fig. 7.9 we have fixed the magnetic field at  $eB = 10m_\pi^2$ . In each of the plots we have compared our full result (dashed lines) with the LLL approximated result

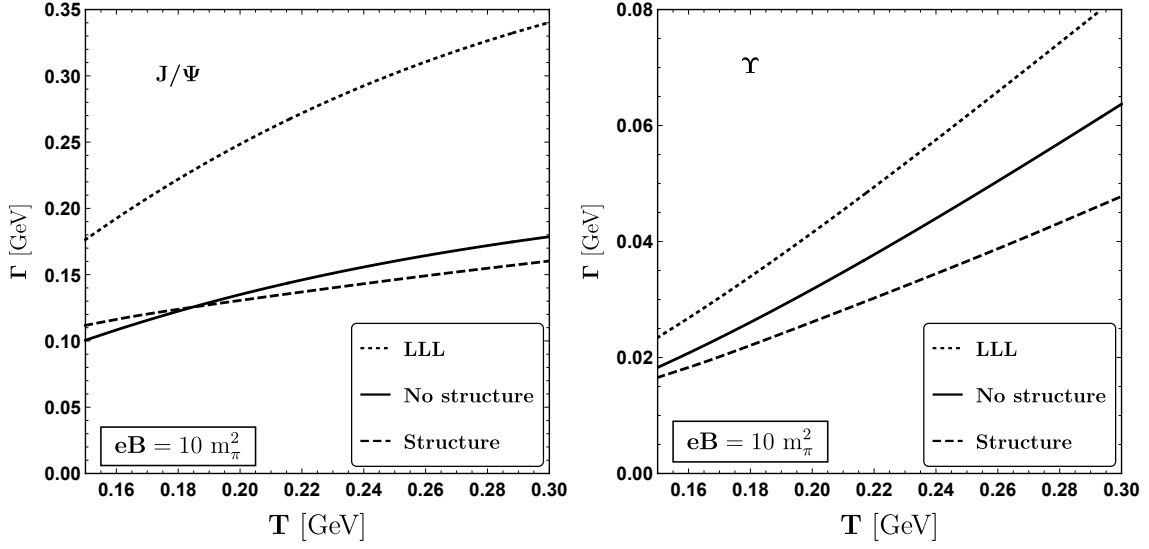


Figure 7.9: Variation of the decay width  $\Gamma$  with respect to the temperature for a fixed external magnetic field shown for the case of Charm quark (left panel) and Bottom quark (right panel). Curves shown for the case of LLL approximated result,  $m_D$  approximated result and full result.

(dotted lines) and the Debye mass approximated result without structure (solid lines). One can notice from fig. 7.8 that the LLL approximation again overestimates the magnitude of the decay width. In comparison with the Debye mass approximated result, our full result of the decay width shows a different  $T$  and  $eB$  profile for both charm and bottom quarks. An increasing behaviour with increasing temperature can also be found in fig. 7.9. As the bottomonium states are smaller in size with larger masses than the charmonium states, the thermal width for  $\Upsilon$  is considerably smaller than the  $J/\Psi$ .

At the end, we want to emphasise once again that with respect to earlier estimations [1, 2] of heavy quark dissociation in presence of finite magnetic field, present results find a new dimension, i.e. a new profile in temperature and magnetic field axes and more intriguingly a rather complex anisotropic tomography in heavy quark dissociation. Former modification is found for adopting the general structure of gluon propagator at finite magnetic field in



#### 7.4. Summary

heavy quark potential framework, which is done here for first time. On the other hand, the later modification - anisotropic tomography of heavy quark dissociation, which can always be expected at finite magnetic field if one carefully considered parallel and perpendicular momentum components during Fourier's transformation. Since earlier Refs. [1, 2] have not included this consideration, so anisotropy structure is missing in their calculations. In this context, our present work is first time pointing out this anisotropic structure in heavy quark potential, which might build an anisotropic dissociation. In near future, our plan is to connect this anisotropic aspect of heavy quark potential due to magnetic field with quarkonia suppression phenomenology, which might unfold how to get signature strong magnetic field through quarkonia phenomenology.

## 7.4 Summary

In the present theoretical study, we have evaluated the imaginary part of heavy quark complex potential formalism at finite temperature and magnetic field, whose preliminary steps are standard and as follows. The imaginary part of heavy quark-antiquark potential in terms of coordinate space, temperature and magnetic field can be estimated by taking Fourier's transform of momentum dependent potential, divided by permittivity of the medium, which carry temperature and magnetic field. This permittivity can be calculated from the temporal component of the effective gluon propagator at finite temperature and magnetic field.

Now, in the present work we have adopted the general structure of the gluon propagator at finite temperature and magnetic field, which was not considered in earlier works. So a new ingredient of temperature and magnetic field field dependent profile in calculations is found. Our adopted generalized gluon propagator consisted four linearly independent tensors. So there are four form factors which can be calculated from the gluon self-energy.

In our case, we have only needed one form factor explicitly for the sake of our calculation. This is evaluated from the one loop gluon self-energy where the quark loop is affected by magnetic field. So the modified quark propagator in presence of magnetic field is considered. We have obtained the results for general magnetic field by summing all Landau level contributions. Comparing our results with the existing works, done with lowest Landau level approximation in the strong field limit as well as weak field approximation, one can consider our work as the more general in nature. Our results are applicable for the entire range from weak to strong magnetic field. This is because we are considering all Landau level summation and most general structure of gluon propagators, which are taking care of corresponding full quantum mechanical and quantum field theoretical effects respectively.

Apart from these new ingredients - all Landau level summation and general structure of propagator, present work has adopted another novel and interesting fact - anisotropic form of heavy quark potential in presence of magnetic field, which were ignored in earlier works, because of some approximations like ignoring the Debye mass independent terms. We have graphically presented the detailed anisotropic tomography of imaginary part of potential, which modifies with temperature and magnetic field. This is one of the main findings of our present study, which to the best of our knowledge, has not been discussed before in the literature for heavy quark potential.

Imaginary part of heavy quark potential basically provides us with its dissociation probability. After doing the co-ordinate space integration by folding with probability density, based on simple wave-function due to Coulomb-type potential, we have obtained the temperature and magnetic field dependent dissociation probability or thermal width of quarkonium states -  $J/\Psi$  and  $\Upsilon$ . Here, we have again found the modified temperature and magnetic field profile due to considering the summation over all possible Landau levels and the general structure of gluon propagator at finite magnetic field with respect to earlier refer-

#### *7.4. Summary*

ences. We believe that the anisotropic aspect of heavy quark potential due to magnetic field might build an interesting quarkonia phenomenology, which is planned for our next work. Further studies on the angular dependence / ellipticity (e.g. for the case of photon emission, see [76] ) of the dissociation probability is also needed to disentangle the anisotropy due to the external magnetic field with the geometrical effects coming from the shape of the plasma produced in non central HIC.



# HADRONIC VISCOSITY COEFFICIENT AT FINITE TEMPERATURE AND MAGNETIC FIELD

---

In this chapter, we calculate the transport coefficient of hadronic matter in the presence of temperature and magnetic field using the linear sigma model within the relaxation time approximation. The point-like interaction rates of hadrons are evaluated through the  $S$ -matrix approach in the presence of a magnetic field to obtain the temperature and magnetic field-dependent relaxation time. By incorporating the estimated relaxation time, the temperature and magnetic field-dependent anisotropic shear viscosity coefficients are obtained. This chapter is based on the work presented in the following paper: *Shear Viscosity of hadronic matter at finite temperature and magnetic field*

Ritesh Ghosh, Najmul Haque, *Phys. Rev. D* **105** (2022) 11, 114029, [[arXiv:2204.01639](https://arxiv.org/abs/2204.01639)] [[hep-ph](#)].

## 8.1 Introduction

In relativistic heavy-ion collision experiments at the Large Hadron Collider (LHC) and Relativistic Heavy Ion Collider (RHIC), a novel state of quarks and gluons, i.e., quark-gluon plasma (QGP) [9] is produced as a near-perfect fluid [20, 263, 264]. The elliptic flow [31, 265] data indicates the smallest viscosity to entropy density ratio ( $\eta/s$ ) of the QGP medium. The produced QGP medium shows the collective behavior, and it undergoes space-time evolution and finally emanates to the hadronic phase. The transverse momentum spectra and the collectivity of the produced particles can be studied from the hydrodynamical modeling [31]. The transport coefficients are used as the input parameters for the hydrodynamic simulations.

More research interests have grown in the non-central heavy-ion collisions through the last decade discussed in introductory Chapter 1. In this chapter we evaluate the shear viscosity coefficients of hadronic matter in a strong magnetic field using the linear sigma model (LSM). The LSM is one of the simple models to study the hadronic system and was first introduced by Gell-Mann and Lévy [266]. Several works have been done considering this as a low-energy effective model during the last few years as it mimics the low-energy QCD region. Recent attempts have extended the LSM by including quarks [224, 267] and vector mesons in this model [268]. Chiral phase transition [269], pion condensate [270] and neutral pion mass [224] in the presence of the external magnetic field and so on have been studied using the LSM. In Refs. [271, 272] the authors have calculated the transport coefficients of hadronic matter at finite temperature using the LSM. The results show that the shear viscosity to entropy density ratio ( $\eta/s$ ) has a minimum at the crossover temperature. In contrast, the bulk viscosity to entropy density ratio ( $\xi/s$ ) has a maximum at the crossover temperature. As a first attempt, we study the viscous shear coefficient of

## *8.2. Anisotropic Viscosity coefficients in non zero magnetic field*

hadronic matter in a magnetic field for zero chemical potential in this present work. There are five shear-viscous coefficients in a nonzero magnetic field, and we have studied all the coefficients. In the presence of a magnetic field, the relaxation times are estimated through the S-matrix approach. In these calculations, we would get the expressions of the matrix elements in terms of the Landau level summation. Our study considers only the lowest Landau level (LLL) contribution.

The chapter is arranged as follows: In Sec. 8.2 we review the formalism for the estimation of the shear viscosity coefficients in the presence of the external magnetic field within relaxation time approximation. In Sec. 8.3 we discuss the basics of the linear sigma model (LSM) and the thermodynamic quantities that are used in the calculations. We have calculated the scattering amplitude and interaction rate in the presence of the magnetic field. In subsection 8.3.2. Expressions for the interaction rate in the pure thermal medium are also discussed here. Incorporating the interaction rate, we finally obtain the anisotropic shear viscous coefficients, and presented is the result Sec. 8.4. Finally, we summarize in section 8.5.

## **8.2 Anisotropic Viscosity coefficients in non zero magnetic field**

We will study the transport properties of a hadronic medium in the presence of a magnetic field. Transport coefficients can be calculated using two popular approaches: kinetic theory [273] and Kubo framework [274–276]. Here we follow the former approach and briefly discuss this formalism in the relaxation approximation (RTA) technique [277, 278]. In a magnetic field, the transport coefficients for the charged particles become anisotropic,

whereas the neutral particles contribute to the isotropic coefficients only.

In a magnetic field, the Boltzmann equation for single hadron species is written as

$$p^\mu \partial_\mu f_a + q F^{\mu\nu} p_\nu \frac{\partial f_a}{\partial p^\mu} = C[f_a], \quad (8.1)$$

where  $F^{\mu\nu}$  is the electromagnetic field tensor. In absence of electric field,  $F^{\mu\nu} = -B b^{\mu\nu}$  where  $b^{\mu\nu} = \epsilon^{\mu\nu\alpha\beta} b_\alpha u_\beta$  with fluid four velocity  $u^\mu$ . The unit vector  $b^\mu$  is defined as  $b^\mu = \frac{B^\mu}{B}$ .  $C[f_a]$  is known as the collision integral,  $p^\mu$  is the four momenta of the particle and  $q$  is the electric charge of the particle.

In relaxation time approximation (RTA), the Boltzmann equation 8.1 is given by

$$p^\mu \partial_\mu f_a + q F_{\mu\nu} p^\nu \frac{\partial f_a}{\partial p^\mu} = -\omega_a (u \cdot p) \delta f_a, \quad (8.2)$$

where  $\omega_a$  is frequency of interaction defined as the inverse of the equilibration time i.e.

$$\omega_a(E) = \tau_a^{-1}(E). \quad (8.3)$$

Assuming that the system is meagerly out of equilibrium, we can write the distribution function as,

$$f_a(x, p) = f_a^0 (1 + \phi_a(x, p)) = f_a^0 + \delta f_a. \quad (8.4)$$

For a small deviation from equilibrium, we can write the Boltzmann equation as

$$p^\mu \partial_\mu f_a^0 = \left( -\frac{u \cdot p}{\tau_a} \right) \left( 1 - \frac{qB\tau_a}{u \cdot p} b^{\mu\nu} p_\nu \frac{\partial}{\partial p^\mu} \right) \delta f_a, \quad (8.5)$$



## 8.2. Anisotropic Viscosity coefficients in non zero magnetic field

where  $f_a^0 = \exp(-u_\alpha p^\alpha/T)$  is equilibrium distribution function. Now, in general, the energy-momentum tensor is written as

$$T^{\mu\nu} = T_0^{\mu\nu} + \Delta T^{\mu\nu}, \quad (8.6)$$

where  $T_0^{\mu\nu}$  represents the energy-momentum tensor in local equilibrium and  $\Delta T^{\mu\nu}$  is the deviation from the equilibrium.  $T^{\mu\nu}$  is given as

$$T^{\mu\nu} = \sum_a \int \frac{d^3p}{(2\pi)^3} \frac{p_a^\mu p_a^\nu}{E_a} f_a + \sum_a \frac{|qB|}{2\pi} \int \frac{dp_3}{2\pi} \frac{\tilde{p}_a^\mu \tilde{p}_a^\nu}{E_a} f_a, \quad (8.7)$$

where the sum is over uncharged and charged particles in the first and second term respectively. In the second term phase factor is modified in presence of strong magnetic field.

For shear viscosity, in presence of magnetic field we can express  $\delta f_a$  in terms of fourth rank projection tensors as

$$\delta f_a = \sum_{m=-2}^2 c^m C_{\mu\nu\alpha\beta}^{(m)} p^\mu p^\nu V^{\alpha\beta}, \quad (8.8)$$

where  $V^{\alpha\beta} = \frac{1}{2}(\partial^\alpha u^\beta + \partial^\beta u^\alpha)$ . There are five complex coefficients  $c_m$ .

Shear viscous tensor ( $\pi^{\mu\nu}$ ) is given as

$$\pi^{\mu\nu} = \eta^{\mu\nu\alpha\beta} V_{\alpha\beta}, \quad (8.9)$$

where the general form of  $\eta^{\mu\nu\alpha\beta}$  in presence of the magnetic field could be expressed with the fourth rank projection tensors as

$$\eta^{\mu\nu\mu'\nu'} = \sum_{m=-2}^2 c^m C^{(m)\mu\nu\mu'\nu'}. \quad (8.10)$$

Here we introduce three second-rank projection tensors given as

$$P_{\mu\nu}^{(0)} = b_\mu b_\nu, \quad (8.11)$$

$$P_{\mu\nu}^{(1)} = \frac{1}{2}(\Delta_{\mu\nu} - b_\mu b_\nu + i b_{\mu\nu}), \quad (8.12)$$

$$P_{\mu\nu}^{(-1)} = \frac{1}{2}(\Delta_{\mu\nu} - b_\mu b_\nu - i b_{\mu\nu}), \quad (8.13)$$

where  $\Delta^{\mu\nu} = g^{\mu\nu} - u^\mu u^\nu$ . Fourth-rank tensor defined in eq. (8.10) can be written in terms of two second-rank tensors as [279, 280]

$$\mathcal{P}_{\mu\nu\alpha\beta}^{(m)} = \sum_{m_1=-1}^1 \sum_{m_2=-1}^1 P_{\mu\alpha}^{(m_1)} P_{\nu\beta}^{(m_2)} \delta(m, m_1 + m_2). \quad (8.14)$$

In terms of real coefficients eq. (8.9) can be written as

$$\begin{aligned} \eta_{\mu\nu\alpha\beta} &= c^0 \mathcal{P}_{\langle\mu\nu\rangle\alpha\beta}^{(0)} + \sum_{m=1}^2 \left\{ c^{m+} \left( \mathcal{P}_{\langle\mu\nu\rangle\alpha\beta}^{(m)} + \mathcal{P}_{\langle\mu\nu\rangle\alpha\beta}^{(-m)} \right) \right. \\ &\quad \left. + i c^{m-} \left( \mathcal{P}_{\langle\mu\nu\rangle\alpha\beta}^{(m)} - \mathcal{P}_{\langle\mu\nu\rangle\alpha\beta}^{(-m)} \right) \right\}, \end{aligned} \quad (8.15)$$

where  $\mathcal{P}_{\langle\mu\nu\rangle\alpha\beta}^{(m)} = \mathcal{P}_{\mu\nu\alpha\beta}^{(m)} + \mathcal{P}_{\nu\mu\alpha\beta}^{(m)}$ . The coefficients  $c^{m+}$  and  $c^{m-}$  are real and imaginary parts of coefficients  $c^m$ . Three coefficients  $c^0$ ,  $c^{1+}$  and  $c^{2+}$  are even functions of the magnetic field whereas other two coefficients  $c^{1-}$  and  $c^{2-}$  are odd functions of magnetic field. The shear viscosity obeys the condition  $\eta^{\mu\nu\mu'\nu'}(B^\alpha) = \eta^{\mu\nu\mu'\nu'}(-B^\alpha)$ , the symmetry principle for transport coefficients.

## 8.2. Anisotropic Viscosity coefficients in non zero magnetic field

Now we can represent eq. (8.8) with real coefficients i.e.

$$\begin{aligned} \delta f_a = & \left[ c^0 \mathcal{P}_{\langle\mu\nu\rangle\alpha\beta}^{(0)} + \sum_{m=1}^2 \left\{ c^{m+} \left( \mathcal{P}_{\langle\mu\nu\rangle\alpha\beta}^{(m)} + \mathcal{P}_{\langle\mu\nu\rangle\alpha\beta}^{(-m)} \right) \right. \right. \\ & \left. \left. + i c^{m-} \left( \mathcal{P}_{\langle\mu\nu\rangle\alpha\beta}^{(m)} - \mathcal{P}_{\langle\mu\nu\rangle\alpha\beta}^{(-m)} \right) \right\} \right] p^\mu p^\nu V^{\alpha\beta}. \end{aligned} \quad (8.16)$$

In integral form we can write the shear viscous tensor as

$$\pi^{\mu\nu} = \frac{1}{15} \sum_a \sum_{m=-2}^2 \int \frac{d^3p}{(2\pi)^3} \frac{(\mathbf{p})^4}{E_a} c^m C^{(m)\mu\nu\alpha\beta} V_{\alpha\beta}. \quad (8.17)$$

The left-hand side of the eq. (8.5) has been written in terms of the projection operators as

$$-\frac{f^0}{2T} p^\mu p^\nu V^{\alpha\beta} \left[ \mathcal{P}_{\langle\mu\nu\rangle\alpha\beta}^{(0)} + \mathcal{P}_{\langle\mu\nu\rangle\alpha\beta}^{(1)} + \mathcal{P}_{\langle\mu\nu\rangle\alpha\beta}^{(-1)} + \mathcal{P}_{\langle\mu\nu\rangle\alpha\beta}^{(2)} + \mathcal{P}_{\langle\mu\nu\rangle\alpha\beta}^{(-2)} \right]. \quad (8.18)$$

Substituting  $\delta f_a$  on the right hand side of eq (8.5), we get

$$-\frac{u \cdot p}{\tau_a} \left( 1 - \frac{qB\tau_a}{u \cdot p} b^{\mu\nu} p_\nu \frac{\partial}{\partial p^\mu} \right) \sum_{m=-2}^2 c^m C_{\mu\nu\alpha\beta}^{(m)} p^\mu p^\nu V^{\alpha\beta}. \quad (8.19)$$

Equating eq. (8.18) and eq. (8.19) after writing the fourth rank tensors in terms of second tensors , we get (see Refs. [277, 279, 281])

$$\begin{aligned} c^0 &= \frac{1}{2T} \frac{f^0 \tau_a}{(u \cdot p)}, \\ c^{1+} &= \frac{1}{2T} \frac{u \cdot p}{(u \cdot p)^2 + (qB\tau_a)^2} f^0 \tau_a, \\ c^{2+} &= \frac{1}{2T} \frac{u \cdot p}{(u \cdot p)^2 + (2qB\tau_a)^2} f^0 \tau_a, \end{aligned}$$

Chapter 8. Hadronic viscosity coefficient at finite temperature and magnetic field

$$\begin{aligned} c^{1-} &= \frac{1}{2T} \frac{qB}{(u \cdot p)^2 + (qB\tau_a)^2} f^0 \tau_a^2, \\ c^{2-} &= \frac{1}{T} \frac{qB}{(u \cdot p)^2 + (2qB\tau_a)^2} f^0 \tau_a^2. \end{aligned} \quad (8.20)$$

Employing eq. (8.17) we can find the shear viscosity coefficients as

$$\eta_{\parallel} = \frac{2}{15} \sum_a \int \frac{d^3p}{(2\pi)^3} \frac{|\mathbf{p}|^4}{E_a} c^0 = \frac{1}{15T} \sum_a \int \frac{d^3p}{(2\pi)^3} \frac{|\mathbf{p}|^4}{E_a^2} f^0 \tau_a, \quad (8.21)$$

$$\eta_{\perp} = \frac{2}{15} \sum_a \int \frac{d^3p}{(2\pi)^3} \frac{|\mathbf{p}|^4}{E_a} c^{1+} = \frac{1}{15T} \sum_a \int \frac{d^3p}{(2\pi)^3} \frac{|\mathbf{p}|^4 f^0 \tau_a}{(u \cdot p)^2 + (qB\tau_a)^2}, \quad (8.22)$$

$$\eta'_{\perp} = \frac{2}{15} \sum_a \int \frac{d^3p}{(2\pi)^3} \frac{|\mathbf{p}|^4}{E_a} c^{2+} = \frac{1}{15T} \sum_a \int \frac{d^3p}{(2\pi)^3} \frac{|\mathbf{p}|^4 f^0 \tau_a}{(u \cdot p)^2 + (2qB\tau_a)^2}, \quad (8.23)$$

$$\eta_{\times} = \frac{2}{15} \sum_a \int \frac{d^3p}{(2\pi)^3} \frac{|\mathbf{p}|^4}{E_a} c^{1-} = \frac{1}{15T} \sum_a \int \frac{d^3p}{(2\pi)^3} \frac{|\mathbf{p}|^4}{E_a} \frac{qB f^0 \tau_a^2}{(u \cdot p)^2 + (qB\tau_a)^2}, \quad (8.24)$$

$$\eta'_{\times} = \frac{2}{15} \sum_a \int \frac{d^3p}{(2\pi)^3} \frac{|\mathbf{p}|^4}{E_a} c^{2-} = \frac{2}{15T} \sum_a \int \frac{d^3p}{(2\pi)^3} \frac{|\mathbf{p}|^4}{E_a} \frac{qB f^0 \tau_a^2}{(u \cdot p)^2 + (2qB\tau_a)^2} \quad (8.25)$$

In the presence of a nonzero magnetic field, the shear stress tensor is written using the available basis (as discussed in this section), having a component parallel to the magnetic field. The subscript  $\parallel$  denotes this parallel component. The subscripts  $\perp$  and  $\times$  are the perpendicular and Hall components. In the absence of a magnetic field, the Hall component is zero, whereas the perpendicular component becomes the same as the parallel component.

From eq. (D.14), the solution of eq. (D.1) for charged particles looks like  $\sim e^{-iP \cdot X_{\bar{x}}} \times \text{Exp}[-eB/2(x - \frac{p_y}{eB})] H_{\nu}(x - \frac{p_y}{eB})$ . To find out the density of state we consider box of length  $[L_1, L_2, L_3]$  and infinite volume limit would be taken at the end.  $p_y$  takes the discrete values i.e.  $p_y = \frac{2\pi n}{L_2}$  with integers  $n$ . The particle is localized in  $x \sim p_y/eB = \frac{2\pi n}{eBL_2}$ . As  $x$  lies in interval  $[0, L_1]$ , we can write  $0 < n < \frac{L_1 L_2}{2\pi} eB$ . So the number of states

## 8.2. Anisotropic Viscosity coefficients in non zero magnetic field

in transverse area is  $\frac{L_1 L_2}{2\pi} eB$ . Now the number of states per unit volume in  $\Delta p_z$  interval becomes  $\sim \frac{1}{V} \frac{L_1 L_2 L_3}{2\pi} eB \frac{\Delta p_z}{2\pi} = eB \frac{\Delta p_z}{(2\pi)^2}$ . Using this argument, for the case of the charged particles we use the phase space [282] as

$$\int \frac{d^3 p}{(2\pi)^3} \longrightarrow \frac{|eB|}{(2\pi)^2} \int dp_z. \quad (8.26)$$

For the neutral particle, the Hall components of the viscosity coefficients are zero, and the perpendicular components are equal to the parallel parts.

In the presence of a finite magnetic field, the momentum of the charged particles becomes anisotropic. The energy dispersion relation of the charged scalar particle of charge  $q$  gets modified as

$$E_n = \sqrt{p_L^2 + (2n + 1)|qB| + m^2}, \quad (8.27)$$

where  $p_z$  is the momentum of the particle parallel to the direction of the magnetic field, and  $m$  is the mass of that particle. Here  $n = 0, 1, 2, 3, \dots$  denotes the Landau levels. In our case, we consider the magnetic field to be in the  $z$ -direction. We also work in a strong magnetic field limit, i.e., the magnetic field is much greater than the temperature square scale. In this approximation, we can safely consider the confinement of charged particles in the lowest Landau level (LLL), and the energy dispersion in LLL is given as

$$E = \sqrt{p_z^2 + m^2 + |qB|}. \quad (8.28)$$

Here, we define the notation  $\tilde{p}^\mu = (E, p^3)$ . For the charged pions equilibrium distribution takes the form as  $f_a^0 = \exp(-u_\alpha \tilde{p}^\alpha / T)$ . Now, the uncharged particles are not affected by the magnetic field, therefore the distribution is given by  $f_a^0 = \exp(-u_\alpha p^\alpha / T)$ , where

$$p^\mu = (E, \mathbf{p}) \text{ with } \omega = \sqrt{\mathbf{p}^2 + m^2}.$$

### 8.3 Linear Sigma Model

The LSM model is a simplistic effective model of pions. Here we use it to calculate transport coefficients. In general, the LSM Lagrangian consists of  $N$  bosonic fields. For  $N = 4$ , it represents the theory of three pions ( $\pi_i$ ) and one sigma ( $\sigma$ ) fields. The LSM Lagrangian density [271, 283] for  $N = 4$  is

$$\mathcal{L} = \frac{1}{2}(\partial_\mu \sigma)^2 + \frac{1}{2}(\partial_\mu \boldsymbol{\pi})^2 - V(\sigma, \boldsymbol{\pi}), \quad (8.29)$$

where the potential term

$$V(\sigma, \boldsymbol{\pi}) = \frac{\lambda}{4}(\sigma^2 + \boldsymbol{\pi}^2 - f^2)^2 - H\sigma. \quad (8.30)$$

Here  $H\sigma$  is the explicit chiral symmetry breaking term that gives the pion mass. The scalar field  $\sigma$  takes the vacuum expectation value  $v$  as  $\sigma = v + \Delta$ , where  $\Delta$  is the fluctuation and  $v$  is determined by the symmetry breaking term as

$$\lambda v(v^2 - f^2) = H. \quad (8.31)$$

Other parameters  $\lambda$ ,  $H$  and  $f$  are expressed in terms of pion decay constant  $f_\pi$ , pion masses ( $m_\pi$ ) and sigma masses ( $m_\sigma$ ) i.e.

$$\begin{aligned} \lambda &= \frac{m_\sigma^2 - m_\pi^2}{2f_\pi^2}, \\ H &= f_\pi m_\pi^2, \end{aligned}$$

### 8.3. Linear Sigma Model

$$f^2 = f_\pi^2 \frac{m_\sigma^2 - 3m_\pi^2}{m_\sigma^2 - m_\pi^2}. \quad (8.32)$$

For calculation we are taking vacuum pion mass  $m_\pi = 140$  MeV, vacuum  $\sigma$  masses  $m_\sigma = \{500, 700\}$  MeV and decay constant  $f_\pi = 93$  MeV.

We would continue our calculations in the isospin pion basis representing the physical pions. The physical pions can be expressed in terms of Cartesian pion fields as,

$$\pi^0 = \pi_3, \quad (8.33)$$

$$\pi^\pm = \frac{1}{\sqrt{2}}(\pi_1 \pm i\pi_2). \quad (8.34)$$

In physical pion basis interaction Lagrangian can be written as

$$\begin{aligned} \mathcal{L}_{int} = & \frac{\lambda}{4} \left( \sigma^4 + (\pi^0)^4 + (\pi^+)^4 + (\pi^-)^4 + 2(\pi^0)^2(\pi^+)^2 \right. \\ & + 2(\pi^0)^2(\pi^-)^2 + 2(\pi^0)^2\sigma^2 + 2(\pi^+)^2(\pi^-)^2 + 2(\pi^+)^2\sigma^2 + 2(\pi^-)^2\sigma^2 \\ & \left. + 4v\sigma(\pi^0)^2 + 4v\sigma(\pi^+)^2 + 4v\sigma(\pi^-)^2 + 4v\sigma^3 \right). \end{aligned} \quad (8.35)$$

From the above interaction Lagrangian, one can find the probable interactions between the mesons.

As we are considering a magnetic field in  $z$ -direction, the magnetic field  $\mathbf{B} = B\hat{z}$ . The covariant four-derivative  $D_\mu = \partial_\mu + QA_\mu$  replaces the four-derivative  $\partial_\mu$  in the kinetic terms of the Lagrangian for the charged pions. Here,  $Q = e$  for  $\pi^\pm$  and  $A^\mu = \{0, 0, xB, 0\}$ .

### 8.3.1 Thermodynamics

The temperature dependence of the effective masses of pions and the condensate  $v$  is rigorously discussed in Refs. [284–286]. There is a significant difference between meson masses at low temperature, i.e., chiral symmetry is broken, and symmetry is restored at around 245 MeV. We are also considering only temperature dependence on effective masses in our case.

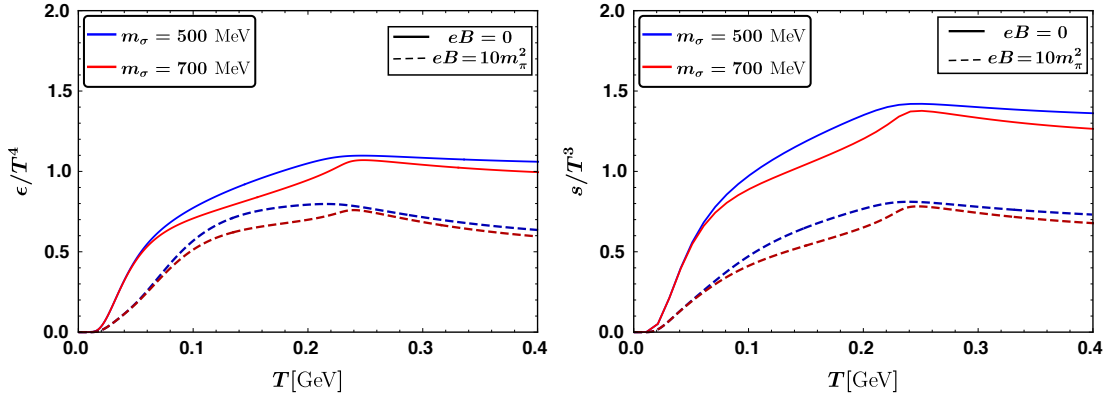


Figure 8.1: Energy density (left) and entropy density (right) as functions of temperature for three different vacuum sigma masses in presence(dashed line) and absence(solid line) of the magnetic field.

In a strong magnetic field, energy density, entropy density, pressure, and other thermodynamics quantities depend on both temperature and magnetic field effect. The phase factors and energy dispersion is modified for the charged particles. So energy density becomes

$$\epsilon_B = \sum_{a=\sigma,\pi^0} \int \frac{d^3p}{(2\pi)^3} E_a f^0(E_a/T) + \sum_{a=\pi^\pm} \frac{|eB|}{2\pi} \int_{-\infty}^{\infty} \frac{dp_z}{2\pi} E_a f^0(E_a/T), \quad (8.36)$$

where  $E_\sigma = \sqrt{p^2 + \bar{m}_\sigma^2}$ ,  $E_{\pi^0} = \sqrt{p^2 + \bar{m}_\pi^2}$  and  $E_{\pi^\pm} = \sqrt{p_z^2 + \bar{m}_\pi^2 + |eB|}$ . Here  $\bar{m}(T)$  is considered as temperature dependent effective mass which comes from the mean field.



### 8.3. Linear Sigma Model

Similarly, the pressure  $P$  and the entropy density  $s$  can be written as

$$P_B = \sum_{a=\sigma,\pi^0} \int \frac{d^3p}{(2\pi)^3} \frac{|\mathbf{p}|^2}{E_a} f^0(E_a/T) + \sum_{a=\pi^\pm} \frac{|eB|}{2\pi} \int_{-\infty}^{\infty} \frac{dp_z}{2\pi} \frac{p_z^2}{E_a} f^0(E_a/T) \quad (8.37)$$

and

$$s_B = \frac{1}{3T^2} \sum_{a=\sigma,\pi^0} \int \frac{d^3p}{(2\pi)^3} |\mathbf{p}|^2 f^0(E_a/T) + \frac{1}{3T^2} \sum_{a=\pi^\pm} \frac{|eB|}{2\pi} \int_{-\infty}^{\infty} \frac{dp_z}{2\pi} p_z^2 f^0(E_a/T). \quad (8.38)$$

In Fig. 8.1 energy density  $\epsilon$  scaled with  $T^4$  and entropy density  $s$  scaled with  $T^3$  are plotted for  $m_\sigma = 500$  MeV and 700 MeV respectively. The dashed lines represent the values of the corresponding thermodynamic quantities in the presence of the magnetic field. In the presence of a magnetic field, both the energy and entropy density decrease.

## 8.3.2 Scattering amplitudes and interaction frequency

### Thermal case

Here we present the interaction frequency for pure thermal medium. For the pure thermal medium, the matrix elements are [271]

$$\begin{aligned} \mathcal{M}_{fi}(\sigma\sigma|\sigma\sigma) &= -6\lambda - 36\lambda^2 v^2 \left( \frac{1}{s - m_\sigma^2} + \frac{1}{t - m_\sigma^2} + \frac{1}{u - m_\sigma^2} \right), \\ \mathcal{M}_{fi}(\pi^a\pi^b|\pi^c\pi^d) &= -2\lambda \left( \frac{s - m_\pi^2}{s - m_\sigma^2} \delta_{ab}\delta_{cd} + \frac{t - m_\pi^2}{t - m_\sigma^2} \delta_{ac}\delta_{bd} + \frac{u - m_\pi^2}{u - m_\sigma^2} \delta_{ad}\delta_{cb} \right), \end{aligned}$$

$$\begin{aligned}
 \mathcal{M}_{fi}(\pi\pi|\sigma\sigma) &= -2\lambda - 4\lambda^2 v^2 \left( \frac{3}{s - m_\sigma^2} + \frac{1}{t - m_\sigma^2} + \frac{1}{u - m_\sigma^2} \right), \\
 \mathcal{M}_{fi}(\pi\sigma|\pi\sigma) &= -2\lambda - 4\lambda^2 v^2 \left( \frac{1}{s - m_\sigma^2} + \frac{1}{t - m_\sigma^2} + \frac{1}{u - m_\sigma^2} \right). \quad (8.39)
 \end{aligned}$$

The poles in the  $s$  and  $u$  channels cause issues in the scattering amplitudes, resulting in divergent integrals. The divergence can be cured by introducing the thermal width of mesons violating the crossing symmetries. These terms come from the three-point vertices, and we have excluded them in the equation of state. So we are avoiding those terms taking the infinity limits of  $s, t$ , and  $u$ . Finally, we are left with the constant scattering amplitudes, and those are given as,

$$\mathcal{M}_{fi}(\sigma\sigma|\sigma\sigma) = -6\lambda, \quad (8.40)$$

$$\mathcal{M}_{fi}(\pi^a\pi^a|\pi^a\pi^a) = -6\lambda, \quad \{a = 0, +, -\} \quad (8.41)$$

$$\mathcal{M}_{fi}(\pi^+\pi^-|\pi^+\pi^-) = -2\lambda, \quad (8.42)$$

$$\mathcal{M}_{fi}(\pi^0\pi^0|\sigma\sigma) = -2\lambda, \quad (8.43)$$

$$\mathcal{M}_{fi}(\pi^a\sigma|\pi^a\sigma) = -2\lambda, \quad \{a = 0, +, -\} \quad (8.44)$$

$$\mathcal{M}_{fi}(\pi^b\pi^0|\pi^b\pi^0) = -2\lambda, \quad \{b = +, -\}. \quad (8.45)$$

For  $a + b \rightarrow c + d$  type interaction, interaction frequency  $\omega_a = 1/\tau_a$  is written as [287]

$$\begin{aligned}
 \omega_{\text{th}}^a(E_a) &\equiv \tau^{-1}(E_a) = \sum_{bcd} \frac{1}{1 + \delta_{ab}} \int \frac{d^3p_b d^3p_c d^3p_d}{(2\pi)^5} \frac{|\mathcal{M}(ab \rightarrow cd)|^2}{16E_a E_b E_c E_d} \\
 &\times \delta^4(p_a + p_b - p_c - p_d) f_b^{eq}. \quad (8.46)
 \end{aligned}$$

In the centre of mass frame, the interaction frequency can be written in simplified form from eq. (8.46) as

### 8.3. Linear Sigma Model

$$\begin{aligned}\omega_{\text{th}}^a &= \frac{1}{256\pi^3 E_a} \sum_{bcd} \frac{1}{1 + \delta_{ab}} \int_{m_b}^{\infty} dE_b \sqrt{E_b^2 - m_b^2} \\ &\times \int_{-1}^1 \frac{dx}{p_{ab}\sqrt{s}} (t_{\text{max}} - t_{\text{min}}) |\mathcal{M}|^2 f^{eq}(E_b),\end{aligned}\quad (8.47)$$

where

$$p_{ab}(s) = \frac{1}{2\sqrt{s}} \sqrt{\lambda(s, m_a^2, m_b^2)},\quad (8.48)$$

with the kinematic function  $\lambda(x, y, z) = x^2 + y^2 + z^2 - 2(xy + yz + zx)$ . Other quantities are defined as

$$s = 2E_a E_b \left( 1 + \frac{m_a^2 + m_b^2}{2E_a E_b} - \frac{p_a p_b}{E_a E_b} x \right),\quad (8.49)$$

$$\begin{aligned}t_{\text{max,min}} &= m_a^2 + m_c^2 - \frac{1}{2s} (s + m_a^2 - m_b^2)(s + m_c^2 - m_d^2) \\ &\pm \frac{1}{2s} \sqrt{\lambda(s, m_a^2, m_b^2)\lambda(s, m_c^2, m_d^2)}.\end{aligned}\quad (8.50)$$

#### In the presence of magnetic field

A finite magnetic field would affect the scattering amplitudes containing charged pions as the charged pions interact with the magnetic field. In this section, we calculate the magnetic field-affected interaction rates. Here we also consider the four-point interactions. Starting from the  $S$ -matrix elements, we end up with the interaction rates of corresponding processes. The calculations of the matrix elements involve the Klein-Gordon solutions of the charged scalar particles in the presence of the magnetic field. The solutions to the Klein-Gordon equation are discussed in Appendix D. As we are confining ourselves in the strong magnetic field case, we have obtained the interaction rates only for the lowest

Landau level.

The  $S$ -matrix element for  $\pi^b(\mathbf{p}_{\bar{x}}, m) + \pi^b(\mathbf{k}_{\bar{x}}, n) \rightarrow \pi^b(\mathbf{p}'_{\bar{x}}, m') + \pi^b(\mathbf{k}'_{\bar{x}}, n')$  scattering in presence of magnetic field is written as

$$\begin{aligned}
 S_{fi} &= 4! \frac{\lambda}{4} \int d^4 X \langle \pi^b(n', \mathbf{k}'_{\bar{x}}) \pi^b(m', \mathbf{p}'_{\bar{x}}) | (\pi^b)^4 | \pi^b(n, \mathbf{k}_{\bar{x}}) \pi^b(m, \mathbf{p}_{\bar{x}}) \rangle, \quad \{b = +, -\} \\
 &= 4! \frac{\lambda}{4} \int d^4 X \frac{e^{-i(P+K-P'-K') \cdot X_{\bar{x}}}}{\sqrt{16 E_n E_m E'_n E'_m (L_y L_z)^4}} f_n(x, \mathbf{k}_{\bar{x}}) f_m(x, \mathbf{p}_{\bar{x}}) f_{n'}^*(x, \mathbf{k}'_{\bar{x}}) f_{m'}^*(x, \mathbf{p}'_{\bar{x}}) \\
 &= (2\pi)^3 \delta_{\bar{x}}^{(3)}(p + k - p' - k') \frac{1}{\sqrt{16 E_n E_m E'_n E'_m (L_y L_z)^4}} \mathcal{M}_{fi}, \quad (8.51)
 \end{aligned}$$

where  $\delta_{\bar{x}}^{(3)}$  implies the  $\delta$ -function for all the space-time coordinates except  $x$ . In this case four-momentum conservation is not appearing through the delta function as the  $x$ -component of the momentum is not a good quantum number. The matrix element  $\mathcal{M}_{fi}$  from eq. (8.51) can be read as

$$\mathcal{M}_{fi}(\pi^b \pi^b | \pi^b \pi^b) = 4! \frac{\lambda}{4} \int dx f_n(x, \mathbf{k}_{\bar{x}}) f_m(x, \mathbf{p}_{\bar{x}}) f_{n'}^*(x, \mathbf{k}'_{\bar{x}}) f_{m'}^*(x, \mathbf{p}'_{\bar{x}}), \quad \{b = +, -\} \quad (8.52)$$

and similarly we can write the scattering amplitudes for  $\pi^+(k') + \pi^-(p') \rightarrow \pi^+(k) + \pi^-(p)$  as

$$\mathcal{M}_{fi}(\pi^+ \pi^- | \pi^+ \pi^-) = 2\lambda \int dx f_n(x, \mathbf{k}_{\bar{x}}) f_m(x, \mathbf{p}_{\bar{x}}) f_n^*(x, \mathbf{k}'_{\bar{x}}) f_m^*(x, \mathbf{p}'_{\bar{x}}). \quad (8.53)$$

Other scattering amplitudes affected by magnetic fields are

$$\mathcal{M}_{fi}(\pi^b \sigma | \pi^b \sigma) = 2\lambda \int dx e^{i(k_x - k'_x)x} f_n(x, \mathbf{k}_{\bar{x}}) f_m^*(x, \mathbf{p}'_{\bar{x}}), \quad \{b = +, -\} \quad (8.54)$$

$$\mathcal{M}_{fi}(\pi^b \pi^0 | \pi^b \pi^0) = 2\lambda \int dx e^{i(k_x - k'_x)x} f_n(x, \mathbf{k}_{\bar{x}}) f_m^*(x, \mathbf{p}'_{\bar{x}}). \quad \{b = +, -\} \quad (8.55)$$

### 8.3. Linear Sigma Model

As we are considering strong magnetic field, we restrict ourselves to the lowest Landau levels. For  $\pi^+(k_a) + \pi^+(k_b) \rightarrow \pi^+(k_c) + \pi^+(k_d)$  and  $\pi^-(k_a) + \pi^-(k_b) \rightarrow \pi^-(k_c) + \pi^-(k_d)$  scatterings, the interaction frequencies of “ $\pi^b(b = \pm)$ ” for these processes are given by

$$\begin{aligned} \omega_1^b &= \frac{1}{2} \int \frac{dk_y^b dk_z^b}{(2\pi)^2} \frac{dk_y^c dk_z^c}{(2\pi)^2} \frac{dk_y^d dk_z^d}{(2\pi)^2} (2\pi)^3 \delta_x^{(3)}(k_a + k_b - k_c - k_d) \\ &\times \frac{1}{16E_a E_b E_c E_d} |\mathcal{M}_{fi}(\pi^+ \pi^+ | \pi^+ \pi^+)|^2 f_b^{eq}, \end{aligned} \quad (8.56)$$

with

$$\begin{aligned} |\mathcal{M}_{fi}|^2 &= (6\lambda)^2 N_0^8 \frac{\pi}{2|eB|} \\ &\exp \left\{ - \frac{(k_y^a + k_y^b + k_y^c + k_y^d)^2 - 4(k_y^a)^2 - 4(k_y^b)^2 - 4(k_y^c)^2 - 4(k_y^d)^2}{4|eB|} \right\}. \end{aligned} \quad (8.57)$$

After integration over  $k_y^b, k_y^c, k_y^d$  we get,

$$\begin{aligned} \omega_1^b &= \frac{1}{2} 6^2 \lambda^2 N_0^8 \frac{\pi^2}{2} \frac{(2\pi)^3}{16(2\pi)^6} \int dk_z^b dk_z^c dk_z^d \\ &\times \delta(E_a + E_b - E_c - E_d) \delta(k_z^a + k_z^b - k_z^c - k_z^d) \frac{1}{E_a E_b E_c E_d} f_b^{eq} \\ &= \frac{1}{2} 6^2 \frac{\lambda^2}{32} \frac{|eB|^2}{\pi^2} \frac{\pi^2}{(2\pi)^3} \int dk_z^b dk_z^c \delta(E_a + E_b - E_c - E_d) \\ &\times \frac{1}{E_a E_b E_c \sqrt{m^2 + (k_z^a + k_z^b - k_z^c)^2 + |eB|}} f_b^{eq} \\ &= \frac{1}{2} 6^2 \frac{\lambda^2}{32} \frac{|eB|^2}{(2\pi)^3} \int dk_z^b dk_z^c \left( \frac{k_z^a}{E_a} - \frac{k_z^b}{E_b} \right)^{-1} \\ &\times \frac{\delta(k_z^c - k_z^a) + \delta(k_z^c - k_z^b)}{E_a E_b E_c \sqrt{m^2 + (k_z^a + k_z^b - k_z^c)^2 + |eB|}} f_b^{eq} \\ &= \frac{1}{2} 6^2 \frac{\lambda^2}{32} \frac{|eB|^2}{(2\pi)^3} \int_{-\infty}^{\infty} dk_z^b \frac{2}{E_a^2 E_b^2} \left( \frac{k_z^a}{E_a} - \frac{k_z^b}{E_b} \right)^{-1} f_b^{eq}. \end{aligned} \quad (8.58)$$

Here we have used the identity

$$\delta[g(x)] = \sum_i \frac{\delta(x - x_i)}{|g'(x_i)|}, \quad (8.59)$$

where  $x_i$  are the roots of  $g(x)$ .

Similarly, for  $\pi^+(k_a) + \pi^-(k_b) \rightarrow \pi^+(k_c) + \pi^-(k_d)$  type scattering the interaction frequencies of “ $\pi^b(b = \pm)$ ” are given by,

$$\omega_2^b = 2^2 \frac{\lambda^2 |eB|^2}{32 (2\pi)^3} \int_{-\infty}^{\infty} dk_z^b \frac{2}{E_a^2 E_b^2} \left( \frac{k_z^a}{E_a} - \frac{k_z^b}{E_b} \right)^{-1} f_b^{eq}. \quad (8.60)$$

Now we are considering the other scatterings  $\pi^b(p) + \sigma(k) \rightarrow \pi^b(p') + \sigma(k')$  and  $\pi^b(p) + \pi^0(k) \rightarrow \pi^b(p') + \pi^0(k')$  with  $\{b = +, -\}$ . In these cases interaction frequency of  $\pi^b$  particle is

$$\omega_3^b(p) = \int \frac{d^3 k}{(2\pi)^3} \frac{d^3 k'}{(2\pi)^3} \frac{d^2 p'}{(2\pi)^2} \frac{(2\pi)^3 \delta_{\vec{x}}^{(3)}(p + k - p' - k')}{16 E_k E_p E_{p'} E_{k'}} |\mathcal{M}_{fi}|^2 f^{eq}(E_k), \quad (8.61)$$

with

$$|\mathcal{M}_{fi}|^2 = (2\lambda)^2 N_0^4 \frac{\pi}{|eB|} \exp \left\{ -\frac{(p_y - p'_y)^2 + (k_x - k'_x)^2}{2|eB|} \right\}. \quad (8.62)$$

After integration over  $p'_y$  and  $k_z$  we get,

$$\begin{aligned} \omega_3^b &= (2\lambda)^2 N_0^4 \frac{\pi}{16|eB|} \int \frac{d^3 k'}{(2\pi)^5} \frac{d^2 k_{\perp} dp'_z}{E_p E_{k'} E_{p'} \sqrt{k_{\perp}^2 + (p'_z + k'_z - p_z)^2}} e^{-\frac{(k-k')_{\perp}^2}{2|eB|}} \\ &\times \delta(E_p + \sqrt{k_{\perp}^2 + (p'_z + k'_z - p_z)^2} - E_{p'} - E_{k'}) f^{eq} \left( \sqrt{k_{\perp}^2 + (p'_z + k'_z - p_z)^2} \right) \end{aligned}$$

### 8.3. Linear Sigma Model

$$\begin{aligned}
&= (2\lambda)^2 \frac{|eB|}{\pi} \frac{\pi}{16|eB|} \int \frac{d^3 k'}{(2\pi)^5} \frac{d^2 k_\perp dp'_z}{E_p E'_k E_{p'} \sqrt{k_\perp^2 + (p'_z + k'_z - p_z)^2}} \\
&\times 2|E_{p'} + E_{k'} - E_p| e^{-\frac{(k-k')^2_\perp}{2|eB|}} f^{eq} \left( \sqrt{k_\perp^2 + (p'_z + k'_z - p_z)^2} \right) \\
&\times \delta(k_\perp^2 - (E_{p'} + E_{k'} - E_p)^2 + (p'_z + k'_z - p_z)^2). \tag{8.63}
\end{aligned}$$

We perform the integration numerically after completing the  $k_\perp$  integration using the delta function.

Next, we are calculating the interaction rate of the neutral scalar particles  $\sigma$  and  $\pi^0$  from  $\pi^b(p) + \sigma(k) \rightarrow \pi^b(p') + \sigma(k')$  and  $\pi^b(p) + \pi^0(k) \rightarrow \pi^b(p') + \pi^0(k')$  scatterings with  $\{b = +, -\}$ . For these types of interactions, we can write the expression of interaction frequencies of  $\pi^0$  and  $\sigma$  as

$$\begin{aligned}
\omega_4^{\sigma, \pi^0}(k) &= \frac{1}{L_x} \int \frac{d^3 k'}{(2\pi)^3} \frac{d^2 p}{(2\pi)^2} \frac{d^2 p'}{(2\pi)^2} \frac{(2\pi)^3 \delta_x^{(3)}(P + K - P' - K')}{16E_k E_p E_{p'} E_{k'}} \\
&\times |\mathcal{M}_{fi}|^2 f^{eq}(E_p), \tag{8.64}
\end{aligned}$$

where the matrix element is same as in Eq. (8.57). After integration over  $p'_y$  and  $k'_z$  we get,

$$\begin{aligned}
\omega_4^{\sigma, \pi^0} &= (2\lambda)^2 N_0^4 \frac{\pi}{16|eB|} \int \frac{d^2 k'_\perp}{(2\pi)^4 L_x} \frac{dp_y dp_z dp'_z}{E_p E_k E_{p'} \sqrt{k'^2_\perp + (p_z + k_z - p'_z)^2}} \\
&\times \delta(E_p + E_k - \sqrt{k'^2_\perp + (p_z + k_z - p'_z)^2} - E_{p'}) e^{-\frac{(k-k')^2_\perp}{2|eB|}} f^{eq}(E_p). \tag{8.65}
\end{aligned}$$

We have performed the integration numerically after using the delta function. Here we have used  $\int dp_y = |eB|L_x$ .

Associated scattering processes to calculate  $\pi^+$  relaxation time i.e.  $\tau_{\pi^+}$  are

$$\pi^+ + \pi^a \rightarrow \pi^+ + \pi^a \quad (a = +, -, 0),$$

$$\pi^+ + \sigma \rightarrow \pi^+ + \sigma. \quad (8.66)$$

Total interaction frequency for  $\pi^+$  is obtained as  $\omega^{\pi^+} = \omega_1^{\pi^+} + \omega_2^{\pi^+} + \omega_3^{\pi^+}$ . The equilibration time  $\tau_{\pi^+}$  is given by  $\tau_{\pi^+} = 1/\omega^{\pi^+}$ . For the only scalar interaction (for example:  $\sigma\sigma \rightarrow \sigma\sigma$ ) we considered the expression of interaction rate from equation (8.47). In the similar fashion we can calculate the interaction frequencies for other particles. Incorporating the estimated relaxation times in eq. (8.22)-eq. (8.25), we can obtain the viscosity coefficients.

## 8.4 Results

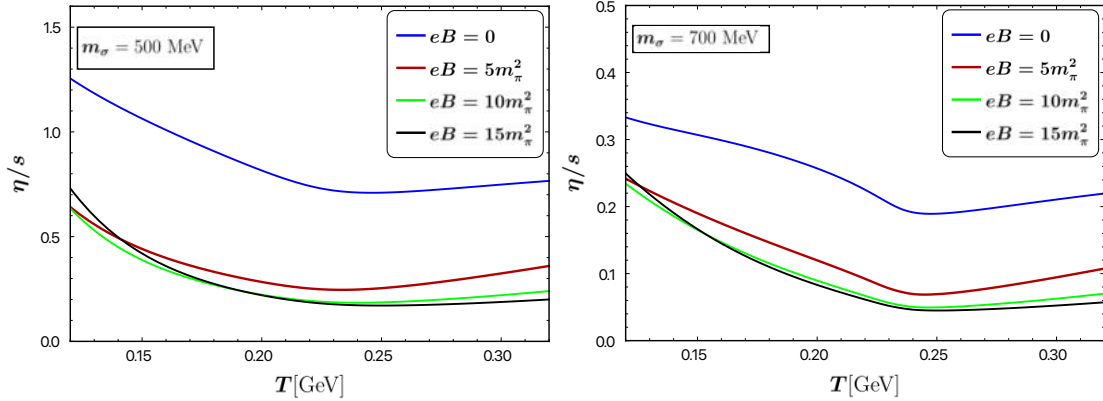


Figure 8.2: The ratio of shear viscosity to entropy density as a function of temperature for vacuum sigma masses  $m_\sigma = 500$  MeV(left) and  $700$  MeV(right). In both the plots blue lines indicate the pure thermal case whereas the other lines represent the parallel components of shear viscosity coefficients to entropy ratio for  $5m_\pi^2$  (red line),  $10m_\pi^2$  (green line),  $15m_\pi^2$  (black line).

We have summarized our results for the anisotropic components of the shear viscosity coefficients in the relaxation time approximation for the nonzero magnetic field. We then briefly discussed the linear sigma model and its thermodynamics. The temperature and



#### 8.4. Results

magnetic field-dependent nature of the thermodynamic quantities like  $s/T^3$  and  $\epsilon/T^3$  are plotted and discussed.

We have revisited the solution of the Klein-Gordon (KG) equation in the presence of a background magnetic field described by a particular vector potential. The quantized nature of the transverse motion of the charged particles emerges to change the particles' energy. The solutions of the KG equation are dependent on the Landau levels. Quantizing the theory, we have calculated the matrix elements using the field operators to obtain the interaction rates. The temperature and magnetic field-dependent interaction rates are incorporated into the thermal relaxation times. In our present study, we have done our evaluation for a strong magnetic field by considering only the lowest Landau level contributions. In Fig. 8.2 we have compared the pure thermal ( $B = 0$  case) isotropic viscous coefficient with parallel component of shear viscosity of the thermo-magnetic medium for vacuum sigma masses  $m_\sigma = 500$  MeV and 700 MeV. The viscous coefficients are scaled with the entropy density. Only temperature-dependent entropy is considered for the thermal case, whereas temperature ( $T$ ) and magnetic field ( $B$ ) dependent entropy is taken for the magnetic case. The plots are shown for three magnetic field strengths, i.e.,  $5m_\pi^2$  (Redline),  $10m_\pi^2$  (Green line), and  $15m_\pi^2$  (Blackline). There is a minimum at crossover temperature of 245 MeV for both thermal and magnetic cases. We can also observe that shear viscosity is reduced in the presence of the magnetic field.

Now we will explore the other shear viscous coefficients. LSM has both charged and neutral hadrons. So we studied the perpendicular components for charged and neutral particles differently. As mentioned earlier, neutral particles have a single viscous coefficient, which only contributes to the isotropic shear viscosity. In Fig. 8.3, the solid black line indicates the variation of the scaled isotropic shear viscous coefficient with temperature. The blue

## Chapter 8. Hadronic viscosity coefficient at finite temperature and magnetic field

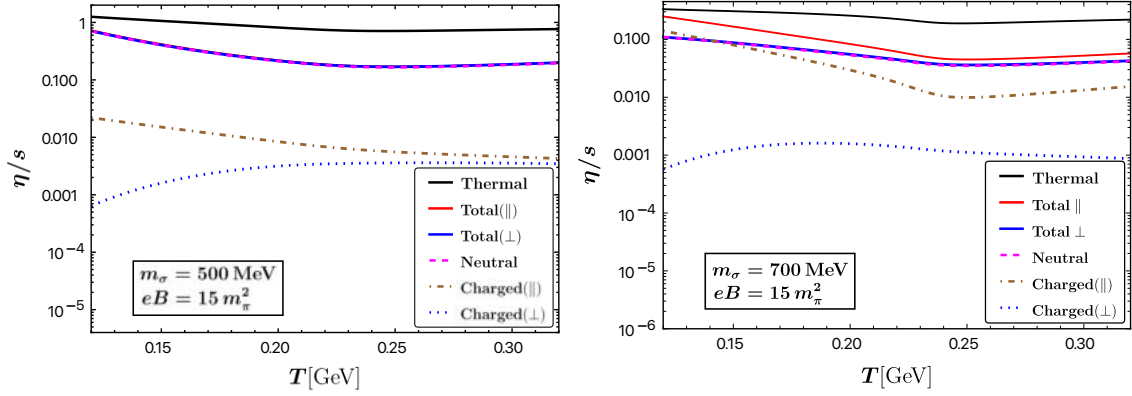


Figure 8.3: Ratio of parallel  $\eta_{\parallel}$  and perpendicular  $\eta_{\perp}$  shear viscosity components to entropy as a function of temperature ( $T$ ) for vacuum sigma mass  $m_\sigma = 500 \text{ MeV}$  (left) and  $m_\sigma = 700 \text{ MeV}$  (right). Magnetic field strength is taken as  $15m_\pi^2$ .

dotted line represents the perpendicular component of shear viscosity for the charged particles, whereas the brown dot-dashed line shows the parallel component. The dashed line (magenta) shows the isotropic contribution to the viscous coefficients coming from neutral particles is shown by the dashed line (magenta). Total parallel (solid red) and perpendicular (solid blue) shear viscous coefficients are also plotted to compare with the pure thermal case. The plots are shown for vacuum sigma mass of 500 MeV (left figure) and 700 (right figure) MeV. It is observed from the figure that the anisotropic viscous coefficients for the charged particles are quite lower than the neutral hadrons. Note that for  $m_\sigma = 500 \text{ MeV}$ , total(parallel), total (perpendicular), and neutral hadron contributions coincide as the contribution from the charged hadrons is very small for this case. It is also noted that the Hall type shear viscosity is zero for vanishing baryon chemical potential even in a finite magnetic field.

## 8.5 Summary

In the presence of the magnetic field, the charged particles get affected, and the system becomes anisotropic. Therefore, the transport coefficients become anisotropic. This work calculates the shear viscosity of hadronic matter in a strong magnetic field and vanishing chemical potential. We have calculated the parallel and perpendicular components of share viscosity in the relaxation time approximation. We have observed that the shear viscosity to entropy ratio for the neutral hadrons gets modified in the presence of a strong magnetic field because of their interaction with the charged particles. In addition, the shear viscosity for charged hadrons is modified in the thermomagnetic medium. We have observed that the contributions to the total shear viscosity to entropy ratio are more dominant for the charged neutral hadrons than the charged hadrons.

The present investigation is limited to the lowest Landau level (LLL) approximation, and it is valid for a very high value of the magnetic field. To study the effect of the magnetic field on the hadronic transport coefficients at a small to moderate strength of the magnetic field, one should include higher Landau levels. Such calculations are in progress and will be presented elsewhere.



---

## CONCLUSIONS

---

The question of modern physics about basic building blocks of the universe has driven the scientists to the particle collision experiments at high energies. The efforts from theorists and experimentalists have led to the recent discovery of Higgs boson,  $W$ ,  $Z$  bosons, quark-gluon plasma and so on. In heavy ion colliders at RHIC and LHC new state of extreme matter i.e. quark-gluon plasma (QGP) is produced. Future experiments at NICA and FAIR are planned to explore the dense matter properties. The dynamics of quark-gluon plasma is governed by the non-abelian quantum field theory of quarks and gluons i.e. Quantum Chromodynamics (QCD). It has two important features: i) the feeble interaction of quarks and gluons at high energy and ii) the confinement in which the interaction strength becomes strong at low energy. The transition between deconfined and confined phases occur at temperature about 160 MeV. One of the main goal of the collider experiments is to unravel the characteristics of QCD phase diagram. Various theoretical tools such as nonperturbative lattice QCD simulation, effective hydrodynamic modeling, perturbative hard thermal loop calculations as well as AdS/CFT inspired studies have made remarkable achievement in

understanding of the experimental data available from the heavy ion colliders.

In this thesis we have explored various characteristics of anisotropic medium. Broadly two types of anisotropies created in HIC are discussed here: i) anisotropic momentum distribution of partons due to the rapid expansion of the medium, ii) magnetic field produced in the noncentral HICs. Partons propagating through the heat bath acquire thermal masses. Unlike vacuum case, gluons have two dispersive modes. In presence of the anisotropies in medium, gluons dispersive modes are modified. In Chapter 3 we have constructed covariant structure of gluon effective propagator in presence of two anisotropy directions. In a thermal QCD medium, anisotropies are characterized by two independent four vectors  $a^\mu$  and  $b^\nu$  having unit norms. The presence of temperature introduces the four vector  $u^\mu$  i.e. heat bath velocity. We have also gluon momentum  $P^\mu$ . These are used to form a set of ten independent symmetric tensors so that the symmetric gluon polarization tensor can be expressed as a linear combination of them. Using the transversality condition  $P^\mu \Pi_{\mu\nu} = 0$ , we have obtained the general structure for the gauge boson self-energy for two anisotropy directions which can be written as a linear combination of six basis tensors [288]. Further the effective propagator has been calculated from the Dyson-Schwinger equation. From the pole of the propagator collective modes are obtained.

The deconfined quark-gluon plasma (QGP) matter produced in the ultra-relativistic heavy ion collision experiments is likely to possess substantial deviation from perfect local isotropic equilibrium. At early times after nuclear impact large pressure anisotropy is expected in the center of the fireball. Incorporating such large momentum space anisotropy, aHydro i.e, anisotropic hydrodynamics [34] is developed. With certain classes of anisotropic momentum distributions, the non-equilibrium plasma properties can be described by studying the collective modes of the quasipartons in the framework of hard thermal loop perturbation theory. Due to the presence of non-equilibrium momentum distributions in QGP

medium, existence of kinetic instabilities is expected. These are, in simple terms, the collective modes that possess a positive imaginary part in their mode frequencies resulting an exponential growth in the chromomagnetic and chromoelectric fields. The presence of such Chromo-Weibel instabilities can influence the thermalization and isotropization of the medium. In Chapter 4, introducing the mass scales corresponding to the collective modes, the occurrence of the unstable modes has been studied for ellipsoidal momentum space anisotropy. The collective modes are obtained from the gauge-boson propagator constructed in Chapter 3. The advantage of considering the general structure of the gauge boson is that the collective modes can be expressed in terms of co-ordinate independent form factors. It is observed that, compared to the spheroidal case, additional unstable mode may appear in presence of ellipsoidal anisotropy depending upon the choice of the parameters.

Another source of anisotropy discussed in this thesis is the magnetic field produced in the direction perpendicular to the reaction plane in non-central heavy ion collisions. We have studied the effect of magnetic field on various quantities like chiral susceptibility, damping rate and so on. In presence of temperature and background magnetic field, the boost and rotational symmetries of the system are broken. In presence of background magnetic field the general structure of gauge-boson self-energy is modified [199]. The presence of magnetic field introduces new four vector  $n^\nu = \frac{1}{B} u_\mu \tilde{F}^{\mu\nu}$ , where  $B$  is the magnetic field strength and  $\tilde{F}^{\mu\nu}$  is the dual of the electromagnetic field tensor. We use the gauge-boson effective propagator structure obtained in Chapter 3. As mentioned earlier, magnetic field produced in heavy ion collisions decreases with time. The QCD matter cools down after the collision and the chiral phase transition occurred at a temperature around 160 MeV. In this region the effect of a weak magnetic field is particularly important. In presence of weak magnetic field, we have calculated photon damping rate in Chapter 5 and chiral susceptibility in Chapter 6 in the QED/QCD medium using the HTL approximation. In presence

of magnetic field and heat bath, the general structure of fermion self-energy is modified and can be written in terms of 16 linearly independent matrices:  $\{\gamma^\mu, \gamma^5, \gamma^5\gamma^\mu, \sigma^{\mu\nu}, \mathbb{I}\}$ . In Chapter 6 we have computed the structure functions upto  $\mathcal{O}[(eB)^2]$  considering the Schwinger propagator for massive fermion in presence of weak magnetic field. In the weak magnetic field limit, we have used the scale hierarchy  $\sqrt{|q_f B|} < gT < T$ .

Magnetized plasma is found in the interiors of neutron stars, magnetospheres of magnetars and central engines of supernovae and gamma ray bursts. The propagation of photon through the hot magnetized electron-positron plasma (EPP) is of great interest of study. High intensity laser beams are used to create ultrarelativistic EPP of temperature around 10 MeV. This EPP can play major role in various astrophysical situations. Some properties of EPP, such as damping rate, transport coefficients, the equation of state and so on are studied using QED at finite temperature. Also the damping rates of hard particles have much interest in heavy ion collisions. For example, damping rate of photon is associated with the mean free path and hard photon production rate of QGP. As photon interacts electromagnetically, it comes out of the hot QCD medium without interacting much. So the photon can be considered as a good probe of the QGP medium. Damping rate of photon is related to the imaginary part of the photon dispersion. This is also connected with the scattering cross-section processes which can be found by cutting the self-energy diagram. In lowest order coupling constant, photons are damped by Compton scattering and pair creation process. In a relativistic hot magnetized QED medium we consider hard photon of momentum  $P^\mu = (p_0, \mathbf{p})$  where  $p = |\mathbf{p}| \gg T$ . To find the soft contribution of the damping rate we introduce a separation scale  $\Lambda$  where  $eT \ll \Lambda \ll T$  ( $gT \ll \Lambda \ll T$  in case of QCD). In case of low momentum transfer, the damping rate shows infrared singularity. So, the effective resummed propagator instead of bare propagator for soft momentum of fermion is considered. We will call this as the soft contribution to the damping rate of photon. The



hard contribution refers to the case where all the fermions in loop have momentum order of or much greater than the system temperature  $T$ . We have calculated the soft contribution of the photon damping rate in weakly magnetized QED medium in Chapter 5. Extension to the case of damping rate of hard photon in weakly magnetized hot QCD medium is straightforward by considering the fermion loops as quark and antiquark. In presence of magnetic field we get one longitudinal and two non-degenerate transverse modes. We have calculated damping rate for two transverse modes of photon. We use the effective fermion propagator in presence of weak magnetic field for the soft fermion and Schwinger propagator for the hard fermion in the loop. The Braaten-Pisarki-Yuan formalism has been used here to calculate the imaginary part of photon self-energy. We have obtained the result upto  $\mathcal{O}[(eB)^2]$ .

Confinement and chiral symmetry breaking are the two nonperturbative features of QCD vacuum. Dynamical chiral symmetry breaking indicates the nonperturbative nature of QCD vacuum at vanishing temperature and/or density. The QCD vacuum undergoes a transition from chiral asymmetric to chiral symmetric phase with the increase in temperature and /or density. The transition is characterized by the order parameter of the chiral phase transition i.e. quark-antiquark scalar condensate. At first order transition, order parameter changes discontinuously near the transition point whereas at the second order phase transition or crossover, it varies smoothly. The fluctuation of this order parameter and the associated susceptibilities are relevant to investigate the properties of QCD matter at extreme condition. Chiral susceptibility is the measure of fluctuation of the order parameter. It estimates the response of the chiral condensate with the variation of current quark mass. We have calculated the chiral susceptibility in weakly magnetized hot QCD medium using HTL approximation in Chapter 6. We expand the result in orders of strong coupling  $g$  and keep it upto  $\mathcal{O}(g)$ . We get the completely analytical result upto  $\mathcal{O}[(eB)^2]$ .

UV divergences appeared in the chiral susceptibility are renormalized within the  $\overline{\text{MS}}$  renormalization scheme. It is found that the chiral susceptibility is increased due to the presence of the chemical potential as well as the background magnetic field. Photon damping rate and chiral susceptibilities are calculated in weak field limit. Extension of these calculations for high and moderate value of magnetic field would be a future direction of study.

The QGP state is very transient. There is no unique signal to confirm the formation of this novel state. There are several signatures for QGP formation. Quarkonium suppression is one of the signatures. Heavy quarkonium [113] i.e. bound state of heavy quark and its anti-quark is considered as one of the important probe to study the deconfining state of the strongly interacting QCD medium under extreme condition. Theoretically heavy quarkonium can be studied through potential models or lattice QCD. Recently several studies [1] have discussed the heavy quark potential in a magnetized medium restricting themselves to limiting cases involving strong or weak magnetic field approximations. We have calculated the imaginary part of heavy quark potential in presence of any finite magnetic field considering all Landau level contributions using the potential models in Chapter 7. We have also used the general structure of gluon propagator in presence of temperature and magnetic field. Due to the presence of magnetic field, the anisotropic nature of potential in space is also explored in our studies which was ignored in earlier works. The imaginary part of potential is related to the decay width ( $\Gamma$ ) of quarkonium bound states which determines the dissociation temperature. The dependency of decay width with temperature and magnetic field has also been estimated.

An out of equilibrium isolated system evolves towards equilibrium state with transporting matter, momentum or energy. For example, viscosity is related to the momenta transfer whereas, thermal conductivity is related to the heat transfer. The microscopic mechanism of the momentum or energy transportation is involved with the interactions with the con-

stituent particles of the system. The investigations of the transport phenomena motivate us to explore about the nature of the interactions and the thermodynamic characteristic of a system. Also, the transport coefficients are used as input parameters for the hydrodynamic simulations. We calculate the transport coefficient of hadronic matter in the presence of temperature and magnetic field using the linear sigma model in Chapter 8. In the relaxation time approximation, we estimated the shear viscosity over entropy density  $\eta/s$ . To estimate the relaxation time, the point-like interaction rates of hadrons are evaluated through the S-matrix approach considering the LLL approximation. Estimation of transport coefficients for moderate value of magnetic field considering the higher Landau levels contributions would be an interesting future direction.



## SPECTRAL REPRESENTATION OF THE PROPAGATORS

---

$$\begin{aligned}
 & \lim_{\epsilon \rightarrow 0} \int_{-\infty}^{\infty} dx \frac{\epsilon}{x^2 + \epsilon^2} f(x) \\
 & \approx f(0) \int_{-\infty}^{\infty} dx \frac{\epsilon}{x^2 + \epsilon^2} \left\{ \begin{array}{l} \text{significant contribution comes from} \\ \text{integration, where } x \simeq 0 \end{array} \right. \\
 & = f(0) \epsilon \int_{-\infty}^{\infty} dx \frac{1}{x^2 + \epsilon^2} = \pi f(0), \tag{A.1}
 \end{aligned}$$

where  $f(x)$  is a test function.

From the above equations we can write,

$$\lim_{\epsilon \rightarrow 0} \frac{\epsilon}{x^2 + \epsilon^2} = \pi \delta(x), \tag{A.2}$$

Chapter A. Spectral representation of the propagators

$$\lim_{\epsilon \rightarrow 0} \text{Im} \frac{1}{x + i\epsilon} = \frac{1}{2i} \lim_{\epsilon \rightarrow 0} \left[ \frac{1}{x + i\epsilon} - \frac{1}{x - i\epsilon} \right] = \frac{1}{2i} \lim_{\epsilon \rightarrow 0} \frac{-2i\epsilon}{x^2 + \epsilon^2} = -\pi \delta(x). \quad (\text{A.3})$$

$$\begin{aligned} \lim_{\epsilon \rightarrow 0} \int_{-\infty}^{\infty} dx \frac{2\epsilon x}{(x^2 + \epsilon^2)^2} f(x) &= \lim_{\epsilon \rightarrow 0} \int_{-\infty}^{\infty} dx \epsilon f(x) \frac{d}{dx} \left[ -\frac{1}{(x^2 + \epsilon^2)} \right] \\ &= \lim_{\epsilon \rightarrow 0} \int_{-\infty}^{\infty} dx f'(x) \frac{\epsilon}{x^2 + \epsilon^2} \\ &= \pi f'(0) = \pi \int dx f'(x) \delta(x) \\ &= -\pi \int dx f(x) \delta'(x) \end{aligned} \quad (\text{A.4})$$

From the above equation we find,

$$\lim_{\epsilon \rightarrow 0} \frac{2\epsilon x}{(x^2 + \epsilon^2)^2} = -\pi \delta'(x). \quad (\text{A.5})$$

Now using Eq. (A.5) one can calculate,

$$\lim_{\epsilon \rightarrow 0} \text{Im} \frac{1}{(x + i\epsilon)^2} = \frac{1}{2i} \lim_{\epsilon \rightarrow 0} \left[ \frac{1}{(x + i\epsilon)^2} - \frac{1}{(x - i\epsilon)^2} \right] = \frac{1}{2i} \lim_{\epsilon \rightarrow 0} \frac{-i4\epsilon x}{(x^2 + \epsilon^2)^2} = \pi \delta'(x). \quad (\text{A.6})$$

Similarly,

$$\begin{aligned} \lim_{\epsilon \rightarrow 0} \int_{-\infty}^{\infty} dx \frac{\epsilon^3 - 3x^2\epsilon}{(x^2 + \epsilon^2)^3} f(x) &= \lim_{\epsilon \rightarrow 0} \int_{-\infty}^{\infty} dx \frac{\epsilon^3}{(x^2 + \epsilon^2)^3} f(x) \\ &\quad - \lim_{\epsilon \rightarrow 0} \int_{-\infty}^{\infty} dx \frac{3x^2\epsilon}{(x^2 + \epsilon^2)^3} f(x) \\ &= I_1 + I_2, \end{aligned} \quad (\text{A.7})$$

where

$$\begin{aligned}
I_1 &= \lim_{\epsilon \rightarrow 0} \int_{-\infty}^{\infty} dx \frac{\epsilon^3 f(x)}{(x^2 + \epsilon^2)^3} \approx \lim_{\epsilon \rightarrow 0} \epsilon^3 f(0) \int_{-\infty}^{\infty} dx \frac{1}{(x^2 + \epsilon^2)^3} \\
&= \lim_{\epsilon \rightarrow 0} \epsilon^3 f(0) \frac{3}{8} \frac{1}{\epsilon^5} = \lim_{\epsilon \rightarrow 0} \frac{3}{8\epsilon^2} f(0), \\
I_2 &= -3 \lim_{\epsilon \rightarrow 0} \int_{-\infty}^{\infty} dx \frac{x^2 \epsilon f(x)}{(x^2 + \epsilon^2)^3} \\
&= -3 \lim_{\epsilon \rightarrow 0} \epsilon \int dx f(x) \left[ \frac{1}{8} \frac{d^2}{dx^2} \left( \frac{1}{x^2 + \epsilon^2} \right) + \frac{1}{8} \frac{2}{(x^2 + \epsilon^2)^2} \right] \\
&= -\lim_{\epsilon \rightarrow 0} \frac{3}{8\epsilon^2} f(0) - \frac{3}{8} \lim_{\epsilon \rightarrow 0} \epsilon \int dx f(x) \frac{d^2}{dx^2} \left( \frac{1}{x^2 + \epsilon^2} \right). \tag{A.8}
\end{aligned}$$

So ,

$$\begin{aligned}
I_1 + I_2 &= -\frac{3}{8} \lim_{\epsilon \rightarrow 0} \epsilon \int dx f(x) \frac{d^2}{dx^2} \left( \frac{1}{x^2 + \epsilon^2} \right) = \frac{3}{8} \lim_{\epsilon \rightarrow 0} \int dx \epsilon f'(x) \frac{d}{dx} \left( \frac{1}{x^2 + \epsilon^2} \right) \\
&= -\frac{3}{8} \lim_{\epsilon \rightarrow 0} \int dx \epsilon f''(x) \frac{1}{x^2 + \epsilon^2} = -\frac{3}{8} \pi \int dx f''(x) \delta(x) \\
&= -\frac{3}{8} \pi \int_{-\infty}^{\infty} dx f(x) \delta''(x). \tag{A.9}
\end{aligned}$$

We can conclude from the last few steps that,

$$\lim_{\epsilon \rightarrow 0} \frac{\epsilon^3 - 3x^2 \epsilon}{(x^2 + \epsilon^2)^3} = -\frac{3}{8} \pi \delta''(x) . \tag{A.10}$$

Using Eq. (A.10) we can find

$$\begin{aligned}
\lim_{\epsilon \rightarrow 0} \text{Im} \frac{1}{(x + i\epsilon)^3} &= \frac{1}{2i} \lim_{\epsilon \rightarrow 0} \left[ \frac{1}{(x + i\epsilon)^2} - \frac{1}{(x - i\epsilon)^3} \right] \\
&= \lim_{\epsilon \rightarrow 0} \frac{\epsilon^3 - 6\epsilon x^2}{(x^2 + \epsilon^2)^3} = -\frac{3}{8} \pi \delta''(x) \tag{A.11}
\end{aligned}$$

## Chapter A. Spectral representation of the propagators

Now ,

$$\lim_{\epsilon \rightarrow 0} \text{Im} \frac{1}{(x + i\epsilon)^4} = \frac{1}{2i} \lim_{\epsilon \rightarrow 0} \left[ \frac{1}{(x + i\epsilon)^4} - \frac{1}{(x - i\epsilon)^4} \right] = \lim_{\epsilon \rightarrow 0} \frac{4x\epsilon^3 - 4x^3\epsilon}{(x^2 + \epsilon^2)^4}, \quad (\text{A.12})$$

$$\begin{aligned} \lim_{\epsilon \rightarrow 0} \int_{-\infty}^{\infty} dx f(x) \frac{4x\epsilon^3 - 4x^3\epsilon}{(x^2 + \epsilon^2)^4} &= \lim_{\epsilon \rightarrow 0} 4\epsilon \int_{-\infty}^{\infty} dx f(x) \frac{1}{24} \frac{d^3}{dx^3} \left( \frac{1}{x^2 + \epsilon^2} \right) \\ &= -\lim_{\epsilon \rightarrow 0} \frac{\epsilon}{6} \int_{-\infty}^{\infty} dx f'''(x) \frac{1}{x^2 + \epsilon^2} = -\frac{\pi f'''(0)}{6} \\ &= \frac{\pi}{6} \int_{-\infty}^{\infty} dx f(x) \delta'''(x). \end{aligned} \quad (\text{A.13})$$

$$\text{Thus, } \lim_{\epsilon \rightarrow 0} \text{Im} \frac{1}{(x + i\epsilon)^4} = \frac{\pi}{6} \delta'''(x). \quad (\text{A.14})$$

Now we write the spectral representations for the free propagators as

$$\begin{aligned} \rho_0^{(1)}(\omega', q) &= \frac{1}{2\pi} \lim_{\epsilon \rightarrow 0} \text{Im} \left[ \frac{1}{\omega' + i\epsilon + \omega_q} + \frac{1}{\omega' + i\epsilon - \omega_q} \right] \\ &= -\frac{1}{2} \left[ \delta(\omega' + \omega_q) + \delta(\omega' - \omega_q) \right], \end{aligned} \quad (\text{A.15})$$

$$\begin{aligned} \rho_0^{(0)}(\omega', q) &= \frac{1}{2\pi\omega_q} \lim_{\epsilon \rightarrow 0} \text{Im} \left[ \frac{1}{\omega' + i\epsilon - \omega_q} - \frac{1}{\omega' + i\epsilon + \omega_q} \right] \\ &= \frac{1}{2\omega_q} \left[ \delta(\omega' + \omega_q) - \delta(\omega' - \omega_q) \right], \end{aligned} \quad (\text{A.16})$$

$$\begin{aligned} \rho_1^{(1)}(\omega', q) &= \frac{1}{4\pi\omega_q} \lim_{\epsilon \rightarrow 0} \text{Im} \left[ \frac{1}{(\omega' + i\epsilon - \omega_q)^2} - \frac{1}{(\omega' + i\epsilon + \omega_q)^2} \right] \\ &= -\frac{1}{4\omega_q} \left[ \delta'(\omega' + \omega_q) - \delta'(\omega' - \omega_q) \right], \end{aligned} \quad (\text{A.17})$$



$$\begin{aligned}
\rho_1^{(0)}(\omega', q) &= \frac{1}{4\pi\omega_q^2} \lim_{\epsilon \rightarrow 0} \text{Im} \left[ \frac{1}{(\omega' + i\epsilon + \omega_q)^2} + \frac{1}{(\omega' + i\epsilon - \omega_q)^2} - \frac{1}{\omega_q} \left( \frac{1}{\omega' + i\epsilon - \omega_q} \right. \right. \\
&\quad \left. \left. - \frac{1}{\omega' + i\epsilon + \omega_q} \right) \right] \\
&= \frac{1}{4\omega_q^2} \left[ \delta'(\omega' + \omega_q) + \delta'(\omega' - \omega_q) - \frac{1}{\omega_q} \left( \delta(\omega' + \omega_q) - \delta(\omega' - \omega_q) \right) \right], \quad (\text{A.18})
\end{aligned}$$

$$\begin{aligned}
\rho_2^{(1)}(\omega', q) &= \frac{1}{8\pi\omega_q^2} \lim_{\epsilon \rightarrow 0} \text{Im} \left[ \frac{1}{(\omega' + i\epsilon + \omega_q)^3} + \frac{1}{(\omega' + i\epsilon - \omega_q)^3} + \frac{1}{2\omega_q} \left\{ \frac{1}{(\omega' + i\epsilon + \omega_q)^2} \right. \right. \\
&\quad \left. \left. - \frac{1}{(\omega' + i\epsilon - \omega_q)^2} \right\} \right] \\
&= \frac{1}{8\omega_q^2} \left[ -\frac{3}{8} \left( \delta''(\omega' + \omega_q) + \delta''(\omega' - \omega_q) \right) + \frac{1}{2\omega_q} \left( \delta'(\omega' + \omega_q) - \delta'(\omega' - \omega_q) \right) \right], \quad (\text{A.19})
\end{aligned}$$

$$\begin{aligned}
\rho_2^{(0)}(\omega', q) &= -\frac{1}{8\pi\omega_q^3} \lim_{\epsilon \rightarrow 0} \text{Im} \left[ \frac{1}{(\omega' + i\epsilon + \omega_q)^3} - \frac{1}{(\omega' + i\epsilon - \omega_q)^3} + \frac{1}{2\omega_q} \left\{ \frac{1}{(\omega' + i\epsilon + \omega_q)^2} \right. \right. \\
&\quad \left. \left. + \frac{1}{(\omega' + i\epsilon - \omega_q)^2} + \frac{3}{\omega_q} \left( \frac{1}{\omega' + i\epsilon + \omega_q} - \frac{1}{\omega' + i\epsilon - \omega_q} \right) \right\} \right] \\
&= -\frac{1}{8\omega_q^3} \left[ -\frac{3}{8} \left( \delta''(\omega' + \omega_q) - \delta''(\omega' - \omega_q) \right) + \frac{1}{2\omega_q} \left\{ \delta'(\omega' + \omega_q) + \delta'(\omega' - \omega_q) \right. \right. \\
&\quad \left. \left. - \frac{3}{\omega_q} \left( \delta(\omega' + \omega_q) - \delta(\omega' - \omega_q) \right) \right\} \right], \quad (\text{A.20})
\end{aligned}$$

$$\begin{aligned}
\rho_3^{(1)}(\omega', q) &= -\frac{1}{16\pi\omega_q^3} \lim_{\epsilon \rightarrow 0} \text{Im} \left[ \frac{1}{(\omega' + i\epsilon + \omega_q)^4} - \frac{1}{(\omega' + i\epsilon - \omega_q)^4} + \frac{1}{\omega_q} \left\{ \frac{1}{(\omega' + i\epsilon + \omega_q)^3} \right. \right. \\
&\quad \left. \left. + \frac{1}{(\omega' + i\epsilon - \omega_q)^3} + \frac{1}{2\omega_q} \left( \frac{1}{(\omega' + i\epsilon + \omega_q)^2} - \frac{1}{(\omega' + i\epsilon - \omega_q)^2} \right) \right\} \right] \quad (\text{A.21})
\end{aligned}$$

$$\begin{aligned}
&= -\frac{1}{16\omega_q^3} \left[ \frac{1}{6} \left( \delta'''(\omega' + \omega_q) - \delta'''(\omega' - \omega_q) \right) + \frac{1}{\omega_q} \left\{ -\frac{3}{8} \left( \delta''(\omega' + \omega_q) \right. \right. \right. \\
&\quad \left. \left. + \delta''(\omega' - \omega_q) \right) + \frac{1}{2\omega_q} \left( \delta'(\omega' + \omega_q) - \delta'(\omega' - \omega_q) \right) \right\} \right], \quad (\text{A.22})
\end{aligned}$$

Chapter A. Spectral representation of the propagators

$$\begin{aligned}
 \rho_3^{(0)}(\omega', q) &= \frac{1}{16\pi\omega_q^4} \lim_{\epsilon \rightarrow 0} \text{Im} \left[ \frac{1}{(\omega' + i\epsilon + \omega_q)^4} + \frac{1}{(\omega' + i\epsilon - \omega_q)^4} + \frac{1}{2\omega_q} \left\{ \frac{4}{(\omega' + i\epsilon + \omega_q)^3} \right. \right. \\
 &- \frac{4}{(\omega' + i\epsilon - \omega_q)^3} + \frac{1}{2\omega_q} \left( \frac{10}{(\omega' + i\epsilon + \omega_q)^2} + \frac{10}{(\omega' + i\epsilon - \omega_q)^2} + \frac{1}{2\omega_q} \right. \\
 &\times \left. \left. \left( \frac{20}{\omega' + i\epsilon + \omega_q} - \frac{20}{\omega' + i\epsilon - \omega_q} \right) \right) \right] \quad (\text{A.23})
 \end{aligned}$$

$$\begin{aligned}
 &= \frac{1}{16\omega_q^4} \left[ \frac{1}{6} \left( \delta'''(\omega' + \omega_q) + \delta'''(\omega' - \omega_q) \right) + \frac{1}{2\omega_q} \left\{ -\frac{3}{2} \left( \delta''(\omega' + \omega_q) \right. \right. \right. \\
 &- \delta''(\omega' - \omega_q) \left. \left. \right) + \frac{5}{\omega_q} \left( \delta'(\omega' + \omega_q) + \delta'(\omega' - \omega_q) - \frac{1}{\omega_q} \left( \delta(\omega' + \omega_q) \right. \right. \right. \\
 &\left. \left. \left. - \delta(\omega' - \omega_q) \right) \right) \right] \quad (\text{A.24})
 \end{aligned}$$

The effective propagators are given as,

$$\frac{1}{D^2} = \frac{1}{D_+ D_-} = \sum_i \left( \frac{\partial D^2}{\partial \omega} \right)^{-1} \Big|_{\omega=\omega_i} \frac{1}{(\omega - \omega_i)}, \quad (\text{A.25})$$

$$\begin{aligned}
 \frac{1}{D^4} &= \frac{1}{(D_+ D_-)^2} \\
 &= \sum_i \left[ \left( \frac{\partial D^2}{\partial \omega} \right)^{-2} \Big|_{\omega=\omega_i} \frac{1}{(\omega - \omega_i)^2} + \frac{\partial}{\partial \omega} \left\{ \frac{(\omega - \omega_i)^2}{D^4} \right\} \Big|_{\omega=\omega_i} \frac{1}{(\omega - \omega_i)} \right] \\
 &= \sum_i \left[ \left( \frac{\partial D^2}{\partial \omega} \right)^{-2} \Big|_{\omega=\omega_i} \frac{1}{(\omega - \omega_i)^2} - \frac{\partial^2 D^2}{\partial \omega^2} \left( \frac{1}{3!} \frac{\partial^3 D^6}{\partial \omega^3} \right)^{-1} \Big|_{\omega=\omega_i} \frac{1}{(\omega - \omega_i)} \right], \quad (\text{A.26})
 \end{aligned}$$

$$\begin{aligned}
\frac{1}{D^6} &= \frac{1}{(D_+ D_-)^3} \\
&= \sum_i \left[ \left( \frac{\partial D^2}{\partial \omega} \right)^{-3} \Big|_{\omega=\omega_i} \frac{1}{(\omega - \omega_i)^3} + \frac{\partial}{\partial \omega} \left\{ \frac{(\omega - \omega_i)^3}{D^6} \right\} \Big|_{\omega=\omega_i} \frac{1}{(\omega - \omega_i)^2} \right. \\
&\quad \left. + \frac{1}{2} \frac{\partial^2}{\partial \omega^2} \left\{ \frac{(\omega - \omega_i)^3}{D^6} \right\} \Big|_{\omega=\omega_i} \frac{1}{(\omega - \omega_i)} \right] \\
&= \sum_i \left[ \left( \frac{\partial D^2}{\partial \omega} \right)^{-3} \Big|_{\omega=\omega_i} \frac{1}{(\omega - \omega_i)^3} - \frac{3}{2} \frac{\partial^2 D^2}{\partial \omega^2} \left( \frac{1}{4!} \frac{\partial^4 D^8}{\partial \omega^4} \right)^{-1} \Big|_{\omega=\omega_i} \frac{1}{(\omega - \omega_i)^2} \right. \\
&\quad \left. - \frac{3}{5} \left( \frac{\partial^3 D^2}{\partial \omega^3} \left\{ 6 \left( \frac{\partial^4 D^8}{\partial \omega^4} \right)^{-1} + \frac{7}{12} \left( \frac{\partial D^2}{\partial \omega} \right)^{-4} \right\} + 6 \frac{\partial^2 D^2}{\partial \omega^2} \frac{\partial}{\partial \omega} \left( \frac{\partial^4 D^8}{\partial \omega^4} \right)^{-1} \right) \Big|_{\omega=\omega_i} \right. \\
&\quad \left. \times \frac{1}{(\omega - \omega_i)} \right], \tag{A.27}
\end{aligned}$$

where  $\omega_i = \pm\omega_{\pm}$  are the poles of  $D_+$  and  $D_-$ .

The spectral functions of the dressed propagators are given as

$$\rho_{D_{\pm}} = -\frac{(\omega^2 - k^2)}{2m_{\text{th}}^2} \left[ \delta(\omega - \omega_{\pm}) + \delta(\omega + \omega_{\mp}) \right] + \beta_{\pm} \Theta(k^2 - \omega^2), \tag{A.28}$$

where

$$\beta_{\pm} = \frac{-\frac{1}{2}(k \mp \omega)m_{\text{th}}^2}{\left[ k(\omega \mp k) - m_{\text{th}}^2 \left\{ Q_0\left(\frac{\omega}{k}\right) \mp Q_1\left(\frac{\omega}{k}\right) \right\} \right]^2 + \left[ \frac{1}{2}(1 \mp \frac{\omega}{k})m_{\text{th}}^2 \pi \right]^2}, \tag{A.29}$$

where we use the Legendre function of second kind

$$Q_0\left(\frac{\omega}{k}\right) = \frac{1}{2} \ln \left| \frac{\omega + k}{\omega - k} \right| - i \frac{\pi}{2} \Theta(k^2 - \omega^2). \tag{A.30}$$

Chapter A. Spectral representation of the propagators

$$\begin{aligned}
\rho_4(\omega, k) &= \frac{1}{\pi} \text{Im} \left( \frac{1}{D^2} \right) = - \sum_i \left( \frac{\partial D^2}{\partial \omega} \right)^{-1} \Big|_{\omega=\omega_i} \delta(\omega - \omega_i) + \beta_4 \Theta(k^2 - \omega^2) \\
&= \frac{\omega^2 - k^2}{4m_{\text{th}}^2(k^2 - \omega^2 + m_{\text{th}}^2)} \left[ (\omega - k) \left( \delta(\omega - \omega_+) + \delta(\omega + \omega_-) \right) \right. \\
&\quad \left. + (\omega + k) \left( \delta(\omega - \omega_-) + \delta(\omega + \omega_+) \right) \right] + \beta_4 \Theta(k^2 - \omega^2),
\end{aligned} \tag{A.31}$$

$$\begin{aligned}
\rho_5(\omega, k) &= \frac{1}{\pi} \text{Im} \left( \frac{1}{D^4} \right) = \sum_i \left[ \left( \frac{\partial D^2}{\partial \omega} \right)^{-2} \Big|_{\omega=\omega_i} \delta'(\omega - \omega_i) + \frac{\partial^2 D^2}{\partial \omega^2} \left( \frac{1}{3!} \frac{\partial^3 D^6}{\partial \omega^3} \right)^{-1} \Big|_{\omega=\omega_i} \right. \\
&\quad \left. \times \delta(\omega - \omega_i) \right] + \beta_5 \Theta(k^2 - \omega^2),
\end{aligned} \tag{A.32}$$

$$\begin{aligned}
\rho_6(\omega, k) &= \frac{1}{\pi} \text{Im} \left( \frac{1}{D^6} \right) \\
&= \sum_i \left[ -\frac{3}{8} \left( \frac{\partial D^2}{\partial \omega} \right)^{-3} \Big|_{\omega=\omega_i} \delta''(\omega - \omega_i) - \frac{3}{2} \frac{\partial^2 D^2}{\partial \omega^2} \left( \frac{1}{4!} \frac{\partial^4 D^8}{\partial \omega^4} \right)^{-1} \Big|_{\omega=\omega_i} \right. \\
&\quad \times \delta'(\omega - \omega_i) + \frac{3}{5} \left( \frac{\partial^3 D^2}{\partial \omega^3} \left\{ 6 \left( \frac{\partial^4 D^8}{\partial \omega^4} \right)^{-1} + \frac{7}{12} \left( \frac{\partial D^2}{\partial \omega} \right)^{-4} \right\} \right. \\
&\quad \left. \left. + 6 \frac{\partial^2 D^2}{\partial \omega^2} \frac{\partial}{\partial \omega} \left( \frac{\partial^4 D^8}{\partial \omega^4} \right)^{-1} \right) \Big|_{\omega=\omega_i} \times \delta(\omega - \omega_i) \right] + \beta_6 \Theta(k^2 - \omega^2),
\end{aligned} \tag{A.33}$$

$$\rho_7(\omega, k) = \frac{1}{\pi} \text{Im} \left( \frac{b'}{D^2} \right) = -b' \sum_i \left( \frac{\partial D^2}{\partial \omega} \Big|_{\omega=\omega_i} \right)^{-1} \delta(\omega - \omega_i) + \beta_7 \Theta(k^2 - \omega^2), \tag{A.34}$$

$$\begin{aligned}\rho_8(\omega, k) &= \frac{1}{\pi} \text{Im} \left( \frac{c'}{D^2} \right) = -c' \sum_i \left( \frac{\partial D^2}{\partial \omega} \Big|_{\omega=\omega_i} \right)^{-1} \delta(\omega - \omega_i) \\ &+ \beta_8 \Theta(k^2 - \omega^2),\end{aligned}\tag{A.35}$$

$$\begin{aligned}\rho_9^{(0)}(\omega, k) &= \frac{1}{\pi} \text{Im} \left( \frac{h(1+a)}{D^4} \right) = h(1+a) \times \sum_i \left[ \left( \frac{\partial D^2}{\partial \omega} \Big|_{\omega=\omega_i} \right)^{-2} \delta'(\omega - \omega_i) \right. \\ &- \left. \frac{\partial}{\partial \omega} \left\{ \frac{(\omega - \omega_i)^2}{D^4} \right\} \Big|_{\omega=\omega_i} \delta(\omega - \omega_i) \right] + \beta_9^{(0)} \Theta(k^2 - \omega^2),\end{aligned}\tag{A.36}$$

$$\begin{aligned}\rho_9^{(1)}(\omega, k) &= \frac{1}{\pi} \text{Im} \left( \frac{h(1+a)\omega}{D^4} \right) = \omega h(1+a) \times \sum_i \left[ \left( \frac{\partial D^2}{\partial \omega} \Big|_{\omega=\omega_i} \right)^{-2} \delta'(\omega - \omega_i) \right. \\ &- \left. \frac{\partial}{\partial \omega} \left\{ \frac{(\omega - \omega_i)^2}{D^4} \right\} \Big|_{\omega=\omega_i} \delta(\omega - \omega_i) \right] + \beta_9^{(1)} \Theta(k^2 - \omega^2),\end{aligned}\tag{A.37}$$

$$\begin{aligned}\rho_{10}(\omega, k) &= \frac{1}{\pi} \text{Im} \left( \frac{hb}{D^4} \right) = hb \times \sum_i \left[ \left( \frac{\partial D^2}{\partial \omega} \Big|_{\omega=\omega_i} \right)^{-2} \delta'(\omega - \omega_i) \right. \\ &- \left. \frac{\partial}{\partial \omega} \left\{ \frac{(\omega - \omega_i)^2}{D^4} \right\} \Big|_{\omega=\omega_i} \times \delta(\omega - \omega_i) \right] + \beta_{10} \Theta(k^2 - \omega^2),\end{aligned}\tag{A.38}$$

$$\begin{aligned}\rho_{11}(\omega, k) &= \frac{1}{\pi} \text{Im} \left[ \frac{hb'}{D^4} \right] = hb' \times \sum_i \left[ \left( \frac{\partial D^2}{\partial \omega} \Big|_{\omega=\omega_i} \right)^{-2} \delta'(\omega - \omega_i) \right. \\ &- \left. \frac{\partial}{\partial \omega} \left\{ \frac{(\omega - \omega_i)^2}{D^4} \right\} \Big|_{\omega=\omega_i} \times \delta(\omega - \omega_i) \right] + \beta_{11} \Theta(k^2 - \omega^2),\end{aligned}\tag{A.39}$$

$$\begin{aligned}\rho_{12}(\omega, k) &= \frac{1}{\pi} \text{Im} \left[ \frac{hc'}{D^4} \right] = hc' \times \sum_i \left[ \left( \frac{\partial D^2}{\partial \omega} \Big|_{\omega=\omega_i} \right)^{-2} \delta'(\omega - \omega_i) \right. \\ &- \left. \frac{\partial}{\partial \omega} \left\{ \frac{(\omega - \omega_i)^2}{D^4} \right\} \Big|_{\omega=\omega_i} \times \delta(\omega - \omega_i) \right] + \beta_{12} \Theta(k^2 - \omega^2),\end{aligned}\tag{A.40}$$

$$\begin{aligned}\rho_{13}(\omega, k) &= \frac{1}{\pi} \text{Im} \left[ \frac{h'b}{D^4} \right] = h'b \times \sum_i \left[ \left( \frac{\partial D^2}{\partial \omega} \Big|_{\omega=\omega_i} \right)^{-2} \delta'(\omega - \omega_i) \right. \\ &- \left. \frac{\partial}{\partial \omega} \left\{ \frac{(\omega - \omega_i)^2}{D^4} \right\} \Big|_{\omega=\omega_i} \times \delta(\omega - \omega_i) \right] + \beta_{13} \Theta(k^2 - \omega^2),\end{aligned}\tag{A.41}$$

$$\begin{aligned}\rho_{14}^{(0)}(\omega, k) &= \frac{1}{\pi} \text{Im} \left[ \frac{h'(1+a)}{D^4} \right] = h'(1+a) \sum_i \left[ \left( \frac{\partial D^2}{\partial \omega} \Big|_{\omega=\omega_i} \right)^{-2} \delta'(\omega - \omega_i) \right. \\ &- \left. \frac{\partial}{\partial \omega} \left\{ \frac{(\omega - \omega_i)^2}{D^4} \right\} \Big|_{\omega=\omega_i} \delta(\omega - \omega_i) \right] + \beta_{14}^{(0)} \Theta(k^2 - \omega^2),\end{aligned}\tag{A.42}$$

Chapter A. Spectral representation of the propagators

$$\begin{aligned}
\rho_{14}^{(1)}(\omega, k) &= \frac{1}{\pi} \text{Im} \left[ \frac{k_0 h'(1+a)}{D^4} \right] = \omega h'(1+a) \sum_i \left[ \left( \frac{\partial D^2}{\partial \omega} \Big|_{\omega=\omega_i} \right)^{-2} \delta'(\omega - \omega_i) \right. \\
&\quad \left. - \frac{\partial}{\partial \omega} \left\{ \frac{(\omega - \omega_i)^2}{D^4} \right\} \Big|_{\omega=\omega_i} \delta(\omega - \omega_i) \right] + \beta_{14}^{(1)} \Theta(k^2 - \omega^2),
\end{aligned} \tag{A.43}$$

$$\begin{aligned}
\rho_{15}^{(0)}(\omega, k) &= \frac{1}{\pi} \text{Im} \left[ \frac{h^2(1+a)}{D^6} \right] = h^2(1+a) \times \sum_i \left[ -\frac{3}{8} \left( \frac{\partial D^2}{\partial \omega} \Big|_{\omega=\omega_i} \right)^{-3} \delta''(\omega - \omega_i) \right. \\
&\quad \left. + \frac{\partial}{\partial \omega} \left\{ \frac{(\omega - \omega_i)^3}{D^6} \right\} \Big|_{\omega=\omega_i} \delta'(\omega - \omega_i) - \frac{\partial^2}{\partial \omega^2} \left\{ \frac{(\omega - \omega_i)^3}{D^6} \right\} \Big|_{\omega=\omega_i} \delta(\omega - \omega_i) \right] \\
&\quad + \beta_{15}^{(0)} \Theta(k^2 - \omega^2),
\end{aligned} \tag{A.44}$$

$$\begin{aligned}
\rho_{15}^{(1)}(\omega, k) &= \frac{1}{\pi} \text{Im} \left[ \frac{h^2(1+a)k_0}{D^6} \right] = \omega h^2(1+a) \times \sum_i \left[ -\frac{3}{8} \left( \frac{\partial D^2}{\partial \omega} \Big|_{\omega=\omega_i} \right)^{-3} \delta''(\omega - \omega_i) \right. \\
&\quad \left. + \frac{\partial}{\partial \omega} \left\{ \frac{(\omega - \omega_i)^3}{D^6} \right\} \Big|_{\omega=\omega_i} \delta'(\omega - \omega_i) - \frac{\partial^2}{\partial \omega^2} \left\{ \frac{(\omega - \omega_i)^3}{D^6} \right\} \Big|_{\omega=\omega_i} \delta(\omega - \omega_i) \right] \\
&\quad + \beta_{15}^{(1)} \Theta(k^2 - \omega^2),
\end{aligned} \tag{A.45}$$

$$\begin{aligned}
\rho_{16}(\omega, k) &= \frac{1}{\pi} \text{Im} \left[ \frac{h^2 b}{D^6} \right] \\
&= h^2 b \times \sum_i \left[ -\frac{3}{8} \left( \frac{\partial D^2}{\partial \omega} \Big|_{\omega=\omega_i} \right)^{-3} \delta''(\omega - \omega_i) + \frac{\partial}{\partial \omega} \left\{ \frac{(\omega - \omega_i)^3}{D^6} \right\} \Big|_{\omega=\omega_i} \right. \\
&\quad \left. \times \delta'(\omega - \omega_i) - \frac{\partial^2}{\partial \omega^2} \left\{ \frac{(\omega - \omega_i)^3}{D^6} \right\} \Big|_{\omega=\omega_i} \delta(\omega - \omega_i) \right] + \beta_{16} \Theta(k^2 - \omega^2),
\end{aligned} \tag{A.46}$$

where cut parts of the spectral functions are given as

$$\beta_4 = \frac{1}{\pi} \text{Im} \left( \frac{1}{D^2} \right) = -\frac{1}{\pi} \frac{\text{Im } D^2}{(\text{Re } D^2)^2 + (\text{Im } D^2)^2}, \quad (\text{A.47})$$

$$\beta_5 = \frac{1}{\pi} \text{Im} \left( \frac{1}{D^4} \right) = -\frac{1}{\pi} \frac{2 \text{Re } D^2 \text{Im } D^2}{\left[ (\text{Re } D^2)^2 + (\text{Im } D^2)^2 \right]^2}, \quad (\text{A.48})$$

$$\beta_6 = \frac{1}{\pi} \text{Im} \left( \frac{1}{D^6} \right) = \frac{1}{\pi} \frac{\left( \text{Im } D^2 \right)^3 - 3 \left( \text{Re } D^2 \right)^2 \text{Im } D^2}{\left[ (\text{Re } D^2)^2 + (\text{Im } D^2)^2 \right]^3}, \quad (\text{A.49})$$

$$\beta_7 = \frac{1}{\pi} \text{Im} \left( \frac{b'}{D^2} \right) = \frac{1}{\pi} \frac{-\text{Re } b' \text{Im } D^2 + \text{Im } b' \text{Re } D^2}{(\text{Re } D^2)^2 + (\text{Im } D^2)^2}, \quad (\text{A.50})$$

$$\beta_8 = \frac{1}{\pi} \text{Im} \left( \frac{c'}{D^2} \right) = \frac{1}{\pi} \frac{-\text{Re } c' \text{Im } D^2 + \text{Im } c' \text{Re } D^2}{(\text{Re } D^2)^2 + (\text{Im } D^2)^2}, \quad (\text{A.51})$$

$$\begin{aligned} \beta_9^{(0)} &= \frac{1}{2} \text{Im} \left( \frac{h(1+a)}{D^4} \right) \\ &= \frac{1}{\pi} \frac{\text{Im} (h(1+a)) \left[ (\text{Re } D^2)^2 - (\text{Im } D^2)^2 \right] - 2 \text{Re } D^2 \text{Im } D^2 \text{Re} (h(1+a))}{\left[ (\text{Re } D^2)^2 + (\text{Im } D^2)^2 \right]^2}, \end{aligned} \quad (\text{A.52})$$

$$\begin{aligned} \beta_9^{(1)} &= \frac{1}{2} \text{Im} \left( \frac{h(1+a)k_0}{D^4} \right) \\ &= \frac{1}{\pi} \frac{\text{Im} (hk_0(1+a)) \left[ (\text{Re } D^2)^2 - (\text{Im } D^2)^2 \right] - 2 \text{Re } D^2 \text{Im } D^2 \text{Re} (hk_0(1+a))}{\left[ (\text{Re } D^2)^2 + (\text{Im } D^2)^2 \right]^2}, \end{aligned} \quad (\text{A.53})$$

$$\beta_{10} = \frac{1}{2} \operatorname{Im} \left( \frac{hb}{D^4} \right) = \frac{1}{\pi} \frac{\operatorname{Im}(hb) \left[ (\operatorname{Re} D^2)^2 - (\operatorname{Im} D^2)^2 \right] - 2 \operatorname{Re} D^2 \operatorname{Im} D^2 \operatorname{Re}(hb)}{\left[ (\operatorname{Re} D^2)^2 + (\operatorname{Im} D^2)^2 \right]^2}, \quad (\text{A.54})$$

$$\beta_{11} = \frac{1}{2} \operatorname{Im} \left( \frac{hb'}{D^4} \right) = \frac{1}{\pi} \frac{\operatorname{Im}(hb') \left[ (\operatorname{Re} D^2)^2 - (\operatorname{Im} D^2)^2 \right] - 2 \operatorname{Re} D^2 \operatorname{Im} D^2 \operatorname{Re}(hb')}{\left[ (\operatorname{Re} D^2)^2 + (\operatorname{Im} D^2)^2 \right]^2}, \quad (\text{A.55})$$

$$\beta_{12} = \frac{1}{2} \operatorname{Im} \left( \frac{hc'}{D^4} \right) = \frac{1}{\pi} \frac{\operatorname{Im}(hc') \left[ (\operatorname{Re} D^2)^2 - (\operatorname{Im} D^2)^2 \right] - 2 \operatorname{Re} D^2 \operatorname{Im} D^2 \operatorname{Re}(hc')}{\left[ (\operatorname{Re} D^2)^2 + (\operatorname{Im} D^2)^2 \right]^2}, \quad (\text{A.56})$$

$$\beta_{13} = \frac{1}{2} \operatorname{Im} \left( \frac{h'b}{D^4} \right) = \frac{1}{\pi} \frac{\operatorname{Im}(h'b) \left[ (\operatorname{Re} D^2)^2 - (\operatorname{Im} D^2)^2 \right] - 2 \operatorname{Re} D^2 \operatorname{Im} D^2 \operatorname{Re}(h'b)}{\left[ (\operatorname{Re} D^2)^2 + (\operatorname{Im} D^2)^2 \right]^2}, \quad (\text{A.57})$$

$$\begin{aligned} \beta_{14}^{(0)} &= \frac{1}{2} \operatorname{Im} \left( \frac{h'(1+a)}{D^4} \right) \\ &= \frac{1}{\pi} \frac{\operatorname{Im}(h'(1+a)) \left[ (\operatorname{Re} D^2)^2 - (\operatorname{Im} D^2)^2 \right] - 2 \operatorname{Re} D^2 \operatorname{Im} D^2 \operatorname{Re}(h'(1+a))}{\left[ (\operatorname{Re} D^2)^2 + (\operatorname{Im} D^2)^2 \right]^2}, \end{aligned} \quad (\text{A.58})$$



$$\begin{aligned}
\beta_{14}^{(1)} &= \frac{1}{2} \text{Im} \left( \frac{h' (1+a) k_0}{D^4} \right) \\
&= \frac{1}{\pi} \frac{\text{Im} (h' (1+a) k_0) \left[ (\text{Re } D^2)^2 - (\text{Im } D^2)^2 \right] - 2 \text{Re } D^2 \text{Im } D^2 \text{Re} (h' (1+a) k_0)}{\left[ (\text{Re } D^2)^2 + (\text{Im } D^2)^2 \right]^2},
\end{aligned} \tag{A.59}$$

$$\begin{aligned}
\beta_{15}^{(0)} &= \frac{1}{\pi} \text{Im} \left( \frac{h^2 (1+a)}{D^6} \right) \\
&= \frac{1}{\pi} \left\{ \text{Im} (h^2 (1+a)) \left[ (\text{Re } D^2)^3 - 3 \text{Re } D^2 (\text{Im } D^2)^2 \right] \right. \\
&\quad \left. + \text{Re} (h^2 (1+a)) \left[ (\text{Im } D^2)^3 - 3 \text{Im } D^2 (\text{Re } D^2)^2 \right] \right\} \left( \left[ (\text{Re } D^2)^2 + (\text{Im } D^2)^2 \right]^3 \right)^{-1},
\end{aligned} \tag{A.60}$$

$$\begin{aligned}
\beta_{15}^{(1)} &= \frac{1}{\pi} \text{Im} \left( \frac{h^2 (1+a) k_0}{D^6} \right) \\
&= \frac{1}{\pi} \left\{ \text{Im} (h^2 (1+a) k_0) \left[ (\text{Re } D^2)^3 - 3 \text{Re } D^2 (\text{Im } D^2)^2 \right] \right. \\
&\quad \left. + \text{Re} (h^2 (1+a) k_0) \left[ (\text{Im } D^2)^3 - 3 \text{Im } D^2 (\text{Re } D^2)^2 \right] \right\} \left( \left[ (\text{Re } D^2)^2 + (\text{Im } D^2)^2 \right]^3 \right)^{-1},
\end{aligned} \tag{A.61}$$

$$\begin{aligned}
\beta_{16} &= \frac{1}{\pi} \text{Im} \left( \frac{h^2 b}{D^6} \right) \\
&= \frac{1}{\pi} \left\{ \text{Im} (h^2 b) \left[ (\text{Re } D^2)^3 - 3 \text{Re } D^2 (\text{Im } D^2)^2 \right] \right. \\
&\quad \left. + \text{Re} (h^2 b) \left[ (\text{Im } D^2)^3 - 3 \text{Im } D^2 (\text{Re } D^2)^2 \right] \right\} \left( \left[ (\text{Re } D^2)^2 + (\text{Im } D^2)^2 \right]^3 \right)^{-1},
\end{aligned} \tag{A.62}$$

where

$$\text{Im}(D^2) = -\frac{\pi m_{\text{th}}^4}{k^2} \left[ \frac{\omega}{k} + \left( 1 - \frac{\omega^2}{k^2} \right) Q_0 \left( \frac{\omega}{k} \right) \right], \tag{A.63}$$

$$\begin{aligned} \text{Re}(D^2) &= \omega^2 - k^2 - 2m_{\text{th}}^2 + \frac{m_{\text{th}}^4}{k^2} \left( \frac{2\omega}{k} Q_0 \left( \frac{\omega}{k} \right) - 1 \right) \\ &+ \frac{m_{\text{th}}^4}{k^2} \left( 1 - \frac{\omega^2}{k^2} \right) \left( Q_0^2 \left( \frac{\omega}{k} \right) - \frac{\pi^2}{4} \right), \end{aligned} \quad (\text{A.64})$$

$$\text{Im}(b') = -4e^2 M^2 \frac{\pi k_3 \omega}{2k^3}, \quad (\text{A.65})$$

$$\text{Re}(b') = 4e^2 M^2 \frac{k_3}{k^2} \left[ \frac{\omega}{k} Q_0 \left( \frac{\omega}{k} \right) - 1 \right], \quad (\text{A.66})$$

$$\text{Im}(c') = -4e^2 M^2 \frac{\pi}{2k}, \quad (\text{A.67})$$

$$\text{Re}(c') = 4e^2 M^2 \frac{1}{k} Q_0 \left( \frac{\omega}{k} \right), \quad (\text{A.68})$$

$$\begin{aligned} \text{Im}(h(1+a)) &= \frac{4\pi e^2 M^2 k_3}{2k^7} \left( -2k^6 - 2k^4 (k_0^2 + 3m_{\text{th}}^2) + 12k^3 k_0 m_{\text{th}}^2 Q_0 \right. \\ &- 4k^2 m_{\text{th}}^2 (k_0^2 + m_{\text{th}}^2) + 4kk_0 m_{\text{th}}^2 Q_0 (k_0^2 + 4m_{\text{th}}^2) \\ &\left. + k_0^2 m_{\text{th}}^4 (\pi^2 - 12Q_0^2) \right), \\ \text{Re}(h(1+a)) &= \frac{4e^2 M^2 k_3}{2k^7} \left( 4k^6 Q_0 - 4k^5 k_0 + 4k^4 Q_0 (k_0^2 + 3m_{\text{th}}^2) \right. \\ &+ k^3 k_0 m_{\text{th}}^2 (-12Q_0^2 + 3\pi^2 - 4) + 8k^2 m_{\text{th}}^2 Q_0 (k_0^2 + m_{\text{th}}^2) \\ &+ kk_0 m_{\text{th}}^2 (\pi^2 - 4Q_0^2) (k_0^2 + 4m_{\text{th}}^2) \\ &\left. + 2k_0^2 m_{\text{th}}^4 Q_0 \times (4Q_0^2 - 3\pi^2) \right), \end{aligned} \quad (\text{A.69})$$

$$\begin{aligned} \text{Im}(hb) &= \frac{4\pi e^2 M^2 k_3 m_{\text{th}}^2}{2k^7} \left( 4k^2 k_0 (k_0^2 + m_{\text{th}}^2) \right. \\ &+ 4kQ_0 (k^4 + 2m_{\text{th}}^2 (k^2 - 2k_0^2) - k_0^4) \\ &+ 12k_0 m_{\text{th}}^2 Q_0^2 (k_0 - k)(k + k_0) \\ &\left. + \pi^2 k_0 m_{\text{th}}^2 (k - k_0)(k + k_0) \right), \end{aligned} \quad (\text{A.70})$$

$$\begin{aligned} \text{Re}(hb) &= \frac{4e^2 M^2 k_3 m_{\text{th}}^2}{2k^7} \left( k^5 (\pi^2 - 4Q_0^2) + 2k^3 (2k_0^2 + m_{\text{th}}^2 (\pi^2 - 4Q_0^2)) \right. \\ &- 2k^2 k_0 Q_0 \times (4k_0^2 + m_{\text{th}}^2 (-4Q_0^2 + 3\pi^2 + 4)) \\ &- kk_0^2 (\pi^2 - 4Q_0^2) (k_0^2 + 4m_{\text{th}}^2) + 2k_0^3 m_{\text{th}}^2 Q_0 \\ &\left. \times (3\pi^2 - 4Q_0^2) \right), \end{aligned} \quad (\text{A.71})$$

$$\begin{aligned}\text{Im}(hb') &= \frac{16\pi e^4 M^4 k_3^2}{2k^7} \left( 2k^4 - 4k^3 k_0 Q_0 + 4k^2 (k_0^2 + m_{\text{th}}^2) - 4kk_0 Q_0 (k_0^2 + 4m_{\text{th}}^2) \right. \\ &\quad \left. - k_0^2 m_{\text{th}}^2 (\pi^2 - 12Q_0^2) \right),\end{aligned}\quad (\text{A.72})$$

$$\begin{aligned}\text{Re}(hb') &= -\frac{16e^4 M^4 k_3^2}{2k^7} \left( 4k^4 Q_0 + k^3 k_0 (\pi^2 - 4(Q_0^2 + 1)) + 8k^2 Q_0 (k_0^2 + m_{\text{th}}^2) \right. \\ &\quad \left. + kk_0 (\pi^2 - 4Q_0^2) (k_0^2 + 4m_{\text{th}}^2) + 2k_0^2 m_{\text{th}}^2 Q_0 (4Q_0^2 - 3\pi^2) \right),\end{aligned}\quad (\text{A.73})$$

$$\begin{aligned}\text{Im}(hc') &= -\frac{16\pi e^4 M^4 k_3}{2k^5} \left( 4k^3 Q_0 - 2k^2 k_0 + 4kQ_0 (k_0^2 + 2m_{\text{th}}^2) \right. \\ &\quad \left. + k_0 m_{\text{th}}^2 (\pi^2 - 12Q_0^2) \right),\end{aligned}\quad (\text{A.74})$$

$$\begin{aligned}\text{Re}(hc') &= -\frac{16e^4 M^4 k_3}{2k^5} \left( k^3 (\pi^2 - 4Q_0^2) + 4k^2 k_0 Q_0 \right. \\ &\quad \left. + k (\pi^2 - 4Q_0^2) (k_0^2 + 2m_{\text{th}}^2) \right. \\ &\quad \left. + 2k_0 m_{\text{th}}^2 Q_0 (4Q_0^2 - 3\pi^2) \right),\end{aligned}\quad (\text{A.75})$$

$$\begin{aligned}\text{Im}(h'b) &= \frac{8\pi e^4 M^4 m_{\text{th}}^2}{k^9} \left( k^6 \left( \frac{\pi^2}{4} - 3Q_0^2 \right) - 2k^5 \omega Q_0 + k^4 \left( k_3^2 - \omega^2 \left( \frac{\pi^2}{4} - 3Q_0^2 \right) \right) \right) \\ &\quad - 4k^3 \omega k_3^2 Q_0 - k^2 \omega^2 k_3^2 \left( -3Q_0^2 + \frac{\pi^2}{4} + 3 \right) + 6k\omega^3 k_3^2 Q_0 \\ &\quad + \omega^4 k_3^2 \left( \frac{\pi^2}{4} - 3Q_0^2 \right),\end{aligned}\quad (\text{A.76})$$

$$\begin{aligned}\text{Re}(h'b) &= \frac{16e^4 M^4 m_{\text{th}}^2}{k^9} \left( k^6 \left( Q_0^3 - \frac{3\pi^2}{4} Q_0 \right) + k^5 \omega \left( Q_0^2 - \frac{\pi^2}{4} \right) \right. \\ &\quad - k^4 Q_0 \left( \omega^2 \left( Q_0^2 - \frac{3\pi^2}{4} \right) + k_3^2 \right) + k^3 \omega k_3^2 \left( 2Q_0^2 - \frac{\pi^2}{2} - 1 \right) \\ &\quad + k^2 \omega^2 k_3^2 Q_0 \left( -Q_0^2 + \frac{3\pi^2}{4} + 3 \right) + 3k\omega^3 k_3^2 \left( \frac{\pi^2}{4} - Q_0^2 \right) \\ &\quad \left. + \omega^4 k_3^2 Q_0 \left( Q_0^2 - \frac{3\pi^2}{4} \right) \right),\end{aligned}\quad (\text{A.77})$$

$$\begin{aligned}\text{Im}(h'(1+a)) &= \frac{8\pi e^4 M^4}{k^9} \left( 2k^7 Q_0 + 2k^5 m_{\text{th}}^2 Q_0 \right. \\ &\quad + k^4 \omega \left( 2k_3^2 + m_{\text{th}}^2 \left( \frac{\pi^2}{4} - 3Q_0^2 \right) \right) - 2k^3 \omega^2 k_3^2 Q_0 + 3k^2 \omega k_3^2 m_{\text{th}}^2 \\ &\quad \left. - 6k\omega^2 k_3^2 m_{\text{th}}^2 Q_0 - \omega^3 k_3^2 m_{\text{th}}^2 \left( \frac{\pi^2}{4} - 3Q_0^2 \right) \right),\end{aligned}\quad (\text{A.78})$$

Chapter A. Spectral representation of the propagators

$$\begin{aligned}
\text{Re}(h'(1+a)) &= \frac{16e^4 M^4}{k^9} \left( k^7 \left( \frac{\pi^2}{4} - Q_0^2 \right) + k^5 \left( k_3^2 + m_{\text{th}}^2 \left( \frac{\pi^2}{4} - Q_0^2 \right) \right) \right) \\
&+ k^4 \omega Q_0 \left( m_{\text{th}}^2 \left( Q_0^2 - \frac{3\pi^2}{4} \right) - 2k_3^2 \right) \\
&+ k^3 k_3^2 \left( \omega^2 \left( Q_0^2 - \frac{\pi^2}{4} \right) + m_{\text{th}}^2 \right) - 3k^2 \omega k_3^2 m_{\text{th}}^2 Q_0 \\
&+ 3k\omega^2 k_3^2 m_{\text{th}}^2 \left( Q_0^2 - \frac{\pi^2}{4} \right) - \omega^3 k_3^2 m_{\text{th}}^2 Q_0 \left( Q_0^2 - \frac{3\pi^2}{4} \right), \quad (\text{A.79})
\end{aligned}$$

$$\begin{aligned}
\text{Im}(h^2(1+a)) &= \frac{16\pi e^4 M^4 k_3^2}{2k^{11}} \left( -8k^9 Q_0 + 8k^8 k_0 - 8k^7 Q_0 (2k_0^2 + 5m_{\text{th}}^2) \right) \\
&+ k^6 k_0 \left( 8k_0^2 + m_{\text{th}}^2 (60Q_0^2 - 5\pi^2 + 24) \right) \\
&- 8k^5 Q_0 (k_0^4 + 12k_0^2 m_{\text{th}}^2 + 8m_{\text{th}}^4) + 2k^4 k_0 m_{\text{th}}^2 \\
&\times \left( k_0^2 (36Q_0^2 - 3\pi^2 + 6) - 8m_{\text{th}}^2 (-12Q_0^2 + \pi^2 - 1) \right) \\
&- 8k^3 m_{\text{th}}^2 Q_0 \left( 3k_0^4 - 4k_0^2 m_{\text{th}}^2 (-4Q_0^2 + \pi^2 - 3) + 4m_{\text{th}}^4 \right) \\
&- k^2 k_0 m_{\text{th}}^2 (\pi^2 - 12Q_0^2) \left( k_0^4 + 12k_0^2 m_{\text{th}}^2 + 12m_{\text{th}}^4 \right) + \\
&+ 16kk_0^2 m_{\text{th}}^4 Q_0 (\pi^2 - 4Q_0^2) (k_0^2 + 3m_{\text{th}}^2) \\
&+ k_0^3 m_{\text{th}}^6 (80Q_0^4 - 40\pi^2 Q_0^2 + \pi^4), \quad (\text{A.80})
\end{aligned}$$

$$\begin{aligned}
\text{Re}(h^2(1+a)) &= -\frac{16e^4 M^4 k_3^2}{k^{11}} \left( k^9 (\pi^2 - 4Q_0^2) + 8k^8 k_0 Q_0 \right) \\
&+ k^7 \left( 2k_0^2 (-4Q_0^2 + \pi^2 - 2) + 5m_{\text{th}}^2 (\pi^2 - 4Q_0^2) \right) \\
&+ k^6 k_0 Q_0 \left( 8k_0^2 + m_{\text{th}}^2 (20Q_0^2 - 15\pi^2 + 24) \right) \\
&+ k^5 \left( k_0^4 (\pi^2 - 4Q_0^2) + 4k_0^2 m_{\text{th}}^2 (-12Q_0^2 + 3\pi^2 - 1) \right) \\
&+ 8m_{\text{th}}^4 (\pi^2 - 4Q_0^2) \\
&+ 2k^4 k_0 m_{\text{th}}^2 Q_0 \left( k_0^2 (12Q_0^2 - 9\pi^2 + 6) + 8m_{\text{th}}^2 (4Q_0^2 - 3\pi^2 + 1) \right)
\end{aligned}$$

$$\begin{aligned}
& + k^3 m_{\text{th}}^2 \left( 3k_0^4 (\pi^2 - 4Q_0^2) - 2k_0^2 m_{\text{th}}^2 (8(2Q_0^2 + 3)Q_0^2 - 6\pi^2(4Q_0^2 + 1) + \pi^4) \right. \\
& + 4m_{\text{th}}^4 (\pi^2 - 4Q_0^2) \left. \right) + k^2 k_0 m_{\text{th}}^2 Q_0 (4Q_0^2 - 3\pi^2) (k_0^4 + 12k_0^2 m_{\text{th}}^2 + 12m_{\text{th}}^4) \\
& - k k_0^2 m_{\text{th}}^4 (16Q_0^4 - 24\pi^2 Q_0^2 + \pi^4) (k_0^2 + 3m_{\text{th}}^2) \\
& + k_0^3 m_{\text{th}}^6 Q_0 (16Q_0^4 - 40\pi^2 Q_0^2 + 5\pi^4) \left. \right), \tag{A.81}
\end{aligned}$$

$$\begin{aligned}
\text{Im}(h^2 b) & = \frac{16\pi e^4 M^4 k_3^2 m_{\text{th}}^2}{2k^{11}} \left( k^8 (- (\pi^2 - 12Q_0^2)) - 8k^7 k_0 Q_0 \right. \\
& - k^6 (k_0^2 (-12Q_0^2 + \pi^2 + 4) \\
& + 4m_{\text{th}}^2 (\pi^2 - 12Q_0^2) \left. \right) + 16k^5 k_0 Q_0 (k_0^2 + m_{\text{th}}^2 (\pi^2 - 4Q_0^2)) \\
& + k^4 \left( k_0^4 (\pi^2 - 12(Q_0^2 + 1)) - 16k_0^2 m_{\text{th}}^2 - 4m_{\text{th}}^4 (\pi^2 - 12Q_0^2) \right) \\
& + 8k^3 k_0 Q_0 (3k_0^4 + 12k_0^2 m_{\text{th}}^2 + 4m_{\text{th}}^4 (-4Q_0^2 + \pi^2 + 1)) \\
& + k^2 k_0^2 \left( k_0^4 (\pi^2 - 12Q_0^2) + 12k_0^2 m_{\text{th}}^2 (\pi^2 - 12Q_0^2) \right. \\
& + m_{\text{th}}^4 (80Q_0^4 - 8(18 + 5\pi^2)Q_0^2 \\
& + \pi^2(12 + \pi^2)) \left. \right) - 16k k_0^3 m_{\text{th}}^2 Q_0 (\pi^2 - 4Q_0^2) (k_0^2 + 3m_{\text{th}}^2) \\
& - k_0^4 m_{\text{th}}^4 (80Q_0^4 - 40\pi^2 Q_0^2 + \pi^4) \left. \right), \tag{A.82}
\end{aligned}$$

Chapter A. Spectral representation of the propagators

$$\begin{aligned}
\text{Re}(h^2b) = & \frac{16e^4 M^4 k_3^2 m_{\text{th}}^2}{k^{11}} \left( k^8 (3\pi^2 Q_0 - 4Q_0^3) - k^7 k_0 (\pi^2 - 4Q_0^2) \right. \\
& + k^6 Q_0 \left( k_0^2 (-4Q_0^2 + 3\pi^2 + 4) + 4 m_{\text{th}}^2 (3\pi^2 - 4Q_0^2) \right) \\
& + k^5 k_0 (2k_0^2 (-4Q_0^2 + \pi^2 - 2) + m_{\text{th}}^2 (16Q_0^4 - 24\pi^2 Q_0^2 + \pi^4)) \\
& + k^4 Q_0 \left( k_0^4 (4Q_0^2 - 3\pi^2 + 12) + 16k_0^2 m_{\text{th}}^2 + 4 m_{\text{th}}^4 (3\pi^2 - 4Q_0^2) \right) \\
& + k^3 k_0 \left( 3k_0^4 (\pi^2 - 4Q_0^2) + 12k_0^2 m_{\text{th}}^2 (\pi^2 - 4Q_0^2) + \right. \\
& \left. + 2 m_{\text{th}}^4 (16Q_0^4 - 8(1 + 3\pi^2) Q_0^2 + \pi^2 (2 + \pi^2)) \right) + k^2 k_0^2 Q_0 \\
& \times \left( 4Q_0^2 (k_0^4 + 12k_0^2 m_{\text{th}}^2 + 2(6 + 5\pi^2) m_{\text{th}}^4) \right. \\
& - \pi^2 (3k_0^4 + 36k_0^2 m_{\text{th}}^2 + (36 + 5\pi^2) m_{\text{th}}^4) \\
& - 16 m_{\text{th}}^4 Q_0^4 \left. \right) - k k_0^3 m_{\text{th}}^2 (16Q_0^4 - 24\pi^2 Q_0^2 + \pi^4) (k_0^2 + 3 m_{\text{th}}^2) \\
& + k_0^4 m_{\text{th}}^4 Q_0 (16Q_0^4 - 40\pi^2 Q_0^2 + 5\pi^4) \left. \right), \tag{A.83}
\end{aligned}$$

where  $M^2$  is defined in Eq. (B.30).

---

## APPENDIX B

---

# STRUCTURE FUNCTIONS

---

The general form of the various structure functions can be written from Eq. (6.4) as

$$a = \frac{1}{4} \frac{\text{Tr}(\Sigma \not{P}) - (P \cdot u) \text{Tr}(\Sigma \not{u})}{(P \cdot u)^2 - P^2}, \quad (\text{B.1})$$

$$b = \frac{1}{4} \frac{-(P \cdot u) \text{Tr}(\Sigma \not{P}) + P^2 \text{Tr}(\Sigma \not{u})}{(P \cdot u)^2 - P^2}, \quad (\text{B.2})$$

$$c' = -\frac{1}{4} \text{Tr}(\not{u} \Sigma \gamma_5), \quad (\text{B.3})$$

$$d' = \frac{1}{4} \text{Tr}(\not{u} \Sigma \gamma_5). \quad (\text{B.4})$$

The structure functions in the presence of magnetic field depends on three Lorentz scalars

$$p_0 = P^\mu u_\mu, \quad (\text{B.5})$$

$$p_3 = P^\mu n_\mu = p_z, \quad (\text{B.6})$$

$$p_\perp = [-(P^\mu P_\mu)^2 + (P^\mu u_\mu)^2 - (P^\mu n_\mu)^2]^{1/2} = (p_1^2 + p_2^2)^{1/2}. \quad (\text{B.7})$$

Free quark propagator in weak magnetic field is given in Eq. (6.18). Now the one loop

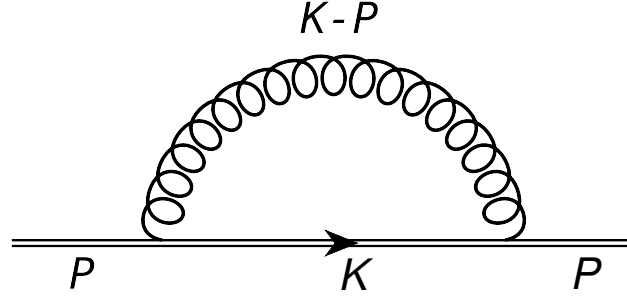


Figure B.1: Self-energy diagram for a quark in presence of background magnetic field. The double line indicates the modified quark propagator in presence of weak magnetic field.

quark self-energy upto  $\mathcal{O}[(q_f B)^2]$  can be written as

$$\begin{aligned}\Sigma(P) &= g^2 C_F \sum_{\{K\}} \gamma_\mu \left( S_0(K) + S_1(K) + S_2(K) \right) \gamma^\mu \frac{1}{(K-P)^2} \\ &= \Sigma_0 + \Sigma_1 + \Sigma_2.\end{aligned}\quad (\text{B.8})$$

From (B.1) structure function  $a$  can be written upto  $\mathcal{O}[(q_f B)^2]$  as

$$a = \frac{1}{4} \frac{\text{Tr}(\Sigma_0 \not{P}) - (P \cdot u) \text{Tr}(\Sigma_0 \not{u})}{(P \cdot u)^2 - P^2} + \frac{1}{4} \frac{\text{Tr}(\Sigma_2 \not{P}) - (P \cdot u) \text{Tr}(\Sigma_2 \not{u})}{(P \cdot u)^2 - P^2}, \quad (\text{B.9})$$

$$= a_0 + a_B, \quad (\text{B.10})$$

where  $a_0$  is purely thermal contribution ( $B = 0$ ) and  $a_B$  is the magnetic correction of  $\mathcal{O}[(q_f B)^2]$  coming from  $\Sigma_2$ . The  $\mathcal{O}[(q_f B)]$  corrections coming from  $\Sigma_1$  vanish due to the trace of odd number of gamma matrices.

Similarly structure function  $b$  can be written as,

$$b = \frac{1 - (P \cdot u) \text{Tr}(\Sigma_0 \not{P}) + P^2 \text{Tr}(\Sigma_0 \not{u})}{4((P \cdot u)^2 - P^2)} + \frac{1 - (P \cdot u) \text{Tr}(\Sigma_2 \not{P}) + P^2 \text{Tr}(\Sigma_2 \not{u})}{4((P \cdot u)^2 - P^2)} \quad (\text{B.11})$$

$$= b_0 + b_B. \quad (\text{B.12})$$



The thermal part of the structure functions  $a$  and  $b$  can be calculated using the quark self energy diagram in Fig. B.1 as [200]

$$a_0(p_0, p) = -\frac{m_{\text{th}}^2}{p^2} \int \frac{d\Omega}{4\pi} \frac{p \cdot \hat{k}}{P \cdot \hat{K}}, \quad (\text{B.13})$$

$$b_0(p_0, p) = \frac{m_{\text{th}}^2}{p} \int \frac{d\Omega}{4\pi} \frac{(P \cdot u)(p \cdot \hat{k}) - p^2}{P \cdot \hat{K}}, \quad (\text{B.14})$$

where thermal mass is given as

$$m_{\text{th}}^2 = \frac{g^2 C_F T^2}{8} (1 + 4\hat{\mu}^2) \quad (\text{B.15})$$

with  $\hat{\mu} = \mu/2\pi T$  and  $C_F = (N_c^2 - 1)/2N_c$ .

Now we derive the  $\mathcal{O}[(q_f B)^2]$  corrections to the structure functions  $a$  and  $b$ . To get the expression of  $a_B$  and  $b_B$  we need to perform the following sum-integrations.

$$\begin{aligned} \text{Tr}(\Sigma_2 \Psi) &= 16g^2 C_F (q_f B)^2 T \sum_{\{K\}} \frac{k_{\perp}^2 k_0}{(K^2 - m_f^2)^4 Q^2} \\ &= \frac{16}{6} g^2 C_F (q_f B)^2 \int \frac{k^2 dk d\Omega}{(2\pi)^3} \frac{\partial^3}{\partial(m_f^2)^3} \left[ -\frac{k_{\perp}^2}{4\sqrt{k^2 + m_f^2}} \right. \\ &\quad \left. \times (n_F(\sqrt{k^2 + m_f^2}) + n_B(\sqrt{k^2 + m_f^2})) \right] \times \left( \frac{1}{p_0 - p \cdot \hat{k}} + \frac{1}{p_0 + p \cdot \hat{k}} \right) \\ &= \frac{g^2 C_F (q_f B)^2}{6\pi^3 T^2} \Gamma(5) \frac{\partial^3}{\partial(y^2)^3} \left[ h_5(y) + f_5(y) \right] \int d\Omega \frac{\hat{k}_{\perp}^2}{P \cdot \hat{K}} \\ &= \frac{g^2 C_F T (q_f B)^2}{8\pi m_f^3} \int \frac{d\Omega}{4\pi} \frac{\hat{k}_{\perp}^2}{P \cdot \hat{K}}, \end{aligned} \quad (\text{B.16})$$

where we have used well-known functions

$$f_{n+1}(y) = \frac{1}{\Gamma(n+1)} \int_0^{\infty} \frac{dx x^n}{\sqrt{x^2 + y^2}} n_F(\sqrt{x^2 + y^2}) \quad (\text{B.17})$$

and

$$h_{n+1}(y) = \frac{1}{\Gamma(n+1)} \int_0^\infty \frac{dx x^n}{\sqrt{x^2+y^2}} n_B(\sqrt{x^2+y^2}), \quad (\text{B.18})$$

which satisfy the recursion relations [202],

$$\frac{\partial f_{n+1}}{\partial y^2} = -\frac{f_{n-1}}{2n}, \quad (\text{B.19})$$

$$\frac{\partial h_{n+1}}{\partial y^2} = -\frac{h_{n-1}}{2n}. \quad (\text{B.20})$$

Expressions for  $f_1(y)$  and  $h_1(y)$  are given as

$$\begin{aligned} f_1(y) &= \frac{\pi}{2y} + \frac{1}{2} \ln\left(\frac{y}{4\pi}\right) + \dots, \\ h_1(y) &= -\frac{1}{2} \ln\left(\frac{y}{4\pi}\right) + \frac{1}{4} \aleph(z) + \dots, \end{aligned} \quad (\text{B.21})$$

where  $\aleph(z)$  is defined in Eq. (B.48).

Now we compute the following trace as

$$\text{Tr}(\Sigma_2 \mathcal{F}) = X_1 + X_2 + X_3 + X_4, \quad (\text{B.22})$$

where

$$\begin{aligned} X_1 &= -16g^2 C_F (q_f B)^2 \sum_{\{K\}} \frac{k(p \cdot \hat{k})}{(K^2 - m_f^2)^3 Q^2} \\ &= -8g^2 C_F (q_f B)^2 \int \frac{k^2 dk d\Omega}{(2\pi)^3} \frac{\partial^2}{\partial (m_f^2)^2} \left[ \frac{k(p \cdot \hat{k})}{4q \sqrt{k^2 + m_f^2}} \right. \\ &\quad \left. \times (n_F(\sqrt{k^2 + m_f^2}) + n_B(\sqrt{k^2 + m_f^2})) \right] \times \left( \frac{1}{p_0 + p \cdot \hat{k}} - \frac{1}{p_0 - p \cdot \hat{k}} \right) \end{aligned}$$

$$\begin{aligned}
&= -\frac{g^2 C_F (q_f B)^2}{8\pi^3 T^2} \frac{\partial}{\partial y^2} \left[ h_1(y) + f_1(y) \right] \int d\Omega \frac{p \cdot \hat{k}}{P \cdot \hat{K}} \\
&= \frac{g^2 C_F T (q_f B)^2}{8\pi m_f^3} \int \frac{d\Omega}{4\pi} \frac{p \cdot \hat{k}}{P \cdot \hat{K}}.
\end{aligned} \tag{B.23}$$

By performing similar calculations we get,

$$\begin{aligned}
X_2 &= 16g^2 C_F (q_f B)^2 \sum_{\{K\}} \frac{k \hat{k}_3 p_3}{(K^2 - m_f^2)^3 Q^2} \\
&= -\frac{g^2 C_F T (q_f B)^2}{8\pi m_f^3} \int \frac{d\Omega}{4\pi} \frac{p_3 \hat{k}_3}{P \cdot \hat{K}},
\end{aligned} \tag{B.24}$$

$$\begin{aligned}
X_3 &= 16g^2 C_F (q_f B)^2 \sum_{\{K\}} \frac{k_\perp^2 k_0 p_0}{(K^2 - m_f^2)^4 Q^2} \\
&= \frac{g^2 C_F T (q_f B)^2}{8\pi m_f^3} \int \frac{d\Omega}{4\pi} \frac{p_0 \hat{k}_\perp^2}{P \cdot \hat{K}},
\end{aligned} \tag{B.25}$$

$$\begin{aligned}
X_4 &= -16g^2 C_F (q_f B)^2 \sum_{\{K\}} \frac{k_\perp^2 k (p \cdot \hat{k})}{(K^2 - m_f^2)^4 Q^2} \\
&= -\frac{g^2 C_F T (q_f B)^2}{8\pi m_f^3} \int \frac{d\Omega}{4\pi} \frac{\hat{k}_\perp^2 (p \cdot \hat{k})}{P \cdot \hat{K}}.
\end{aligned} \tag{B.26}$$

So we obtain the expression of  $a_B$  and  $b_B$  as

$$\begin{aligned}
a_B &= \frac{g^2 C_F T (q_f B)^2}{32\pi m_f^3} \frac{1}{p^2} \int \frac{d\Omega}{4\pi} \frac{\hat{k}_3^2 (p \cdot \hat{k}) - p_3 \hat{k}_3}{P \cdot \hat{K}}, \\
b_B &= \frac{g^2 C_F T (q_f B)^2}{32\pi m_f^3} \frac{1}{p} \int \frac{d\Omega}{4\pi} \frac{\hat{k}_3 (P \cdot u) (\hat{p}_3 - \hat{p} \cdot \hat{k} \hat{k}_3) - p \hat{k}_\perp^2}{P \cdot \hat{K}}.
\end{aligned} \tag{B.27}$$

Other two structure functions are given as [200]

$$c' = -m_{\text{eff}}^2 \int \frac{d\Omega}{4\pi} \frac{\hat{K} \cdot n}{P \cdot \hat{K}},$$

$$d' = m_{\text{eff}}^2 \int \frac{d\Omega}{4\pi} \frac{\hat{K} \cdot u}{P \cdot \hat{K}}, \quad (\text{B.28})$$

where the contribution comes only from  $\Sigma_1$  term. The contributions from  $\Sigma_0$  and  $\Sigma_2$  vanish due the trace of odd number of gamma matrices.

Here we note that

$$m_{\text{eff}}^2 = 4g^2 C_F M_f^2(T, m_f, q_f B), \quad (\text{B.29})$$

where the thermomagnetic mass for flavor  $f$  is given as

$$M_f^2(T, m_f, q_f B) = \frac{q_f B}{16\pi^2} \left[ -\frac{1}{4} \aleph(z) - \frac{\pi T}{2m_f} - \frac{\gamma_E}{2} \right], \quad (\text{B.30})$$

where  $\aleph(z)$  is defined in Eq. (B.51).

We rearrange the inverse of effective propagator in different way,

$$\begin{aligned} S_{\text{eff}}^{-1}(P) &= (1+a)\not{P} + b\not{\psi} + c' \gamma_5 \not{\psi} + d' \gamma_5 \not{\eta} - m_f \mathbb{I} \\ &= c p_0 \gamma_0 - d p_i \gamma_i + c' \gamma_5 \not{\psi} + d' \gamma_5 \not{\eta} - m_f \mathbb{I}, \end{aligned} \quad (\text{B.31})$$

where

$$\begin{aligned} c &= 1 + \left(a_0 + \frac{b_0}{p_0}\right) + \left(a_B + \frac{b_B}{p_0}\right) = 1 - a'_0 - a'_B, \\ d &= 1 + a_0 + a_B, \end{aligned} \quad (\text{B.32})$$

with

$$\begin{aligned}
a_0 &= \frac{m_{\text{th}}^2}{p^2}(1 - \mathcal{T}_p), \\
a'_0 &= \frac{m_{\text{th}}^2}{p_0^2}\mathcal{T}_p, \\
a_B &= \frac{m_{\text{eff}}'^2}{6p^2}\left(1 - \frac{3p_3^2}{p^2}\right)\left(\frac{3p_0^2}{p^2}(1 - \mathcal{T}_p) - 2 + 3\mathcal{T}_p\right), \\
a'_B &= \frac{m_{\text{eff}}'^2}{2p_0^2}\left(3\frac{p_0^2 p_3^2}{p^4}(1 - \mathcal{T}_p) + \mathcal{T}_p + \frac{1}{p^2}\left(p_3^2 \mathcal{T}_p - p_0^2(1 - \mathcal{T}_p)\right)\right), \\
c' &= \frac{p_3 m_{\text{eff}}'^2}{p^2}(1 - \mathcal{T}_p), \\
d' &= \frac{m_{\text{eff}}'^2}{p_0}\mathcal{T}_p.
\end{aligned} \tag{B.33}$$

We expressed all the structure functions in terms of

$$\mathcal{T}_p = \int \frac{d\Omega}{4\pi} \frac{p_0}{p_0 - p \cdot \hat{k}}. \tag{B.34}$$

Here we have defined

$$m_{\text{eff}}'^2 = \frac{g^2 C_F (q_f B)^2 T}{32 \pi m_f^3} \tag{B.35}$$

with  $C_F = (N_c^2 - 1)/2N_c$ . We can see that  $m_{\text{eff}}'^2$  and  $m_{\text{eff}}^2$  diverge when current quark mass vanishes ( $m_f \rightarrow 0$ ). It is regulated by thermal mass  $m_{th}$  of the fermion as discussed in Refs. [204, 259].

## B.1 Sum-integrals

The dimensionally regularized sum integrals are defined as

$$\not\int_{\{P\}} = \left( \frac{e^{\gamma_E} \Lambda^2}{4\pi} \right)^\epsilon T \sum_{p_0=(2n+1)\pi T i + \mu} \int \frac{d^{d-2\epsilon} p}{(2\pi)^{d-2\epsilon}}, \quad (\text{B.36})$$

where  $\Lambda$  can be identified as the  $\overline{MS}$  renormalization scale which also introduces the factor  $\left(\frac{e^{\gamma_E}}{4\pi}\right)^\epsilon$  along with it where  $\gamma_E$  is the Euler-Mascheroni constant.

The sum integrals are related by the following equations.

$$\not\int_{\{P\}} \frac{1}{P^4} = -\frac{d-2}{2} \not\int_{\{P\}} \frac{1}{p^2 P^2}, \quad (\text{B.37})$$

$$\not\int_{\{P\}} \frac{1}{p^2 P^4} = -\frac{d-4}{2} \not\int_{\{P\}} \frac{1}{p^4 P^2}. \quad (\text{B.38})$$

### B.1.1 One-loop sum integrals

We list the fermionic sum-integrals as [202, 217]

$$\not\int_{\{P\}} \frac{1}{P^2} = \frac{T^2}{24} \left( \frac{\Lambda}{4\pi T} \right)^{2\epsilon} [1 + 12\hat{\mu}^2], \quad (\text{B.39})$$

$$\not\int_{\{P\}} \frac{1}{P^4} = \frac{1}{(4\pi)^2} \left( \frac{\Lambda}{4\pi T} \right)^{2\epsilon} \left[ \frac{1}{\epsilon} - \aleph(z) \right], \quad (\text{B.40})$$

$$(\text{B.41})$$

### B.1. Sum-integrals

$$\sum_{\{P\}} \frac{p_3^2}{p^2 P^4} = \frac{1}{3(4\pi)^2} \left( \frac{\Lambda}{4\pi T} \right)^{2\epsilon} \left[ \frac{1}{\epsilon} + \frac{2}{3} - \aleph(z) \right], \quad (\text{B.42})$$

$$\sum_{\{P\}} \frac{1}{P^6} = \frac{1}{(2\pi)^4} \left( \frac{\Lambda}{4\pi T} \right)^{2\epsilon} \frac{\mathfrak{J}(z)}{32T^2}, \quad (\text{B.43})$$

$$\sum_{\{P\}} \frac{1}{p^4 P^2} = -\frac{1}{(2\pi)^4} \left( \frac{\Lambda}{4\pi T} \right)^{2\epsilon} \frac{\mathfrak{J}(z)}{4T^2}, \quad (\text{B.44})$$

$$\sum_{\{P\}} \frac{1}{p^2 P^4} = -\frac{1}{(2\pi)^4} \left( \frac{\Lambda}{4\pi T} \right)^{2\epsilon} \frac{\mathfrak{J}(z)}{8T^2}, \quad (\text{B.45})$$

$$\sum_{\{P\}} \frac{p_3^2}{p^2 P^6} = \frac{1}{(2\pi)^4} \left( \frac{\Lambda}{4\pi T} \right)^{2\epsilon} \frac{\mathfrak{J}(z)}{96T^2}, \quad (\text{B.46})$$

$$\sum_{\{P\}} \frac{p_3^2}{p^4 P^4} = -\frac{1}{(2\pi)^4} \left( \frac{\Lambda}{4\pi T} \right)^{2\epsilon} \frac{\mathfrak{J}(z)}{24T^2}. \quad (\text{B.47})$$

Here we list the frequently used functions in the sum-integrals

$$\aleph(z) \equiv \Psi(z) + \Psi(z^*), \quad (\text{B.48})$$

$$\mathfrak{J}(z) \equiv \frac{d^2}{dz^2} \left( \Psi(z) + \Psi(z^*) \right), \quad (\text{B.49})$$

where  $z$  is a general complex number, here  $z = 1/2 - i\hat{\mu}$ .  $\zeta$  and  $\Psi$  denote the Riemann Zeta function and the digamma function respectively. The digamma function can be written as

$$\Psi(z) \equiv \frac{\Gamma'(z)}{\Gamma(z)}. \quad (\text{B.50})$$

We write the functional form of  $\aleph(1/2 - i\hat{\mu})$  and  $\beth(1/2 - i\hat{\mu})$  for small  $\hat{\mu}$  below.

$$\aleph(z) = -2\gamma_E - 4\ln 2 + 14\zeta(3)\hat{\mu}^2 - 62\zeta(5)\hat{\mu}^4 + 254\zeta(7)\hat{\mu}^6 + \mathcal{O}(\hat{\mu}^8), \quad (\text{B.51})$$

$$\beth(z) = -4 \left[ 7\zeta(3) - 186\zeta(5)\hat{\mu}^2 + 1905\zeta(7)\hat{\mu}^4 - 14308\zeta(9)\hat{\mu}^6 \right] + \mathcal{O}(\hat{\mu}^8). \quad (\text{B.52})$$

## B.1.2 One-loop HTL sum integrals used in the magnetic case

We also need one-loop HTL sum integrals which involve the angular average defined earlier in Eq. (B.34). For brevity, henceforth we will use the notation  $c = \cos \theta$  for single angular average and  $c_i = \cos \theta_i$  for multiple angular averages. We list the sum integrals below:

$$\sum_{\{P\}} \frac{1}{P^4} \mathcal{T}_p = \frac{d-4}{d-5} \sum_{\{P\}} \frac{1}{P^4} \quad (\text{B.53})$$

$$\sum_{\{P\}} \frac{1}{p^2 P^4} \mathcal{T}_p = \left( \Delta_1 - \frac{d-4}{2} \Delta_2 \right) \sum_{\{P\}} \frac{1}{p^4 P^2}, \quad (\text{B.54})$$

$$\sum_{\{P\}} \frac{p_3^2}{p^2 P^4} \mathcal{T}_p = \left( \frac{d-4}{d-2} (1 + \Delta_0) + \frac{2}{d-2} \Delta_3' \right) \Delta_3 \sum_{\{P\}} \frac{1}{P^4} \quad (\text{B.55})$$

$$\sum_{\{P\}} \frac{\mathcal{T}_p^2}{p^2 p_0^2 P^2} = \Delta_4 \sum_{\{P\}} \frac{1}{p^4 P^2}, \quad (\text{B.56})$$

$$\sum_{\{P\}} \frac{p_3^2}{p^4 P^4} \mathcal{T}_p = \left( \Delta_1 - \frac{d-4}{2} \Delta_2 \right) \Delta_3 \sum_{\{P\}} \frac{1}{p^4 P^2}, \quad (\text{B.57})$$

$$(\text{B.58})$$



### B.1. Sum-integrals

$$\sum_{\{P\}} \frac{1}{p_0^2 P^4} \mathcal{T}_p^2 = \Delta_5 \sum_{\{P\}} \frac{1}{p^4 P^2}, \quad (\text{B.59})$$

$$\sum_{\{P\}} \frac{p_3^2}{p^4 P^4} \mathcal{T}_p^2 = \Delta_3 \Delta_6 \sum_{\{P\}} \frac{1}{p^4 P^2}, \quad (\text{B.60})$$

$$\sum_{\{P\}} \frac{p_3^2}{p^2 p_0^2 P^4} \mathcal{T}_p^2 = \Delta_3 \Delta_5 \sum_{\{P\}} \frac{1}{p^4 P^2}, \quad (\text{B.61})$$

where  $\Delta$ 's are the various angular averages which we list below. The symbol  $\langle \rangle_c$  in the angular averages depicts the standard definition used in Ref. [289].

$$\Delta_0 = \left\langle \frac{c^2}{1-c^2} \right\rangle_c = -\frac{1}{2\epsilon} + \mathcal{O}[\epsilon]^3, \quad (\text{B.62})$$

$$\Delta_1 = \left\langle \frac{c^{6-d} - c^2}{(1-c^2)^2} \right\rangle_c = \frac{1}{4\epsilon} - \frac{1}{4} + \ln 2 + \epsilon \left[ -\frac{3}{4} + \frac{\pi^2}{6} + (\ln 2)^2 - 2 \ln 2 \right] + \mathcal{O}[\epsilon]^3, \quad (\text{B.63})$$

$$\Delta_2 = \left\langle \frac{1}{1-c^2} \right\rangle_c = -\frac{1}{2\epsilon} + 1 + \mathcal{O}[\epsilon], \quad (\text{B.64})$$

$$\Delta_3 = \langle c^2 \rangle_c = \frac{1}{3} + \frac{2\epsilon}{9} + \mathcal{O}[\epsilon]^2, \quad (\text{B.65})$$

$$\Delta'_3 = \left\langle \frac{1-c^{4-d}}{(1-c^2)^2} \right\rangle_c = -\frac{1}{4\epsilon} + \frac{1}{4} + \frac{3\epsilon}{4} - \frac{3\epsilon^2}{4} + \mathcal{O}[\epsilon]^3, \quad (\text{B.66})$$

$$\Delta_4 = \left\langle \frac{1-c_1^{6-d}}{(c_1^2 - c_2^2)(1-c_1^2)} + c_1 \leftrightarrow c_2 \right\rangle_{c_1, c_2} = \frac{1}{12} \left[ 24 \ln 2 - \pi^2 \right] + \mathcal{O}[\epsilon], \quad (\text{B.67})$$

$$\begin{aligned} \Delta_5 &= \left\langle \frac{c_1^{6-d} - c_1^2}{(c_1^2 - c_2^2)(1-c_1^2)^2} - \frac{d-4}{2} \frac{1}{(c_1^2 - c_2^2)(1-c_1^2)} + c_1 \leftrightarrow c_2 \right\rangle_{c_1, c_2} \\ &= \frac{1}{24} \left[ 6 - \pi^2 \right] + \mathcal{O}[\epsilon], \end{aligned} \quad (\text{B.68})$$

$$\begin{aligned} \Delta_6 &= \left\langle \frac{1 - 2c_1^2 + c_1^{8-d}}{(c_1^2 - c_2^2)(1-c_1^2)^2} - \frac{d-4}{2} \frac{1}{(c_1^2 - c_2^2)(1-c_1^2)} + c_1 \leftrightarrow c_2 \right\rangle_{c_1, c_2} \\ &= \frac{1}{8} \left[ 2 - \pi^2 + 16 \ln 2 \right] + \mathcal{O}[\epsilon]. \end{aligned} \quad (\text{B.69})$$

Using the expressions of angular averages we obtain the results of HTL sum integrals for magnetic case as

$$\sum_{\{P\}} \frac{1}{P^4} \mathcal{T}_p = \frac{1}{2(4\pi)^2} \left( \frac{\Lambda}{4\pi T} \right)^{2\epsilon} \left[ \frac{1}{\epsilon} + 1 - \aleph(z) \right], \quad (\text{B.70})$$

$$\sum_{\{P\}} \frac{1}{p^2 P^4} \mathcal{T}_p = -\frac{1}{(2\pi)^4} \left( \frac{\Lambda}{4\pi T} \right)^{2\epsilon} \frac{\mathfrak{J}(z)}{16T^2} (-1 + 4 \ln 2), \quad (\text{B.71})$$

$$\sum_{\{P\}} \frac{p_3^2}{p^2 P^4} \mathcal{T}_p = \frac{1}{6(4\pi)^2} \left( \frac{\Lambda}{4\pi T} \right)^{2\epsilon} \left[ \frac{1}{\epsilon} + \frac{5}{3} - \aleph(z) \right], \quad (\text{B.72})$$

$$\sum_{\{P\}} \frac{1}{p^2 p_0^2 P^2} \mathcal{T}_p^2 = \frac{1}{(2\pi)^4} \left( \frac{\Lambda}{4\pi T} \right)^{2\epsilon} \frac{\mathfrak{J}(z)}{48T^2} (\pi^2 - 24 \ln 2), \quad (\text{B.73})$$

$$\sum_{\{P\}} \frac{p_3^2}{p^4 P^4} \mathcal{T}_p = -\frac{1}{(2\pi)^4} \left( \frac{\Lambda}{4\pi T} \right)^{2\epsilon} \frac{\mathfrak{J}(z)}{48T^2} (-1 + 4 \ln 2), \quad (\text{B.74})$$

$$\sum_{\{P\}} \frac{1}{p_0^2 P^4} \mathcal{T}_p^2 = \frac{1}{(2\pi)^4} \left( \frac{\Lambda}{4\pi T} \right)^{2\epsilon} \frac{\mathfrak{J}(z)}{96T^2} (\pi^2 - 6), \quad (\text{B.75})$$

$$\sum_{\{P\}} \frac{p_3^2}{p^4 P^4} \mathcal{T}_p^2 = \frac{1}{(2\pi)^4} \left( \frac{\Lambda}{4\pi T} \right)^{2\epsilon} \frac{\mathfrak{J}(z)}{96T^2} (-2 + \pi^2 - 16 \ln 2), \quad (\text{B.76})$$

$$\sum_{\{P\}} \frac{p_3^2}{p^2 p_0^2 P^4} \mathcal{T}_p^2 = \frac{1}{(2\pi)^4} \left( \frac{\Lambda}{4\pi T} \right)^{2\epsilon} \frac{\mathfrak{J}(z)}{288T^2} (\pi^2 - 6). \quad (\text{B.77})$$

# CALCULATIONS RELATED TO HEAVY QUARK POTENTIAL

---

## C.1 Gluon effective propagator in presence of magnetic field

The general structure of effective gluon propagator for two anisotropic direction is formulated in Chapter 3. Here we revisited it for particular one anisotropic case i.e. in presence of magnetic field. In presence of thermal medium, the Lorentz (boost) invariance is broken, whereas the presence of magnetic field breaks the rotational symmetry of the system. Heat bath velocity  $u^\mu = (1, 0, 0, 0)$  is introduced in presence of thermal medium. We consider the magnetic field along  $z$  direction i.e.,  $n_\mu = (0, 0, 0, 1)$ . We define  $\bar{n}^\mu = A^{\mu\nu}n_\nu$ . Now gluon self energy in the presence of thermomagnetic medium can be written as

$$\Pi^{\mu\nu} = bB^{\mu\nu} + cR^{\mu\nu} + dQ^{\mu\nu} + aN^{\mu\nu} \quad (\text{C.1})$$

where the basis tensors are given as [199]

$$B^{\mu\nu} = \frac{\bar{u}^\mu \bar{u}^\nu}{\bar{u}^2}, \quad (\text{C.2})$$

$$Q^{\mu\nu} = \frac{\bar{n}^\mu \bar{n}^\nu}{\bar{n}^2}, \quad (\text{C.3})$$

$$N^{\mu\nu} = \frac{\bar{u}^\mu \bar{n}^\nu + \bar{u}^\nu \bar{n}^\mu}{\sqrt{\bar{u}^2} \sqrt{\bar{n}^2}},$$

$$R^{\mu\nu} = V^{\mu\nu} - B^{\mu\nu} - Q^{\mu\nu}. \quad (\text{C.4})$$

$b$ ,  $c$ ,  $d$  and  $a$  are the corresponding form factors. The vacuum projection tensor is

$$V^{\mu\nu} = g^{\mu\nu} - \frac{P^\mu P^\nu}{P^2}. \quad (\text{C.5})$$

$\bar{u}^\mu$  is defined by projecting the vacuum projection tensor upon  $u^\mu$  i.e.  $\bar{u}^\mu = V^{\mu\nu} u_\nu$  and  $\bar{n}^\mu$  is defined as  $\bar{n}^\mu = A^{\mu\nu} n_\nu$ . The form factors can be calculated using the following relations.

$$b = b_g + b_q = -\frac{p_0^2 - p^2}{p^2} \left[ \Pi_{00}^g(P) + \Pi_{00}^q(P) \right], \quad (\text{C.6})$$

$$\begin{aligned} c &= c_g + c_q = R^{\mu\nu} \left[ \Pi_{\mu\nu}^g(P) + \Pi_{\mu\nu}^q(P) \right] \\ &= (\Pi^g)^\mu{}_\mu(P) + (\Pi^q)^\mu{}_\mu(P) + \frac{1}{p_\perp^2} \left[ (p_0^2 - p_\perp^2) \left\{ \Pi_{00}^g(P) + \Pi_{00}^q(P) \right\} \right. \\ &\quad \left. \times p^2 \left\{ \Pi_{33}^g(P) + \Pi_{33}^q(P) \right\} - 2p_0 p_3 \left\{ \Pi_{03}^g(P) + \Pi_{03}^q(P) \right\} \right], \end{aligned} \quad (\text{C.7})$$

$$\begin{aligned} d &= d_g + d_q = Q^{\mu\nu} \left[ \Pi_{\mu\nu}^g(P) + \Pi_{\mu\nu}^q(P) \right] \\ &= -\frac{p^2}{p_\perp^2} \left[ \left\{ \Pi_{33}^g(P) + \Pi_{33}^q(P) \right\} - \frac{2p_0 p_3}{p^2} \left\{ \Pi_{03}^g(P) + \Pi_{03}^q(P) \right\} \right. \\ &\quad \left. + \frac{p_0^2 p_3^2}{p^4} \left\{ \Pi_{00}^g(P) + \Pi_{00}^q(P) \right\} \right], \end{aligned} \quad (\text{C.8})$$

$$\begin{aligned} a &= a_g + a_q = \frac{1}{2} N^{\mu\nu} \left[ \Pi_{\mu\nu}^g + \Pi_{\mu\nu}^q \right] \\ &= \frac{1}{2\sqrt{\bar{u}^2} \sqrt{\bar{n}^2}} \left[ -2 \frac{\bar{u} \cdot \bar{n}}{\bar{u}^2} \left\{ \Pi_{00}^g + \Pi_{00}^q \right\} + 2 \left\{ \Pi_{03}^g + \Pi_{03}^q \right\} \right]. \end{aligned} \quad (\text{C.9})$$

## C.2. Frequency sum

where  $\Pi_{\mu\nu}^g$  and  $\Pi_{\mu\nu}^q$  are the self energy contributions from the gluon loop, ghost loop and from the quark loop respectively. The form factors would be calculated from one loop gluon self energy diagram.

The general structure of the gluon effective propagator using Eq. (C.1) is given as [199]

$$D^{\mu\nu} = \frac{\xi P^\mu P^\nu}{P^4} + \frac{P^2 - d}{(P^2 - b)(P^2 - d) - a^2} B^{\mu\nu} + \frac{1}{P^2 - c} R^{\mu\nu} + \frac{P^2 - d}{(P^2 - b)(P^2 - b) - a^2} Q^{\mu\nu} + \frac{a}{(P^2 - b)(P^2 - d) - a^2} N^{\mu\nu}. \quad (\text{C.10})$$

## C.2 Frequency sum

We write the fermionic Matsubara sums. Here  $\omega_n = (2n + 1)\pi T$  and  $\omega_m = 2m\pi T$  are the fermionic and bosonic Matsubara frequencies respectively.

$$T \sum_{n=-\infty}^{\infty} \frac{1}{[(i\omega_n)^2 - E_k^2][(i\omega_n - i\omega_m)^2 - E_q^2]} = \sum_{s_1, s_2 = \pm 1} \frac{1}{4s_1 E_k E_q} \frac{n_F(E_k) - n_F(s_1 E_q)}{i s_2 \omega_m + E_k - s_1 E_q}, \quad (\text{C.11})$$

and

$$T \sum_{n=-\infty}^{\infty} \frac{i\omega_n(i\omega_n - i\omega_m)}{[(i\omega_n)^2 - E_k^2][(i\omega_n - i\omega_m)^2 - E_q^2]} = \sum_{s_1, s_2 = \pm 1} \frac{1}{4} \frac{n_F(E_k) - n_F(s_1 E_q)}{i s_2 \omega_m + E_k - s_1 E_q}. \quad (\text{C.12})$$

The fermi-Dirac distribution function is given as,  $n_F(E) = \frac{1}{\exp(E/T)+1}$ .

### C.3 Definition of functions $X_{m,n}$ and $X_{m,n}^1$

$$X_{m,n} = \frac{m!}{n!} e^{-p_{\perp}^2 d_f^2/2} \left( \frac{p_{\perp}^2 d_f^2}{2} \right)^{n-m} \left[ L_m^{n-m} \left( \frac{p_{\perp}^2 d_f^2}{2} \right) \right]^2, \quad \text{for } n \geq m \quad (\text{C.13})$$

$$= \frac{n!}{m!} e^{-p_{\perp}^2 d_f^2/2} \left( \frac{p_{\perp}^2 d_f^2}{2} \right)^{m-n} \left[ L_n^{m-n} \left( \frac{p_{\perp}^2 d_f^2}{2} \right) \right]^2, \quad \text{for } n < m \quad (\text{C.14})$$

$$X_{m,n}^1 = 2 \frac{(m+1)!}{n!} e^{-p_{\perp}^2 d_f^2/2} \left( \frac{p_{\perp}^2 d_f^2}{2} \right)^{n-m} L_m^{n-m} \left( \frac{p_{\perp}^2 d_f^2}{2} \right) L_{m+1}^{n-m} \left( \frac{p_{\perp}^2 d_f^2}{2} \right), \quad \text{for } n \geq m \quad (\text{C.15})$$

$$= 2 \frac{(n+1)!}{m!} e^{-p_{\perp}^2 d_f^2/2} \left( \frac{p_{\perp}^2 d_f^2}{2} \right)^{m-n} L_n^{m-n} \left( \frac{p_{\perp}^2 d_f^2}{2} \right) L_{n+1}^{m-n} \left( \frac{p_{\perp}^2 d_f^2}{2} \right), \quad \text{for } n < m \quad (\text{C.16})$$

### C.4 Debye mass approximated $\text{Im } V$

In this case, one usually does not consider the general structure of the gluon propagator in the presence of temperature and external magnetic field and instead incorporates the effect of the magnetic field solely through the modification in the Debye mass. Hence the imaginary part of the potential in this case can be written as [252, 256]

$$\text{Im}V(r) = -\alpha T \phi_2(m_D r) - \frac{\sigma T}{m_D^2} \chi(m_D r), \quad (\text{C.17})$$

where  $m_D$  is the Debye screening mass. In order to calculate the Debye screening mass we have taken the static limit of the temporal component of the gluon self-energy i.e.  $m_D^2 = \Pi^{00}(\omega \rightarrow 0, \mathbf{p} = 0)$ , where  $\Pi^{00}(P) = \Pi_g^{00}(P) + \Pi_q^{00}(P)$ . First term in eq. C.17 comes from the Coulombic contribution whereas the second term is related to the string part of the Cornell potential.

#### C.4. Debye mass approximated $\text{Im } V$

The functions  $\phi_2(x)$  and  $\chi(x)$  are defined as,

$$\phi_2(x) = 2 \int_0^\infty dz \frac{z}{(z^2 + 1)^2} \left( 1 - \frac{\sin(zx)}{zx} \right), \quad (\text{C.18})$$

$$\chi(x) = 2 \int_0^\infty dz \frac{1}{z(z^2 + 1)^2} \left( 1 - \frac{\sin(zx)}{zx} \right). \quad (\text{C.19})$$

Both the functions  $\phi_2(x)$  and  $\chi(x)$  are monotonically increasing functions with  $\phi_2(0) = 0$  and  $\chi(0) = 1$ . At large  $x$ ,  $\chi(x)$  is logarithmically divergent, whereas  $\phi_2(\infty) = 1$ .

## CHARGED SCALAR FIELD

### D.1 wave function

We consider charged particles in a constant magnetic field. The Klein-Gordon equation becomes [290, 291]

$$\left(i\frac{\partial}{\partial t} - eA_0\right)^2 \phi(x, y, z, t) = \left((i\vec{\nabla} + e\vec{A})^2 + m^2\right) \phi(x, y, z, t), \quad (\text{D.1})$$

where the wave function can be written in the following form

$$\phi(x, y, z, t) = \phi(x, y, z) e^{-iEt}. \quad (\text{D.2})$$

In our case magnetic field is in  $z$ -direction i.e.  $\vec{B} = B\hat{z}$ . We choose vector potential as

$$A^\mu = (0, 0, xB, 0). \quad (\text{D.3})$$



### D.1. wave function

Using the vector potential from Eq. (D.3), Eq. (D.1) becomes

$$(E^2 - m^2) \phi(x, y, z) = \left( -\nabla^2 + 2ieBx \frac{\partial}{\partial y} + e^2 B^2 x^2 \right) \phi(x, y, z). \quad (\text{D.4})$$

The coordinate  $x$  appears through the derivatives, so we expect solution as

$$\phi(x, y, z) = f(x) e^{ik_y y + k_z z}. \quad (\text{D.5})$$

Putting it in above equation we get,

$$\begin{aligned} \left( \frac{d^2}{dx^2} + 2eBxk_y - e^2 B^2 x^2 + \epsilon \right) f(x) &= 0 \\ \left[ \frac{d^2}{dx^2} - (eBx - k_y)^2 + (E^2 - k_z^2 - m^2) \right] f(x) &= 0. \end{aligned} \quad (\text{D.6})$$

After doing variable transformation i.e.

$$\xi = \sqrt{|eB|} \left( x - \frac{k_y}{eB} \right), \quad (\text{D.7})$$

we arrive to equation

$$\left( \frac{d^2}{d\xi^2} - \xi^2 + a \right) f(x) = 0, \quad (\text{D.8})$$

where  $a = \frac{E^2 - k_z^2 - m^2}{|eB|}$ . The solution of above equation exists when  $a = 2\nu + 1$  for  $\nu = 0, 1, 2, \dots$ . Energy eigenvalues becomes,

$$E^2 = k_z^2 + m^2 + (2\nu + 1)|eB|, \quad (\text{D.9})$$

and the solution for  $f$  is

$$f_\nu(\xi) \equiv N_\nu e^{-\xi^2/2} H_\nu(\xi), \quad (\text{D.10})$$

where  $H_\nu$  are Hermite polynomials and normalization constant is

$$N_\nu = \left( \frac{\sqrt{|eB|}}{\nu! 2^\nu \sqrt{\pi}} \right)^{1/2}. \quad (\text{D.11})$$

$f_\nu(\xi)$  satisfy the completeness relation

$$\sum_n f_n(\xi) f_n(\xi') = \delta(x - x'), \quad (\text{D.12})$$

and also

$$\int_{-\infty}^{\infty} f_\mu(x) f_\nu(x) dx = \sqrt{eB} \delta_{\mu,\nu}. \quad (\text{D.13})$$

Finally we can write

$$\phi_n(x, y, z, t) = e^{-iK \cdot X_{\hat{x}}} f_n(x, k_y), \quad (\text{D.14})$$

where  $X_{\hat{x}}$  is position four vector setting  $x$  component to zero. We would use  $X$  to represent spacial co-ordinates.

## D.2 Quantization

The scalar field operator can be written in terms of annihilation and creation operator as

$$\Phi(X) = \sum_{n=0}^{\infty} \int \frac{dk_y dk_z}{2\pi\sqrt{2E_n}} \left[ e^{-iK \cdot X_{\vec{x}}} f_n(x, \vec{k}_{\vec{x}}) a(n, \vec{k}_{\vec{x}}) + e^{iK \cdot X_{\vec{x}}} f_n^*(x, \vec{k}_{\vec{x}}) b^\dagger(n, \vec{k}_{\vec{x}}) \right] \quad (\text{D.15})$$

The field  $\Phi(X)$  and  $\Pi(X) = \dot{\Phi}^\dagger$  satisfy the commutation relation

$$[\Phi(X), \Pi(Y)] = \delta^{(3)}(\vec{x} - \vec{y}). \quad (\text{D.16})$$

We can obtain the commutation relation for annihilation and creation operator as

$$[a(n, p_{\vec{x}}), a^\dagger(m, p'_{\vec{x}})] = \delta_{n,m} \delta(k_y - k'_y) \delta(k_z - k'_z), \quad (\text{D.17})$$

and similar for  $b$  and  $b^\dagger$ . Now we define the one-particle states

$$|n, \vec{k}_{\vec{x}}\rangle = \frac{2\pi}{\sqrt{L_y L_z}} a^\dagger(n, \vec{k}_{\vec{x}}) |0\rangle. \quad (\text{D.18})$$

Here we have considered a finite box of sides  $(L_x, L_y, L_z)$ , which is taken to infinite volume limit at the end. The action of field operators on one-particle states reads as

$$\begin{aligned} \Phi |\pi^-(n, \vec{k}_{\vec{x}})\rangle &= \frac{1}{\sqrt{2E_n L_y L_z}} e^{-iK \cdot X_{\vec{x}}} f_n(x, \vec{k}_{\vec{x}}) |0\rangle, \\ \Phi^\dagger |\pi^+(n, \vec{k}_{\vec{x}})\rangle &= \frac{1}{\sqrt{2E_n L_y L_z}} e^{-iK \cdot X_{\vec{x}}} f_n(x, \vec{k}_{\vec{x}}) |0\rangle. \end{aligned} \quad (\text{D.19})$$



---

---

## BIBLIOGRAPHY

---

- [1] B. Singh, L. Thakur and H. Mishra, *Heavy quark complex potential in a strongly magnetized hot QGP medium*, *Phys. Rev. D* **97** (2018) 096011, [[1711.03071](#)].
- [2] M. Hasan and B. K. Patra, *Dissociation of heavy quarkonia in a weak magnetic field*, *Phys. Rev. D* **102** (2020) 036020, [[2004.12857](#)].
- [3] T. Muta, *Foundations of Quantum Chromodynamics: An Introduction to Perturbative Methods in Gauge Theories*, (3rd ed.), vol. 78 of *World scientific Lecture Notes in Physics*. World Scientific, Hackensack, N.J., 3rd ed., 2010.
- [4] F. Halzen and A. D. Martin, *QUARKS AND LEPTONS: AN INTRODUCTORY COURSE IN MODERN PARTICLE PHYSICS*. 1984.
- [5] S. Bethke, *Experimental tests of asymptotic freedom*, *Prog. Part. Nucl. Phys.* **58** (2007) 351–386, [[hep-ex/0606035](#)].
- [6] D. J. Gross and F. Wilczek, *Ultraviolet Behavior of Nonabelian Gauge Theories*, *Phys. Rev. Lett.* **30** (1973) 1343–1346.

- [7] H. D. Politzer, *Reliable Perturbative Results for Strong Interactions?*, *Phys. Rev. Lett.* **30** (1973) 1346–1349.
- [8] K. Yagi, T. Hatsuda and Y. Miake, *Quark-gluon plasma: From big bang to little bang*, vol. 23. 2005.
- [9] B. Muller, *THE PHYSICS OF THE QUARK - GLUON PLASMA*, *Lect. Notes Phys.* **225** (1985) 1.
- [10] M. Gyulassy and L. McLerran, *New forms of QCD matter discovered at RHIC*, *Nucl. Phys. A* **750** (2005) 30–63, [nucl-th/0405013].
- [11] E. V. Shuryak, *Quantum Chromodynamics and the Theory of Superdense Matter*, *Phys. Rept.* **61** (1980) 71–158.
- [12] P. Petreczky, *Lattice QCD at non-zero temperature*, *J. Phys. G* **39** (2012) 093002, [1203.5320].
- [13] S. Borsanyi, G. Endrodi, Z. Fodor, A. Jakovac, S. D. Katz, S. Krieg et al., *The QCD equation of state with dynamical quarks*, *JHEP* **11** (2010) 077, [1007.2580].
- [14] S. Borsanyi, Z. Fodor, C. Hoelbling, S. D. Katz, S. Krieg and K. K. Szabo, *Full result for the QCD equation of state with 2+1 flavors*, *Phys. Lett. B* **730** (2014) 99–104, [1309.5258].
- [15] A. Bazavov et al., *Equation of state and QCD transition at finite temperature*, *Phys. Rev. D* **80** (2009) 014504, [0903.4379].
- [16] ALICE collaboration, P. Cortese et al., *ALICE: Physics performance report, volume I*, *J. Phys. G* **30** (2004) 1517–1763.

## BIBLIOGRAPHY

- [17] ALICE collaboration, C. W. Fabjan et al., *ALICE: Physics performance report, volume II*, *J. Phys. G* **32** (2006) 1295–2040.
- [18] BRAHMS collaboration, I. Arsene et al., *Quark gluon plasma and color glass condensate at RHIC? The Perspective from the BRAHMS experiment*, *Nucl. Phys. A* **757** (2005) 1–27, [[nucl-ex/0410020](#)].
- [19] PHOBOS collaboration, B. B. Back et al., *The PHOBOS perspective on discoveries at RHIC*, *Nucl. Phys. A* **757** (2005) 28–101, [[nucl-ex/0410022](#)].
- [20] PHENIX collaboration, K. Adcox et al., *Formation of dense partonic matter in relativistic nucleus-nucleus collisions at RHIC: Experimental evaluation by the PHENIX collaboration*, *Nucl. Phys. A* **757** (2005) 184–283, [[nucl-ex/0410003](#)].
- [21] P. Senger, *The compressed baryonic matter experiment at FAIR in Darmstadt*, *J. Phys. G* **30** (2004) S1087–S1090.
- [22] B. Friman, C. Hohne, J. Knoll, S. Leupold, J. Randrup, R. Rapp et al., eds., *The CBM physics book: Compressed baryonic matter in laboratory experiments*, vol. 814. 2011, [10.1007/978-3-642-13293-3](#).
- [23] V. Toneev, *The NICA/MPD project at JINR (Dubna)*, *PoS CPOD07* (2007) 057, [[0709.1459](#)].
- [24] NICA collaboration, A. N. Sissakian and A. S. Sorin, *The nuclotron-based ion collider facility (NICA) at JINR: New prospects for heavy ion collisions and spin physics*, *J. Phys. G* **36** (2009) 064069.

- [25] W. Busza, K. Rajagopal and W. van der Schee, *Heavy Ion Collisions: The Big Picture, and the Big Questions*, *Ann. Rev. Nucl. Part. Sci.* **68** (2018) 339–376, [[1802.04801](#)].
- [26] E. Iancu, *QCD in heavy ion collisions*, in *2011 European School of High-Energy Physics*, pp. 197–266, 2014. [1205.0579](#). DOI.
- [27] P. Romatschke and U. Romatschke, *Relativistic Fluid Dynamics In and Out of Equilibrium*. Cambridge Monographs on Mathematical Physics. Cambridge University Press, 5, 2019, [10.1017/9781108651998](#).
- [28] F. Gelis, E. Iancu, J. Jalilian-Marian and R. Venugopalan, *The Color Glass Condensate*, *Ann. Rev. Nucl. Part. Sci.* **60** (2010) 463–489, [[1002.0333](#)].
- [29] P. Romatschke, *Do nuclear collisions create a locally equilibrated quark–gluon plasma?*, *Eur. Phys. J. C* **77** (2017) 21, [[1609.02820](#)].
- [30] P. M. Chesler and W. van der Schee, *Early thermalization, hydrodynamics and energy loss in AdS/CFT*, *Int. J. Mod. Phys. E* **24** (2015) 1530011, [[1501.04952](#)].
- [31] C. Gale, S. Jeon and B. Schenke, *Hydrodynamic Modeling of Heavy-Ion Collisions*, *Int. J. Mod. Phys. A* **28** (2013) 1340011, [[1301.5893](#)].
- [32] S. Jeon and U. Heinz, *Introduction to Hydrodynamics*, *Int. J. Mod. Phys. E* **24** (2015) 1530010, [[1503.03931](#)].
- [33] P. F. Kolb and U. W. Heinz, *Hydrodynamic description of ultrarelativistic heavy ion collisions*, [nucl-th/0305084](#).



## BIBLIOGRAPHY

- [34] M. Alqahtani, M. Nopoush, R. Ryblewski and M. Strickland, *(3+1)D Quasiparticle Anisotropic Hydrodynamics for Ultrarelativistic Heavy-Ion Collisions*, *Phys. Rev. Lett.* **119** (2017) 042301, [[1703.05808](#)].
- [35] M. Strickland, *Anisotropic Hydrodynamics: Three lectures*, *Acta Phys. Polon. B* **45** (2014) 2355–2394, [[1410.5786](#)].
- [36] T. H. Hansson and I. Zahed, *Electric and Magnetic Properties of Hot Gluons*, *Phys. Rev. Lett.* **58** (1987) 2397.
- [37] H. T. Elze, U. W. Heinz, K. Kajantie and T. Toimela, *High Temperature Gluon Matter in the Background Gauge*, *Z. Phys. C* **37** (1988) 305.
- [38] D. J. Gross, R. D. Pisarski and L. G. Yaffe, *QCD and Instantons at Finite Temperature*, *Rev. Mod. Phys.* **53** (1981) 43.
- [39] R. D. Pisarski, *Computing Finite Temperature Loops with Ease*, *Nucl. Phys. B* **309** (1988) 476–492.
- [40] E. Braaten and R. D. Pisarski, *Soft Amplitudes in Hot Gauge Theories: A General Analysis*, *Nucl. Phys. B* **337** (1990) 569–634.
- [41] R. D. Pisarski, *Scattering Amplitudes in Hot Gauge Theories*, *Phys. Rev. Lett.* **63** (1989) 1129.
- [42] R. D. Pisarski, *How to Compute Scattering Amplitudes in Hot Gauge Theories*, *Physica A* **158** (1989) 246–250.
- [43] O. K. Kalashnikov, *QCD AT FINITE TEMPERATURE*, *Fortsch. Phys.* **32** (1984) 525.

- [44] J. O. Andersen, E. Braaten and M. Strickland, *Hard thermal loop resummation of the free energy of a hot gluon plasma*, *Phys. Rev. Lett.* **83** (1999) 2139–2142, [[hep-ph/9902327](#)].
- [45] J. O. Andersen, E. Braaten and M. Strickland, *Hard thermal loop resummation of the thermodynamics of a hot gluon plasma*, *Phys. Rev. D* **61** (2000) 014017, [[hep-ph/9905337](#)].
- [46] J. O. Andersen, E. Braaten and M. Strickland, *Hard thermal loop resummation of the free energy of a hot quark - gluon plasma*, *Phys. Rev. D* **61** (2000) 074016, [[hep-ph/9908323](#)].
- [47] Y. Jiang, H.-x. Zhu, W.-m. Sun and H.-s. Zong, *The Quark Number Susceptibility in Hard-Thermal-Loop Approximation*, *J. Phys. G* **37** (2010) 055001, [[1003.5031](#)].
- [48] M. Strickland, J. O. Andersen, A. Bandyopadhyay, N. Haque, M. G. Mustafa and N. Su, *Three loop HTL perturbation theory at finite temperature and chemical potential*, *Nucl. Phys. A* **931** (2014) 841–845, [[1407.3671](#)].
- [49] N. Haque, M. G. Mustafa and M. Strickland, *Two-loop hard thermal loop pressure at finite temperature and chemical potential*, *Phys. Rev. D* **87** (2013) 105007, [[1212.1797](#)].
- [50] J. B. Kogut, *A Review of the Lattice Gauge Theory Approach to Quantum Chromodynamics*, *Rev. Mod. Phys.* **55** (1983) 775.
- [51] M. Creutz, L. Jacobs and C. Rebbi, *Monte Carlo Computations in Lattice Gauge Theories*, *Phys. Rept.* **95** (1983) 201–282.

## BIBLIOGRAPHY

- [52] K. G. Wilson and J. B. Kogut, *The Renormalization group and the epsilon expansion*, *Phys. Rept.* **12** (1974) 75–199.
- [53] F. Karsch, *Lattice QCD at high temperature and density*, *Lect. Notes Phys.* **583** (2002) 209–249, [[hep-lat/0106019](#)].
- [54] S. P. Klevansky, *The Nambu-Jona-Lasinio model of quantum chromodynamics*, *Rev. Mod. Phys.* **64** (1992) 649–708.
- [55] P. Rehberg, S. P. Klevansky and J. Hufner, *Hadronization in the SU(3) Nambu-Jona-Lasinio model*, *Phys. Rev. C* **53** (1996) 410–429, [[hep-ph/9506436](#)].
- [56] M. K. Volkov and A. E. Radzhabov, *The Nambu-Jona-Lasinio model and its development*, *Phys. Usp.* **49** (2006) 551–561, [[hep-ph/0508263](#)].
- [57] B.-J. Schaefer and J. Wambach, *The Phase diagram of the quark meson model*, *Nucl. Phys. A* **757** (2005) 479–492, [[nucl-th/0403039](#)].
- [58] N. Petropoulos, *Linear sigma model and chiral symmetry at finite temperature*, *J. Phys. G* **25** (1999) 2225–2241, [[hep-ph/9807331](#)].
- [59] C. Ratti, S. Roessner, M. A. Thaler and W. Weise, *Thermodynamics of the PNJL model*, *Eur. Phys. J. C* **49** (2007) 213–217, [[hep-ph/0609218](#)].
- [60] S. Mukherjee, M. G. Mustafa and R. Ray, *Thermodynamics of the PNJL model with nonzero baryon and isospin chemical potentials*, *Phys. Rev. D* **75** (2007) 094015, [[hep-ph/0609249](#)].
- [61] B.-J. Schaefer, J. M. Pawłowski and J. Wambach, *The Phase Structure of the Polyakov–Quark-Meson Model*, *Phys. Rev. D* **76** (2007) 074023, [[0704.3234](#)].

- [62] P. Huovinen and P. Petreczky, *QCD Equation of State and Hadron Resonance Gas*, *Nucl. Phys. A* **837** (2010) 26–53, [0912.2541].
- [63] K. Tuchin, *Particle production in strong electromagnetic fields in relativistic heavy-ion collisions*, *Adv. High Energy Phys.* **2013** (2013) 490495, [1301.0099].
- [64] V. Skokov, A. Y. Illarionov and V. Toneev, *Estimate of the magnetic field strength in heavy-ion collisions*, *Int. J. Mod. Phys. A* **24** (2009) 5925–5932, [0907.1396].
- [65] A. Bzdak and V. Skokov, *Event-by-event fluctuations of magnetic and electric fields in heavy ion collisions*, *Phys. Lett. B* **710** (2012) 171–174, [1111.1949].
- [66] V. Voronyuk, V. D. Toneev, W. Cassing, E. L. Bratkovskaya, V. P. Konchakovski and S. A. Voloshin, *(Electro-)Magnetic field evolution in relativistic heavy-ion collisions*, *Phys. Rev. C* **83** (2011) 054911, [1103.4239].
- [67] V. Roy, S. Pu, L. Rezzolla and D. H. Rischke, *Effect of intense magnetic fields on reduced-MHD evolution in  $\sqrt{s_{NN}} = 200$  GeV Au+Au collisions*, *Phys. Rev. C* **96** (2017) 054909, [1706.05326].
- [68] X.-G. Huang, *Electromagnetic fields and anomalous transports in heavy-ion collisions — A pedagogical review*, *Rept. Prog. Phys.* **79** (2016) 076302, [1509.04073].
- [69] K. Tuchin, *Time and space dependence of the electromagnetic field in relativistic heavy-ion collisions*, *Phys. Rev. C* **88** (2013) 024911, [1305.5806].
- [70] K. Fukushima, D. E. Kharzeev and H. J. Warringa, *The Chiral Magnetic Effect*, *Phys. Rev. D* **78** (2008) 074033, [0808.3382].

## BIBLIOGRAPHY

- [71] J. O. Andersen, *Chiral perturbation theory in a magnetic background - finite-temperature effects*, *JHEP* **10** (2012) 005, [[1205.6978](#)].
- [72] S. Rath and B. K. Patra, *One-loop QCD thermodynamics in a strong homogeneous and static magnetic field*, *JHEP* **12** (2017) 098, [[1707.02890](#)].
- [73] M. Strickland, V. Dexheimer and D. P. Menezes, *Bulk Properties of a Fermi Gas in a Magnetic Field*, *Phys. Rev. D* **86** (2012) 125032, [[1209.3276](#)].
- [74] R. L. S. Farias, V. S. Timoteo, S. S. Avancini, M. B. Pinto and G. Krein, *Thermo-magnetic effects in quark matter: Nambu–Jona-Lasinio model constrained by lattice QCD*, *Eur. Phys. J. A* **53** (2017) 101, [[1603.03847](#)].
- [75] R. Ghosh, A. Bandyopadhyay, I. Nilima and S. Ghosh, *Anisotropic tomography of heavy quark dissociation by using general propagator structure at finite magnetic field*, [2204.02312](#).
- [76] X. Wang, I. A. Shovkovy, L. Yu and M. Huang, *Ellipticity of photon emission from strongly magnetized hot QCD plasma*, *Phys. Rev. D* **102** (2020) 076010, [[2006.16254](#)].
- [77] K. Hattori, H. Taya and S. Yoshida, *Di-lepton production from a single photon in strong magnetic fields: vacuum dichroism*, *JHEP* **01** (2021) 093, [[2010.13492](#)].
- [78] S. Ghosh and V. Chandra, *Electromagnetic spectral function and dilepton rate in a hot magnetized QCD medium*, *Phys. Rev. D* **98** (2018) 076006, [[1808.05176](#)].
- [79] A. Das, A. Bandyopadhyay and C. A. Islam, *Lepton pair production from a hot and dense QCD medium in presence of an arbitrary magnetic field*, [2109.00019](#).

- [80] A. Bandyopadhyay, C. A. Islam and M. G. Mustafa, *Electromagnetic spectral properties and Debye screening of a strongly magnetized hot medium*, *Phys. Rev. D* **94** (2016) 114034, [[1602.06769](#)].
- [81] M. Kurian, S. Mitra, S. Ghosh and V. Chandra, *Transport coefficients of hot magnetized QCD matter beyond the lowest Landau level approximation*, *Eur. Phys. J. C* **79** (2019) 134, [[1805.07313](#)].
- [82] M. Kurian and V. Chandra, *Bulk viscosity of a hot QCD medium in a strong magnetic field within the relaxation-time approximation*, *Phys. Rev. D* **97** (2018) 116008, [[1802.07904](#)].
- [83] S. Schramm, B. Muller and A. J. Schramm, *Quark - anti-quark condensates in strong magnetic fields*, *Mod. Phys. Lett. A* **7** (1992) 973–982.
- [84] E. S. Fraga and A. J. Mizher, *Chiral transition in a strong magnetic background*, *Phys. Rev. D* **78** (2008) 025016, [[0804.1452](#)].
- [85] B. Chatterjee, H. Mishra and A. Mishra, *Vacuum structure and chiral symmetry breaking in strong magnetic fields for hot and dense quark matter*, *Phys. Rev. D* **84** (2011) 014016, [[1101.0498](#)].
- [86] R. Gatto and M. Ruggieri, *Deconfinement and Chiral Symmetry Restoration in a Strong Magnetic Background*, *Phys. Rev. D* **83** (2011) 034016, [[1012.1291](#)].
- [87] M. D’Elia, S. Mukherjee and F. Sanfilippo, *QCD Phase Transition in a Strong Magnetic Background*, *Phys. Rev. D* **82** (2010) 051501, [[1005.5365](#)].

## BIBLIOGRAPHY

- [88] G. Endrodi, M. Giordano, S. D. Katz, T. G. Kovács and F. Pittler, *Magnetic catalysis and inverse catalysis for heavy pions*, *JHEP* **07** (2019) 007, [[1904.10296](#)].
- [89] M. D'Elia, F. Manigrasso, F. Negro and F. Sanfilippo, *QCD phase diagram in a magnetic background for different values of the pion mass*, *Phys. Rev. D* **98** (2018) 054509, [[1808.07008](#)].
- [90] G. S. Bali, F. Bruckmann, G. Endrodi, Z. Fodor, S. D. Katz and A. Schafer, *QCD quark condensate in external magnetic fields*, *Phys. Rev. D* **86** (2012) 071502, [[1206.4205](#)].
- [91] G. S. Bali, F. Bruckmann, G. Endrodi, Z. Fodor, S. D. Katz, S. Krieg et al., *The QCD phase diagram for external magnetic fields*, *JHEP* **02** (2012) 044, [[1111.4956](#)].
- [92] R. L. S. Farias, K. P. Gomes, G. I. Krein and M. B. Pinto, *Importance of asymptotic freedom for the pseudocritical temperature in magnetized quark matter*, *Phys. Rev. C* **90** (2014) 025203, [[1404.3931](#)].
- [93] M. Ferreira, P. Costa, O. Lourenço, T. Frederico and C. Providência, *Inverse magnetic catalysis in the (2+1)-flavor Nambu-Jona-Lasinio and Polyakov-Nambu-Jona-Lasinio models*, *Phys. Rev. D* **89** (2014) 116011, [[1404.5577](#)].
- [94] A. Ayala, M. Loewe and R. Zamora, *Inverse magnetic catalysis in the linear sigma model with quarks*, *Phys. Rev. D* **91** (2015) 016002, [[1406.7408](#)].

- [95] S. Mao, *Inverse magnetic catalysis in Nambu–Jona-Lasinio model beyond mean field*, *Phys. Lett. B* **758** (2016) 195–199, [[1602.06503](#)].
- [96] V. P. Pagura, D. Gomez Dumm, S. Noguera and N. N. Scoccola, *Magnetic catalysis and inverse magnetic catalysis in nonlocal chiral quark models*, *Phys. Rev. D* **95** (2017) 034013, [[1609.02025](#)].
- [97] J. O. Andersen, W. R. Naylor and A. Tranberg, *Phase diagram of QCD in a magnetic field: A review*, *Rev. Mod. Phys.* **88** (2016) 025001, [[1411.7176](#)].
- [98] M. S. Ali, C. A. Islam and R. Sharma, *Studying explicit  $U(1)_A$  symmetry breaking in a hot and magnetized two flavor nonlocal NJL model constrained using lattice results*, *Phys. Rev. D* **104** (2021) 114026, [[2009.13563](#)].
- [99] B. Karmakar, R. Ghosh, A. Bandyopadhyay, N. Haque and M. G. Mustafa, *Anisotropic pressure of deconfined QCD matter in presence of strong magnetic field within one-loop approximation*, *Phys. Rev. D* **99** (2019) 094002, [[1902.02607](#)].
- [100] T.-K. Chyi, C.-W. Hwang, W. F. Kao, G.-L. Lin, K.-W. Ng and J.-J. Tseng, *The weak field expansion for processes in a homogeneous background magnetic field*, *Phys. Rev. D* **62** (2000) 105014, [[hep-th/9912134](#)].
- [101] S. A. Bass, M. Gyulassy, H. Stoecker and W. Greiner, *Signatures of quark gluon plasma formation in high-energy heavy ion collisions: A Critical review*, *J. Phys. G* **25** (1999) R1–R57, [[hep-ph/9810281](#)].
- [102] J. W. Harris and B. Muller, *The Search for the quark - gluon plasma*, *Ann. Rev. Nucl. Part. Sci.* **46** (1996) 71–107, [[hep-ph/9602235](#)].



## BIBLIOGRAPHY

- [103] T. Niida and Y. Miake, *Signatures of QGP at RHIC and the LHC*, *AAPPS Bull.* **31** (2021) 12, [[2104.11406](#)].
- [104] J. I. Kapusta, P. Lichard and D. Seibert, *High-energy photons from quark - gluon plasma versus hot hadronic gas*, *Phys. Rev. D* **44** (1991) 2774–2788.
- [105] W. Cassing and E. L. Bratkovskaya, *Hadronic and electromagnetic probes of hot and dense nuclear matter*, *Phys. Rept.* **308** (1999) 65–233.
- [106] J. I. Kapusta, *Photons and lepton pairs from high-energy nuclear collisions*, *Nucl. Phys. A* **566** (1994) 45C–59C.
- [107] P. V. Ruuskanen, *Electromagnetic probes of quark - gluon plasma in relativistic heavy ion collisions*, *Nucl. Phys. A* **544** (1992) 169–182.
- [108] J. Rafelski and B. Muller, *Strangeness Production in the Quark - Gluon Plasma*, *Phys. Rev. Lett.* **48** (1982) 1066.
- [109] P. Koch, B. Muller and J. Rafelski, *Strangeness in Relativistic Heavy Ion Collisions*, *Phys. Rept.* **142** (1986) 167–262.
- [110] C. Blume and C. Markert, *Strange hadron production in heavy ion collisions from SPS to RHIC*, *Prog. Part. Nucl. Phys.* **66** (2011) 834–879, [[1105.2798](#)].
- [111] S. Margetis, K. Safarik and O. Villalobos Baillie, *Strangeness production in heavy-ion collisions*, *Ann. Rev. Nucl. Part. Sci.* **50** (2000) 299–342.
- [112] F. Wang, *Strangeness in dense nuclear matter: A Review of AGS results*, *J. Phys. G* **27** (2001) 283–300, [[nucl-ex/0010002](#)].

- [113] T. Matsui and H. Satz, *J/ψ Suppression by Quark-Gluon Plasma Formation*, *Phys. Lett. B* **178** (1986) 416–422.
- [114] F. Karsch, M. T. Mehr and H. Satz, *Color Screening and Deconfinement for Bound States of Heavy Quarks*, *Z. Phys. C* **37** (1988) 617.
- [115] L. D. McLerran and T. Toimela, *Photon and Dilepton Emission from the Quark - Gluon Plasma: Some General Considerations*, *Phys. Rev. D* **31** (1985) 545.
- [116] E. V. Shuryak and I. Zahed, *Towards a theory of binary bound states in the quark gluon plasma*, *Phys. Rev. D* **70** (2004) 054507, [[hep-ph/0403127](#)].
- [117] C.-Y. Wong, *Heavy quarkonia in quark-gluon plasma*, *Phys. Rev. C* **72** (2005) 034906, [[hep-ph/0408020](#)].
- [118] H. Satz, *Quarkonium Binding and Dissociation: The Spectral Analysis of the QGP*, *Nucl. Phys. A* **783** (2007) 249–260, [[hep-ph/0609197](#)].
- [119] S. Cao and X.-N. Wang, *Jet quenching and medium response in high-energy heavy-ion collisions: a review*, *Rept. Prog. Phys.* **84** (2021) 024301, [[2002.04028](#)].
- [120] Y. Mehtar-Tani, J. G. Milhano and K. Tywoniuk, *Jet physics in heavy-ion collisions*, *Int. J. Mod. Phys. A* **28** (2013) 1340013, [[1302.2579](#)].
- [121] M. Spusta, *Jet Quenching at LHC*, *Mod. Phys. Lett. A* **28** (2013) 1330017, [[1305.6400](#)].
- [122] J.-P. Blaizot and Y. Mehtar-Tani, *Jet Structure in Heavy Ion Collisions*, *Int. J. Mod. Phys. E* **24** (2015) 1530012, [[1503.05958](#)].

## BIBLIOGRAPHY

- [123] U. A. Wiedemann, *Jet Quenching in Heavy Ion Collisions*, [0908.2306](#).
- [124] STAR collaboration, J. Adams et al., *Distributions of charged hadrons associated with high transverse momentum particles in pp and Au + Au collisions at  $\sqrt{s_{NN}} = 200$ -GeV*, *Phys. Rev. Lett.* **95** (2005) 152301, [[nucl-ex/0501016](#)].
- [125] CMS collaboration, S. Chatrchyan et al., *Observation and studies of jet quenching in PbPb collisions at nucleon-nucleon center-of-mass energy = 2.76 TeV*, *Phys. Rev. C* **84** (2011) 024906, [[1102.1957](#)].
- [126] S. Voloshin and Y. Zhang, *Flow study in relativistic nuclear collisions by Fourier expansion of Azimuthal particle distributions*, *Z. Phys. C* **70** (1996) 665–672, [[hep-ph/9407282](#)].
- [127] A. M. Poskanzer and S. A. Voloshin, *Methods for analyzing anisotropic flow in relativistic nuclear collisions*, *Phys. Rev. C* **58** (1998) 1671–1678, [[nucl-ex/9805001](#)].
- [128] CMS collaboration, S. Chatrchyan et al., *Measurement of the elliptic anisotropy of charged particles produced in PbPb collisions at  $\sqrt{s_{NN}} = 2.76$  TeV*, *Phys. Rev. C* **87** (2013) 014902, [[1204.1409](#)].
- [129] P. F. Kolb, J. Sollfrank and U. W. Heinz, *Anisotropic transverse flow and the quark hadron phase transition*, *Phys. Rev. C* **62** (2000) 054909, [[hep-ph/0006129](#)].
- [130] C. Villani, *A review of mathematical topics in collisional kinetic theory*, *Handbook of mathematical fluid dynamics* **1** (2002) 3–8.
- [131] S. R. De Groot, *Relativistic Kinetic Theory. Principles and Applications*. 1980.

- [132] P. Romatschke, *New Developments in Relativistic Viscous Hydrodynamics*, *Int. J. Mod. Phys. E* **19** (2010) 1–53, [[0902.3663](#)].
- [133] L. D. Landau, *On the multiparticle production in high-energy collisions*, *Izv. Akad. Nauk Ser. Fiz.* **17** (1953) 51–64.
- [134] J. D. Bjorken, *Highly Relativistic Nucleus-Nucleus Collisions: The Central Rapidity Region*, *Phys. Rev. D* **27** (1983) 140–151.
- [135] R. M. Weiner, *Surprises from the search for quark-gluon plasma? When was quark-gluon plasma seen?*, *Int. J. Mod. Phys. E* **15** (2006) 37–70, [[hep-ph/0507115](#)].
- [136] U. W. Heinz, *Early collective expansion: Relativistic hydrodynamics and the transport properties of QCD matter*, *Landolt-Bornstein* **23** (2010) 240, [[0901.4355](#)].
- [137] W. Scheid, H. Muller and W. Greiner, *Nuclear Shock Waves in Heavy-Ion Collisions*, *Phys. Rev. Lett.* **32** (1974) 741–745.
- [138] M. I. Sobel, H. A. Bethe, P. J. Siemens and J. P. Bondorf, *Shock Waves in Colliding Nuclei*, *Nucl. Phys. A* **251** (1975) 502–529.
- [139] P. B. Arnold, J. Lenaghan and G. D. Moore, *QCD plasma instabilities and bottom up thermalization*, *JHEP* **08** (2003) 002, [[hep-ph/0307325](#)].
- [140] S. Mrowczynski, *Plasma instability at the initial stage of ultrarelativistic heavy ion collisions*, *Phys. Lett. B* **314** (1993) 118–121.
- [141] S. Mrowczynski and M. H. Thoma, *Hard loop approach to anisotropic systems*, *Phys. Rev. D* **62** (2000) 036011, [[hep-ph/0001164](#)].

## BIBLIOGRAPHY

- [142] R. Baier, A. H. Mueller, D. Schiff and D. T. Son, 'Bottom up' thermalization in heavy ion collisions, *Phys. Lett. B* **502** (2001) 51–58, [[hep-ph/0009237](#)].
- [143] S. Mrowczynski, B. Schenke and M. Strickland, Color instabilities in the quark–gluon plasma, *Phys. Rept.* **682** (2017) 1–97, [[1603.08946](#)].
- [144] B. S. Kasmaei and M. Strickland, Parton self-energies for general momentum-space anisotropy, *Phys. Rev. D* **97** (2018) 054022, [[1801.00863](#)].
- [145] T. Matsubara, A New Approach to Quantum-Statistical Mechanics, *Progress of Theoretical Physics* **14** (10, 1955) 351–378.
- [146] J. S. Schwinger, Brownian motion of a quantum oscillator, *J. Math. Phys.* **2** (1961) 407–432.
- [147] L. V. Keldysh, Diagram technique for nonequilibrium processes, *Zh. Eksp. Teor. Fiz.* **47** (1964) 1515–1527.
- [148] A. K. Das, *Finite Temperature Field Theory*. World Scientific, New York, 1997.
- [149] S. Mallik and S. Sarkar, *Hadrons at Finite Temperature*. Cambridge Monographs on Mathematical Physics. Cambridge University Press, 2016, [10.1017/9781316535585](#).
- [150] M. L. Bellac, *Thermal Field Theory*. Cambridge Monographs on Mathematical Physics. Cambridge University Press, 3, 2011, [10.1017/CBO9780511721700](#).
- [151] H.-T. Ding, F. Karsch and S. Mukherjee, Thermodynamics of strong-interaction matter from Lattice QCD, *Int. J. Mod. Phys. E* **24** (2015) 1530007, [[1504.05274](#)].

- [152] C. Ratti, *Lattice QCD and heavy ion collisions: a review of recent progress*, *Rept. Prog. Phys.* **81** (2018) 084301, [[1804.07810](#)].
- [153] USQCD collaboration, A. Bazavov, F. Karsch, S. Mukherjee and P. Petreczky, *Hot-dense Lattice QCD: USQCD whitepaper 2018*, *Eur. Phys. J. A* **55** (2019) 194, [[1904.09951](#)].
- [154] J. O. Andersen and M. Strickland, *Resummation in hot field theories*, *Annals Phys.* **317** (2005) 281–353, [[hep-ph/0404164](#)].
- [155] N. Haque, A. Bandyopadhyay, J. O. Andersen, M. G. Mustafa, M. Strickland and N. Su, *Three-loop HTLpt thermodynamics at finite temperature and chemical potential*, *JHEP* **05** (2014) 027, [[1402.6907](#)].
- [156] N. Su, *Recent progress in hard-thermal-loop QCD thermodynamics and collective excitations*, *Int. J. Mod. Phys. A* **30** (2015) 1530025, [[1502.04589](#)].
- [157] A. Jaiswal and V. Roy, *Relativistic hydrodynamics in heavy-ion collisions: general aspects and recent developments*, *Adv. High Energy Phys.* **2016** (2016) 9623034, [[1605.08694](#)].
- [158] D. T. Son and A. O. Starinets, *Viscosity, Black Holes, and Quantum Field Theory*, *Ann. Rev. Nucl. Part. Sci.* **57** (2007) 95–118, [[0704.0240](#)].
- [159] H. Nastase, *Introduction to AdS-CFT*, [0712.0689](#).
- [160] R. Peschanski, *Introduction to String Theory and Gauge/Gravity duality for students in QCD and QGP phenomenology*, *Acta Phys. Polon. B* **39** (2008) 2479–2510, [[0804.3210](#)].

## BIBLIOGRAPHY

- [161] J. Sadeghi, B. Pourhassan and S. Heshmatian, *Application of AdS/CFT in Quark-Gluon Plasma*, *Adv. High Energy Phys.* **2013** (2013) 759804.
- [162] R. Stock, ed., *Relativistic Heavy Ion Physics*, vol. 23 of *Landolt-Boernstein - Group I Elementary Particles, Nuclei and Atoms*. Springer, 2010, 10.1007/978-3-642-01539-7.
- [163] M. Strickland, *Thermalization and isotropization in heavy-ion collisions*, *Pramana* **84** (2015) 671–684, [1312.2285].
- [164] M. Alqahtani, M. Nopoush and M. Strickland, *Relativistic anisotropic hydrodynamics*, *Prog. Part. Nucl. Phys.* **101** (2018) 204–248, [1712.03282].
- [165] S. Mrowczynski, A. Rebhan and M. Strickland, *Hard loop effective action for anisotropic plasmas*, *Phys. Rev. D* **70** (2004) 025004, [hep-ph/0403256].
- [166] P. Romatschke and M. Strickland, *Collective modes of an anisotropic quark gluon plasma*, *Phys. Rev. D* **68** (2003) 036004, [hep-ph/0304092].
- [167] P. Romatschke and M. Strickland, *Collective modes of an anisotropic quark-gluon plasma II*, *Phys. Rev. D* **70** (2004) 116006, [hep-ph/0406188].
- [168] B. Schenke and M. Strickland, *Fermionic Collective Modes of an Anisotropic Quark-Gluon Plasma*, *Phys. Rev. D* **74** (2006) 065004, [hep-ph/0606160].
- [169] L. Bhattacharya and P. Roy, *Photons from anisotropic Quark-Gluon-Plasma*, *Phys. Rev. C* **78** (2008) 064904, [0809.4596].
- [170] L. Bhattacharya and P. Roy, *Measuring isotropization time of Quark-Gluon-Plasma from direct photon at RHIC*, *Phys. Rev. C* **79** (2009) 054910, [0812.1478].

- [171] L. Bhattacharya, R. Ryblewski and M. Strickland, *Photon production from a nonequilibrium quark-gluon plasma*, *Phys. Rev. D* **93** (2016) 065005, [[1507.06605](#)].
- [172] M. Nopoush, Y. Guo and M. Strickland, *The static hard-loop gluon propagator to all orders in anisotropy*, *JHEP* **09** (2017) 063, [[1706.08091](#)].
- [173] B. Krouppa and M. Strickland, *Predictions for bottomonia suppression in 5.023 TeV Pb-Pb collisions*, *Universe* **2** (2016) 16, [[1605.03561](#)].
- [174] M. Mandal and P. Roy, *Wake in anisotropic quark-gluon plasma*, *Phys. Rev. D* **86** (2012) 114002, [[1310.4657](#)].
- [175] M. Mandal and P. Roy, *Wake potential in collisional anisotropic quark-gluon plasma*, *Phys. Rev. D* **88** (2013) 074013, [[1310.4660](#)].
- [176] M. Mandal, L. Bhattacharya and P. Roy, *Nuclear modification factor in an anisotropic  $\gamma$  Quark-Gluon-Plasma*, *Phys. Rev. C* **84** (2011) 044910, [[1101.5855](#)].
- [177] V. Chandra and V. Sreekanth, *Impact of momentum anisotropy and turbulent chromo-fields on thermal particle production in quark-gluon-plasma medium*, *Eur. Phys. J. C* **77** (2017) 427, [[1602.07142](#)].
- [178] M. Strickland, *The Chromo-Weibel instability*, *Braz. J. Phys.* **37** (2007) 762–765, [[hep-ph/0611349](#)].
- [179] A. Rebhan, P. Romatschke and M. Strickland, *Hard-loop dynamics of non-Abelian plasma instabilities*, *Phys. Rev. Lett.* **94** (2005) 102303, [[hep-ph/0412016](#)].



## BIBLIOGRAPHY

- [180] D. Bazow, U. W. Heinz and M. Strickland, *Second-order (2+1)-dimensional anisotropic hydrodynamics*, *Phys. Rev. C* **90** (2014) 054910, [[1311.6720](#)].
- [181] L. Tinti and W. Florkowski, *Projection method and new formulation of leading-order anisotropic hydrodynamics*, *Phys. Rev. C* **89** (2014) 034907, [[1312.6614](#)].
- [182] M. Nopoush, R. Ryblewski and M. Strickland, *Bulk viscous evolution within anisotropic hydrodynamics*, *Phys. Rev. C* **90** (2014) 014908, [[1405.1355](#)].
- [183] M. Alqahtani, M. Nopoush and M. Strickland, *Quasiparticle equation of state for anisotropic hydrodynamics*, *Phys. Rev. C* **92** (2015) 054910, [[1509.02913](#)].
- [184] M. Nopoush and M. Strickland, *Including off-diagonal anisotropies in anisotropic hydrodynamics*, *Phys. Rev. C* **100** (2019) 014904, [[1902.03303](#)].
- [185] B. S. Kasmaei, M. Nopoush and M. Strickland, *Quark self-energy in an ellipsoidally anisotropic quark-gluon plasma*, *Phys. Rev. D* **94** (2016) 125001, [[1608.06018](#)].
- [186] B. S. Kasmaei and M. Strickland, *Photon production and elliptic flow from a momentum-anisotropic quark-gluon plasma*, *Phys. Rev. D* **102** (2020) 014037, [[1911.03370](#)].
- [187] B. S. Kasmaei and M. Strickland, *Dilepton production and elliptic flow from an anisotropic quark-gluon plasma*, *Phys. Rev. D* **99** (2019) 034015, [[1811.07486](#)].
- [188] A. Dumitru, Y. Guo and M. Strickland, *The Heavy-quark potential in an anisotropic (viscous) plasma*, *Phys. Lett. B* **662** (2008) 37–42, [[0711.4722](#)].

- [189] A. Dumitru, Y. Guo and M. Strickland, *The Imaginary part of the static gluon propagator in an anisotropic (viscous) QCD plasma*, *Phys. Rev. D* **79** (2009) 114003, [[0903.4703](#)].
- [190] D. A. Uzdensky and S. Rightley, *Plasma Physics of Extreme Astrophysical Environments*, *Rept. Prog. Phys.* **77** (2014) 036902, [[1401.5110](#)].
- [191] A. K. Ganguly, S. Konar and P. B. Pal, *Faraday effect: A Field theoretical point of view*, *Phys. Rev. D* **60** (1999) 105014, [[hep-ph/9905206](#)].
- [192] M. Giovannini, *Cosmic microwave background polarization, Faraday rotation, and stochastic gravity-waves backgrounds*, *Phys. Rev. D* **56** (1997) 3198–3206, [[hep-th/9706201](#)].
- [193] E. P. Liang, S. C. Wilks and M. Tabak, *Pair Production by Ultraintense Lasers*, *Phys. Rev. Lett.* **81** (1998) 4887–4890.
- [194] M. H. Thoma, *Field Theoretic Description of Ultrarelativistic Electron-Positron Plasmas*, *Rev. Mod. Phys.* **81** (2009) 959–968, [[0801.0956](#)].
- [195] M. H. Thoma, *What can we learn from electromagnetic plasmas about the quark-gluon plasma?*, *J. Phys. A* **42** (2009) 214004, [[0809.1507](#)].
- [196] M. H. Thoma, *Parton interaction rates in the quark - gluon plasma*, *Phys. Rev. D* **49** (1994) 451–459, [[hep-ph/9308257](#)].
- [197] M. H. Thoma, *Damping rate of a hard photon in a relativistic plasma*, *Phys. Rev. D* **51** (1995) 862–865, [[hep-ph/9405309](#)].
- [198] H. A. Weldon, *Simple Rules for Discontinuities in Finite Temperature Field Theory*, *Phys. Rev. D* **28** (1983) 2007.

## BIBLIOGRAPHY

- [199] B. Karmakar, A. Bandyopadhyay, N. Haque and M. G. Mustafa, *General structure of gauge boson propagator and its spectra in a hot magnetized medium*, *Eur. Phys. J. C* **79** (2019) 658, [[1804.11336](#)].
- [200] A. Das, A. Bandyopadhyay, P. K. Roy and M. G. Mustafa, *General structure of fermion two-point function and its spectral representation in a hot magnetized medium*, *Phys. Rev. D* **97** (2018) 034024, [[1709.08365](#)].
- [201] E. Braaten, R. D. Pisarski and T.-C. Yuan, *Production of Soft Dileptons in the Quark - Gluon Plasma*, *Phys. Rev. Lett.* **64** (1990) 2242.
- [202] A. Bandyopadhyay, B. Karmakar, N. Haque and M. G. Mustafa, *Pressure of a weakly magnetized hot and dense deconfined QCD matter in one-loop hard-thermal-loop perturbation theory*, *Phys. Rev. D* **100** (2019) 034031, [[1702.02875](#)].
- [203] M. H. Thoma, *New developments and applications of thermal field theory*, [hep-ph/0010164](#).
- [204] J. I. Kapusta and C. Gale, *Finite-temperature field theory: Principles and applications*. Cambridge Monographs on Mathematical Physics. Cambridge University Press, 2011, [10.1017/CBO9780511535130](#).
- [205] Y. Aoki, G. Endrodi, Z. Fodor, S. D. Katz and K. K. Szabo, *The Order of the quantum chromodynamics transition predicted by the standard model of particle physics*, *Nature* **443** (2006) 675–678, [[hep-lat/0611014](#)].
- [206] T. Bhattacharya et al., *QCD Phase Transition with Chiral Quarks and Physical Quark Masses*, *Phys. Rev. Lett.* **113** (2014) 082001, [[1402.5175](#)].

- [207] K. Fukushima, *Chiral effective model with the Polyakov loop*, *Phys. Lett. B* **591** (2004) 277–284, [[hep-ph/0310121](#)].
- [208] C. Ratti, M. A. Thaler and W. Weise, *Phases of QCD: Lattice thermodynamics and a field theoretical model*, *Phys. Rev. D* **73** (2006) 014019, [[hep-ph/0506234](#)].
- [209] Z. Fang, Y.-L. Wu and L. Zhang, *Chiral phase transition and QCD phase diagram from AdS/QCD*, *Phys. Rev. D* **99** (2019) 034028, [[1810.12525](#)].
- [210] C. S. Fischer, *Deconfinement phase transition and the quark condensate*, *Phys. Rev. Lett.* **103** (2009) 052003, [[0904.2700](#)].
- [211] J. Braun, L. M. Haas, F. Marhauser and J. M. Pawłowski, *Phase Structure of Two-Flavor QCD at Finite Chemical Potential*, *Phys. Rev. Lett.* **106** (2011) 022002, [[0908.0008](#)].
- [212] F. Karsch and E. Laermann, *Susceptibilities, the specific heat and a cumulant in two flavor QCD*, *Phys. Rev. D* **50** (1994) 6954–6962, [[hep-lat/9406008](#)].
- [213] MILC collaboration, C. Bernard, T. Burch, E. B. Gregory, D. Toussaint, C. E. DeTar, J. Osborn et al., *QCD thermodynamics with three flavors of improved staggered quarks*, *Phys. Rev. D* **71** (2005) 034504, [[hep-lat/0405029](#)].
- [214] M. Cheng et al., *The Transition temperature in QCD*, *Phys. Rev. D* **74** (2006) 054507, [[hep-lat/0608013](#)].
- [215] L.-K. Wu, X.-Q. Luo and H.-S. Chen, *Phase structure of lattice QCD with two flavors of Wilson quarks at finite temperature and chemical potential*, *Phys. Rev. D* **76** (2007) 034505, [[hep-lat/0611035](#)].

## BIBLIOGRAPHY

- [216] S. Digal, E. Laermann and H. Satz, *Deconfinement through chiral symmetry restoration in two flavor QCD*, *Eur. Phys. J. C* **18** (2001) 583–586, [[hep-ph/0007175](#)].
- [217] P. Chakraborty, M. G. Mustafa and M. H. Thoma, *Chiral susceptibility in hard thermal loop approximation*, *Phys. Rev. D* **67** (2003) 114004, [[hep-ph/0210159](#)].
- [218] A. V. Smilga and J. J. M. Verbaarschot, *Scalar susceptibility in QCD and the multiflavor Schwinger model*, *Phys. Rev. D* **54** (1996) 1087–1093, [[hep-ph/9511471](#)].
- [219] P. Zhuang, J. Hufner and S. P. Klevansky, *Thermodynamics of a quark - meson plasma in the Nambu-Jona-Lasinio model*, *Nucl. Phys. A* **576** (1994) 525–552.
- [220] C. Sasaki, B. Friman and K. Redlich, *Susceptibilities and the Phase Structure of a Chiral Model with Polyakov Loops*, *Phys. Rev. D* **75** (2007) 074013, [[hep-ph/0611147](#)].
- [221] D. Blaschke, A. Holl, C. D. Roberts and S. M. Schmidt, *Analysis of chiral and thermal susceptibilities*, *Phys. Rev. C* **58** (1998) 1758–1766, [[nucl-th/9803030](#)].
- [222] I. A. Shovkovy, *Magnetic Catalysis: A Review*, *Lect. Notes Phys.* **871** (2013) 13–49, [[1207.5081](#)].
- [223] A. Das, D. Kumar and H. Mishra, *Chiral susceptibility in the Nambu–Jona-Lasinio model: A Wigner function approach*, *Phys. Rev. D* **100** (2019) 094030, [[1907.12332](#)].

- [224] A. Das and N. Haque, *Neutral pion mass in the linear sigma model coupled to quarks at arbitrary magnetic field*, *Phys. Rev. D* **101** (2020) 074033, [[1908.10323](#)].
- [225] A. Ayala, C. A. Dominguez, S. Hernandez-Ortiz, L. A. Hernandez, M. Loewe, D. Manreza Paret et al., *Thermomagnetic evolution of the QCD strong coupling*, *Phys. Rev. D* **98** (2018) 031501, [[1805.08198](#)].
- [226] PARTICLE DATA GROUP collaboration, J. Beringer et al., *Review of Particle Physics (RPP)*, *Phys. Rev. D* **86** (2012) 010001.
- [227] D. E. Kharzeev, K. Landsteiner, A. Schmitt and H.-U. Yee, '*Strongly interacting matter in magnetic fields*': an overview, *Lect. Notes Phys.* **871** (2013) 1–11, [[1211.6245](#)].
- [228] V. A. Miransky and I. A. Shovkovy, *Quantum field theory in a magnetic field: From quantum chromodynamics to graphene and Dirac semimetals*, *Phys. Rept.* **576** (2015) 1–209, [[1503.00732](#)].
- [229] A. Mocsy, *Potential Models for Quarkonia*, *Eur. Phys. J. C* **61** (2009) 705–710, [[0811.0337](#)].
- [230] D. Cabrera and R. Rapp, *T-Matrix Approach to Quarkonium Correlation Functions in the QGP*, *Phys. Rev. D* **76** (2007) 114506, [[hep-ph/0611134](#)].
- [231] L. Thakur, N. Haque, U. Kakade and B. K. Patra, *Dissociation of quarkonium in an anisotropic hot QCD medium*, *Phys. Rev. D* **88** (2013) 054022, [[1212.2803](#)].

## BIBLIOGRAPHY

- [232] W. M. Alberico, A. Beraudo, A. De Pace and A. Molinari, *Potential models and lattice correlators for quarkonia at finite temperature*, *Phys. Rev. D* **77** (2008) 017502, [[0706.2846](#)].
- [233] C. S. Machado, F. S. Navarra, E. G. de Oliveira, J. Noronha and M. Strickland, *Heavy quarkonium production in a strong magnetic field*, *Phys. Rev. D* **88** (2013) 034009, [[1305.3308](#)].
- [234] X. Guo, S. Shi, N. Xu, Z. Xu and P. Zhuang, *Magnetic Field Effect on Charmonium Production in High Energy Nuclear Collisions*, *Phys. Lett. B* **751** (2015) 215–219, [[1502.04407](#)].
- [235] K. Marasinghe and K. Tuchin, *Quarkonium dissociation in quark-gluon plasma via ionization in magnetic field*, *Phys. Rev. C* **84** (2011) 044908, [[1103.1329](#)].
- [236] D.-L. Yang and B. Muller,  *$J/\psi$  Production by Magnetic Excitation of  $\eta_c$* , *J. Phys. G* **39** (2012) 015007, [[1108.2525](#)].
- [237] M. Hasan, B. Chatterjee and B. K. Patra, *Heavy Quark Potential in a static and strong homogeneous magnetic field*, *Eur. Phys. J. C* **77** (2017) 767, [[1703.10508](#)].
- [238] C. Bonati, M. D’Elia, M. Mariti, M. Mesiti, F. Negro, A. Rucci et al., *Magnetic field effects on the static quark potential at zero and finite temperature*, *Phys. Rev. D* **94** (2016) 094007, [[1607.08160](#)].
- [239] C. Bonati, M. D’Elia, M. Mariti, M. Mesiti, F. Negro, A. Rucci et al., *Screening masses in strong external magnetic fields*, *Phys. Rev. D* **95** (2017) 074515, [[1703.00842](#)].

- [240] K. Fukushima, K. Hattori, H.-U. Yee and Y. Yin, *Heavy Quark Diffusion in Strong Magnetic Fields at Weak Coupling and Implications for Elliptic Flow*, *Phys. Rev. D* **93** (2016) 074028, [[1512.03689](#)].
- [241] S. K. Das, S. Plumari, S. Chatterjee, J. Alam, F. Scardina and V. Greco, *Directed Flow of Charm Quarks as a Witness of the Initial Strong Magnetic Field in Ultra-Relativistic Heavy Ion Collisions*, *Phys. Lett. B* **768** (2017) 260–264, [[1608.02231](#)].
- [242] A. E. Shabad and V. V. Usov, *Real and virtual photons in an external constant electromagnetic field of most general form*, *Phys. Rev. D* **81** (2010) 125008, [[1002.1813](#)].
- [243] K. Hattori and K. Itakura, *Vacuum birefringence in strong magnetic fields: (I) Photon polarization tensor with all the Landau levels*, *Annals Phys.* **330** (2013) 23–54, [[1209.2663](#)].
- [244] M. Bordag and V. Skalozub, *Polarization tensor of charged gluons in color magnetic background field at finite temperature*, *Phys. Rev. D* **77** (2008) 105013, [[0801.2306](#)].
- [245] J. Chao, L. Yu and M. Huang, *Zeta function regularization of the photon polarization tensor for a magnetized vacuum*, *Phys. Rev. D* **90** (2014) 045033, [[1403.0442](#)].
- [246] N. Mueller, J. A. Bonnet and C. S. Fischer, *Dynamical quark mass generation in a strong external magnetic field*, *Phys. Rev. D* **89** (2014) 094023, [[1401.1647](#)].



## BIBLIOGRAPHY

- [247] A. Ayala, J. D. Castaño Yepes, C. A. Dominguez, S. Hernández-Ortiz, L. A. Hernández, M. Loewe et al., *Thermal corrections to the gluon magnetic Debye mass*, *Rev. Mex. Fis.* **66** (2020) 446–461, [[1805.07344](#)].
- [248] A. Ayala, J. D. Castaño Yepes, L. A. Hernández, J. Salinas San Martín and R. Zamora, *Gluon polarization tensor and dispersion relation in a weakly magnetized medium*, *Eur. Phys. J. A* **57** (2021) 140, [[2009.00830](#)].
- [249] A. Ayala, J. D. Castaño Yepes, M. Loewe and E. Muñoz, *Fermion mass and width in QED in a magnetic field*, *Phys. Rev. D* **104** (2021) 016006, [[2104.04019](#)].
- [250] E. Eichten, K. Gottfried, T. Kinoshita, J. B. Kogut, K. D. Lane and T.-M. Yan, *The Spectrum of Charmonium*, *Phys. Rev. Lett.* **34** (1975) 369–372.
- [251] V. Agotiya, V. Chandra and B. K. Patra, *Dissociation of quarkonium in hot QCD medium: Modification of the inter-quark potential*, *Phys. Rev. C* **80** (2009) 025210, [[0808.2699](#)].
- [252] L. Thakur, U. Kakade and B. K. Patra, *Dissociation of Quarkonium in a Complex Potential*, *Phys. Rev. D* **89** (2014) 094020, [[1401.0172](#)].
- [253] U. Kakade, B. K. Patra and L. Thakur, *Complex potential and bottomonium suppression at LHC energy*, *Int. J. Mod. Phys. A* **30** (2015) 1550043.
- [254] V. K. Agotiya, V. Chandra, M. Y. Jamal and I. Nilima, *Dissociation of heavy quarkonium in hot QCD medium in a quasiparticle model*, *Phys. Rev. D* **94** (2016) 094006, [[1610.03170](#)].

- [255] D. Lafferty and A. Rothkopf, *Improved Gauss law model and in-medium heavy quarkonium at finite density and velocity*, *Phys. Rev. D* **101** (2020) 056010, [[1906.00035](#)].
- [256] L. Thakur, N. Haque and Y. Hirono, *Heavy quarkonia in a bulk viscous medium*, *JHEP* **06** (2020) 071, [[2004.03426](#)].
- [257] J. Alexandre, *Vacuum polarization in thermal QED with an external magnetic field*, *Phys. Rev. D* **63** (2001) 073010, [[hep-th/0009204](#)].
- [258] H. A. Weldon, *Reformulation of finite temperature dilepton production*, *Phys. Rev. D* **42** (1990) 2384–2387.
- [259] A. Ayala, J. J. Cobos-Martínez, M. Loewe, M. E. Tejeda-Yeomans and R. Zamora, *Finite temperature quark-gluon vertex with a magnetic field in the Hard Thermal Loop approximation*, *Phys. Rev. D* **91** (2015) 016007, [[1410.6388](#)].
- [260] E. J. Ferrer, V. de la Incera and X. J. Wen, *Quark Antiscreening at Strong Magnetic Field and Inverse Magnetic Catalysis*, *Phys. Rev. D* **91** (2015) 054006, [[1407.3503](#)].
- [261] Y. Burnier and A. Rothkopf, *A gauge invariant Debye mass and the complex heavy-quark potential*, *Phys. Lett. B* **753** (2016) 232–236, [[1506.08684](#)].
- [262] PARTICLE DATA GROUP collaboration, K. A. Olive et al., *Review of Particle Physics*, *Chin. Phys. C* **38** (2014) 090001.
- [263] ALICE collaboration, K. Aamodt et al., *Charged-particle multiplicity density at mid-rapidity in central Pb-Pb collisions at  $\sqrt{s_{NN}} = 2.76$  TeV*, *Phys. Rev. Lett.* **105** (2010) 252301, [[1011.3916](#)].

## BIBLIOGRAPHY

- [264] STAR collaboration, J. Adams et al., *Experimental and theoretical challenges in the search for the quark gluon plasma: The STAR Collaboration's critical assessment of the evidence from RHIC collisions*, *Nucl. Phys. A* **757** (2005) 102–183, [[nucl-ex/0501009](#)].
- [265] P. Romatschke and U. Romatschke, *Viscosity Information from Relativistic Nuclear Collisions: How Perfect is the Fluid Observed at RHIC?*, *Phys. Rev. Lett.* **99** (2007) 172301, [[0706.1522](#)].
- [266] M. Gell-Mann and M. Levy, *The axial vector current in beta decay*, *Nuovo Cim.* **16** (1960) 705.
- [267] A. Ayala, R. L. S. Farias, S. Hernández-Ortiz, L. A. Hernández, D. M. Paret and R. Zamora, *Magnetic field-dependence of the neutral pion mass in the linear sigma model coupled to quarks: The weak field case*, *Phys. Rev. D* **98** (2018) 114008, [[1809.08312](#)].
- [268] F. Divotgey, P. Kovacs, F. Giacosa and D. H. Rischke, *Low-energy limit of the extended Linear Sigma Model*, *Eur. Phys. J. A* **54** (2018) 5, [[1605.05154](#)].
- [269] N. Petropoulos, *Linear sigma model at finite temperature*, other thesis, 2, 2004.
- [270] M. Loewe, C. Villavicencio and R. Zamora, *Linear sigma model and the formation of a charged pion condensate in the presence of an external magnetic field*, *Phys. Rev. D* **89** (2014) 016004, [[1310.5789](#)].
- [271] P. Chakraborty and J. I. Kapusta, *Quasi-Particle Theory of Shear and Bulk Viscosities of Hadronic Matter*, *Phys. Rev. C* **83** (2011) 014906, [[1006.0257](#)].

- [272] M. Heffernan, S. Jeon and C. Gale, *Hadronic transport coefficients from the linear  $\sigma$  model at finite temperature*, *Phys. Rev. C* **102** (2020) 034906, [[2005.12793](#)].
- [273] S. Gavin, *TRANSPORT COEFFICIENTS IN ULTRARELATIVISTIC HEAVY ION COLLISIONS*, *Nucl. Phys. A* **435** (1985) 826–843.
- [274] S. Jeon, *Hydrodynamic transport coefficients in relativistic scalar field theory*, *Phys. Rev. D* **52** (1995) 3591–3642, [[hep-ph/9409250](#)].
- [275] S. Ghosh and S. Ghosh, *One-loop Kubo estimations of the shear and bulk viscous coefficients for hot and magnetized Bosonic and Fermionic systems*, *Phys. Rev. D* **103** (2021) 096015, [[2011.04261](#)].
- [276] S. Satapathy, S. Ghosh and S. Ghosh, *Kubo estimation of the electrical conductivity for a hot relativistic fluid in the presence of a magnetic field*, *Phys. Rev. D* **104** (2021) 056030, [[2104.03917](#)].
- [277] K. Tuchin, *On viscous flow and azimuthal anisotropy of quark-gluon plasma in strong magnetic field*, *J. Phys. G* **39** (2012) 025010, [[1108.4394](#)].
- [278] S. Ghosh, B. Chatterjee, P. Mohanty, A. Mukharjee and H. Mishra, *Impact of magnetic field on shear viscosity of quark matter in Nambu–Jona-Lasinio model*, *Phys. Rev. D* **100** (2019) 034024, [[1804.00812](#)].
- [279] A. Dash, S. Samanta, J. Dey, U. Gangopadhyaya, S. Ghosh and V. Roy, *Anisotropic transport properties of a hadron resonance gas in a magnetic field*, *Phys. Rev. D* **102** (2020) 016016, [[2002.08781](#)].
- [280] S. Hess, *Tensors for Physics*. 2015, [10.1007/978-3-319-12787-3](#).

## BIBLIOGRAPHY

- [281] A. Das, H. Mishra and R. K. Mohapatra, *Transport coefficients of hot and dense hadron gas in a magnetic field: a relaxation time approach*, *Phys. Rev. D* **100** (2019) 114004, [[1909.06202](#)].
- [282] K. Hattori, S. Li, D. Satow and H.-U. Yee, *Longitudinal Conductivity in Strong Magnetic Field in Perturbative QCD: Complete Leading Order*, *Phys. Rev. D* **95** (2017) 076008, [[1610.06839](#)].
- [283] O. Scavenius, A. Mocsy, I. N. Mishustin and D. H. Rischke, *Chiral phase transition within effective models with constituent quarks*, *Phys. Rev. C* **64** (2001) 045202, [[nucl-th/0007030](#)].
- [284] G. P. Kadam and H. Mishra, *Medium modification of hadron masses and the thermodynamics of the hadron resonance gas model*, *Phys. Rev. C* **93** (2016) 025205, [[1509.06998](#)].
- [285] A. Ayala, P. Amore and A. Aranda, *Pion dispersion relation at finite density and temperature*, *Phys. Rev. C* **66** (2002) 045205, [[hep-ph/0207081](#)].
- [286] A. Ayala and S. Sahu, *Pion propagation in the linear sigma model at finite temperature*, *Phys. Rev. D* **62** (2000) 056007, [[hep-ph/0003266](#)].
- [287] A. Abhishek, H. Mishra and S. Ghosh, *Transport coefficients in the Polyakov quark meson coupling model: A relaxation time approximation*, *Phys. Rev. D* **97** (2018) 014005, [[1709.08013](#)].
- [288] R. Ghosh, B. Karmakar and A. Mukherjee, *Covariant formulation of gluon self-energy in presence of ellipsoidal anisotropy*, *Phys. Rev. D* **102** (2020) 114002, [[2011.03374](#)].

## Bibliography

- [289] J. O. Andersen, E. Braaten, E. Petitgirard and M. Strickland, *HTL perturbation theory to two loops*, *Phys. Rev. D* **66** (2002) 085016, [[hep-ph/0205085](#)].
- [290] W. Greiner, *Relativistic quantum mechanics: Wave equations*. 1990.
- [291] M. R. Setare and O. Hatami, *Exact Solution of Klein–Gordon Equation for Charged Particle in Magnetic Field with Shape Invariant Method*, *Commun. Theor. Phys.* **51** (2009) 1000–1002.